Quantitative characterization of amyloid-beta interaction with artificial compounds designed for Alzheimer´s disease therapy

Inaugural-Dissertation

zur Erlangung des Doktorgrades
der Mathematisch-Naturwissenschaftlichen Fakultät
der Heinrich-Heine-Universität Düsseldorf

vorgelegt von

Tamar Magdalena Ziehm
aus Kevelaer

Jülich, Februar 2018

aus dem Institut für Physikalische Biologie

der Heinrich-Heine-Universität Düsseldorf

Gedruckt mit der Genehmigung der

Mathematisch-Naturwissenschaftlichen Fakultät der

Heinrich-Heine-Universität Düsseldorf

Referent: Prof. Dr. Dieter Willbold

Korreferent: Jun.-Prof. Dr. Alexander K. Büll

Tag der mündlichen Prüfung: 09. Mai 2017

“We ask ourselves, who am I to be brilliant, gorgeous, talented, fabulous?

Actually, who are you *not* to be?”

Marianne Williamson

Table of Contents

List of figures

List of tables

Abbreviations

Aβ	amyloid-beta
AD	Alzheimer's disease
ADMET	adsorption, distribution, metabolism, excretion, toxicity
AGP	α1-acid glycoprotein
ApoE4	apolipoprotein E4
APP	amyloid precursor protein
BLI	biolayer interferometry
CSF	cerebrospinal fluid
CT	computed tomography
fAD	familiar Alzheimer's disease
FDA	U.S. Food and Drug Administration
FDG	fluorodeoxyglucose
HSA	human serum albumin
IDP	intrinsically disordered protein
K_D	equilibrium dissociation constant
MMSE	mini-mental state examination
MRI	magnetic resonance imaging
NMDA	N-methyl-D-aspartate
pEAβ	pyroglutamate-modified amyloid-beta
PET	positron emission tomography
PiB	Pittsburgh compound B
PSEN	presenilin
sAD	sporadic Alzheimer´s disease
SPR	surface plasmon resonance

Abstract

The overall risk for any individual of developing dementia is approximately 10 to 12 %. The most common type of dementia, Alzheimer´s disease (AD), is number 6 of the top 10 leading causes of deaths in the United States and the only one which cannot be prevented, retarded or cured. Therefore, alternative approaches are demanded for the development of AD therapy. Based on the amyloid cascade hypothesis, the aggregation of amyloid-beta (Aβ) has been manifested as the major hallmark of AD. We hypothesize that stabilization of Aβ monomers in its intrinsically disordered protein (IDP) like conformation will sequester them from the aggregation cascade and simultaneously eliminate pre-formed cytotoxic Aβ oligomers. To validate and confirm this strategy, the lead compound D3, a peptide consisting of twelve D-enantiomeric amino acid residues, was selected by mirror image phage display with monomeric Aβ(1-42) as target and intensively characterized in vitro and in vivo regarding its efficacy as a potential therapeutic agent for AD.

Pre-clinical results approved that D3 as a D-peptide is characterized by a high oral bioavailability and long plasma half-lives due to increased metabolic stability as compared to the L-enantiomer. Additionally, a free fraction of 8 % was determined in plasma for D3 which is mainly attributed to low binding affinity to human serum albumin.

Additionally, the lead compound D3 was optimized regarding its efficacy and potency for AD therapy. Two different strategies were applied which were either rational or systematic yielding several D3 derivatives. We found out that increased net charge, cyclization and design of multivalent derivatives are suitable modifications to further increase the potency of D3. Those strategies yielded up to 75-fold increased affinity to Aβ which was linked to increased oligomer elimination efficacy and subsequent rescue of cytotoxicity. Furthermore, peptide microarrays turned out to be a powerful tool for systematic compound optimization. Derivatives derived from those were especially characterized by increased potency. Thus, two compounds were investigated in detail regarding their interaction with Aβ in order to gain a clearer understanding of the molecular mechanism. Kinetics, stoichiometry and epitopes were studied using surface plasmon resonance (SPR). The results suggest an additional contribution of hydrophobic interactions to Aβ in the case of the optimized compounds in comparison to the mostly electrostatic Aβ interaction of the lead compound. These findings were supported by thermodynamic

profiles of complex formation which indicated an increase in entropy for the interaction between optimized compounds and Aβ monomers.

Recently, N-terminally modified pEAβ is getting more and more in focus due to its high prevalence in senile plaques of AD patients and increased aggregation propensity as compared to full-length Aβ. To further study the suitability for AD therapy involving this aggressive isoform of Aβ, the effects of D3 and its tandem version D3D3 on pEAβ were analyzed. Quantitative affinity determinations revealed a high cross-reactivity of the compounds for pEAβ and thus, D3D3 was able to rescue pEAβ-derived cytotoxicity.

Based on the present work, we could extent the knowledge of the molecular mechanism of interaction between Aβ and D3 and its derivatives. Lead optimization strategies were established and validated in vitro and in vivo. From a scientific point of view, promising candidates were developed and merit further pre-clinical investigations.

Zusammenfassung

Das Risiko eines Jeden von uns an einer Demenz zu erkranken, beträgt ca. 10 bis 12 %. Die üblichste Art der Demenz, die Alzheimer-Demenz (AD), ist auf Platz 6 der zehn häufigsten Todesursachen in den Vereinigten Staaten von Amerika und die einzige, die nicht vorgebeugt, aufgehalten oder geheilt werden kann. Daher herrscht eine große Nachfrage nach alternativen Ansätzen um eine Therapie für die AD zu entwickeln. Basierend auf der Amyloid-Kaskaden-Hypothese hat sich die Aggregation von Amyloid-beta (Aβ) als der wahrscheinlichste Auslöser der AD manifestiert. Wir haben die Hypothese aufgestellt, dass die Stabilisierung von Monomeren in ihrer IDP-ähnlichen Konformation diese von der Aggregation abhält und gleichzeitigt schon gebildete zytotoxische Aβ-Oligomere eliminiert. Um diese Strategie zu validieren und bestätigen, haben wir den Leitwirkstoff D3, ein Peptid bestehend aus D-enantiomeren Aminosäuren, mittels Spiegelbild-Phagen-Display mit monomerem Aβ(1-42) selektiert und intensiv in vitro und in vivo hinsichtlich seiner Wirksamkeit als potentielles Medikament für die AD charakterisiert.

Präklinische Ergebnisse bestätigten, dass D3 als ein D-Peptid von hoher oraler Bioverfügbarkeit und langer Halbwertszeit im Plasma als eine Folge von gesteigerter metabolischer Stabilität im Vergleich zu dem L-Enantiomer gekennzeichnet ist. Weiterhin wurde eine freie Fraktion von 8 % im Plasma für D3 bestimmt, was hauptsächlich der geringen Affinität zu humanem Serumalbumin zugeschrieben werden kann.

Zusätzlich wurde der Leitwirkstoff D3 hinsichtlich seiner Wirksamkeit für die Behandlung von der AD optimiert. Dabei wurden zwei verschiedene Strategie angewendet, welche entweder rational oder systematisch waren, und verschiedene D3-Derivate ergaben. Wir haben herausgefunden, dass die Erhöhung der Nettoladung, Zyklisierung und das Entwerfen von multivalenten Derivaten geeignete Modifikationen sind um die Wirksamkeit von D3 weiter zu erhöhen. Diese Strategien ergaben eine bis zu 75-fach erhöhte Affinität für Aβ, welche an erhöhte Effizienz für Oligomer-Eliminierung und anschließende Aufhebung der Zytotoxizität gekoppelt war. Weiterhin haben sich Peptid-Mikroarrays als ein wirksames Instrument für systematische Wirkstoff-Optimierung herausgestellt. Die Derivate, die davon abgeleitet wurden, waren besonders von gesteigerter Wirksamkeit gekennzeichnet. Deswegen wurden zwei Wirkstoffe detailliert hinsichtlich ihrer Interaktion mit Aβ untersucht, um ein klareres Verständnis von dem molekularen Mechanismus zu bekommen. Kinetik, Stöchiometrie und Epitope wurden mittels Oberflächenplasmonen-

resonanz untersucht. Die Ergebnisse lassen für die optimierten Wirkstoffe einen zusätzlichen Anteil von hydrophoben Wechselwirkungen vermuten im Vergleich zu dem hauptsächlich elektrostatisch-getriebenen Leitwirkstoff. Dies wurde von dem thermodynamischen Profil der Komplex-Bildung unterstütz, welches einen Anstieg der Entropie für die Interaktion zwischen optimierten Wirkstoffen und Aβ-Monomeren zeigt.

Kürzlich ist das N-terminal modifizierte pEAβ aufgrund seines hohen Vorkommens in senilen Plaques von AD-Patienten und gesteigerte Aggregations-Tendenz im Vergleich zum Volllängen-Aβ mehr und mehr in den Fokus gerückt. Um die Eignung für die Behandlung der AD zu testen, wo diese aggressive Aβ-Isoform involviert ist, wurden die Effekte von D3 und dem Tandem-Derivat D3D3 auf pEAβ getestet. Quantitative Affinitäts-Bestimmungen offenbarten eine hohe Kreuzreaktivität der Wirkstoffe für pEAβ und folglich war D3D3 in der Lage, pEAβ-induzierte Zytotoxizität aufzuheben.

Basierend auf der vorliegenden Arbeit konnten wir das Wissen über den molekularen Interaktions-Mechanismus zwischen Aβ und D3 und seinen Derivaten erweitern. Es wurden Optimierungsstrategien des Leitwirkstoffes etabliert und in vitro sowie in vivo validiert. Von der wissenschaftlichen Sichtweise aus wurden vielversprechende Kandidaten entwickelt, für welche weitere präklinische Untersuchungen lohnenswert sind.

1 Introduction

1.1 Alzheimer's disease

Alzheimer's disease (AD) was first described in 1907 by the German psychiatrist and neuropathologist Alois Alzheimer as a peculiar disease of the cerebral cortex (Alzheimer 1907). Since 1968, AD is accepted to be the most common cause for senile dementia (Blessed et al. 1968). Nowadays, 47 million people suffer from dementia worldwide and this number is projected to increase to more than 131 million by 2050 (Prince et al. 2016). AD is accounted to 60-70 % of all dementia cases (Alzheimer's Association 2017).

The clinical manifestation of AD typically begins with subtle failure of memory and slowly becomes more severe and incapacitating. Other symptoms include confusion, poor judgment, language disturbance, agitation, withdrawal and hallucinations. Death is more caused by comorbidities, e.g. general inanition, malnutrition or pneumonia, than by AD itself. The typical clinical duration of the disease is eight to ten years and AD prevalence increases significantly with age (Bird 1993).

AD is a heterogeneous disorder with both familial and sporadic forms. Familial AD (fAD) covers less than 1 % of all AD cases and develops as a result of dominantly inherited mutations (Bekris et al. 2010). Three specific genes are known to be involved. The first mutation causing fAD was identified in the amyloid precursor protein (APP) (Goate et al. 1991). However, this mutation explains only a few familial cases. Instead, mutations in the presenilin genes PSEN1 and PSEN2 account for most cases of fAD (Levy-Lahad et al. 1995, Sherrington et al. 1995, Blennow et al. 2006). Individuals inheriting at least one of these mutations on APP, PSEN1 or PSEN2 have a risk of > 95 % to develop AD. fAD is typically linked to early-onset AD which starts before age 65 (Alzheimer's Association 2017).

The sporadic form of AD (sAD) is highly prevalent and covers the majority of all AD cases (Blennow et al. 2006). Risk factors are mostly non-genetic but environmental such as low educational level, head injury or cardiovascular diseases (Mayeux 2003). A major genetic risk factor for sAD is the apolipoprotein E ε4 allele which was found to increase the risk of AD by three times in heterozygotes and by 15 times in homozygote carriers (Farrer et al. 1997). However, ageing is the most important risk factor for the disease (Blennow et al. 2006).

The major pathologies of AD are the progressive accumulation of senile plaques in the extracellular space consisting of fibrillar amyloid-beta (Aβ) and neurofibrillary tangles inside neurons formed by aggregated hyperphosphorylated tau protein in the brain (Figure 1) accompanied by a degeneration of the neurons and synapses (Blennow et al. 2006).

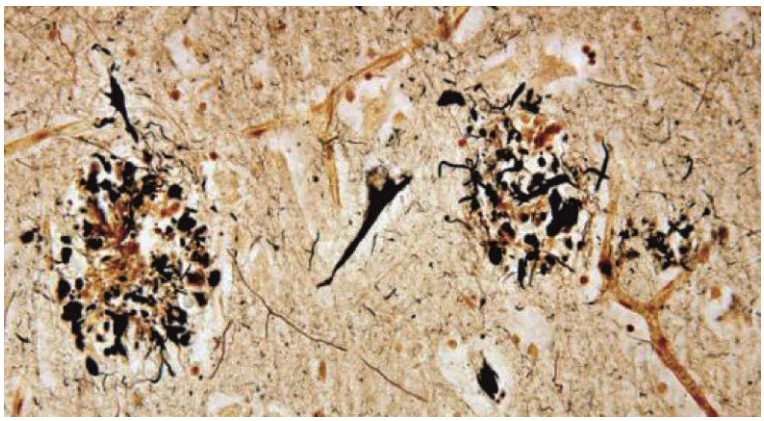

Figure 1 Photomicrograph of two senile plaques and a neurofibrillary tangle in between. Modified Bielschowsky stain of the temporal cortex of an AD patient, adapted from Perl (2010).

1.1.1 Amyloid-beta

Although the underlying disease mechanism is still not clear, the primary role of Aβ in the development of AD has been widely accepted (LaFerla et al. 2007). Aβ is an approx. 4 kDa peptide which was identified by isolation from amyloid deposits in the brain of AD and Down´s syndrome patients and subsequently characterized (Glenner and Wong 1984, Masters et al. 1985).

Aβ is generated by cleavage and processing of the amyloid precursor protein (APP) (Figure 2).

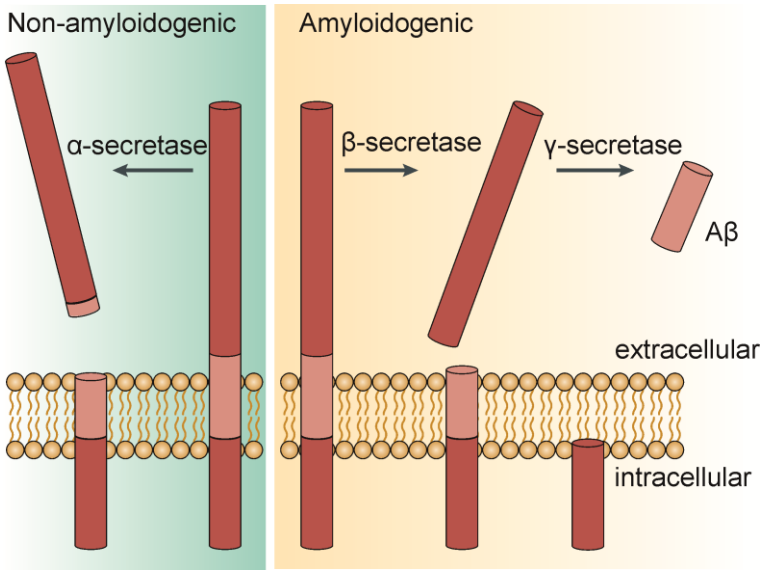

Figure 2 Non-amyloidogenic and amyloidogenic pathway of APP processing adapted from LaFerla et al. (2007).

Under physiological conditions, APP is extracellularly cleaved by the α-secretases within the Aβ region resulting in the prevalent non-amyloidogenic pathway. In AD, APP is cleaved by β- and γ-secretases leading to the release of amyloidogenic Aβ (LaFerla et al. 2007). Due to imprecise cleavage by γ-secretase, C-terminal heterogeneity of Aβ occurs. Hence, various different Aβ isoforms exist but Aβ(1-40) is the most abundant (80-90 %), followed by Aβ(1-42) (5-10 %) (Murphy and LeVine 2010). The slightly longer forms of Aβ, particularly Aβ(1-42), are more hydrophobic and prone to aggregate and are the principal species deposited in senile plaques (Selkoe 2001). Additional posttranslational modifications further increase the diversity of Aβ species. N-terminally truncated pyroglutamate Aβ (pEAβ(3-42)) gets more and more in focus since it was found together with Aβ(1-42) in up to equivalent amounts in senile plaques (Wirths et al. 2009, Gunn et al. 2010). In vitro, pEAβ(3-42) was characterized by increased aggregation propensity and the resulting assemblies have a stronger cross-seeding potential for other Aβ isoforms (Schilling et al. 2006, D'Arrigo et al. 2009).

The amyloid cascade hypothesis offers broad theory to explain both fAD and sAD pathogenesis and has become the most-researched fundamental framework of AD (Figure 3).

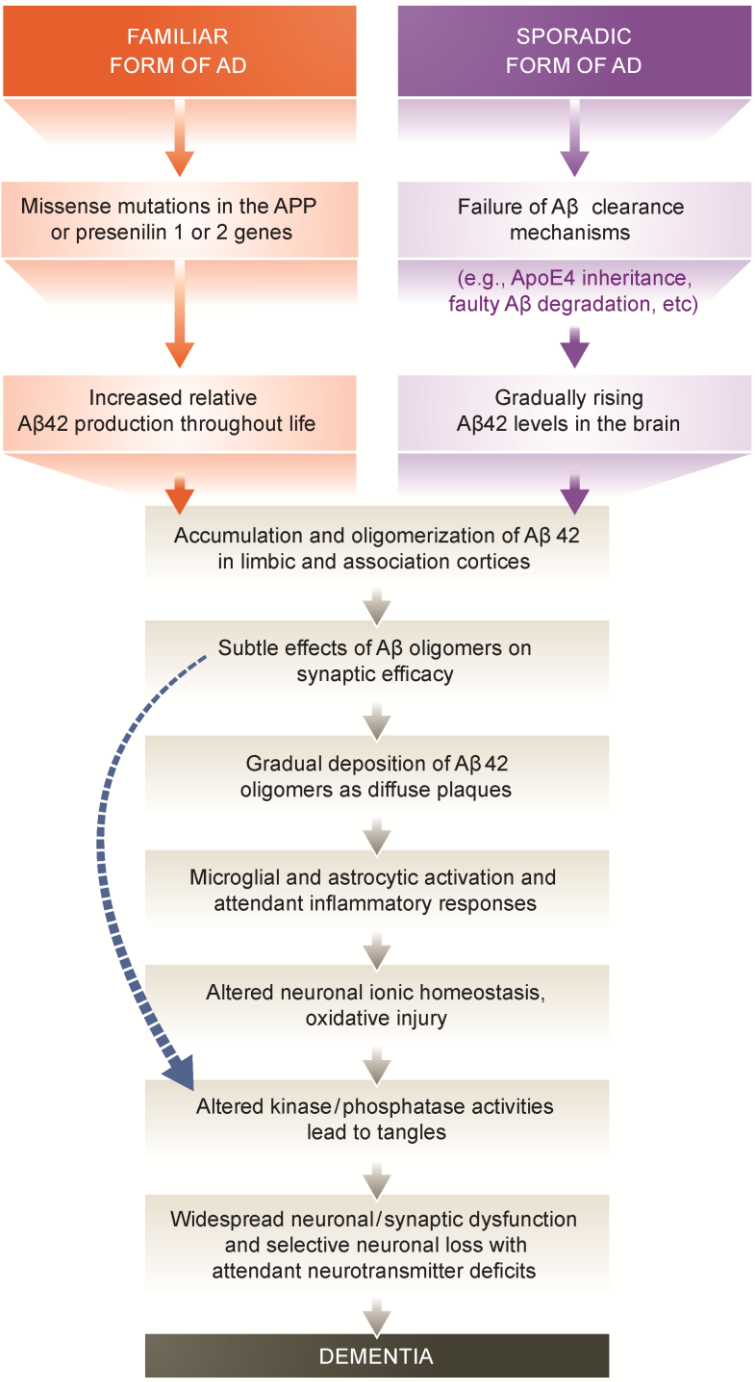

Figure 3 Amyloid cascade hypothesis consisting of major pathogenic events leading to AD. The blue arrow indicates that Aβ oligomers may directly injure the synapses and neurites of brain neurons, adapted from Selkoe and Hardy (2016).

Developed in the 1990s, it states that the imbalance between production and clearance of Aβ in the brain is the main event ultimately leading to neuronal degeneration (Beyreuther and Masters 1991, Hardy and Allsop 1991, Selkoe 1991). Thereby, monomers aggregate into soluble oligomers and finally into amyloid fibrils which are found in AD plaques. Despite those are a major hallmark of AD, the number of amyloid plaques in the brain

does not correlate well with the degree of cognitive impairment and it is controversially discussed which Aβ species the toxic ones are leading to AD pathogenesis. At the moment, small soluble oligomers are thought to be the most neurotoxic species (Hardy and Selkoe 2002, Walsh and Selkoe 2007, Karran and De Strooper 2016). In 2013, a revised and updated model of the aggregation cascade of Aβ was published by Cohen et al. which reveals a novel source of neurotoxic oligomers (Figure 4).

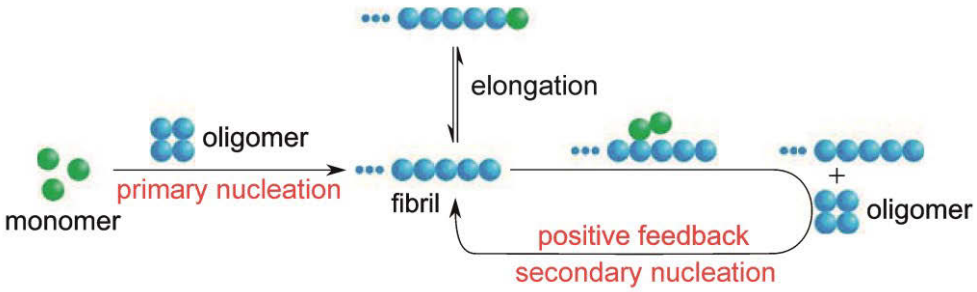

Figure 4 Schematic model of the self-assembly process of Aβ(1-42) adapted from Cohen et al. (2013).

Here, the well-known homogeneous aggregation of monomer units into oligomers and fibrils is called primary nucleation and the model is expanded by the rate-limiting secondary nucleation process. This is a positive feedback loop where the surface of formed fibrils shows autocatalytic functions and serves as a template for further generation of oligomers. As compared to the primary nucleation, the secondary nucleation is a very rapid and efficient process and small critical concentrations of formed fibrils are sufficient to induce this pathway (Cohen et al. 2013). Thus, secondary nucleation is thought to be the major oligomer source and a promising target to intervene selectively in toxic oligomer formation on a critical microscopic level (Cohen et al. 2015).

1.1.2 Diagnosis

Nowadays, clinical diagnosis of AD is most commonly based on a complex testing procedure by physicians obtaining family history and history of cognitive and behavioral changes with input from family members. Consulting cognitive tests accompanied with physical and neurologic examinations help to assess cognitive impairment of the patient (Blennow et al. 2006, Alzheimer's Association 2017). Thereby, the mini-mental state examination (MMSE) which is a 30-point questionnaire plays an important role but allows diagnosis of dementia only (Folstein et al. 1975). Additionally, biomarkers and imaging techniques such as computed tomography (CT) or magnetic resonance imaging (MRI) are consulted. Those enable to visualize the morphology of the brain with regards to a

possible atrophy but seem to be too expensive to conduct as a standard procedure (Dubois et al. 2014, Knight et al. 2016).

At the moment, the most studied and best validated biomarkers are Aβ(1-42), total and phosphorylated tau in CSF and amyloid imaging by positron emission tomography (PET) (Blennow et al. 2006, Vlassenko et al. 2012). For this, the ^{11}C-labeled PET tracer Pittsburgh compound B (PiB) is widely used. PiB is a derivative of Thioflavin T and binds specifically to Aβ plaque depositions in the brain of AD patients (Klunk et al. 2004). Another common PET tracer is the glucose analog ^{18}F-labeled fluorodeoxyglucose (FDG) which monitors glucose metabolism in the brain (Newberg et al. 2002). Since cerebral metabolic rates of glucose were found to correlate with AD progression and histopathological diagnosis, FDG was approved for the diagnosis of AD (Mosconi et al. 2010). A hypothetical model for the course of AD biomarker level over disease progression can be obtained from Figure 5.

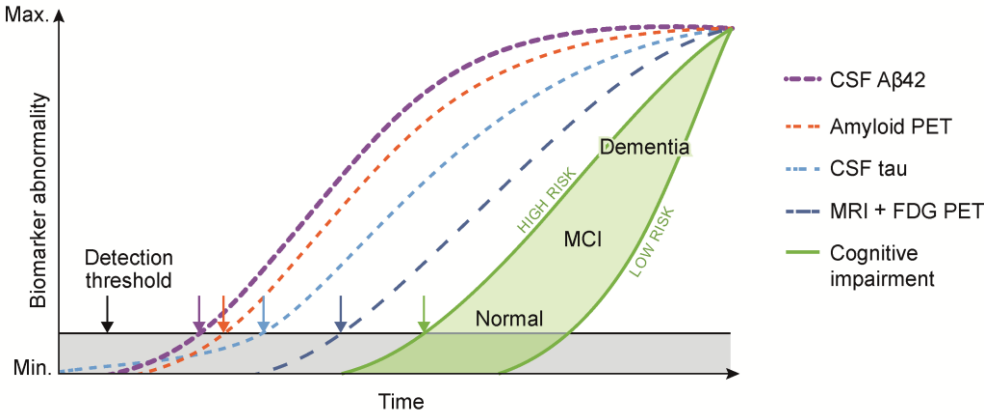

Figure 5 A hypothetical temporal model for the course of AD biomarkers over disease progression adapted from Selkoe and Hardy (2016).

The diagnosis of AD based on a combination of clinical and pathological examinations is accurate in 71-87 % of cases and reads “possible AD” or “probable AD” only (Jack et al. 2011, Beach et al. 2012). Up until now, definite diagnosis of AD can only be made post mortem by demonstrating the senile plaques and neurofibrillary tangles in the brain after an autopsy (Ballard et al. 2011). A huge demand on reliable biomarkers exist which cover the full range of disease stages from the asymptomatic through the most severe stages of AD to ensure accurate diagnosis followed by early therapeutic intervention (Dubois et al. 2007, Jack et al. 2011).

Also increasing numbers of clinical studies for AD therapy need to be accompanied with sensitive and valid detection of AD biomarkers. Only thus, clinical study individuals can involve patients with the brain changes that treatments target (McKhann et al. 2012). Furthermore, the outcomes of clinical trials can be certainly analyzed and compared with each other (Golde et al. 2011). Therefore, much effort is made for the identification and validation of specific biomarkers in cerebrospinal fluid (CSF) or plasma of AD patients (Blennow et al. 2010). Additionally, highly sensitive and selective detection methods are required to quantify very low amounts of potential biomarkers in biological samples.

1.1.3 Therapy

Despite intensive research, no curative or preventive care exists for AD patients and the current therapies are palliative only. That means slowing down the progression of the symptoms without changing the underlying disease mechanism (Alzheimer's Association 2017).

Nowadays, pharmacologic treatment temporarily improves symptoms by increasing the amounts of neurotransmitters in the brain (Francis 2005). Thereby, cholinergic and glutamatergic pathways are affected. For treatment of mild to moderate AD, the acetylcholinesterase inhibitors donepezil, rivastigmine and galantamine are approved by the U.S. Food and Drug Administration (FDA) and currently used. Memantine is an N-methyl-D-aspartate (NMDA) receptor antagonist and used to treat moderate to severe AD, also in combination with donepezil (Noetzli and Eap 2013, Alzheimer's Association 2017). Non-pharmacologic therapies, e.g. memory training or music therapy, are often used to reduce behavioral symptoms and maintain cognitive functions and the overall quality of life. Both pharmacologic and non-pharmacologic therapies have not been shown to alter the course of AD (Alzheimer's Association 2017). Therefore, much effort is made to look beyond treating symptoms and develop preventive or even curative care for AD. Most of the strategies are based on intervention in the Aβ aggregation cascade or Aβ generation, clearance or redistribution from the brain to systemic circulation. Therefore, common targets are β- and γ-secretases or Aβ itself with inhibitors, antibodies or aggregation modulators. Additionally, anti-tau therapeutics are under development which reduce tau phosphorylation by inhibiting tau kinases, (Hardy and Selkoe 2002, Blennow et al. 2006, Selkoe and Hardy 2016).

1.2 Peptides as potential drugs

In recent years, peptides received a revival of interest, especially as potential therapeutics (Marx 2005). Those peptides can be derived from three different sources: isolated from a genetic or recombinant library, selected from a synthetic library or derived from nature such as bioactive peptides or protein fragments (Vlieghe et al. 2010). Due to the high diversity of natural occurring amino acids, peptides are characterized by very high affinity and specificity to their targets which leads to high biological activity and low toxicity in vivo (Sun et al. 2012, Khazanov and Carlson 2013, Otvos and Wade 2014). If the size is between 5 and 50 amino acid residues, the peptide might be suitable for synthetic production. This has the advantage of less limited access as compared to recombinant biologics and the diversity increases due to unnatural amino acids and pseudo-peptide bonds (Vlieghe et al. 2010).

However, peptides show a variety of favorable characteristics, also some limitations for the use as therapeutics are known. The most challenging problem is the proteolytic instability in plasma which can lead to the clearance of peptides within a few minutes after application (Vlieghe et al. 2010). As a consequence of pre-systemic degradation, peptides suffer from low oral bioavailability (Hamman et al. 2005). Furthermore, peptides often have hydrophilic features. Therefore, they might not cross membranes and the blood brain barrier. Thus, they often cannot reach targets in the in the cytoplasm or in the central nervous system (Witt et al. 2001, Joo 2012).

1.2.1 D-peptides

Although the majority of proteins derived from nature consists of L-amino acid residues only also naturally occurring D-amino acid residues were described (Neuberger 1948). The main sources are bacteria where D-enantiomers were found in the peptidoglycan (Stevens et al. 1951, Radkov and Moe 2014). Furthermore, D-serine is known to be an important neurotransmitter in the mammalian brain (Wolosker et al. 2008). The above described unfavorable characteristics of peptides as therapeutics belong to peptides consisting of L-enantiomeric amino acid residues only. In order to overcome some of these disadvantages, the stereoisomers in D-enantiomeric configurations are a suitable alternative. D-peptides are characterized by increased stability against proteolysis in vivo as compared to their L-enantiomeric equivalent due to high stereoisomeric selectivity of most proteases (van Regenmortel and Muller 1998, Hamamoto et al. 2002). This results in reduced immunogenicity and increased bioavailability of D-peptides (Dintzis et al. 1993,

Werle and Bernkop-Schnurch 2006). Therefore, the suitability of peptides as a class of therapeutics is highly increased by replacing L-amino acid residues with less naturally abundant D-amino acid residues.

1.2.2 Further optimization strategies

In addition to the improvement of clinical parameters, further strategies exist to optimize the potency of therapeutic peptides. Various techniques aim for higher affinity and thus specificity with the therapeutic target molecule. One promising rational strategy is the cyclization of peptides between termini and side chains (Hummel et al. 2006). In comparison to linear peptides, the decrease in conformational flexibility reduces the entropic contribution to Gibbs free binding energy leading to enhanced binding affinities to the target (Joo 2012). The rigidity of cyclic compounds further increases membrane permeability and cyclization involving the free termini reduces the risk of proteolysis. Blocking the N-terminus by acylation and the C-terminus by amidation or pegylation also contributes to increased bioavailability (Edman 1959, Horton et al. 2000, Vlieghe et al. 2010). Another optimization strategy is the design of multivalent peptides, e.g. bivalent tandem peptides. Thereby, homodimers are supposed to show increased affinity due to avidity effects similar to antibodies whereas heterodimers are able to bind two different targets resulting in improved potency and selectivity (Duggineni et al. 2013, Liu et al. 2017).

A systematic screening approach to improve therapeutic efficacy of peptides based on increased binding affinity to the target can be rapidly realized by a high-throughput screening, i.e. a peptide microarray approach (Lin et al. 2009). By N- or C-terminal truncations or consecutive deletions, the minimum active sequence can be ascertained. Additionally, peptide microarrays are a convenient tool to conduct an alanine scan in order to identify important amino acid residues for the interaction with the target molecule or even create a complete amino acid substitution profile (Vlieghe et al. 2010).

1.2.3 D-peptides for therapy of AD

Within the last years, several therapeutic strategies have been reported involving D-peptides for the treatment of AD. Thereby, Aβ monomers are a highly validated target for early intervention resulting in the inhibition of the Aβ aggregation process (Kumar and Sim 2014).

A variety of Aβ-targeting approaches include D-peptides which were designed based on the key amyloidogenic motif KLVFF of Aβ (residues 16 to 20) in order to interfere with potential aggregation sites (Lowe et al. 2001). These peptides are discussed to underlie a β-sheet breaking mechanism which turned out to be highly efficient for the inhibition of Aβ aggregation and subsequent reduction of Aβ-mediated cytotoxicity (Soto et al. 1996, Tjernberg et al. 1997, Findeis et al. 1999, Chalifour et al. 2003). Arai and coworkers were able to further increase the potency of Aβ-targeting D-peptides by cyclization (Arai et al. 2014). Interestingly, most of these studies revealed that the D-peptides show increased potency in the investigated properties as compared to the L-enantiomeric equivalents. Therefore, a heterochiral stereoselectivity of naturally occurring L-Aβ for inhibitory D-peptides might exist and should be considered for the development of AD therapy (Chalifour et al. 2003).

1.2.4 D3 as a lead compound

To develop a curative therapy for AD, we hypothesize that the stabilization of monomers in order to prevent further aggregation and simultaneous elimination of pre-formed cytotoxic Aβ oligomers by D-peptides might be a promising strategy. To address this, mirror image phage display was performed using soluble low-molecular weight Aβ(1-42) species as target yielding the lead compound D3 (Schumacher et al. 1996, Esteras-Chopo et al. 2008, van Groen et al. 2008). D3 is a polycationic peptide with the sequence rprtrlhthrnr in D-enantiomeric configuration. In vitro, it was shown that D3 indeed binds to monomeric Aβ(1-42) with micromolar affinity driven by electrostatic interactions, as suggested by in silico studies (Olubiyi and Strodel 2012, Olubiyi et al. 2014). It inhibits the aggregation into cytotoxic species in a concentration-dependent manner (van Groen et al. 2008). Additionally, pre-formed oligomers are eliminated by D3 and recovered in high molecular-weight co-precipitates which are non-fibrillar and non-toxic. Thus, oligomer-induced cytotoxicity is abolished (van Groen et al. 2008, Funke et al. 2010, Brener et al. 2015). Based on a cell culture model, it was shown that D3 is efficiently transported across the blood brain barrier by transcytosis (Liu et al. 2010).

In double transgenic APP/PS1 mice, treatment with D3 reduces Aβ plaque deposition and inflammation and improves cognition, also in aged mice with full-blown AD pathology without adverse side effects (van Groen et al. 2008, van Groen et al. 2012, van Groen et al. 2013). Even after oral administration of D3, improvement in cognitive paradigms was reported (Funke et al. 2010).

2 Objective

Despite intensive efforts, a causative therapy for AD is not yet available. In order to address this in our institute, the D-peptide D3 was previously selected by mirror image phage display using Aβ(1-42) as target. D3 as the lead compound was characterized in detail regarding the efficacy in vitro and in vivo and optimized during the drug development process. Thereby, rational design and systematic approaches were applied resulting in a variety of D3 derivatives.

The aim of this work was the detailed biophysical characterization of the interaction between Aβ(1-42) and optimized D3 derivatives in order to gain a deeper understanding of the molecular mechanism of interaction in comparison to the original compound D3. This was realized by biophysical methods such as surface plasmon resonance (SPR) and biolayer interferometry (BLI). Details on the interaction, e.g. affinity, kinetics, stoichiometry, epitopes and thermodynamics, as well as potency characteristics such as Aβ oligomer elimination and toxicity neutralization efficacy were investigated. These data were used to analyze the influence of positive net charge, rigidity, valence and hydrophobicity and allowed to conclude successful lead optimization strategies for D3.

Additionally to Aβ(1-42), the N-terminally truncated pyroglutamate-modified isoform pEAβ(3-42) got more and more in focus because it was found to play a critical role in the development of AD. Due to promising perspectives of D3 and derivatives to modulate Aβ(1-42)-mediated progression of AD, the potency of D3 and its tandem variant D3D3 to interfere with pEAβ-induced AD should be investigated. Therefore, cross-reactivity of D3 and D3D3 for pEAβ(3-42) was analyzed by affinity determination followed by further in vitro and in vivo investigations.

3 Publications

Preclinical Pharmacokinetic Studies of the Tritium Labelled D-Enantiomeric Peptide D3 Developed for the Treatment of Alzheimer´s Disease

Jiang N, Leithold LH, Post J, Ziehm T, Mauler J, Gremer L, Cremer M, Schartmann E, Shah NJ, Kutzsche J, Langen KJ, Breitkreutz J, Willbold D, Willuweit A

Journal: PLOS ONE
Impact Factor: 2.81 (2016)

Contributions: 10 % (analysis of plasma protein binding, contributed to manuscript writing)

Increase of Positive Net Charge and Conformational Rigidity Enhances the Efficacy of D-Enantiomeric Peptides Designed to Eliminate Cytotoxic Aβ Species

Ziehm T, Brener O, van Groen T, Kadish I, Frenzel D, Tusche M, Kutzsche J, Reiß K, Gremer L, Nagel-Steger L, Willbold D

Journal: ACS Chemical Neuroscience
Impact Factor: 3.88 (2016)

Contributions: 65 % (performance and analysis of SPR studies, TEM images and cell viability assays, statistical analysis, main part of manuscript writing)

Optimization of the All-D Peptide D3 for Aβ Oligomer Elimination

Klein AN, Ziehm T, Tusche M, Buitenhuis J, Bartnik D, Boeddrich A, Wiglenda T, Wanker E, Funke SA, Brener O, Gremer L, Kutzsche J, Willbold D

Journal: PLOS ONE
Impact Factor: 2.81 (2016)

Contributions: 15 % (performance and analysis of BLI studies, contributed to manuscript writing)

Optimization of D-peptides for Aβ monomer binding specificity enhances their potential to eliminate toxic Aβ oligomers

Klein AN, Ziehm T, van Groen T, Kadish I, Elfgen A, Tusche M, Thomaier M, Reiss K, Brener O, Gremer L, Kutzsche J, Willbold D

Journal: ACS Chemical Neuroscience
Impact Factor: 3.88 (2016)

Contributions: 20 % (performance and analysis of BLI studies, contributed to data analysis (QIAD, MTT, statistical analysis) and manuscript writing)

The role of hydrophobicity and charge of amyloid-beta oligomer eliminating D-peptides in the interaction with amyloid-beta monomers

Ziehm T, Buell AK, Willbold D

Journal: Chemical Science (submitted)
Impact Factor: 8.67 (2016)

Contributions: 85 % (study design, performance and analysis of all experiments, main part of manuscript writing)

Aβ oligomer eliminating compounds interfere successfully with pEAβ(3-42) induced motor neurodegenerative phenotype in transgenic mice

Dunkelmann T, Teichmann K, Ziehm T, Schemmert S, Frenzel D, Tusche M, Dammers C, Jürgens D, Langen KJ, Demuth HU, Shah NJ, Kutzsche J, Willuweit A, Willbold D

Journal: Neuropeptides
Impact Factor: 2.49 (2016)

Contributions: 10 % (performance and analysis of SPR studies, contributed to manuscript writing)

3.1 Preclinical Pharmacokinetic Studies of the Tritium Labelled D-Enantiomeric Peptide D3 Developed for the Treatment of Alzheimer´s Disease

Nan Jiang, Leonie H Leithold, Julia Post, Tamar Ziehm, Jörg Mauler, Lothar Gremer, Markus Cremer, Elena Schartmann, Nadim J Shah, Janine Kutzsche, Karl-Josef Langen, Jörg Breitkreutz, Dieter Willbold, Antje Willuweit

PLoS One. 2015 Jun 5;10(6):e0128553

doi: 10.1371/journal.pone.0128553

PLOS | ONE

RESEARCH ARTICLE

Preclinical Pharmacokinetic Studies of the Tritium Labelled D-Enantiomeric Peptide D3 Developed for the Treatment of Alzheimer´s Disease

Nan Jiang[1], Leonie H. E. Leithold[1], Julia Post[1], Tamar Ziehm[1], Jörg Mauler[2], Lothar Gremer[1], Markus Cremer[3], Elena Schartmann[1], N. Jon Shah[2], Janine Kutzsche[1], Karl-Josef Langen[2,4], Jörg Breitkreutz[5], Dieter Willbold[1,6]*, Antje Willuweit[2]*

1 Structural Biochemistry, Institute of Complex Systems (ICS-6), Forschungszentrum Jülich GmbH, Jülich, Germany, **2** Medical Imaging Physics, Institute of Neuroscience and Medicine (INM-4), Forschungszentrum Jülich GmbH, Jülich, Germany, **3** Structural and functional organisation of the brain, Institute of Neuroscience and Medicine (INM-1), Forschungszentrum Jülich GmbH, Jülich, Germany, **4** Department of Nuclear Medicine, Universitätsklinikum der RWTH Aachen, Aachen, Germany, **5** Institute of Pharmaceutics and Biopharmaceutics, Heinrich-Heine-Universität Düsseldorf, Düsseldorf, Germany, **6** Institut für Physikalische Biologie, Heinrich-Heine-Universität Düsseldorf, Düsseldorf, Germany

* D.Willbold@fz-juelich.de (DW); A.Willuweit@fz-juelich.de (AW)

OPEN ACCESS

Citation: Jiang N, Leithold LHE, Post J, Ziehm T, Mauler J, Gremer L, et al. (2015) Preclinical Pharmacokinetic Studies of the Tritium Labelled D-Enantiomeric Peptide D3 Developed for the Treatment of Alzheimer´s Disease. PLoS ONE 10(6): e0128553. doi:10.1371/journal.pone.0128553

Academic Editor: Riqiang Yan, Cleveland Clinic Foundation, UNITED STATES

Received: March 4, 2015

Accepted: April 28, 2015

Published: June 5, 2015

Data Availability Statement: All relevant data are within the paper and its Supporting Information files.

Funding: DW was supported by grants from the "Portfolio Technology and Medicine" and the Helmholtz-Validierungsfonds of the Impuls und Vernetzungs-Fonds der Helmholtzgemeinschaft; KJL and DW were supported by the "Portfolio Drug Design" of the Impuls und Vernetzungs-Fonds der Helmholtzgemeinschaft (http://www.helmholtz.de/ueber_uns/impuls_und_vernetzungsfonds; no grant numbers available). The funders had no role in study

Abstract

Targeting toxic amyloid beta (Aβ) oligomers is currently a very attractive drug development strategy for treatment of Alzheimer´s disease. Using mirror-image phage display against Aβ1-42, we have previously identified the fully D-enantiomeric peptide D3, which is able to eliminate Aβ oligomers and has proven therapeutic potential in transgenic Alzheimer´s disease animal models. However, there is little information on the pharmacokinetic behaviour of D-enantiomeric peptides in general. Therefore, we conducted experiments with the tritium labelled D-peptide D3 (^{3}H-D3) in mice with different administration routes to study its distribution in liver, kidney, brain, plasma and gastrointestinal tract, as well as its bioavailability by i.p. and p.o. administration. In addition, we investigated the metabolic stability in liver microsomes, mouse plasma, brain, liver and kidney homogenates, and estimated the plasma protein binding. Based on its high stability and long biological half-life, our pharmacokinetic results support the therapeutic potential of D-peptides in general, with D3 being a new promising drug candidate for Alzheimer´s disease treatment.

Introduction

After the initial description by Alois Alzheimer in 1906 [1], Alzheimer's disease (AD), a progressive neurodegenerative disorder, has become nowadays the most common form (60–80%) of dementia [2]. According to the World Alzheimer Report 2014, nearly 36 million people worldwide are suffering from AD or related dementia. Even after years of intensive

design, data collection and analysis, decision to publish, or preparation of the manuscript.

Competing Interests: The authors have declared that no competing interests exist.

investigation and research, it is still an incurable disease [3]. Current treatments are only supportive against some of its symptoms. Clinical duration of AD varies from one to 25 years, typically eight to ten years [4].

Amyloid beta (Aβ) is produced by sequential cleavage of a type I integral transmembrane protein, called amyloid precursor protein (APP) by β- and γ-secretases. Variable lengths of Aβ isomers differing at the C-terminus are produced due to imprecise cleavage by γ-secretase [5, 6]. The most abundant isomers are Aβ1–40 (approximately 80–90%) and Aβ1–42 (approximately 5–10%). Aβ1–42 is more hydrophobic and fibrillogenic, and therefore the main component of Aβ plaques in the brain of AD patients [7]. It also aggregates readily into oligomers, which are considered to be the most toxic form of Aβ [8–10].

In recent years, many substances have been developed targeting Aβ production and clearance [11], including peptide-based drugs [12, 13]. In spite of the many advantages of peptide drugs, for example high specificity and low toxicity, their short half-life time *in vivo* due to rapid degradation by proteases, and low bioavailability by oral administration, restrict their clinical usage. In comparison to naturally occurring L-form peptides, peptides derived from partial D-amino acid substitutions or D-enantiomeric peptides, which are composed entirely of D-amino acids, have advantages over L-enantiomers. Because of the stereoisomeric selectivity of proteolytic enzymes they are less prone to proteolysis, therefore longer half-lives and higher bioavailability after oral administration are to be expected [14–16]. Furthermore, they are less or even not immunogenic at all [13].

The fully D-enantiomeric peptide D3, which was identified by mirror-image phage display [17, 18] for binding to Aβ (1–42), has been shown to have interesting properties. D3 inhibits Aβ fibril formation and eliminates Aβ-oligomers *in vitro*. *Ex vivo*, D3 has been shown to specifically bind to amyloid plaques in transgenic mice [19]. *In vivo*, D3 was able to reduce plaque load and inflammation markers in the brains of treated transgenic mice, as well as improve their cognition even after oral administration [20–23]. Here we investigate the pharmacokinetic properties of D3 in mice.

We present the first comprehensive preclinical pharmacokinetic study of a peptide consisting solely of D-enantiomeric amino acid residues in general and in particular for such a D-peptide developed for the treatment of Alzheimer's disease.

Materials and Methods

Materials

^{3}H-D3 (rprtr-(4,5-^{3}H-Leu)-hthrnr) and its L-form enantiomer ^{3}H-(L)-D3 (RPRTR-(4,5-^{3}H-Leu)-HTHRNR) were purchased from Quotient Bioresearch (Radiochemicals) Ltd. (Cardiff, United Kingdom) with 10–100 Ci/mmol, 1 mCi/ml and purity >95%.

All chemicals were supplied by Fluka Chemie AG (Buchs, Switzerland), Merck (Darmstadt, Germany), AppliChem (Darmstadt, Germany) and VWR (Darmstadt, Germany) in research grade. Micro-osmotic pumps (model 1007D) were purchased from Alzet DURECT Corporation, (Cupertino, CA, USA).

Animals

Male C57Bl/6 mice (Charles River, Sulzfeld Germany) with an average age of 13 weeks and body weight of 28.5 g were used in this study. For micro-osmotic pump i.p. implantation experiment, 19 months old mice were used with average body weight of 34 g. The mice were hosted in the animal facility of the Forschungszentrum Juelich under standard housing conditions with free access to food and water for at least 2 weeks before experiment. All animal experiments were approved by the Animal Protection Committee of the local government

(LANUV (Landesamt für Natur, Umwelt und Verbraucherschutz), North-Rhine-Westphalia, Germany, AZ84-02.04.2011. A359 and AZ84-02.04.2011. A356) according to the Deutsche Tierschutzgesetz). All sections of this study adhere to the ARRIVE Guidelines for reporting animal research [24]. A completed ARRIVE guidelines checklist was included in Supporting Information (S1 File).

Pharmacokinetic studies

Mice were administered with 100 μl radioactive working solution consisting of 5 μCi ^{3}H-D3 in 5 μl with 95 μl buffer (0.1 M phosphate buffer, pH 8) as a single bolus dose either i.v. (tail vein), i.p. or p.o. (gavaging). In order to achieve the desired total D3 concentration, non-radioactive D3 was added to a concentration of 1 mg/ml (i.v.) or 3 mg/ml (i.p. and p.o.). Doses were selected from previous tolerability studies and were not causing any adverse effects. I.v. injections and i.p micro-osmotic pump implantations were performed under anaesthesia with ketamine/medetomidine per i.p. administration. Antisedan was administered s.c. to reverse the anaesthesia directly after the intervention, which took about 10 min. Sampling times were chosen depending on the route of administration (i.p.: 10, 20, 30, 60, 120, 240, 360, 1440 and 2880 min.; p.o.: 10, 20, 30, 60, 120, 240, 360, 1080, 1440, 2880 and 4320 min.; i.v.: 3, 5, 10, 15, 30, 60, 240, 1440 and 2880 min.; 3 animals per time point). For i.p. micro-osmotic pump implantation, delivery dose of pumps was set to 5 μCi ^{3}H-D3 plus 0.3 mg non-radioactive D3 per 24 hours per mouse. Sampling times were 2, 4 and 6 days after implantation (3 mice per time point).

Upon sampling time, blood was drawn per heart puncture under isoflurane anaesthesia and heparinized plasma was isolated. A small piece of liver (approx. 0.2 g), the left kidney and the right brain hemisphere were sampled. To study the gastrointestinal absorption and elimination by p.o. administration, mice were fasted 18 hours before the experiment and their complete gastrointestinal tracts were prepared. Small intestine was dissected into 4 equal parts and marked from oral to aboral as 1 to 4, respectively. Organ samples were weighted and homogenized in homogenizer tubes (Precellys Ceramic Kit 1.4 mm, Precellys 24, Bertin technologies SAS, Montigny le Bretonneux, France) with 500 μl PBS. 10 ml scintillation cocktail (Ultima Gold XR, PerkinElmer, Waltham, Massachusetts, USA) was added to 100 μl of each organ homogenate or plasma (diluted 1:1 with PBS) and mixed well. Disintegrations per unit time (dpm) were obtained in triplicates with a liquid scintillation counter (Packard Tri-Carb 2100TR Liquid Scintillation Analyser, PerkinElmer, Waltham, MA, USA). Blank values of each sample were obtained by omitting radioactive substance following the same protocol.

Radioactivity counted in each sample was adjusted (subtraction of the blank value) and was expressed as percentage injected dose per gram tissue or millilitre plasma (%ID/g or %ID/ml), or as milligram of total D3 per gram tissue or millilitre plasma (mg/g or mg/ml).

Pharmacokinetic analysis

Pharmacokinetic parameters were calculated with non-compartmental analysis using Phoenix WinNonlin, version 6.3 (Pharsight Corp., St. Louis, USA). Mean D3 concentrations per time point were used to calculate the PK parameters (model type: plasma (200–202); calculation method: linear trapezoidal linear interpolation; dose options: "IV Bolus" for i.v. or "Extravascular" for i.p. and p.o. administration). The same model setting was used to estimate pharmacokinetic parameters of brain. For i.v. administration, plasma concentration at time zero (C0) was back extrapolated with a log-linear regression of the first two observed plasma concentrations, while brain C0 was set to be zero. For the i.p. and p.o. administrations, all concentrations at time zero were set to be zero.

The last three to five observed mean plasma concentrations were used to estimate the first order rate constant in the terminal elimination phase (Lambda_z) based on the largest adjusted square of the correlation coefficient (R^2) of the log-linear regression lines. The area under the curve (AUC) from C0 extrapolated to infinity ($AUC_{C0\text{-}inf}$) was calculated as the sum of $AUC_{C0\text{-}last}$+(Clast/Lambda_z), calculated from the last determined concentration derived by Lambda_z, and $AUC_{C0\text{-}last}$ representing the AUC from time point zero to the last observed concentration (Clast). Parameters that do not require Lambda_z were calculated for brain data: time of maximal observed concentration (Tmax), maximal observed concentration (Cmax), maximal observed concentration normalized to dose (Cmax/D), $AUC_{C0\text{-}last}$ and mean residence time from the time of dosing to the last time point ($MRT_{C0\text{-}last}$). Additional parameters requiring estimated Lambda_z were calculated for plasma data: Lambda_z, terminal half-life (HL_Lambda_z), $AUC_{C0\text{-}inf}$, terminal volume of distribution (Vz), plasma clearance (Cl), $MRT_{C0\text{-}inf}$ and volume of distribution at steady state (Vss). Absolute bioavailability of i.p. and p.o. administration was calculated with $AUC_{C0\text{-}inf}$ by: F(bioavailability) = [AUC(non-iv)*Dose (iv)]/[AUC(iv)*Dose(non-iv)]*100.

To minimize the time dependence of brain-plasma ratio by bolus dosing, brain-plasma ratio was calculated from the areas under the brain and plasma concentration curves in the terminal elimination phase starting from 4 hours to infinity (brain_$AUC_{4h\text{-}inf}$/plasma_$AUC_{4h\text{-}inf}$).

Plasma protein binding

Plasma protein binding was estimated by incubation of D3 with varying concentrations of protein using TRANSIL^{XL} binding kits (Sovicell GmbH, Leipzig, Germany). K_D values were determined by titrating a constant drug concentration against different concentrations of human serum albumin (HSA) and α_1-acid glycoprotein (AGP). Experiments were performed as recommended for the kit. To obtain the desired D3 stock solution of 80 μM, non-radioactively labelled D3 was dissolved in PBS and 5% ^{3}H-labelled D3 solution was added for detection purposes. A final concentration of 5 μM D3 was applied in the assay. After incubation and centrifugation 15 μl supernatant were taken and scintillation cocktail was added. This was done in triplicate. Radioactivity was then quantified using liquid scintillation counting. After measuring the disintegrations per minute (dpm) of the supernatant containing the unbound peptide, the D3 fraction bound to the titrated protein was calculated and plotted against the protein concentrations. The curves were fitted to the Michaelis Menten ligand binding equation (SigmaPlot 11.0, Systat Software, Inc., San Jose, California, USA) to obtain the K_D. Mean and relative standard error (%) of multiple measurements are given (AGP n = 3, HSA n = 2).

For bioavailability determination, the unbound fraction of D3 (f_u) was calculated using the equation below:

$$f_u = 100 * \frac{\frac{C_{D3}-K_D-C_{physiol}}{2} + \sqrt{K_D * C_{D3} + \left(\frac{C_{D3}-K_D-C_{physiol}}{2}\right)^2}}{C_{D3}} \quad (1)$$

For very low D3 concentrations in blood (C_{D3}), Eq (1) can be simplified by Eq (2), where the unbound fraction of D3 can be calculated independently of the applied D3 concentration. Since this is true for our *in vivo* experiments we used Eq (2) for the total free fraction of D3, combining the binding of D3 to HSA and AGP. For calculation of the overall unbound fraction according to Eq (2), physiological concentrations ($C_{physiol}$) of 0.65 mM HSA and 0.02 mM

AGP were assumed.

$$f_{u,total} = 100 * \frac{1}{1 + \frac{C_{physiolHSA}}{K_D HSA} + \frac{C_{physiolAGP}}{K_D AGP}} \quad (2)$$

Calibration curves and internal standard

Calibration curves were prepared by adding a corresponding ^{3}H-D3 dilution series with certain dpm range to plasma or organ homogenates in comparison to those diluted in PBS. The dpm ranges of each ^{3}H-D3 dilution series were set to cover the measured dpm ranges of each sample (for plasma 400–40000; for brain 100–1200; for liver 3000–15000; for kidney 40000–400000). Plasma and organ homogenates obtained from C57Bl/6 mice were prepared following the same procedure as outlined above.

No differences were found comparing the calibration curves of ^{3}H-D3 in organ homogenates or plasma to those in PBS. The measured dpm values of the internal standard with ^{3}H-D3 in PBS matched closely the expected ones.

Thin layer chromatography

In order to study the proteolytic stability of peptides in biological extracts, tritium labelled peptides were incubated with liver microsomes (pooled from mouse (CD-1), Sigma-Aldrich), freshly prepared mouse plasma or extracts of brain, liver and kidney at 37°C for different time periods (from 0 min to 2 days). 1 μCi (approx. 0.08–0.8 μg) radioactive labelled peptide was mixed with 1 μl microsomes stock solution, plasma or organ extracts, respectively (in great excess to peptide). Mixtures containing tritium-labelled peptides were applied onto HPTLC Silica Gel 60 plates (OMNILAB, Essen, Germany) for thin layer chromatography (TLC) with a mobile solvent (2-Butanol/Pyridine/Ammonia(28%)/Water(39/34/10/26)). After development, a phosphor imaging plate for ^{3}H-autoradiography (FUJIFILM, Tokyo, Japan) was exposed to the TLC plates for 3 days. Images were acquired with a BAS reader and AIDA software (Raytest, Freiburg, Germany). Retardation factor (Rf) of each substance was defined as the ratio of the migration distance of the centre of a separated spot to the migration distance of the solvent front.

Results

Proteolytic stability of D3 in comparison to its L-enantiomer

Before meaningful pharmacokinetic studies could be performed with ^{3}H-D3, it was essential to show that the D-peptide is stable under near *in vivo* conditions. First, we compared the stability of ^{3}H-D3 with its exact enantiomer, ^{3}H-(L)-D3 in plasma (Fig 1). ^{3}H-(L)-D3 shows significant degradation already after 60 min incubation in plasma as concluded by the appearance of additional bands as compared to the mixture at 0 min on the TLC plate after detection by autoradiography. In contrast, ^{3}H-D3 did not show any degradation products even after 2 d incubation in the same plasma preparation.

More importantly, ^{3}H-D3, was neither degraded after 2 h incubation in liver microsomes nor after 2 days incubation in homogenates of kidney, brain and liver as shown by TLC and detection by autoradiography (Fig 2). Microsomes were checked for proteolytic activity using L-peptide substrates.

Due to high but unspecific affinity of D3 and (L)-D3 to the TLC plate support material (glass), artefacts were observed at the starting points of the TLC as well as light smears

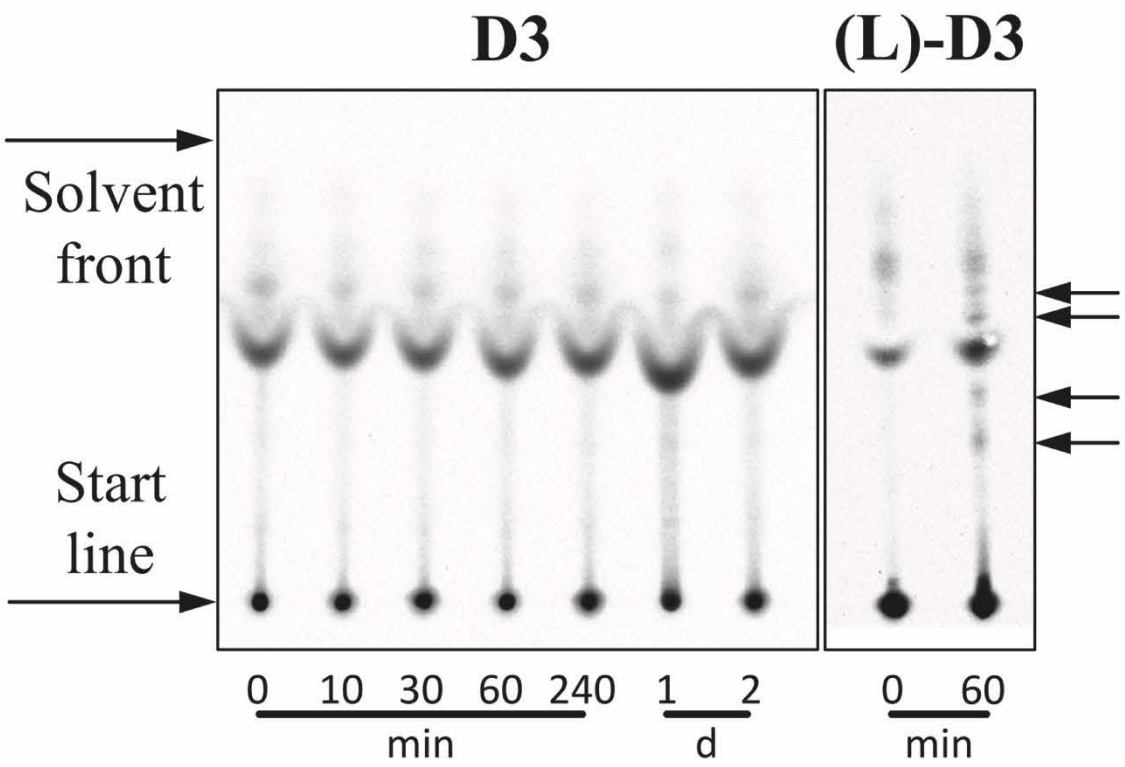

Fig 1. Autoradiogram demonstrating proteolytic stability of ^{3}H labelled peptides in plasma. ^{3}H-D3 was incubated with plasma for different times at 37°C and developed on TLC plates. For comparison, the exact enantiomer of D3, (L)-D3, was used in this stability assay. ^{3}H-(L)-D3 was incubated with plasma for 0 and 60 min at 37°C. Please note that free ^{3}H-(L)-D3 and free ^{3}H-D3 are perfect enantiomers to each other and because the TLC material is not chiral, both compounds show identical Rf values. Additional bands in the 0 min lanes of ^{3}H-(L)-D3 and ^{3}H-D3 that arise from binding and co-migration of ^{3}H-D3 and ^{3}H-(L)-D3 to plasma components do not necessarily have identical Rf values in the 0 min lanes of ^{3}H-(L)-D3 and ^{3}H-D3, because some of the plasma components are enantiomers themselves. Therefore, any effect of degradation will lead to extra additional bands as compared to the 0 min lane of the very same compound. Obvious proteolytic degradation can be observed for ^{3}H-(L)-D3 already after 60 min incubation with plasma leading to additionally appearing bands (black arrows) as compared to the 0 min lane ^{3}H-(L)-D3. Additionally appearing bands as compared to 0 min incubation are not observed for ^{3}H-D3 even after 2 days incubation.

doi:10.1371/journal.pone.0128553.g001

originating thereof. To prove that these compounds were not located in the layer of the TLC matrices, a control experiment was performed by placing a new TLC plate to a freshly developed plate to transfer only the ^{3}H-peptides within matrices, but not those on the glass surface support (Fig 3). Artefacts could thus be eliminated.

Pharmacokinetics

Time dependent distribution of D3 in organs and plasma after different administration routes was analysed using tritium labelled D3 (^{3}H-D3) as shown in Fig 4. The corresponding pharmacokinetic parameters calculated with non-compartmental analysis based on the absolute amount of administered D3 are shown in Tables 1 and 2.

After i.v. and i.p. administration, pharmacokinetic curves showed similar patterns with highest concentration of tritium per gram tissue found in kidney, followed by liver and plasma.

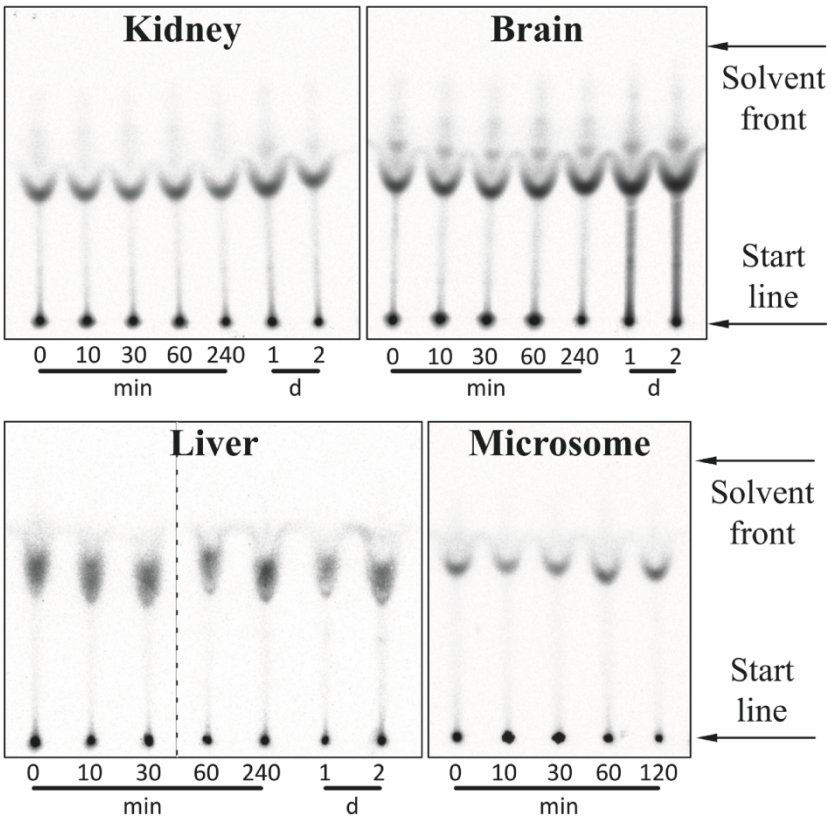

Fig 2. Autoradiogram demonstrating proteolytic stability of ^{3}H labelled peptides in liver microsomes and organ homogenates. ^{3}H-D3 was incubated with kidney, brain and liver homogenate for 0, 10, 30, 60, 240 min and 1, 2 days at 37°C and developed on TLC plates. For liver microsomes, the incubation time was 0, 10, 30, 60 and 120 min. Slight difference in Rf values of ^{3}H-D3 in liver homogenate might be due to incompletely homogenized liver tissues, which was not observed after incubation with liver microsomes. (Two autoradiograms of liver homogenate were presented in one image and separated through a dashed line.) No obvious proteolytic degradation of D3 can be observed in all the organ homogenates with up to two days' incubation.

doi:10.1371/journal.pone.0128553.g002

However, after oral administration ^{3}H-D3 concentrations measured in kidney and liver did not exceed concentrations in plasma (Fig 4). Plasma Cmax/D after i.v. administration reached 78 μg/ml/mg at Tmax 3 min (the first sampling time point), while after i.p. and p.o. administration plasma Cmax/D were 47 μg/ml/mg at 10 min and 1.5 μg/ml/mg at 240 min (Table 1). In brain, the Cmax/D and their corresponding Tmax values for i.v., i.p. and p.o. administration were 2.8, 2.2 and 1.3 μg/ml/mg at 3, 20 and 240 min, respectively (Table 2). However, after 4 hours concentrations in brain reached similar concentrations irrespectively of the administration route (Fig 4). Although plasma concentrations after p.o. administration appeared to be very low in comparison to i.v. and i.p. administration, comparable concentrations of ^{3}H-D3 were found in the brain resulting in high brain/plasma ratio after 4 h (Fig 5).

4 hours after a ^{3}H-D3 bolus dose, brain/plasma ratio of all administration routes reached a plateau between 0.7 and 1.0 (Fig 5). To minimize the time dependence of brain/plasma ratio, the absolute ratios were calculated from the area under the brain and plasma concentration

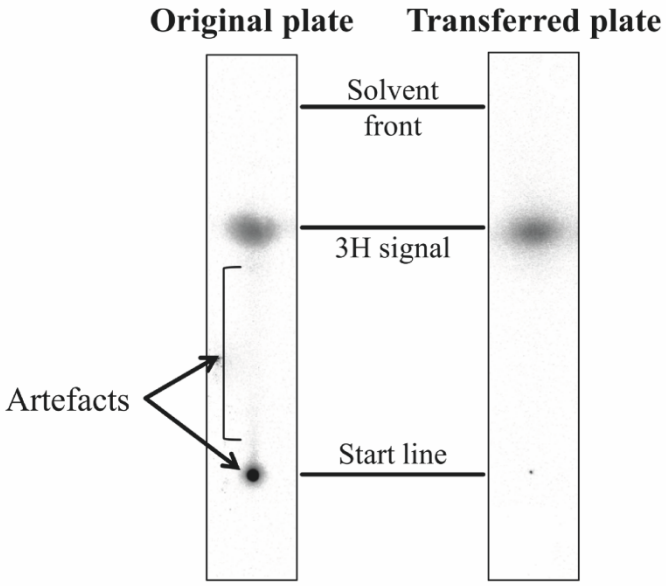

Fig 3. Plate-transfer of ^{3}H-D3 in TLC matrices. A control experiment was performed by placing a new TLC plate to a freshly developed plate to transfer only the ^{3}H-D3 within matrices. On the mirror image of the transferred plate, the ^{3}H signals at the start points as well as the smears were obviously reduced, while the intensity of separated ^{3}H-D3 did only change slightly. This result suggests that the observed artefacts arise from unspecific ^{3}H-D3 binding to the glass surface.

doi:10.1371/journal.pone.0128553.g003

curves from 4 hours to infinity (brain_AUC$_{4h\text{-}inf}$/plasma_AUC$_{4h\text{-}inf}$) with 1.07 for i.v., 0.69 for i.p., and 0.85 for p.o. administration.

After bolus administration, D3 showed relatively long elimination half-lives in plasma of 31.8 h, 41.2 h and 40.7 h after i.v., i.p. and p.o. administration, respectively. Plasma clearance was 0.12 ml/min after i.v. administration. Apparent volumes of distribution were different among i.v., i.p. and p.o. administration with 316, 444 and 684 ml, respectively (Table 1).

Absolute bioavailability was high with 92.2% after i.p. administration and 58.3% after p.o. administration (Table 1). When studying gastrointestinal distribution of D3 after p.o. administration (Fig 6), most of the radioactivity was found in the lower intestinal tract after 4 hours, which suggested that the majority of D3 did not enter the system circulation within 4 hours. Still, the AUC of D3 in brain after p.o. administration was comparable to those after i.p. and i.v. administration (Table 2).

We were also interested in answering the question, whether continuous dosing over several days using an i.p. implanted osmotic pump is showing specific effects in D3 distribution. We found linearly increasing D3 concentrations in plasma and all tested organs over 6 days (Fig 7). Although D3 highly accumulated in liver and kidney at day 6, the mice did not show any obvious signs of intoxication. The brain/plasma ratio increased with time from 0.53 at day 2 to 0.77 at day 6.

Plasma protein binding of D3

To estimate the free fraction of D3 in plasma *in vivo* ($f_{u,total}$), D3 was incubated with human serum albumin (HSA) and α_1-acid glycoprotein (AGP) in an *in vitro* assay (Fig 8). The plasma

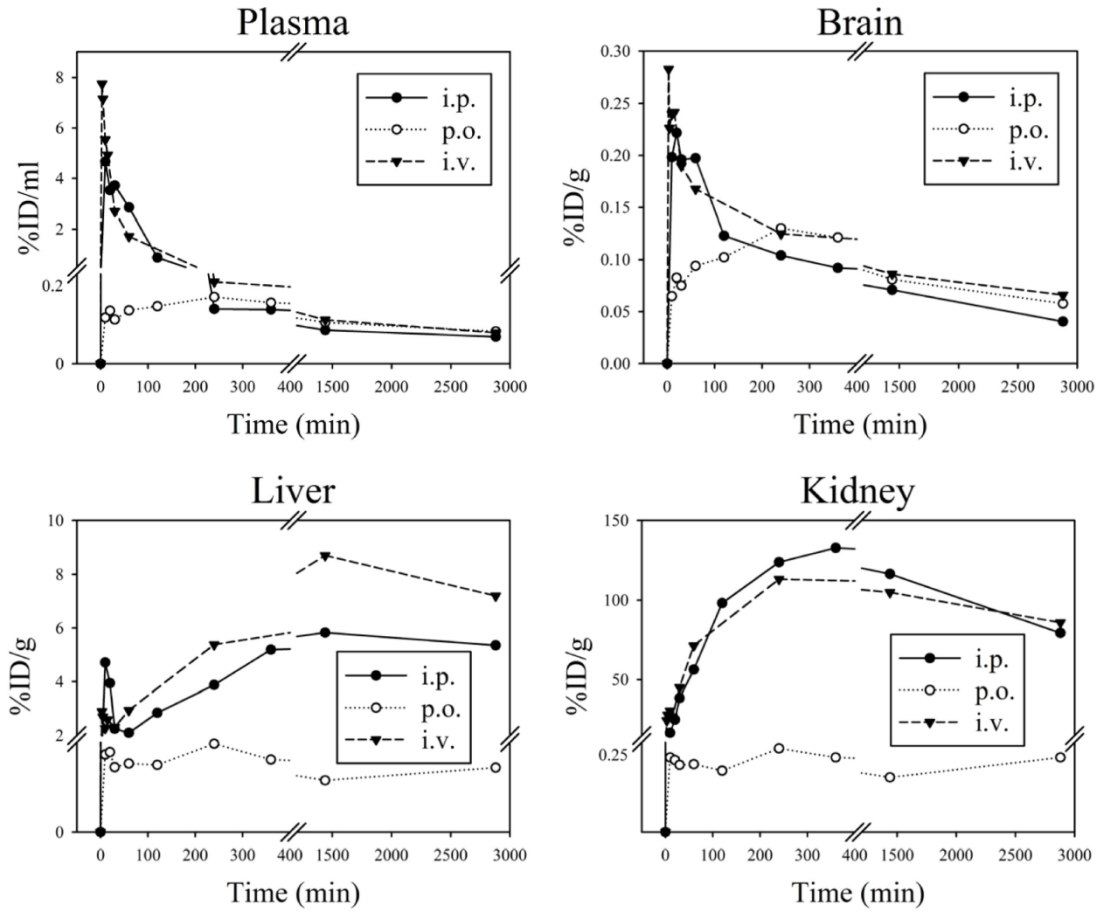

Fig 4. Mean pharmacokinetic profiles of ^{3}H-D3 in organs and plasma after i.p., p.o. and i.v. administration. ^{3}H-D3 (5 μCi) mixed with D3 in a total concentration of 3.5 mg/kg (i.v.) or 10.5 mg/kg (i.p. and p.o.) was applied per mouse. D3 concentrations are shown as percentage of injected dose per gram tissue or milliliter plasma (%ID/g or %ID/ml) dependent of time after administration. Mean values from 3 mice are shown.

doi:10.1371/journal.pone.0128553.g004

protein binding assay for AGP resulted in a K_D of 1.8 μM ± 7.9%. Assuming a D3 concentration in blood of 0.1 μM (C_{D3}, measured 4 h after i.p. injection) calculation of binding to AGP according to Eq (1) predicts a free fraction of 8.3%. For HSA, the K_D was above the detection limit of the kit (> 1.4 mM) indicating very low affinity of D3 to HSA. Nevertheless, calculation of the free fraction with an assumed K_D of 1.4 mM resulted in 68.3% free D3. Taken together, using Eq (2), the estimated free fraction of D3 in plasma was calculated to be approximately 8%.

Discussion

In the current study we have analysed the distribution of the D-enantiomeric peptide D3 after single intravenous, intraperitoneal and per oral administration, as well as continuous dosing

Table 1. Pharmacokinetic parameters for D3 from noncompartmental analysis of plasma.

Parameter	Units	i.v. (3.5 mg/kg)	i.p. (10.5 mg/kg)	p.o. (10.5 mg/kg)
Tmax	min	3	10	240
Cmax	µg/ml	7.75	14	0.45
Cmax/D	µg/ml/mg	77.5	46.7	1.48
$AUC_{C0\text{-}last}$	min*µg/ml	679	1763	1095
$MRT_{C0\text{-}last}$	min	547	527	1718
Lambda_z	1/min	0.00036	0.00028	0.00028
HL_Lambda_z	min	1907	2471	2439
$AUC_{C0\text{-}inf}$	min*µg/ml	869	2404	1521
$MRT_{C0\text{-}inf}$	min	1658	2104	3430
Vz	ml	317	445	684
Cl	ml/min	0.115	N.A.	N.A.
Vss	ml	190	N.A.	N.A.
Bioavailability	%	N.A.	92.2	58.3

N.A.: Parameters not applicable for this administration route. For abbreviations see methods section.

doi:10.1371/journal.pone.0128553.t001

via intraperitoneally implanted osmotic pumps. To the best of our knowledge, this is the first report of a comprehensive pharmacokinetic study of a peptide consisting solely of D-enantiomeric amino acid residues in rodents demonstrating excellent proteolytic stability, long plasma half-life and very high oral bioavailability.

D3 showed high proteolytic resistance exactly as it was shown *in vitro* previously with other all-D-peptides [14–16]. Thanks to this stability, metabolites can be neglected and the measured ^{3}H radioactivity represents the concentration of D3 after administration *in vivo*.

Estimated terminal plasma half-lives of D3 were between 32 and 41 h and were thus much higher than those reported for L-enantiomeric peptides which are typically only a few minutes [25]. Four hours after administration, irrespective of the administration routes, the temporal distribution of D3 in brain closely followed that in plasma resulting in brain/plasma ratios between 0.7 and 1.0 (Fig 5). While substances with a brain/plasma ratio larger than 0.3 are considered to have sufficient access to the central nervous system [26], our results suggest that D3 efficiently overcomes the blood-brain barrier.

Interestingly, by p.o. administration of D3, in spite of only a small rate of D3 being absorbed via the enteric tract, the bioavailability was 58.3% (Table 1), which is relatively high in comparison to that of L-peptide drugs, which were described to be less than 1% without delivery enhancement [27–30]. This finding can be explained by slow oral absorption of D3 and particularly long terminal half-life in plasma resulting in high AUC-values after p.o.

Table 2. Pharmacokinetic parameters for D3 from noncompartmental analysis of brain.

Parameter	Units	i.v. (3.5 mg/kg)	i.p. (10.5 mg/kg)	p.o. (10.5 mg/kg)
Tmax	min	3	20	240
Cmax	µg/g	0.283	0.665	0.390
Cmax/D	µg/g/mg	2.83	2.22	1.30
$AUC_{C0\text{-}last}$	min*µg/g	275	643	935
$MRT_{C0\text{-}last}$	min	1173	1108	1693

For abbreviations see methods section.

doi:10.1371/journal.pone.0128553.t002

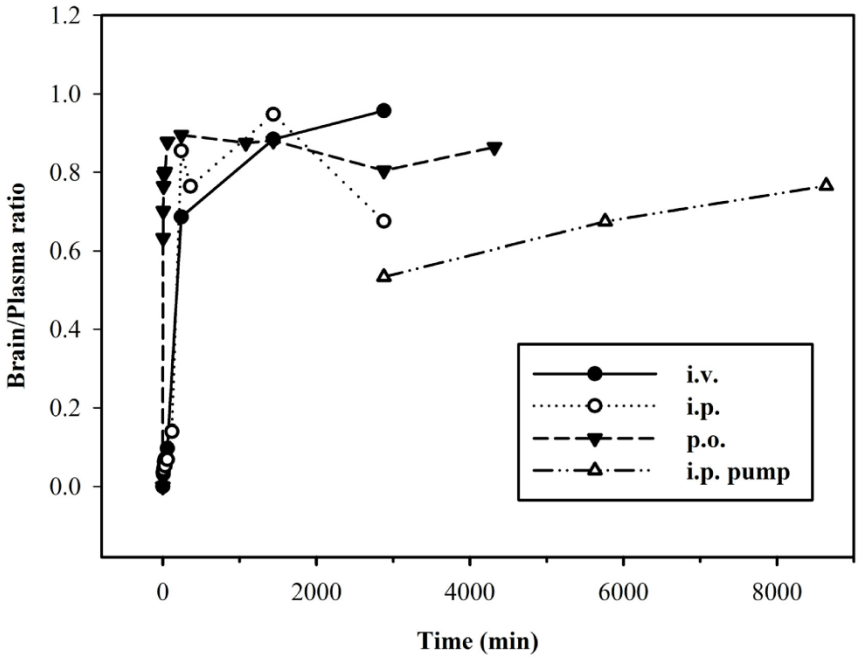

Fig 5. Temporal distribution of brain/plasma ratio of ^{3}H-D3 after different administration routes. Following bolus dose administration, low brain/plasma ratios were found at the starting time points. After 4 hours, the ratios reached relative high values and varied between 0.7–1.0. Upon i.p. pump implantation the ratio increased constantly with time.

doi:10.1371/journal.pone.0128553.g005

administration (Table 1). Low concentrations of D3 as found in kidney and liver after p.o. administration are desirable because this lowers the risk of possible intoxication of important organs. With absorption enhancers and a more suitable formulation of D3, even higher oral bioavailabilities seem to be feasible. Due to the observed high stability of D3 against proteolysis under biological conditions and its hydrophilic properties, elimination via biliary excretion (without re-absorption) and renal clearance in unchanged form could be expected.

Estimated volumes of distribution were 11.1 (i.v.), 15.6 (i.p.) and 24.0 l/kg (p.o.), respectively considering the body weight of the mice (28.5 g in average). The total body water in C57Bl/6 mice is approximately 0.6 l/kg [31], suggesting a distribution of D3 beyond the body fluid and some uptake in peripheral tissues.

Plasma volume of distribution at steady state was also high with 191 ml and 6.69 l/kg considering the body weight of the mice and the fraction of unbound D3 in plasma was predicted to be around 8%. High volume of distribution promotes low plasma clearance, which in our study was approximately between 0.12–0.19 ml/min observed in all routes of administration.

In summary, the current study demonstrates high proteolytic stability for the D-enantiomeric peptide D3. Furthermore, D3 enters the brain very efficiently and shows high oral bioavailability. The terminal half-life in mice after p.o. administration was approximately 41 hours with a brain/plasma ratio between 0.7 and 1.0, and a bioavailability of about 60%.

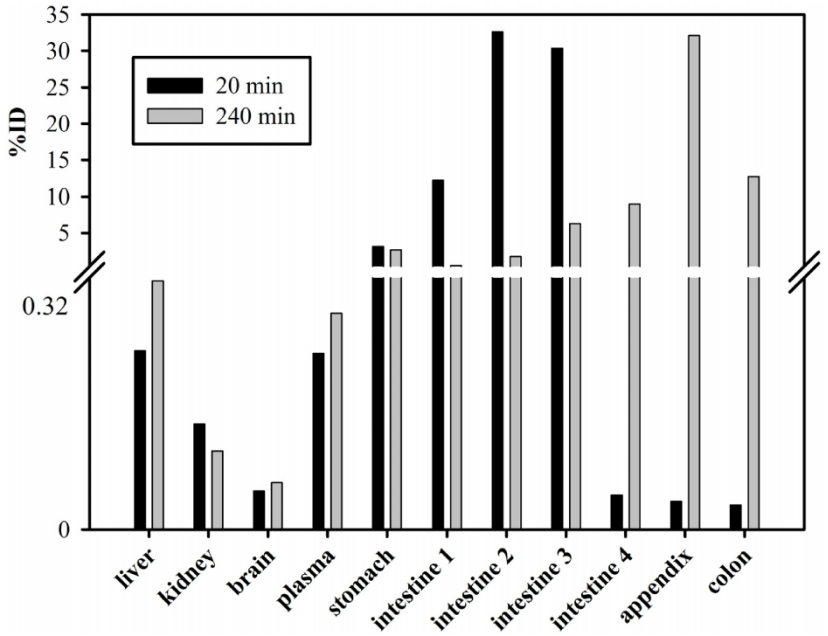

Fig 6. Distribution of ^{3}H-D3 after p.o. administration in organs and plasma. 20 min after gavaging of 100 µl, 5 µCi ^{3}H-D3 with a total D3 concentration of 10.5 mg/kg, most of the radioactivity was located in the middle of small intestine (intestine 2 and 3); 4 hours later, it spread to the lower intestinal tract. Of note is the high concentration of D3 observed in the appendix. At this time point, D3 could already be detected in feces. In comparison to the gastrointestinal tract, the amount of D3 in other organs or plasma after p.o. administration was very low.

doi:10.1371/journal.pone.0128553.g006

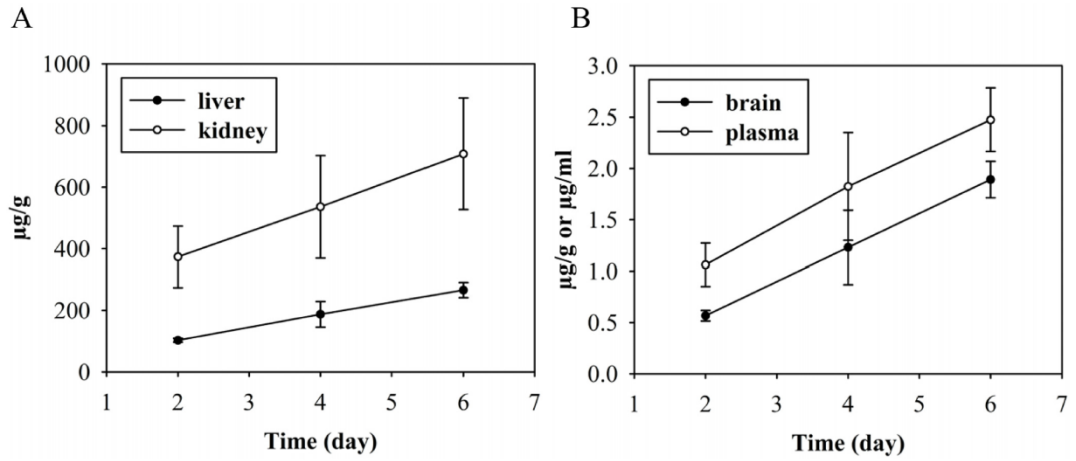

Fig 7. Concentration of ^{3}H-D3 in kidney, liver, brain and plasma administered via i.p. implanted osmotic pump. Alzet mini pumps with a delivery rate of 0.3 mg D3 (plus 5 µCi ^{3}H-D3) per 24 hours were implanted i.p. and organs were sampled after 2 to 6 days. Similar to bolus i.p. administration, more ^{3}H-D3 was found in kidney than in liver (A), whereas D3 concentrations in plasma and brain were considerably lower (B). The concentration of D3 was increasing linearly over time suggesting that the saturation concentration in the respective organs and plasma was not reached by 6 days of continuous dosing.

doi:10.1371/journal.pone.0128553.g007

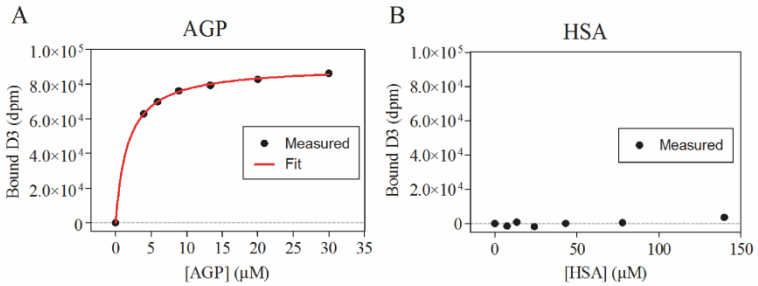

Fig 8. The bound D3 (in dpm) over the protein concentration as determined using the TRANSIL^{XL} kits. Each sample contained 5 µM D3 added to varying concentrations of AGP or HSA. (A) AGP fitted to the Michaelis Menten equation (red). (B) The binding of D3 to HSA was below the detection limit of the kit (K_D > 1.4 mM).

doi:10.1371/journal.pone.0128553.g008

In our previous studies, D3 already proved to be therapeutically active in reversing cognitive deficits and amyloid plaque load *in vivo*. Given its high oral bioavailability, suitably formulated D3 with multiple dosing might be a promising drug candidate against Alzheimer's disease.

Supporting Information

S1 File. ARRIVE Checklist. Completed "The ARRIVE Guidelines Checklist" for reporting animal data in this manuscript.
(DOCX)

Acknowledgments

We thank Michael Schöneck, Nicole Niemietz and Daniela Schumacher for excellent technical assistance and Dr. Dagmar Jürgens for discussions on the data analysis.

Author Contributions

Conceived and designed the experiments: NJ LL JB LG MC NJS JK KJL DW AW. Performed the experiments: NJ LL JP ES. Analyzed the data: NJ LL JP TZ JM DW AW. Wrote the paper: NJ LL NJS JB DW AW.

References

1. Berchtold NC, Cotman CW. Evolution in the conceptualization of dementia and Alzheimer's disease: Greco-Roman period to the 1960s. Neurobiology of aging. 1998; 19(3):173–89. Epub 1998/07/14. PMID: 9661992.
2. Fletcher LC, Burke KE, Caine PL, Rinne NL, Braniff CA, Davis HR, et al. Diagnosing Alzheimer's disease: are we any nearer to useful biomarker-based, non-invasive tests? GMS health technology assessment. 2013; 9:Doc01. Epub 2013/06/12. doi: 10.3205/hta000107 PMID: 23755087; PubMed Central PMCID: PMC3677379.
3. Nygaard HB. Current and emerging therapies for Alzheimer's disease. Clinical therapeutics. 2013; 35 (10):1480–9. Epub 2013/10/22. doi: 10.1016/j.clinthera.2013.09.009 PMID: 24139420.
4. TD B. Alzheimer Disease Overview. 1993. In: GeneReviews(R) [Internet]. University of Washington, Seattle.
5. Mikulca JA, Nguyen V, Gajdosik DA, Teklu SG, Giunta EA, Lessa EA, et al. Potential novel targets for Alzheimer pharmacotherapy: II. Update on secretase inhibitors and related approaches. Journal of clinical pharmacy and therapeutics. 2014; 39(1):25–37. Epub 2013/12/10. doi: 10.1111/jcpt.12112 PMID: 24313554.

6. Stockley JH, O'Neill C. Understanding BACE1: essential protease for amyloid-beta production in Alzheimer's disease. Cellular and molecular life sciences: CMLS. 2008; 65(20):3265–89. Epub 2008/08/13. doi: 10.1007/s00018-008-8271-3 PMID: 18695942.

7. Selkoe DJ. Alzheimer's disease: genes, proteins, and therapy. Physiological reviews. 2001; 81(2):741–66. Epub 2001/03/29. PMID: 11274343.

8. Bitan G, Kirkitadze MD, Lomakin A, Vollers SS, Benedek GB, Teplow DB. Amyloid beta-protein (Abeta) assembly: Abeta 40 and Abeta 42 oligomerize through distinct pathways. Proceedings of the National Academy of Sciences of the United States of America. 2003; 100(1):330–5. Epub 2002/12/31. doi: 10.1073/pnas.222681699 PMID: 12506200; PubMed Central PMCID: PMC140968.

9. Kayed R, Lasagna-Reeves CA. Molecular mechanisms of amyloid oligomers toxicity. Journal of Alzheimer's disease: JAD. 2013; 33 Suppl 1:S67–78. Epub 2012/04/26. doi: 10.3233/JAD-2012-129001 PMID: 22531422.

10. Tamaoka A. [The pathophysiology of Alzheimer's disease with special reference to "amyloid cascade hypothesis"]. Rinsho byori The Japanese journal of clinical pathology. 2013; 61(11):1060–9. Epub 2014/01/24. PMID: 24450113.

11. Schenk D, Basi GS, Pangalos MN. Treatment strategies targeting amyloid beta-protein. Cold Spring Harbor perspectives in medicine. 2012; 2(9):a006387. Epub 2012/09/07. doi: 10.1101/cshperspect.a006387 PMID: 22951439; PubMed Central PMCID: PMC3426815.

12. Citron M. Alzheimer's disease: strategies for disease modification. Nature reviews Drug discovery. 2010; 9(5):387–98. doi: 10.1038/nrd2896 PMID: 20431570

13. Sun N, Funke SA, Willbold D. A Survey of Peptides with Effective Therapeutic Potential in Alzheimer's Disease Rodent Models or in Human Clinical Studies. Mini-Rev Med Chem. 2012; 12(5):388–98. PMID: ISI:000303103600005.

14. Liu M, Li C, Pazgier M, Mao Y, Lv Y, Gu B, et al. D-peptide inhibitors of the p53-MDM2 interaction for targeted molecular therapy of malignant neoplasms. Proceedings of the National Academy of Sciences of the United States of America. 2010; 107(32):14321–6. Epub 2010/07/28. doi: 10.1073/pnas.1008930107 PMID: 20660730; PubMed Central PMCID: PMC2922601.

15. Zawadzke LE, Berg JM. A Racemic Protein. Journal of the American Chemical Society. 1992; 114 (10):4002–3. doi: 10.1021/Ja00036a073 PMID: ISI:A1992HT80100073.

16. Milton RCD, Milton SCF, Kent SBH. Total Chemical Synthesis of a D-Enzyme—the Enantiomers of Hiv-1 Protease Show Demonstration of Reciprocal Chiral Substrate-Specificity. Science. 1992; 256 (5062):1445–8. doi: 10.1126/science.1604320 PMID: ISI:A1992HX33700036.

17. Wiesehan K, Willbold D. Mirror-image phage display: aiming at the mirror. Chembiochem: a European journal of chemical biology. 2003; 4(9):811–5. Epub 2003/09/10. doi: 10.1002/cbic.200300570 PMID: 12964153.

18. Schumacher TN, Mayr LM, Minor DL Jr., Milhollen MA, Burgess MW, Kim PS. Identification of D-peptide ligands through mirror-image phage display. Science. 1996; 271(5257):1854–7. PMID: 8596952

19. van Groen T, Kadish I, Wiesehan K, Funke SA, Willbold D. In vitro and in vivo staining characteristics of small, fluorescent, Abeta42-binding D-enantiomeric peptides in transgenic AD mouse models. ChemMedChem. 2009; 4(2):276–82. Epub 2008/12/17. doi: 10.1002/cmdc.200800289 PMID: 19072935.

20. van Groen T, Kadish I, Funke SA, Bartnik D, Willbold D. Treatment with D3 removes amyloid deposits, reduces inflammation, and improves cognition in aged AbetaPP/PS1 double transgenic mice. J Alzheimers Dis. 2013; 34(3):609–20. Epub 2012/12/29. doi: 10.3233/JAD-121792 PMID: 23271316.

21. van Groen T, Kadish I, Funke A, Bartnik D, Willbold D. Treatment with Abeta42 binding D-amino acid peptides reduce amyloid deposition and inflammation in APP/PS1 double transgenic mice. Advances in protein chemistry and structural biology. 2012; 88:133–52. Epub 2012/07/21. doi: 10.1016/B978-0-12-398314-5.00005-2 PMID: 22814708.

22. Aileen Funke S, van Groen T, Kadish I, Bartnik D, Nagel-Steger L, Brener O, et al. Oral treatment with the d-enantiomeric peptide D3 improves the pathology and behavior of Alzheimer's Disease transgenic mice. ACS chemical neuroscience. 2010; 1(9):639–48. Epub 2010/09/15. doi: 10.1021/cn100057j PMID: 22778851; PubMed Central PMCID: PMC3368690.

23. van Groen T, Wiesehan K, Funke SA, Kadish I, Nagel-Steger L, Willbold D. Reduction of Alzheimer's disease amyloid plaque load in transgenic mice by D3, A D-enantiomeric peptide identified by mirror image phage display. ChemMedChem. 2008; 3(12):1848–52. Epub 2008/11/19. doi: 10.1002/cmdc.200800273 PMID: 19016284.

24. Kilkenny C, Browne WJ, Cuthill IC, Emerson M, Altman DG. Improving Bioscience Research Reporting: The ARRIVE Guidelines for Reporting Animal Research. Plos Biol. 2010; 8(6). ARTN e1000412 doi: 10.1371/journal.pbio.1000412 PMID: ISI:000279355600022.

25. Pollaro L, Heinis C. Strategies to prolong the plasma residence time of peptide drugs. MedChemComm. 2010; 1(5):319–24. doi: 10.1039/c0md00111b

26. Reichel A. The role of blood-brain barrier studies in the pharmaceutical industry. Current drug metabolism. 2006; 7(2):183–203. Epub 2006/02/14. PMID: 16472107.

27. Wong TW. Design of oral insulin delivery systems. Journal of drug targeting. 2010; 18(2):79–92. Epub 2009/12/09. doi: 10.3109/10611860903302815 PMID: 19968567.

28. Takagi H, Hiroi T, Hirose S, Yang L, Takaiwa F. Rice seed ER-derived protein body as an efficient delivery vehicle for oral tolerogenic peptides. Peptides. 2010; 31(8):1421–5. Epub 2010/05/12. doi: 10.1016/j.peptides.2010.04.032 PMID: 20457197.

29. Mason JM. Design and development of peptides and peptide mimetics as antagonists for therapeutic intervention. Future medicinal chemistry. 2010; 2(12):1813–22. Epub 2011/03/25. doi: 10.4155/fmc.10.259 PMID: 21428804.

30. Lalatsa A, Garrett NL, Ferrarelli T, Moger J, Schatzlein AG, Uchegbu IF. Delivery of Peptides to the Blood and Brain after Oral Uptake of Quaternary Ammonium Palmitoyl Glycol Chitosan Nanoparticles. Molecular pharmaceutics. 2012; 9(6):1764–74. doi: 10.1021/Mp300068j PMID: ISI:000304728700022.

31. Chapman ME, Hu L, Plato CF, Kohan DE. Bioimpedance spectroscopy for the estimation of body fluid volumes in mice. American journal of physiology Renal physiology. 2010; 299(1):F280–3. Epub 2010/05/14. doi: 10.1152/ajprenal.00113.2010 PMID: 20462974; PubMed Central PMCID: PMC2904176.

3.2 Increase of Positive Net Charge and Conformational Rigidity Enhances the Efficacy of D-Enantiomeric Peptides Designed to Eliminate Cytotoxic Aβ Species

Tamar Ziehm, Oleksandr Brener, Thomas van Groen, Inga Kadish, Daniel Frenzel, Markus Tusche, Janine Kutzsche, Kerstin Reiß, Lothar Gremer, Luitgard Nagel-Steger, Dieter Willbold

ACS Chem Neurosci. 2016 Aug 17;7(8):1088-96

doi: 10.1021/acschemneuro.6b00047

http://pubs.acs.org/doi/abs/10.1021/acschemneuro.6b00047

ACS Chemical Neuroscience

Research Article

pubs.acs.org/chemneuro

Increase of Positive Net Charge and Conformational Rigidity Enhances the Efficacy of D-Enantiomeric Peptides Designed to Eliminate Cytotoxic Aβ Species

Tamar Ziehm,[†] Oleksandr Brener,[†,‡] Thomas van Groen,[§] Inga Kadish,[§] Daniel Frenzel,[†] Markus Tusche,[†] Janine Kutzsche,[†] Kerstin Reiß,[†] Lothar Gremer,[†,‡] Luitgard Nagel-Steger,[†,‡] and Dieter Willbold*[,†,‡]

[†]Institute of Complex Systems, Structural Biochemistry (ICS-6), Forschungszentrum Jülich, 52425 Jülich, Germany

[‡]Institut für Physikalische Biologie, Heinrich-Heine-Universität Düsseldorf, 40225 Düsseldorf, Germany

[§]Department of Cell, Developmental and Integrative Biology, University of Alabama at Birmingham (UAB), Birmingham, Alabama 35233, United States

Supporting Information

ABSTRACT: Alzheimer's disease (AD) is a neurodegenerative disorder and the most common type of dementia. Until now, there is no curative therapy available. Previously, we selected the amyloid-beta (Aβ) targeting peptide D3 consisting of 12 D-enantiomeric amino acid residues by mirror image phage display as a potential drug candidate for the treatment of AD. In the current approach, we investigated the optimization potential of linear D3 with free C-terminus ($D3_{COOH}$) by chemical modifications. First, the impact of the net charge was investigated and second, cyclization was introduced which is a well-known tool for the optimization of peptides for enhanced target affinity. Following this strategy, three D3 derivatives in addition to $D3_{COOH}$ were designed: C-terminally amidated linear D3 ($D3_{CONH_2}$), cyclic D3 (cD3), and cyclic D3 with an additional arginine residue (cD3r) to maintain the net charge of linear $D3_{CONH_2}$. These four compounds were compared to each other according to their binding affinities to Aβ(1−42), their efficacy to eliminate cytotoxic oligomers, and consequently their potency to neutralize Aβ(1−42) oligomer induced neurotoxicity. $D3_{CONH_2}$ and cD3r versions with equally increased net charge showed superior properties over $D3_{COOH}$ and cD3, respectively. The cyclic versions showed superior properties compared to their linear version with equal net charge, suggesting cD3r to be the most efficient compound among these four. Indeed, treatment of the transgenic AD mouse model Tg-SwDI with cD3r significantly enhanced spatial memory and cognition of these animals as revealed by water maze performance. Therefore, charge increase and cyclization imply suitable modification steps for an optimization approach of the Aβ targeting compound D3.

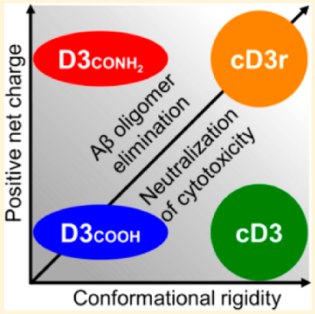

KEYWORDS: *Alzheimer's disease, amyloid-beta, drug discovery, D-enantiomeric peptides, cyclization, charge increase*

1. INTRODUCTION

Alzheimer's disease (AD) is a progressive and devastating neurodegenerative disorder and the most common type of dementia. The number of patients is continually increasing and expected to reach 42 million people worldwide in the year 2020.[1] Although a curative therapy is utterly important, there is no disease modifying drug available yet.[2]

AD is an amyloid related disorder which is associated with misfolding of the amyloid-beta peptide (Aβ) resulting in Aβ self-assembly.[3,4] Expected Aβ states and assemblies include soluble monomer units, low molecular weight oligomers, protofibrils, and insoluble, fibrillar aggregates.[5] Fibrillar Aβ is the major component of extracellular senile plaques which are histopathologically characteristic features in the brain of AD patients.[3,4] However, studies over the past decade implicate oligomeric assembly states of Aβ as the major neurotoxic agents in AD.[6,7] Therefore, these soluble species represent a suitable target for the treatment of AD. An attractive strategy is the development of a compound that interferes with the Aβ self-assembly process resulting in nonamyloidogenic and nontoxic Aβ species.[2,8]

Previous studies in our group describe the peptide D3 which was selected against Aβ(1−42) monomers via mirror image phage display with the intention to destabilize Aβ oligomers.[9−12] D3 consists of 12 D-enantiomeric amino acid residues (rprtrlhthrnr). Therefore, D3 shows superior proteolytic stability compared to its stereoisomer resulting in longer biological half-life.[13] In vitro, D3 induces the conversion of

Received: February 17, 2016
Accepted: May 31, 2016
Published: May 31, 2016

DOI: 10.1021/acschemneuro.6b00047
ACS Chem. Neurosci. 2016, 7, 1088−1096

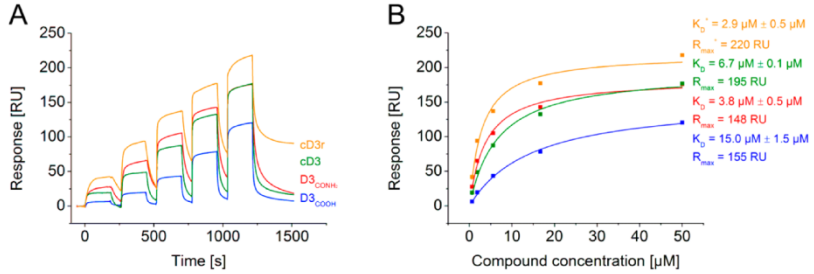

Figure 1. Interaction studies of $D3_{COOH}$, $D3_{CONH_2}$, cD3, and cD3r with Aβ(1−42) monomers. Interaction between the designed D3 derivatives and Aβ(1−42) was examined using SPR with immobilized biotinylated Aβ(1−42) monomers via streptavidin−biotin coupling. The compounds were injected over the surface with increasing concentrations (0.6 μM, 1.9 μM, 5.6 μM, 16.7 μM, 50 μM) in single cycles. The sensorgrams of $D3_{COOH}$, $D3_{CONH_2}$, cD3, and cD3r binding to Aβ(1−42) are shown (A). For evaluation, the steady state binding responses were plotted against the compound concentrations and the data points were fitted using the Langmuir 1:1 binding model (B). The calculated K_D values ± SE and saturation binding levels (R_{max}) are indicated. cD3r shows a heterogeneous interaction with Aβ. Therefore, the evaluated K_D and R_{max} values represent apparent binding affinity and saturation level in case of cD3r consisting of two kinetics, indicated with K_D* and R_{max}*. Blue, $D3_{COOH}$; red, $D3_{CONH_2}$; green, cD3; orange, cD3r.

cytotoxic Aβ oligomers into high molecular weight aggregates, which are not cytotoxic.[14−16] In transgenic AD mice, D3 binds to Aβ plaques, reduces Aβ plaque load and cerebral inflammation, and improves cognition after oral treatment.[9,15,17,18] Pharmacokinetic data report that D3 reaches a high oral bioavailability and enters the brain efficiently.[13] Nevertheless, the potency of D3 as a drug candidate for the treatment of AD can further be optimized by applying general tools for peptide modification.

In this study, the impact of net charge and cyclization of D3 was systematically investigated. The analyzed D3 derivatives were characterized according to their binding affinity to Aβ(1−42), their efficacy to eliminate cytotoxic Aβ(1−42) oligomers, and the resulting potency to neutralize Aβ(1−42) oligomer induced cytotoxicity to neuronal cells. Finally, the most promising compound based on the in vitro characterization was evaluated in an in vivo study.

2. RESULTS AND DISCUSSION

Design of D3 Derivatives. The peptide D3 (rprtrlhthrnr) is characterized by a high content of positively charged amino acid residues. At physiological pH, the net charge of D3 with free N- and C-termini amounts to +5 due to the five arginine residues. In silico, it was shown that the basic side chains of D3 form the electrostatically driven interaction with the acidic residues E11, E22, and D23 of Aβ(1−42).[19] Thus, we hypothesized that increasing the net charge of D3 represents one possibility for increasing its affinity to Aβ(1−42). Additionally, cyclization of peptides was reported to implicate several advantages. Hydrogen bonding is reduced in cyclic compounds, which can increase their membrane permeability.[20] Furthermore, cyclic peptides are less affected by both endo- and exopeptidases as they lack free termini and are conformationally less flexible compared to linear peptides. These effects often result in increased pharmaceutical efficacy.[21,22] The rigidity of cyclic compounds further implies a reduction of the entropic part of Gibbs free binding energy leading to enhanced binding affinity.[23] To investigate the impact of net charge and cyclization on the therapeutic effect of D3, four peptides based on the sequence of D3 were investigated: the linear D3 peptide with free N- and C-termini ($D3_{COOH}$), the C-terminally amidated peptide ($D3_{CONH_2}$), the head to tail cyclized version of D3 (cD3) that maintains the net charge of $D3_{COOH}$, and the head to tail cyclized D3 with an additional arginine inserted to remain the net charge of $D3_{CONH_2}$ (rprtrlhthrnrr, cD3r).

D3 Derivatives Bind to Aβ(1−42) with Increased Affinity. The interaction between the four compounds and Aβ(1−42) was investigated using surface plasmon resonance (SPR). N-Terminally biotinylated Aβ(1−42) was used as ligand and immobilized via streptavidin−biotin coupling to the sensor surface. Five ascending compound concentrations were injected in single cycles to the surface.

The interactions between Aβ(1−42) and $D3_{COOH}$, $D3_{CONH_2}$, and cD3 were characterized by fast on- and off-rates and the equilibrium phases were rapidly achieved (Figure 1A). Furthermore, the interactions were characterized by a homogeneous 1:1 binding. In contrast, the sensorgram of cD3r binding to Aβ(1−42) indicated a heterogeneous interaction comprising two kinetics. In order to keep all four compounds comparable to each other, we determined the equilibrium dissociation constants (K_D) by plotting the steady state responses against the corresponding compound concentrations and the data points were fitted applying the Langmuir 1:1 binding model (Figure 1B). K_D values of 15 μM, 3.8 μM, and 6.7 μM were determined for $D3_{COOH}$, $D3_{CONH_2}$, and cD3, respectively. Despite the heterogeneous binding mode, one apparent overall K_D value (K_D*) of 2.9 μM was determined for the interaction between cD3r and Aβ(1−42). Charge elevation of $D3_{COOH}$ by amidation of the acidic C-terminus and cyclization equally enhanced the affinity to Aβ(1−42). For cD3r, both optimization strategies were combined, leading to enhanced affinity with a 5-fold lower K_D value for the Aβ(1−42) interaction compared to the unmodified compound $D3_{COOH}$.

Modified D3 Compounds Efficiently Eliminate Aβ(1−42) Oligomers. Aβ(1−42) oligomer elimination efficacies of the four compounds $D3_{COOH}$, $D3_{CONH_2}$, cD3, or cD3r were studied using QIAD (quantitative determination of interference with Aβ aggregate size distribution). QIAD is a method for quantitative determination of Aβ oligomer elimination efficacy by a given compound. The outcome of the assay allows comparison between various drug candidates regarding their Aβ oligomer elimination efficacies.[16]

DOI: 10.1021/acschemneuro.6b00047
ACS Chem. Neurosci. 2016, 7, 1088−1096

In the current study, 80 μM Aβ(1−42) was preincubated in order to enrich Aβ(1−42) oligomers. After this step, Aβ(1−42) was coincubated with 20 μM of the respective compound. The resulting Aβ(1−42) assemblies were separated by density gradient centrifugation and subsequent fractionation. Fractions 1 to 15 represented the density gradient from the top to the bottom containing particles with increasing s-values.[24] The Aβ(1−42) content in each fraction was quantified using RP-HPLC (Figure 2). Fractions 4−6 contain cytotoxic Aβ(1−42)

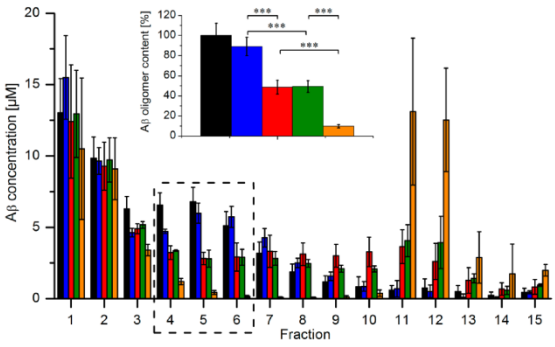

Figure 2. Quantitative determination of interference with Aβ aggregate size distribution. Influences of $D3_{COOH}$, $D3_{CONH_2}$, cD3, or cD3r on preformed Aβ(1−42) aggregates were examined with emphasis on cytotoxic Aβ(1−42) oligomer species. 80 μM Aβ(1−42) was preincubated for 4.5 h and coincubated with 20 μM of the respective compound for further 40 min. Aβ(1−42) species were separated using density gradient centrifugation. The gradient was fractionated from the top to the bottom and the Aβ(1−42) concentrations of all 15 fractions were determined using RP-HPLC. A reduction of Aβ(1−42) species in the presence of compound was observed in fractions 4−6 which contain Aβ oligomers. For quantitation of the oligomer elimination influenced by the compounds, the Aβ(1−42) concentrations in fractions 4 to 6 were pooled and statistically analyzed (inset). The data represent mean ± SD of quadruplicate (for Aβ(1−42) without compound: n = 21). One-way ANOVA ($p < 0.001$) with Bonferroni post hoc analysis: $^{***}p \leq 0.001$. Black, Aβ(1−42); blue, Aβ(1−42) + $D3_{COOH}$; red, Aβ(1−42) + $D3_{CONH_2}$; green, Aβ(1−42) + cD3; orange, Aβ(1−42) + cD3r.

oligomers with an s-value of 7 S, consisting of approximately 23 Aβ(1−42) monomer units.[16] Aβ protofibrils, Aβ fibrils and large Aβ aggregates are known to be located in the bottom six fractions of the gradient.[24,25]

The concentrations of Aβ(1−42) monomers and low molecular weight assemblies in the upper fractions of the gradient were not significantly affected by all four compounds (p = 0.23). The most affected Aβ(1−42) species which were drastically reduced by the compounds were located in fractions 4−6, i.e., the cytotoxic Aβ(1−42) oligomers. Within these fractions, the total Aβ(1−42) concentration was diminished by 14% ($D3_{COOH}$), 51% ($D3_{CONH_2}$ and cD3), and 90% (cD3r) compared to Aβ(1−42) without compound (Figure 2 inset). As the QIAD assay is a matrix free and closed approach, Aβ(1−42) was completely recovered and its redistribution can be conveniently monitored. Eliminated Aβ(1−42) oligomers from fractions 4−6 were converted into species that moved into higher density material of the gradient and were recovered in fractions 11−13. While the compounds shifted the equilibrium of Aβ(1−42) from oligomers to high molecular weight coprecipitates, the monomeric and low molecular weight Aβ(1−42) present in fractions 1−3 was not affected. Comparing these modified compounds according to their efficacy, we conclude that both charge increase and cyclization of the peptides lead to a significant increase of Aβ(1−42) oligomer elimination in a comparable way. cD3r almost completely eliminated the Aβ(1−42) oligomers of fractions 4−6, indicating that cD3r acts as the most efficient compound in Aβ(1−42) oligomer elimination.

High Molecular Weight Coprecipitates in the Presence of the Compounds. The morphology of the resulting high molecular weight Aβ(1−42) coprecipitates in the presence of the compounds shown by QIAD was examined using transmission electron microscopy (TEM). Aβ(1−42) incubated without compound shows the well-known structure of amyloid fibrils with its highly ordered and elongated aggregates (Figure 3A).[26] Addition of the compounds to an oligomer enriched Aβ(1−42) mixture resulted in the formation of high molecular weight coprecipitates (Figure 3B−E). However, the morphology of the coprecipitates altered between the compounds. In the presence of $D3_{COOH}$, the aggregates still exhibited remaining fibrillar parts which were less pronounced in the presence of $D3_{CONH_2}$ or cD3. The formed coprecipitates in the presence of cD3r lacked any fibrillar morphology but were completely amorphous.

Reduction of Aβ(1−42) Oligomer Induced Cytotoxicity. Aβ(1−42) aggregates are known to exert cytotoxic effects on neuronal cells.[16,27] As an in vitro system to investigate Aβ(1−42) induced cytotoxicity, the human derived neuroblastoma cell line SH-SY5Y is commonly used.[16,28] In this study, we examined the cytotoxicity of an Aβ(1−42) oligomer enriched mixture on SH-SY5Y cells in the presence or absence of the compounds $D3_{COOH}$, $D3_{CONH_2}$, cD3, or cD3r. By this, we investigated if the formed high molecular weight Aβ(1−42) coprecipitates in the presence of the compounds shown by QIAD are cytotoxic. The cell viability was determined using the tetrazolium dye MTT which is reduced to its purple formazan by dehydrogenase enzymes in active mitochondria. Thus, the color change reflects metabolic activity and correlates with total cell viability.[29]

Aβ(1−42) was preincubated for 4.5 h in order to enrich cytotoxic oligomeric Aβ(1−42) assemblies followed by coincubation with the four compounds, respectively. The mixture of Aβ(1−42) assemblies and respective compound was added to SH-SY5Y cells and the cell viability was determined (Figure 4). Normalized to the buffer control, 1 μM Aβ(1−42), mostly consisting of oligomers, reduced the cell viability of SH-SY5Y cells to 55%. The presence of 5 μM $D3_{COOH}$ did not show a significant influence on the Aβ(1−42) oligomer induced cytotoxicity. However, in the presence of $D3_{CONH_2}$, the cell viability was increased to 60%. cD3 enhanced the cell viability to 82%. cD3r further reduced Aβ(1−42) oligomer induced cytotoxicity, resulting in 97% cell viability. The compounds themselves showed no significant effect on the cell viability in the applied concentration (Figure S2). Thus, the high molecular weight Aβ(1−42) coprecipitates which are formed in the presence of the compounds are nontoxic to SH-SY5Y cells, independent of their morphology. Furthermore, cyclization and charge increase yielded in a compound which inhibited Aβ(1−42) oligomer induced cytotoxicity. Both modifications, cyclization and charge increase, contributed synergistically to this effect.

DOI: 10.1021/acschemneuro.6b00047
ACS Chem. Neurosci. 2016, 7, 1088−1096

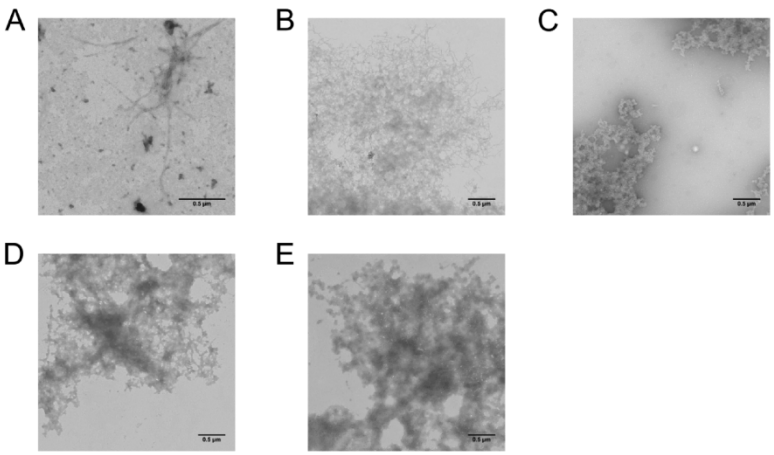

Figure 3. Transmission electron microscopy (TEM) images of Aβ(1−42) coincubated with $D3_{COOH}$, $D3_{CONH_2}$, cD3, or cD3r. Via TEM, the morphology of Aβ(1−42) aggregates in the absence (A) or presence of the compounds $D3_{COOH}$ (B), $D3_{CONH_2}$ (C), cD3 (D), and cD3r (E) was investigated. After preincubation of 20 μM Aβ(1−42) for 4.5 h, 20 μM of the respective compound was added and coincubated for 16 h.

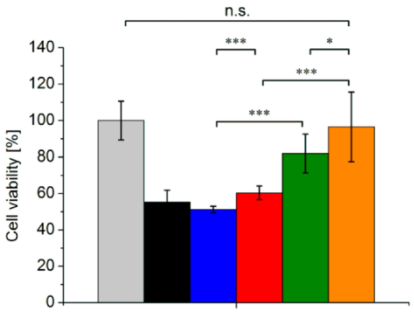

Figure 4. MTT based cytotoxicity test of oligomer enriched Aβ(1−42) coincubated with $D3_{COOH}$, $D3_{CONH_2}$, cD3, or cD3r. 50 μM Aβ(1−42) was preincubated for 4.5 h to enrich cytotoxic Aβ(1−42) oligomers, followed by coincubation for 40 min with 250 μM of the respective compound. Cytotoxicity of the Aβ-compound mixtures was examined based on the MTT assay principle using SH-SY5Y cells. The cells were exposed to final concentrations of 1 μM Aβ(1−42) with 5 μM compound. The data represent mean ± SD of three independent experiments with n = 5 for each compound in the respective experiment, normalized to the buffer control. Kruskal−Wallis ANOVA ($p < 0.001$) with Bonferroni corrected Mann−Whitney U-test: *$p \leq 0.05$, ***$p \leq 0.001$, n.s. not significant ($p > 0.05$). Gray, buffer control; black, Aβ(1−42); blue, Aβ(1−42) + $D3_{COOH}$; red, Aβ(1−42) + $D3_{CONH_2}$; green, Aβ(1−42) + cD3; orange, Aβ(1−42) + cD3r.

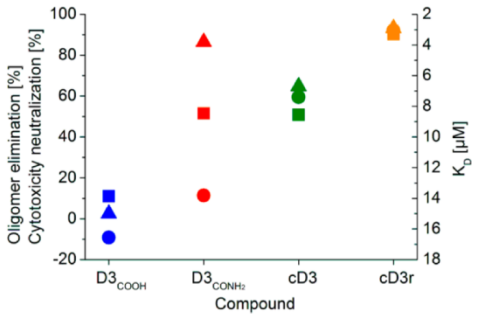

Figure 5. Summary of quantitative assays. Binding affinities given as K_D values derived by SPR (triangle), oligomer elimination efficacies analyzed by QIAD (square), and cytotoxicity neutralization efficacies (circle) derived from MTT based cytotoxicity assays of the four compounds are shown.

Correlation between the Quantitative in Vitro Assays. Concerning the efficacies of $D3_{COOH}$, $D3_{CONH_2}$, cD3, and cD3r within the applied quantitative in vitro assays (SPR, QIAD, cytotoxicity assay), we can conclude that the efficacy correlates with positive charge and cyclization of the investigated compounds (Figure 5). $D3_{COOH}$ bound to Aβ(1−42) with a K_D value of 15 μM and showed no significant effects in the performed assays under the applied conditions. By amidating the C-terminus, the net charge was increased, resulting in a 4-fold increase in binding affinity to Aβ(1−42) and in enhanced Aβ(1−42) oligomer elimination. Interestingly, the neutralization effect of Aβ(1−42) oligomer induced cytotoxicity was only slightly increased for $D3_{CONH_2}$ compared to $D3_{COOH}$. Therefore, the correlation between the quantitative assays was very weak for this compound. Nevertheless, the efficacy of $D3_{COOH}$ could be improved by charge increase.

The second optimization strategy, cyclization, presents a well-established method to yield increased compound efficacy and is already described for the drug development process for AD treatment.[30−32] In our study, cyclization of $D3_{COOH}$ leading to cD3 resulted in similar enhancement of binding affinity and Aβ(1−42) oligomer elimination efficacy as achieved by charge increase. Thus, charge increase and cyclization facilitate a similar degree of optimization concerning binding affinity and Aβ(1−42) oligomer elimination efficacy, while the neutralization effect on Aβ(1−42) oligomer induced cytotoxicity was enhanced in the presence of cD3 compared to $D3_{CONH_2}$. The correlation between the quantitative assays was also very strong for cD3, as already shown in case of $D3_{COOH}$.

The combination of both optimization strategies, cyclization and charge increase, was realized in cD3r. This compound showed the strongest binding affinity to Aβ(1−42) and eliminated 90% of the cytotoxic Aβ(1−42) oligomers by shifting the equilibrium to high molecular weight nonfibrillar

DOI: 10.1021/acschemneuro.6b00047
ACS Chem. Neurosci. 2016, 7, 1088−1096

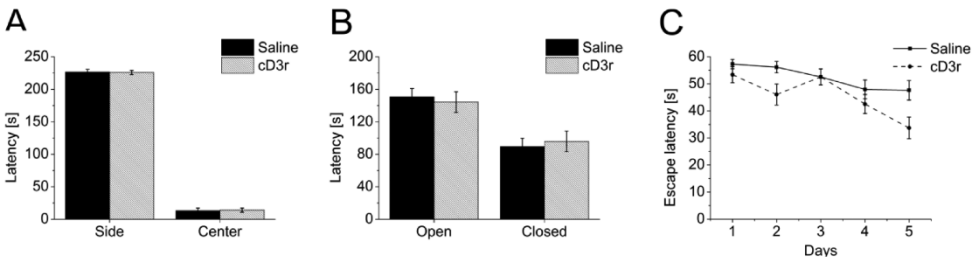

Figure 6. In vivo cognition study of cD3r treated transgenic AD mice. Transgenic AD mice (Tg-SwDI) were treated with cD3r (n = 9) or saline (n = 10) over 4 weeks. After 3 weeks of treatment, the influence of cD3r treatment on normal behavior of Tg-SwDI mice was investigated in an open field (A) and zero maze test (B). The latencies of the mice in the respective area are plotted as means ± SEM. Mann−Whitney U-test saline vs cD3r: p = 0.775 for open field test; p = 0.965 for zero maze test. Subsequently, the cognition was examined in a water maze consecutively over 5 days (C). The animals were placed into a maze with a hidden platform and allowed to find the platform for 60 s. The escape latency of the mice before they found the platform is plotted as mean ± SEM of three trials per day of all animals of the respective group. Friedman's one-way repeated measures ANOVA by ranks: p = 0.014 for cD3r group; p = 0.238 for saline group.

coprecipitates. Consequently, Aβ(1−42) oligomer induced cytotoxicity was completely neutralized and there were no significant differences between buffer treated cells and Aβ(1−42) plus cD3r treated cells (p = 0.110). These findings support the theory of Aβ oligomers being the major cytotoxic species in AD. Additionally, our data show clearly that net charge increase and cyclization enhance the efficacy of D3. Thereby, Aβ(1−42) binding affinities, Aβ(1−42) oligomer elimination, and cytotoxic neutralization efficacies strongly correlated, except for the compound $D3_{CONH_2}$. Thereby, the morphology of the high molecular weight coprecipitates which are formed in the presence of the compounds seemed to have no influence on the cytotoxicity.

cD3r Improves Cognition of Transgenic AD Mice. In vitro experiments revealed that the compounds $D3_{CONH_2}$, cD3, and cD3r show enhanced performance in Aβ(1−42) binding affinity, elimination of Aβ(1−42) oligomers, and reduction of the cytotoxic effect of Aβ(1−42) compared to $D3_{COOH}$. The cyclic version with an arginine insertion, cD3r, showed the highest efficacy in these experiments. To evaluate cD3r as a potential therapeutic, the influence of cD3r treatment on the cognition of transgenic AD mice was examined. Tg-SwDI mice were used as mouse model. These mice express human Swedish, Dutch, and Iowa multiple mutant APP. From the age of three months, Tg-SwDI mice show Aβ deposits in the subiculum and impaired learning and memory effects without developing differences in mobility, strength, or coordination as compared to wildtype.[33,34]

In the current study, 48 weeks old male mice were intraperitoneally (i.p.) treated with a total amount of 5 mg cD3r (n = 9) or saline as a control (n = 10) over 4 weeks using osmotic minipumps (4.2 ± 0.1 mg kg^{-1} day^{-1}). The influence of the treatment on the exploratory behavior and anxiolytic activity was examined in the zero maze and open field tests.[35,36] cD3r treatment did not significantly affect the proportion of time spent in the center of the arena (open field, Figure 6A) or in the open quadrants (zero maze, Figure 6B), suggesting that the treatment with compound or saline had no side effects regarding exploratory behavior and anxiolytic activity of Tg-SwDI mice.

During the last week of treatment, the cognition of cD3r treated animals was investigated in a water maze over a period of 5 days, modified after the procedure developed by Morris.[37] Daily, the latency until each mouse found a hidden platform within the maze was measured for both groups (Figure 6C). Over a period of 5 days, the control group showed no significant differences in latency (p = 0.238), indicating neither spatial learning effects nor improved cognition. In contrast, cD3r treated animals required significantly less time over the tested period until they found the hidden platform (p = 0.014). Thus, Tg-SwDI mice improved in spatial cognition and memory after cD3r treatment.

In order to investigate whether cD3r influenced the Aβ plaque load, we performed an immunohistochemical analysis of the hippocampus of saline and cD3r treated animals. As already described for Tg-SwDI mice at the age of 12 months,[33] human Aβ was highly expressed and accumulated in the hippocampus area (Figure 7). Nevertheless, there were no significant changes

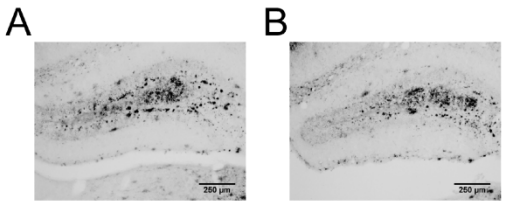

Figure 7. Aβ plaque load of saline and cD3r treated Tg-SwDI mice. After 4 weeks of treatment, Aβ plaque load in the hippocampus of saline or cD3r treated Tg-SwDI mice was analyzed by immunohistochemistry. Exemplary, brain slides of animal no. 5 (saline, A) and no. 8 (cD3r, B) are shown.

in Aβ plaque load analyzed after saline or cD3r treatment (p = 0.094, Table 1). Thus, we can conclude that therapeutic activity of cD3r shown by water maze performance did not result from alterations in Aβ plaque load. In accordance to our findings, Karran et al. reported that the correlation between cognitive alterations and Aβ plaque load in the brain is not linear.[2]

To further investigate the mechanism of action of cD3r in vivo, the concentrations of the cytokines interleukin-10 (IL-10), tumor necrosis factor alpha (TNFα), and interferon gamma (IFNγ) were determined in plasma samples after 4 weeks of treatment (Table 1). Although some values were below the limit of detection (LoD) and were excluded from evaluation, the data revealed that cD3r treatment had no significant influence on these cytokines in Tg-SwDI mice (p > 0.2). Therefore, we concluded that cD3r had no side effects on

DOI: 10.1021/acschemneuro.6b00047
ACS Chem. Neurosci. 2016, 7, 1088−1096

Table 1. Aβ plaque load is presented as staining density analyzed by immunohistochemistry of the hippocampus of saline or cD3r treated Tg-SwDi mice after 4 weeks of treatment. Cytokine concentrations in pg mL^{-1} were examined in plasma samples. Values below the limit of detection (LoD) were excluded from evaluation. Mann−Whitney U-test for saline vs. cD3r was applied

	Aβ plaque load		IL-10		TNFα		IFNγ	
animal	saline	cD3r	saline	cD3r	saline	cD3r	saline	cD3r
1	170.0	184.5	8.5	< LoD	< LoD	< LoD	< LoD	< LoD
2	173.0	170.5	25.9	31.1	1.1	0.6	< LoD	< LoD
3	164.0	160.0	< LoD	< LoD	< LoD	< LoD	< LoD	< LoD
4	169.5	167.0	27.4	13.1	0.6	< LoD	< LoD	< LoD
5	159.5	163.5	3.4	8.9	0.3	< LoD	< LoD	< LoD
6	138.5	157.0	9.2	34.4	< LoD	0.8	< LoD	< LoD
7	152.0	171.0	25.7	28.3	1.0	0.9	20.6	22.7
8	151.5	168.5	34.3	31.1	1.0	1.4	23.7	< LoD
9	139.5	169.0	11.6	28.1	0.4	0.8	22.5	21.7
10	139.0		31.6		0.6		23.1	
mean	155.7	167.9	19.7	25.0	0.7	0.9	22.5	22.2
SEM	4.1	2.5	3.6	3.5	0.1	0.1	0.6	0.4
p		0.094		0.244		0.511		0.817

inflammation and that the observed in vivo activity of cD3r in transgenic AD mice cannot be attributed to potential reduction of inflammation.

3. CONCLUSION

In this study, we showed that the compound $D3_{COOH}$ and its derivatives $D3_{CONH_2}$, cD3, and cD3r bound to Aβ(1−42) and eliminated cytotoxic Aβ(1−42) oligomers. In vitro, the eliminated Aβ(1−42) oligomers were converted into high molecular weight Aβ(1−42) coprecipitates which were non-toxic as shown using SH-SY5Y cells, independent of their morphology.

According to the efficacy of the compounds as a drug for the treatment of AD, the lead compound D3 can be already optimized by charge increase. Most probably, the electrostatic-driven interaction of D3 with negatively charged residues of Aβ is enhanced by net charge increase. This effect can especially be amplified by introducing arginine residues. Cyclization implied another optimization step with a similar degree of optimization. These two minor modifications are readily implemented and provide high potential to increase the therapeutic effect of D3. Indeed, by applying both modifications, $D3_{COOH}$ was successfully upgraded into the superior compound cD3r. Because treatment with cD3r yielded cognition enhancement in transgenic AD mice, we conclude that this compound shows therapeutic activity in vivo without changing Aβ plaque load or inflammation markers. Although various other mechanisms of action might underlay the observed cognition improvement, the elimination of Aβ oligomers is one potential mechanism. Therefore, cD3r represents a suitable candidate for further fit-for-purpose validation during clinical translation.

4. METHODS

Peptides. The compounds $D3_{COOH}$, $D3_{CONH_2}$, cD3, and cD3r consisted of D-enantiomeric amino acids and were synthesized by peptides and elephants (Germany) following the Fmoc strategy of solid phase peptide synthesis.[38] The cyclization was carried out with BOP while the peptides were still attached to the resin.[39,40] The compounds were acquired as lyophilized powder with >95% purity (Figure S1, Table S1).

Aβ(1−42) and N-terminally biotinylated Aβ(1−42) were purchased from Bachem (Germany) as lyophilized powder with >95% purity.

Preparation of Aβ(1−42) Solution. Lyophilized Aβ(1−42) and N-terminally biotinylated Aβ(1−42) were dissolved in 1,1,1,3,3,3-hexafluoro-2-propanol "overnight" (HFIP, Sigma-Aldrich, Germany) to destroy any existing aggregates, aliquoted, and stored at −20 °C. Before using, HFIP was evaporated in a vacuum concentrator 5301 (Eppendorf, Germany) and the Aβ(1−42) film was dissolved in 10 mM sodium phosphate buffer, pH 7.4.

Surface Plasmon Resonance. The affinity dissociation constants (K_D) of the compounds binding to monomeric Aβ(1−42) was determined by surface plasmon resonance (SPR) using a T200 device (Biacore, GE Healthcare, Sweden). The immobilization was performed as described by Frenzel et al. with minor modifications.[41] N-Terminally biotinylated Aβ(1−42) (8 μM) was dissolved and Aβ(1−42) monomers were purified via density gradient centrifugation using a discontinuous gradient containing 5 to 50% (w/v) iodixanol (OptiPrep, Axis-Shield, Norway). The species were separated at 259 000 × g for 3 h at 4 °C by ultracentrifugation (Optima MAX-XP, Beckman Coulter, USA). Afterward, the gradient was fractionated into 14 fractions of 140 μL. Aβ(1−42) monomers from the top fraction 1 were directly immobilized onto a series S SA sensor chip (Biacore, GE Healthcare, Sweden) by biotin−streptavidin coupling to a final level of 600 RU. The ligand flow cell and a reference flow cell were quenched with 10 μg mL^{-1} biotin for 7 min. For affinity determination of the compounds, single cycle kinetic experiments were applied at 25 °C and 30 μL min^{-1} flow rate. Concentrations of 0.6, 1.9, 5.6, 16.7, and 50 μM of the compounds diluted in 20 mM sodium phosphate buffer including 50 mM sodium chloride, pH 7.4 were injected over the flow cells for 180 s. A conditional regeneration step was implemented using 2 M guanidine hydrochloride for cD3r. The quenched flow cell and buffer cycles were used for double referencing of the sensorgrams. For evaluation, the sensorgrams were fitted applying the steady state Langmuir 1:1 fit model of the Biacore T200 Evaluation Software 2.0 and the offset was constantly set to zero.

QIAD Assay. The assay for quantitative determination of interference with Aβ aggregate size distribution (QIAD) of the compounds $D3_{COOH}$, $D3_{CONH_2}$, cD3, and cD3r was performed according to Brener et al.[16] In brief, 80 μM Aβ(1−42) was preincubated for 4.5 h followed by the addition of 20 μM of the respective compound for another 40 min. The Aβ(1−42) species were separated via density gradient centrifugation using a discontinuous gradient containing 5 to 50% (w/v) iodixanol (OptiPrep, Axis-Shield, Norway). Afterward, the gradient was fractionated into 15 fractions from top to bottom and the Aβ(1−42) distribution influenced by the compounds was quantified via analytical reversed-phase HPLC (Agilent 1260 Infinity system) using a C8 column (Zorbax 300SB-C8, 4.6 mm × 250 mm, 5 μm Agilent, Germany). The determined

DOI: 10.1021/acschemneuro.6b00047
ACS Chem. Neurosci. 2016, 7, 1088−1096

Aβ(1−42) concentrations in each fraction were normalized to the recovery rate of the whole gradient. The recovery rate for Aβ(1−42) without compound (n = 20) averaged to 99.3% ± 11.3%, for Aβ(1−42) with compound (n = 16) to 84.5% ± 15.6%.

Transmission Electron Microscopy. 20 μM Aβ(1−42) was preincubated for 4.5 h shaking at 600 rpm. Afterward, 20 μM $D3_{COOH}$, $D3_{CONH_2}$, cD3, or cD3r was added and coincubated for 16 h. A sample of 20 μL was dropped on a Formvar/carbon coated 200 mesh copper grid (Plano, Germany) for 7 min, and the grid was washed with deionized water. It was stained with 1% (w/v) uranyl acetate for 1 min, washed, and dried. Images were recorded at 120 kV using a Libra 120 transmission electron microscope (Zeiss, Germany).

Cell Viability Assay. 3-(4,5-Dimethylthiazol-2-yl)-2,5-diphenyltetrazolium bromide (MTT) based cell viability assays were performed to investigate the cytotoxicity of Aβ(1−42) in the presence of $D3_{COOH}$, $D3_{CONH_2}$, cD3, or cD3r. SH-SY5Y cells (DSMZ, Germany) were cultivated in DMEM supplemented with 20% fetal calf serum at 37 °C, 5% CO_2, and 95% humidity. The assay was performed using the Cell Proliferation Kit I (Roche, Switzerland) according to the manufacturer's protocol "Cytotoxicity assay procedure" whereby the seeded cell concentration was reduced to 1000 cells per well. A concentration of 50 μM Aβ(1−42) was incubated for 4.5 h shaking at 600 rpm before adding 250 μM $D3_{COOH}$, $D3_{CONH_2}$, cD3, or cD3r for another 40 min. During the assay the cells were exposed to final concentrations of 1 μM Aβ(1−42) plus 5 μM compound. For evaluation, the viability of buffer treated cells was set to 100%.

Animals. For evaluation of in vivo efficacy of cD3r, homozygous Tg-SwDI mice were used which are C57BL/6 mice expressing human APP with Swedish K670N/M671L and Dutch/Iowa E693Q/D694N mutations.[33] The animals housed four per cage in a controlled environment (22 °C, 50−60% humidity, light from 7 am to 7 pm) on food and water ad libitum. Animal experiments were conducted according to the local Institutional Animal Care and Use Committee (IACUC) guidelines.

Treatment of Tg-SwDI Mice. Male Tg-SwDI mice, 48 weeks old, were treated with cD3r compound or saline as a control for 4 weeks. Both groups started with n = 10, decided on the basis of previous studies.[15] After the study, one cD3r treated animal was excluded due to incorrect genotype. cD3r and saline were dosed intraperitoneally by osmotic minipumps (Alzet, #1004) which were implanted into the peritoneal cavity. After the implantation each animal housed separately. cD3r was applied in a concentration of 67.5 mg mL^{-1} with a flow rate of 0.11 μL h^{-1}, yielding a total applied amount of 5 mg. Three weeks after start of the treatment, the animals were double-blinded tested in open field and zero maze and the water maze experiments started. After 4 weeks, plasma samples were taken for cytokine analysis and the animals were sacrificed for Aβ plaque load analysis in the brain.

Open Field Test. The maze consisted of an arena of 42 cm × 42 cm with clear plexiglass sides (20 cm high). The arena was subdivided into two areas: the open center and the sides nearby the wall. The animal was put in the arena and observed for 4 min with a camera driven tracker system (Ethovision XT10, Noldus, The Netherlands). The system recorded the position of the animal within the arena at 5 frames per second and the data were analyzed with respect to the time spent in both areas. After each test, the apparatus was wiped out with chlorhexidine and 70% ethanol.

Zero Maze Test. The maze consisted of an annular maze (70 cm diameter) that is raised 40 cm above the table. The maze was separated into four equal parts by two 15 cm high walls of opaque material and two only 0.5 cm high walls. Therefore, it consisted of two open and two closed areas. The animal was put into the circle and observed for 4 min with a camera driven tracker system (Ethovision XT10, Noldus, The Netherlands). The system recorded the position of the animal at 5 frames per second and the data were analyzed with respect to the time spent in each area. After each test, the apparatus was wiped out with chlorhexidine and 70% ethanol.

Water Maze Test. To investigate the influence of cD3r on the cognition of Tg-SwDI mice, a water maze test was performed as described before.[42] Briefly, a blue plastic pool (120 cm diameter) with an opaque round platform (10 cm diameter) located 0.5 cm below the water surface was used. During 5 days, the mice were trained to find the hidden platform that was kept in a constant position throughout this period. Each day, three trials were run where all starting positions were equally used in a random order. The mice were given 60 s to find the platform and 10 s afterward to stay on the platform. If the animals did not locate the platform within this time they were placed there by the experimenter. The intertrial interval was 2 min. The task was evaluated by recording the latency of each animal until the platform was found.

Cytokine Assay. Plasma samples of saline and cD3r treated Tg-SwDI mice were tested for interleukin-2 (IL-2), interleukin-4 (IL-4), interleukin-6 (IL-6), interleukin-10 (IL-10), tumor necrosis factor alpha (TNFα), and interferon gamma (IFNγ) biomarkers using LUNARIS Mouse Cytokine 6-Plex Kit (Ayoxxa, Germany) according to the manufacturer's protocol. The limits of detection (LoD) were: IL-2: 0 pg mL^{-1}; IL-4: 55.4 pg mL^{-1}; IL-6: 11.3 pg mL^{-1}; IL-10: 2.2 pg mL^{-1}; TNFα: 0.3 pg mL^{-1}; IFNγ: 18.8 pg mL^{-1}. All samples were diluted 1:2. Results were analyzed using the LUNARIS Analysis Suite Software. The determined IL-2, IL-4, and IL-6 concentrations within the samples were, with a few exceptions, below the LoD and no statement was possible concerning these cytokines.

Aβ Plaque Analysis. Aβ plaque load of saline and cD3r treated Tg-SwDI mice was determined by immunohistochemistry. After 4 weeks of treatment, mice were anesthetized and transcardially perfused with cold saline. The brains were sagittally cut in half and the right hemisphere of the brain was fixed in 4% paraformaldehyde overnight and afterward placed in 30% sucrose for 24 h for cryoprotection. Thirty μm thick coronal sections were cut on a freezing sliding microtome. For staining, free floating sections were pretreated with sodium citrate solution, pH 6.5 for 30 min at 85 °C, washed with TBS including 0.5% Triton X-100 (TBS-T), and incubated in W0−2 antibody (The Genetics Company, Switzerland), diluted 1:2000 in TBS-T overnight. Afterward, the Mouse ExtrAvidin Peroxidase Staining Kit (Sigma-Aldrich) was used according to the manufacturer's protocol. After washing, the sections were stained for 3 min with Ni^{2+}-enhanced DAB solution. All sections from all animals were processed in the same tray.

After staining, sections were mounted on slides with coverslips. The hippocampus area of the brain was digitized using an Olympus DP70 digital camera. To avoid changes in lighting which might affect measurements, all images were acquired in one session. For evaluation, the average density of staining by the antibody in the measured area was calculated. All density measurements were performed in triplicate by an investigator who was blinded to the treatment of the animals.

Statistical Analysis. Data were averaged and represented as mean ± standard deviation (SD), standard error (SE), or standard error of the mean (SEM), as indicated. For plotting and statistical evaluation, OriginPro 8.5G (OrigínLab) was used; $p > 0.05$ was considered as not significant (n.s.).

QIAD assay: Data of each group were normally distributed (Shapiro-Wilk test: $p \leq 0.05$). One-way ANOVA and Bonferroni post hoc analysis were applied. Aβ(1−42) without compound: n = 21; Aβ(1−42) with compound: n = 4.

Cell viability assay: Data were not normally distributed (Shapiro-Wilk test: $p > 0.05$). Kruskal−Wallis ANOVA and Bonferroni corrected Mann−Whitney U-test were applied. Aβ(1−42) without compound: n = 45; Aβ(1−42) with compound: n = 15.

Open field test: Data were not normally distributed (Shapiro-Wilk test: $p > 0.05$) and Mann−Whitney U-test was applied. Saline group: n = 10; cD3r group: n = 9.

Zero maze test: Data were not normally distributed (Shapiro-Wilk test: $p > 0.05$) and Mann−Whitney U-test was applied. Saline group: n = 10; cD3r group: n = 8.

Water maze test: Data were not normally distributed (Shapiro-Wilk test: $p > 0.05$) and Friedman's one-way repeated measures ANOVA by ranks was applied. Saline group: n = 10; cD3r group: n = 9.

Cytokine assay and Aβ plaque analysis: Data were not normally distributed (Shapiro-Wilk test: $p > 0.05$) and Mann−Whitney U-test

DOI: 10.1021/acschemneuro.6b00047
ACS Chem. Neurosci. 2016, 7, 1088−1096

was applied. Values < LoD were excluded from statistics. Thus, *n* varied between the tests and can be obtained from Table 1.

■ ASSOCIATED CONTENT

Supporting Information

The Supporting Information is available free of charge on the ACS Publications website at DOI: 10.1021/acschemneuro.6b00047.

Analytical RP-HPLC chromatograms of the compounds and controls for cell viability assay (PDF)

■ AUTHOR INFORMATION

Corresponding Author

*E-mail: d.willbold@fz-juelich.de.

Author Contributions

T.Z., O.B., T.v.G., I.K., D.F., J.K., L.G., L.N.-S., and D.W. designed the experiments. T.Z., O.B., T.v.G., I.K., and M.T. performed experiments. T.Z., O.B., J.K., K.R., L.G., L.N.-S., and D.W. analyzed the data. T.Z., L.G., and D.W. wrote the paper with input from coauthors.

Funding

This work was funded by the Portfolio Technology and Medicine, the Portfolio Drug Research, and the "Helmholtz-Validierungsfond" of the "Impuls- und Vernetzungsfond der Helmholtzgemeinschaft", and by the Technology Transfer Department of the Forschungszentrum Jülich.

Notes

The authors declare no competing financial interest.

■ ABBREVIATIONS

$D3_{COOH}$, unmodified D3 peptide (rprtrlhthrnr); $D3_{CONH_2}$, C-terminally amidated D3 peptide; cD3, head to tail cyclized version of D3; cD3r, head to tail cyclized D3 with an additional arginine (rprtrlhthrnrr)

■ REFERENCES

(1) Jellinger, K. A. (2006) Alzheimer 100–highlights in the history of Alzheimer research. *J. Neural Transm 113*, 1603−1623.

(2) Karran, E., Mercken, M., and De Strooper, B. (2011) The amyloid cascade hypothesis for Alzheimer's disease: an appraisal for the development of therapeutics. *Nat. Rev. Drug Discovery 10*, 698−712.

(3) Selkoe, D. J. (2003) Folding proteins in fatal ways. *Nature 426*, 900−904.

(4) Haass, C., and Selkoe, D. J. (2007) Soluble protein oligomers in neurodegeneration: lessons from the Alzheimer's amyloid beta-peptide. *Nat. Rev. Mol. Cell Biol. 8*, 101−112.

(5) Finder, V. H., and Glockshuber, R. (2007) Amyloid-beta aggregation. *Neurodegener. Dis. 4*, 13−27.

(6) Walsh, D. M., Klyubin, I., Fadeeva, J. V., Cullen, W. K., Anwyl, R., Wolfe, M. S., Rowan, M. J., and Selkoe, D. J. (2002) Naturally secreted oligomers of amyloid beta protein potently inhibit hippocampal long-term potentiation in vivo. *Nature 416*, 535−539.

(7) Glabe, C. G., and Kayed, R. (2006) Common structure and toxic function of amyloid oligomers implies a common mechanism of pathogenesis. *Neurology 66*, S74−78.

(8) Cohen, S. I., Arosio, P., Presto, J., Kurudenkandy, F. R., Biverstal, H., Dolfe, L., Dunning, C., Yang, X., Frohm, B., Vendruscolo, M., Johansson, J., Dobson, C. M., Fisahn, A., Knowles, T. P., and Linse, S. (2015) A molecular chaperone breaks the catalytic cycle that generates toxic Abeta oligomers. *Nat. Struct. Mol. Biol. 22*, 207−213.

(9) van Groen, T., Wiesehan, K., Funke, S. A., Kadish, I., Nagel-Steger, L., and Willbold, D. (2008) Reduction of Alzheimer's disease amyloid plaque load in transgenic mice by D3, A D-enantiomeric peptide identified by mirror image phage display. *ChemMedChem 3*, 1848−1852.

(10) Schumacher, T. N., Mayr, L. M., Minor, D. L., Jr., Milhollen, M. A., Burgess, M. W., and Kim, P. S. (1996) Identification of D-peptide ligands through mirror-image phage display. *Science 271*, 1854−1857.

(11) Wiesehan, K., and Willbold, D. (2003) Mirror-image phage display: aiming at the mirror. *ChemBioChem 4*, 811−815.

(12) Funke, S. A., Liu, H., Sehl, T., Bartnik, D., Brener, O., Nagel-Steger, L., Wiesehan, K., and Willbold, D. (2012) Identification and characterization of an abeta oligomer precipitating peptide that may be useful to explore gene therapeutic approaches to Alzheimer disease. *Rejuvenation Res. 15*, 144−147.

(13) Jiang, N., Leithold, L. H., Post, J., Ziehm, T., Mauler, J., Gremer, L., Cremer, M., Schartmann, E., Shah, N. J., Kutzsche, J., Langen, K. J., Breitkreutz, J., Willbold, D., and Willuweit, A. (2015) Preclinical Pharmacokinetic Studies of the Tritium Labelled D-Enantiomeric Peptide D3 Developed for the Treatment of Alzheimer s Disease. *PLoS One 10*, e0128553.

(14) Wiesehan, K., Stohr, J., Nagel-Steger, L., van Groen, T., Riesner, D., and Willbold, D. (2008) Inhibition of cytotoxicity and amyloid fibril formation by a D-amino acid peptide that specifically binds to Alzheimer's disease amyloid peptide. *Protein Eng., Des. Sel. 21*, 241−246.

(15) Aileen Funke, S., van Groen, T., Kadish, I., Bartnik, D., Nagel-Steger, L., Brener, O., Sehl, T., Batra-Safferling, R., Moriscot, C., Schoehn, G., Horn, A. H., Muller-Schiffmann, A., Korth, C., Sticht, H., and Willbold, D. (2010) Oral treatment with the d-enantiomeric peptide D3 improves the pathology and behavior of Alzheimer's Disease transgenic mice. *ACS Chem. Neurosci. 1*, 639−648.

(16) Brener, O., Dunkelmann, T., Gremer, L., van Groen, T., Mirecka, E. A., Kadish, I., Willuweit, A., Kutzsche, J., Jurgens, D., Rudolph, S., Tusche, M., Bongen, P., Pietruszka, J., Oesterhelt, F., Langen, K. J., Demuth, H. U., Janssen, A., Hoyer, W., Funke, S. A., Nagel-Steger, L., and Willbold, D. (2015) QIAD assay for quantitating a compound's efficacy in elimination of toxic Abeta oligomers. *Sci. Rep. 5*, 13222.

(17) van Groen, T., Kadish, I., Funke, A., Bartnik, D., and Willbold, D. (2012) Treatment with Abeta42 binding D-amino acid peptides reduce amyloid deposition and inflammation in APP/PS1 double transgenic mice. *Adv. Protein Chem. Struct. Biol. 88*, 133−152.

(18) van Groen, T., Kadish, I., Wiesehan, K., Funke, S. A., and Willbold, D. (2009) In vitro and in vivo staining characteristics of small, fluorescent, Abeta42-binding D-enantiomeric peptides in transgenic AD mouse models. *ChemMedChem 4*, 276−282.

(19) Olubiyi, O. O., Frenzel, D., Bartnik, D., Gluck, J. M., Brener, O., Nagel-Steger, L., Funke, S. A., Willbold, D., and Strodel, B. (2014) Amyloid aggregation inhibitory mechanism of arginine-rich D-peptides. *Curr. Med. Chem. 21*, 1448−1457.

(20) Vlieghe, P., Lisowski, V., Martinez, J., and Khrestchatisky, M. (2010) Synthetic therapeutic peptides: science and market. *Drug Discovery Today 15*, 40−56.

(21) Edman, P. (1959) Chemistry of amino acids and peptides. *Annu. Rev. Biochem. 28*, 69−96.

(22) Horton, D. A., Bourne, G. T., and Smythe, M. L. (2000) Exploring privileged structures: the combinatorial synthesis of cyclic peptides. *Mol. Diversity 5*, 289−304.

(23) Joo, S. H. (2012) Cyclic peptides as therapeutic agents and biochemical tools. *Biomol. Ther. 20*, 19−26.

(24) Rzepecki, P., Nagel-Steger, L., Feuerstein, S., Linne, U., Molt, O., Zadmard, R., Aschermann, K., Wehner, M., Schrader, T., and Riesner, D. (2004) Prevention of Alzheimer's disease-associated Abeta aggregation by rationally designed nonpeptidic beta-sheet ligands. *J. Biol. Chem. 279*, 47497−47505.

(25) Ward, R. V., Jennings, K. H., Jepras, R., Neville, W., Owen, D. E., Hawkins, J., Christie, G., Davis, J. B., George, A., Karran, E. H., and Howlett, D. R. (2000) Fractionation and characterization of oligomeric, protofibrillar and fibrillar forms of beta-amyloid peptide. *Biochem. J. 348* (Pt 1), 137−144.

DOI: 10.1021/acschemneuro.6b00047
ACS Chem. Neurosci. 2016, 7, 1088−1096

(26) Cukalevski, R., Yang, X. T., Meisl, G., Weininger, U., Bernfur, K., Frohm, B., Knowles, T. P. J., and Linse, S. (2015) The A beta 40 and A beta 42 peptides self-assemble into separate homomolecular fibrils in binary mixtures but cross-react during primary nucleation. *Chem. Sci. 6*, 4215−4233.
(27) Yankner, B. A., Duffy, L. K., and Kirschner, D. A. (1990) Neurotrophic and neurotoxic effects of amyloid beta protein: reversal by tachykinin neuropeptides. *Science 250*, 279−282.
(28) Li, Y. P., Bushnell, A. F., Lee, C. M., Perlmutter, L. S., and Wong, S. K. (1996) Beta-amyloid induces apoptosis in human-derived neurotypic SH-SY5Y cells. *Brain Res. 738*, 196−204.
(29) Mosmann, T. (1983) Rapid colorimetric assay for cellular growth and survival: application to proliferation and cytotoxicity assays. *J. Immunol. Methods 65*, 55−63.
(30) Arai, T., Araya, T., Sasaki, D., Taniguchi, A., Sato, T., Sohma, Y., and Kanai, M. (2014) Rational design and identification of a non-peptidic aggregation inhibitor of amyloid-beta based on a pharmacophore motif obtained from cyclo[-Lys-Leu-Val-Phe-Phe-]. *Angew. Chem., Int. Ed. 53*, 8236−8239.
(31) Cho, P. Y., Joshi, G., Boersma, M. D., Johnson, J. A., and Murphy, R. M. (2015) A Cyclic Peptide Mimic of the beta-Amyloid Binding Domain on Transthyretin. *ACS Chem. Neurosci. 6*, 778−789.
(32) Hoogerhout, P., Kamphuis, W., Brugghe, H. F., Sluijs, J. A., Timmermans, H. A., Westdijk, J., Zomer, G., Boog, C. J., Hol, E. M., and van den Dobbelsteen, G. P. (2011) A cyclic undecamer peptide mimics a turn in folded Alzheimer amyloid beta and elicits antibodies against oligomeric and fibrillar amyloid and plaques. *PLoS One 6*, e19110.
(33) Davis, J., Xu, F., Deane, R., Romanov, G., Previti, M. L., Zeigler, K., Zlokovic, B. V., and Van Nostrand, W. E. (2004) Early-onset and robust cerebral microvascular accumulation of amyloid beta-protein in transgenic mice expressing low levels of a vasculotropic Dutch/Iowa mutant form of amyloid beta-protein precursor. *J. Biol. Chem. 279*, 20296−20306.
(34) Xu, F., Grande, A. M., Robinson, J. K., Previti, M. L., Vasek, M., Davis, J., and Van Nostrand, W. E. (2007) Early-onset subicular microvascular amyloid and neuroinflammation correlate with behavioral deficits in vasculotropic mutant amyloid beta-protein precursor transgenic mice. *Neuroscience 146*, 98−107.
(35) Archer, J. (1973) Tests for emotionality in rats and mice: a review. *Anim. Behav. 21*, 205−235.
(36) Shepherd, J. K., Grewal, S. S., Fletcher, A., Bill, D. J., and Dourish, C. T. (1994) Behavioural and pharmacological characterisation of the elevated "zero-maze" as an animal model of anxiety. *Psychopharmacology 116*, 56−64.
(37) Morris, R. (1984) Developments of a water-maze procedure for studying spatial learning in the rat. *J. Neurosci. Methods 11*, 47−60.
(38) Stawikowski, M., and Fields, G. B. (2012) Introduction to peptide synthesis. *Curr. Protoc. Protein Sci. 69*, 18.1.1−18.1.13.
(39) Fournier, A., Wang, C. T., and Felix, A. M. (1988) Applications of BOP reagent in solid phase synthesis. Advantages of BOP reagent for difficult couplings exemplified by a synthesis of [Ala 15]-GRF(1−29)-NH2. *Int. J. Pept. Protein Res. 31*, 86−97.
(40) Plaue, S. (1990) Synthesis of cyclic peptides on solid support. Application to analogs of hemagglutinin of influenza virus. *Int. J. Pept. Protein Res. 35*, 510−517.
(41) Frenzel, D., Gluck, J. M., Brener, O., Oesterhelt, F., Nagel-Steger, L., and Willbold, D. (2014) Immobilization of homogeneous monomeric, oligomeric and fibrillar Abeta species for reliable SPR measurements. *PLoS One 9*, e89490.
(42) van Groen, T., Kadish, I., Funke, S. A., Bartnik, D., and Willbold, D. (2013) Treatment with D3 removes amyloid deposits, reduces inflammation, and improves cognition in aged AbetaPP/PS1 double transgenic mice. *J. Alzheimer's Dis. 34*, 609−620.

DOI: 10.1021/acschemneuro.6b00047
ACS Chem. Neurosci. 2016, 7, 1088−1096

Supporting Information

Increase of Positive Net Charge and Conformational Rigidity Enhances the Efficacy of D-Enantiomeric Peptides Designed to Eliminate Cytotoxic Aβ Species

Tamar Ziehm[1], Oleksandr Brener[1,2], Thomas van Groen[3], Inga Kadish[3], Daniel Frenzel[1], Markus Tusche[1], Janine Kutzsche[1], Kerstin Reiß[1], Lothar Gremer[1,2], Luitgard Nagel-Steger[1,2], Dieter Willbold[1,2,*]

[1]Institute of Complex Systems, Structural Biochemistry (ICS-6), Forschungszentrum Jülich, 52425 Jülich, Germany
[2]Institut für Physikalische Biologie, Heinrich-Heine-Universität Düsseldorf, 40225 Düsseldorf,
Germany
[3]Department of Cell, Developmental and Integrative Biology, University of Alabama at Birmingham (UAB), Birmingham, Alabama 35233, United States
[*]Corresponding Author: d.willbold@fz-juelich.de

Keywords: Alzheimer´s disease, amyloid-beta, drug discovery, D-enantiomeric peptides, cyclization, charge increase

1. SI Methods

Analytical RP-HPLC: To evaluate the compounds´ purity of > 95%, analytical reversed-phase high performance liquid chromatography (RP-HPLC) was used. 20 µL of a 20 µM compound solution in H_2O were injected on a Zorbax 300SB-C8 column (4.6 mm × 250 mm, 5 µm, Agilent, Germany) connected to an Agilent 1260 Infinity system and analyzed isocratically at 14% acetonitrile containing 0.1% trifluoroacetic acid (TFA) at 21°C and a flow rate of 1 mL min^{-1}. Absorbance was measured at 214 nm and the data were analyzed using ChemStation (Agilent, Germany).

Cell viability assay: MTT based cell viability assays were performed as described in the manuscript. Here, the cytotoxicity of the compounds $D3_{COOH}$, $D3_{CONH2}$, cD3, or cD3r themselves were investigated. During the assay the cells were exposed to a final concentration of 5 µM compound.

Statistical analysis: Data were averaged and represented as mean ± standard deviation (SD). For plotting and statistical evaluation OriginPro 8.5G (OriginLab, USA) was used; $p > 0.05$ was considered as not significant (n.s.).
Cell viability assay: Data were not normally distributed (Shapiro-Wilk test: $p > 0.05$). Kruskal-Wallis ANOVA and Bonferroni corrected Mann-Whitney U-test were applied. Buffer and all compounds: $n = 5$.

2. SI Figures

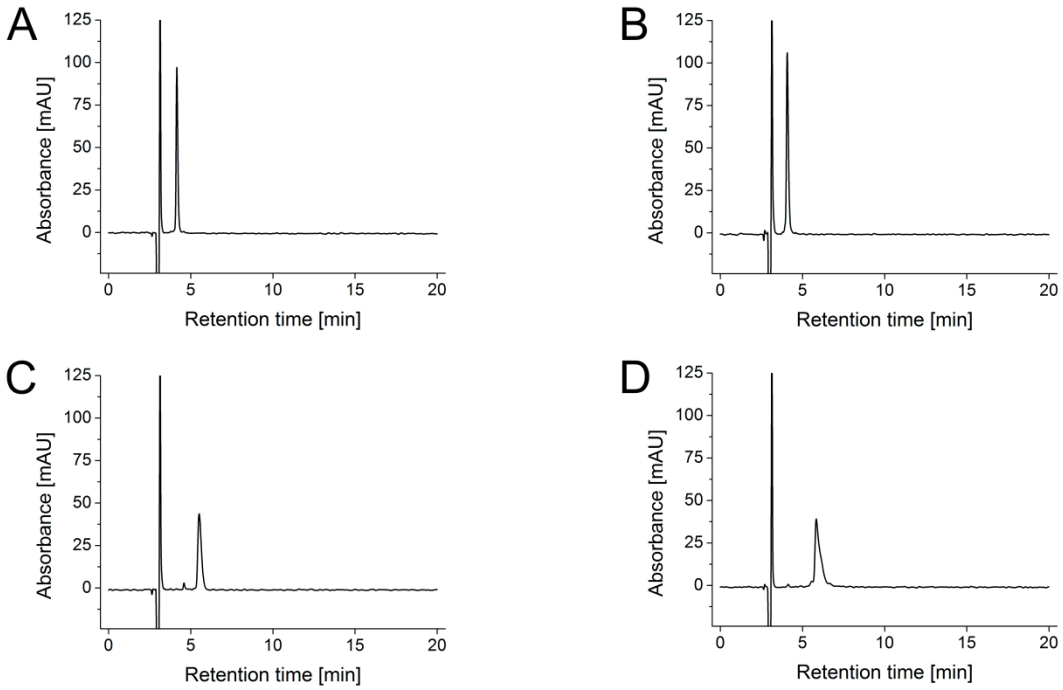

Figure S1: RP-HPLC chromatograms of $D3_{COOH}$, $D3_{CONH_2}$, cD3, or cD3r.

The purity of $D3_{COOH}$ (A), $D3_{CONH_2}$ (B), cD3 (C), and cD3r (D) was evaluated using analytical reversed-phase high performance liquid chromatography (RP-HPLC). Absorbance was measured at 214 nm and the data were analyzed using ChemStation (Agilent, Germany).

Table S1: Purity of the compounds analyzed by peak integration of RP-HPLC chromatograms. Peaks which show > 95% of the total peak area represent the respective compound.

Compound	Peak no.	Retention time [min]	Peak area [%]
$D3_{COOH}$	1	3.78	1.1
	2	4.15	97.2
	3	4.58	1.7
$D3_{CONH_2}$	1	3.79	0.7
	2	4.07	98.2
	3	4.42	1.1
cD3	1	4.59	3.1
	2	5.27	0.9
	3	5.51	96.0
cD3r	1	4.14	1.5
	2	5.48	2.9
	3	5.84	95.7

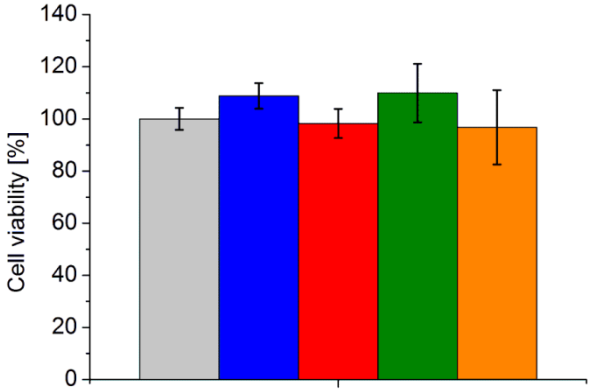

Figure S2: MTT based cytotoxicity test of the compounds $D3_{COOH}$, $D3_{CONH_2}$, cD3, or cD3r.
As a control experiment, the cytotoxicity of 5 μM compound was examined based on the MTT assay principle using SH-SY5Y cells. The data represent mean ± SD of one experiment with n = 5 for each compound, normalized to the buffer control. Kruskal-Wallis ANOVA (p = 0.098) with Bonferroni corrected Mann-Whitney U-test were not significant (p > 0.05) for all compounds. Gray, buffer control; blue, $D3_{COOH}$; red, $D3_{CONH_2}$; green, cD3; orange, cD3r.

3.3 Optimization of the All-D Peptide D3 for Aβ Oligomer Elimination

Antonia N Klein, Tamar Ziehm, Markus Tusche, Johan Buitenhuis, Dirk Bartnik, Annett Boeddrich, Thomas Wiglenda, Erich Wanker, Susanne A Funke, Oleksandr Brener, Lothar Gremer, Janine Kutzsche, Dieter Willbold

PLoS One. 2016 Apr 22;11(4):e0153035

doi: 10.1371/journal.pone.0153035

PLOS ONE

RESEARCH ARTICLE

Optimization of the All-D Peptide D3 for Aβ Oligomer Elimination

Antonia Nicole Klein[1], Tamar Ziehm[1], Markus Tusche[1], Johan Buitenhuis[2], Dirk Bartnik[1], Annett Boeddrich[3], Thomas Wiglenda[3], Erich Wanker[3], Susanne Aileen Funke[1,4], Oleksandr Brener[1,5], Lothar Gremer[1,5], Janine Kutzsche[1], Dieter Willbold[1,5]*

1 Institute of Complex Systems, Structural Biochemistry (ICS-6), Research Center Jülich, 52425, Jülich, Germany, **2** Institute of Complex Systems, Soft Matter (ICS-3), Research Center Jülich, 52425, Jülich, Germany, **3** Neuroproteomforschung und Molekulare Mechanismen Neurodegenerativer Erkrankungen, Max-Delbrück-Centrum für Molekulare Medizin, Berlin, Germany, **4** Bioanalytik, Fakultät angewandte Naturwissenschaften, Hochschule für angewandte Wissenschaften Coburg, 96450, Coburg, Germany, **5** Institut für Physikalische Biologie, Heinrich-Heine-Universität Düsseldorf, 40225, Düsseldorf, Germany

* d.willbold@fz-juelich.de

OPEN ACCESS

Citation: Klein AN, Ziehm T, Tusche M, Buitenhuis J, Bartnik D, Boeddrich A, et al. (2016) Optimization of the All-D Peptide D3 for Aβ Oligomer Elimination. PLoS ONE 11(4): e0153035. doi:10.1371/journal.pone.0153035

Editor: Damian Christopher Crowther, MedImmune Ltd Research and Development, UNITED KINGDOM

Received: November 16, 2015

Accepted: March 22, 2016

Published: April 22, 2016

Data Availability Statement: All data are within this paper.

Funding: D. W. was supported by grants from the "Portfolio Technology and Medicine", the "Portfolio Drug Research" and the Helmholtz-Validierungsfonds of the Impuls und Vernetzungs-Fonds der Helmholtzgemeinschaft. D.W. was also supported by the TT-Fonds of the Technology Transfer Department of the Forschungszentrum Jülich.

Competing Interests: The authors have declared that no competing interests exist.

Abstract

The aggregation of amyloid-β (Aβ) is postulated to be the crucial event in Alzheimer's disease (AD). In particular, small neurotoxic Aβ oligomers are considered to be responsible for the development and progression of AD. Therefore, elimination of thesis oligomers represents a potential causal therapy of AD. Starting from the well-characterized D-enantiomeric peptide D3, we identified D3 derivatives that bind monomeric Aβ. The underlying hypothesis is that ligands bind monomeric Aβ and stabilize these species within the various equilibria with Aβ assemblies, leading ultimately to the elimination of Aβ oligomers. One of the hereby identified D-peptides, DB3, and a head-to-tail tandem of DB3, DB3DB3, were studied in detail. Both peptides were found to: (i) inhibit the formation of Thioflavin T-positive fibrils; (ii) bind to Aβ monomers with micromolar affinities; (iii) eliminate Aβ oligomers; (iv) reduce Aβ-induced cytotoxicity; and (v) disassemble preformed Aβ aggregates. The beneficial effects of DB3 were improved by DB3DB3, which showed highly enhanced efficacy. Our approach yielded Aβ monomer-stabilizing ligands that can be investigated as a suitable therapeutic strategy against AD.

Introduction

There are 4.2 million new cases of dementia worldwide each year with Alzheimer's disease (AD) being the most common cause. Currently, there is no causal treatment for AD available [1, 2].

Intracellular neurofibrillary tangles (NFTs), consisting of hyperphosphorylated tau and extracellular plaques, consisting predominantly of amyloid-β (Aβ), are the major pathological hallmarks of AD. The cleavage of the amyloid precursor protein (APP) by the β- and γ- secretases releases Aβ. Various species of Aβ are formed because the N- and C-terminal cleavage events are non-homogeneous. The most abundant species of Aβ is Aβ(1–40), consisting of 40 amino acids. The second most dominant species is Aβ(1–42) [3, 4].

According to the amyloid cascade hypothesis the aggregation of Aβ is responsible for the development and the progression of AD. Various Aβ aggregate species have been described, including Aβ oligomers and Aβ protofibrils [5]. In particular, soluble, toxic Aβ oligomers are thought to be responsible for damage of synaptic plasticity, formation of free radicals, disequilibrium of intracellular calcium distribution, chronic inflammation and increased phosphorylation of tau [6, 7]. Thus, inhibition of Aβ oligomerization and the elimination of Aβ oligomers are promising treatment strategies for the development of a causal therapy of AD.

We have previously selected the 12mer all-D-enantiomeric peptide D3 via mirror image phage display [8, 9]. *In vitro*, D3 binds to amyloid plaques, reduces Aβ aggregation to regular fibrils, eliminates Aβ oligomers and converts preformed fibrils into non-amyloidogenic, non-fibrillar, non-toxic aggregates [10–14]. *In vivo*, the plaque load and cerebral inflammation of transgenic mice is reduced after injection of D3 into the brain and cognitive impairment of transgenic mice is improved after oral application [10, 15, 16]. The original phage library, from which D3 was selected, coded for about 10^9 different peptides. A fully randomized 12mer library would contain 20^{12} different peptides. That equals 4 x 10^{15} theoretically possible 12mer sequences and is absolutely impossible to achieve due to limitations in the transformation efficiency during generation of the original phage library. Thus, it can be expected that variation of the D3 sequence will lead to even more potent D3 derivatives.

In the present study, we screened for D3 derivatives with optimized efficiency. To facilitate the screening for various derivatives, peptide microarrays were used because they allow miniaturization, parallelization and automation, and enable high-throughput screenings [17, 18]. In addition, non-natural amino acids and linker groups, like biotin or fluorescein, can be introduced easily.

We screened more than 600 different D3 derivatives for their ability to bind monomeric Aβ and characterized the five most promising candidates by examining their ability to prevent Aβ fibril formation. For further optimization, the most promising D3 derivative DB3 was modified by designing a head-to-tail tandem peptide, called DB3DB3. Both peptides were characterized in more detail regarding their affinity to Aβ monomers and their efficiency to eliminate Aβ oligomers.

Material and Methods

Peptides

Aβ(1–42), N-terminally biotinylated Aβ(1–42) and FITC-Aβ(1–42) were purchased from Bachem (Heidelberg, Germany). D3 (RPRTRLHTHRNR), DB1 (RPITRLHTDRNR), DB2 (RPITTLQTHQNR), DB3 (RPITRLRTHQNR), DB4 (RPRTRLRTHQNR) and DB5 (RPITRLQTHEQR) were purchased from JPT (Berlin, Germany). DB3DB3 (RPITRLRTHQNRRPITRLRTHQNR) was purchased from peptides&elephants (Potsdam, Germany). All D-peptides consisted of D-enantiomeric amino acids, were C-terminally amidated and > 95% pure.

HFIP pretreatment of Aβ(1–42)

For obtaining monomeric Aβ(1–42), N-terminally biotinylated Aβ(1–42) and FITC-Aβ(1–42) were dissolved in 1,1,1,3,3,3-hexafluoroisopropanol (HFIP) overnight to a final concentration of 1 mg/ml and aliquoted. HFIP was evaporated by vacuum concentration (Concentrator 5301, Eppendorf, Germany) for 20 min and the aliquots were stored at -20°C until further usage.

Peptide Microarrays

Pepspot membranes. In a first generation peptide array, every position of the 12 amino acid residue D-peptide D3 was replaced against all 20 naturally occurring amino acids in their D-enantiomeric conformation. The nitrocellulose membrane spotted with these 240 different

peptides (JPT, Berlin, Germany) was blocked using TBS pH 7.4 with 10% v/v blocking solution (Roche, Basel, Switzerland) for 2.5 h at room temperature. After 5 min washing with TBS and 0.1% v/v Tween 20 (TBS-T), the membrane was incubated with 5 μM Aβ(1–42) in 10 mM sodium phosphate buffer pH 7.4 for 1 h. The potential of all 240 derivatives to bind monomeric Aβ was measured by applying 6E10 (BioLegend, San Diego, USA, diluted 1:10.000 in TBS pH 7.4) and a horseradish peroxidase (HRP)-conjugated goat anti-mouse antibody (Fisher Scientific, Schwerte, Germany, diluted 1:10.000 in TBS pH 7.4). The membrane was washed with TBS-T pH 7.4 for 2 h. HRP activity was measured after incubation with HRP substrate (Pierce, Waltham, USA) by using a ChemiDoc 200 detection system (Bio-Rad Laboratories, Munich, Germany) and the ImageLab software (Bio-Rad Laboratories, Hercules, Munich, Germany).

Pepscan. For the second generation a peptide microarray was produced by Pepscan (Lelystad, Netherlands).

For the Pepscan chip, the peptides were covalently coupled on glass slides in triplicate (spots with diameter of 100 μm). Slides were incubated with 5 μM FITC-Aβ(1–42) in 10 mM sodium phosphate buffer pH 7.4 for 1 h at room temperature with gentle agitation. After incubation, the slides were washed three times with TBS-T for 10 min, three times with water for 10 min and subsequently dried using a stream of nitrogen gas.

Fluorescence intensity of FITC-Aβ(1–42) bound to the peptide spots was measured by a FLA800 fluorescence image system (Fujifilm Medical Systems USA Inc, Stamford, USA) with a slide carrier employing a 473 nm laser for excitation. Digital images were recorded at 5 μm resolution. Fluorescence was analyzed by the software AIDA Array Metrix (Raytest, Staubenhardt, Germany). Signals were integrated for each spot (diameter 80 μm). The background signal was detected from local dot rings with diameter widths of 150 μm and background ring widths of 30 μm, and subtracted from the peptide spot signal.

Thioflavin T (ThT) Assay

20 μM Aβ(1–42) was mixed with 20 μM Thioflavin T (ThT) and 31 μg/ml DB3 or DB3DB3 in 10 mM sodium phosphate buffer, pH 7.4. The assay was performed using a non-binding 96 well plate (Greiner Bio-One, Frickenhausen, Germany). ThT fluorescence was measured every 15 min at λ_{ex} = 440 nm and λ_{em} = 490 nm in a temperature-controlled plate reader (Polarstar Optima, BMG, Offenburg, Germany) at 37°C with 1 min agitation before every measurement. Each value was background corrected using the ThT fluorescence of a peptide solution without Aβ(1–42).

Biolayer interferometry (BLI)

BLI experiments were performed using an Octet RED96 instrument (fortéBIO, PALL Life Science, Menlo Park, USA). N-terminally biotinylated Aβ(1–42) was dissolved in HFIP, lyophilized and dissolved in 2 mM aqueous sodium hydroxide (1 mg/ml) in order to destroy any pre-existing aggregates. The Aβ(1–42) solution was neutralized by dilution in running buffer (20 mM sodium phosphate buffer, pH 7.4) to a final concentration of 20 μg/ml and directly immobilized on Super Streptavidin biosensors (SSA) (fortéBIO, PALL Life Science, Menlo Park, USA) to a final depth of 3 nm. Ligand biosensors and reference biosensors were quenched with 20 μg/ml biotin for 7 min.

For K_D determinations, the binding of a dilution series of DB3 (200, 100, 50, 25, 12.5, 6.25, 3.125 μM) or DBDB3 (20, 10, 5, 2.5, 1.25, 0.625, 0.3125 μM) was detected in parallel to the ligand biosensors and reference biosensors. A separate buffer cycle was used for double referencing. For evaluation, steady state response levels were plotted against the applied peptide concentrations and fitted according to Langmuir´s 1:1 binding model (Hill function with $n = 1$, OriginPro 8.5G, OriginLab, Northampton, USA).

QIAD assay

The quantitative determination of interference with Aβ(1–42) aggregate size distribution (QIAD) was performed as described before [14]. In brief, 80 μM Aβ(1–42) was incubated in 10 mM sodium phosphate buffer, pH 7.4 for 4.5 h at 22°C with 600 rpm agitation. Aβ(1–42) aggregation was continued for an additional 40 min with or without DB peptide. The obtained partial size distribution was analyzed by applying density gradient centrifugation. 100 μl of the incubated sample was placed on top of a gradient with 5 to 50% iodixanol (Optiprep, Axis-shield, Oslo, Norway) and separated at 259.000 x g for 3 h at 4°C using an ultracentrifuge (Optima MAX-XP, Beckman Coulter, Brea, USA). Fourteen fractions of 140 μl were taken from top to bottom. The pellet was dissolved by adding 60 μl of 6 M guanidine hydrochloride to the centrifugation tube. After boiling for 5 min, the dissolved pellet sample was collected. The samples were stored at -80°C until further use.

For quantification of the Aβ(1–42) amount in each fraction, reversed-phase high performance liquid chromatography (RP-HPLC) was performed using a Zorbax SB-300 C8 column (Agilent, Böblingen, Germany) connected to an Agilent 1260 Infinity system using 30% (v/v) acetonitrile with 0.1% (v/v) trifluoroacetic acid (TFA) as the mobile phase with a flow of 1 ml/min and a column temperature of 80°C. The applied sample volume was 20 μl. The UV absorption at 214 nm was measured. For quantification of the Aβ(1–42) amount, the area under the peak representing Aβ(1–42) was calculated and the molar concentration was determined using a calibration curve.

For additional control and visualization of the Aβ content in each fraction, a 16% tricine-SDS-PAGE was performed and Aβ(1–42) was visualized by silver staining according to Schagger [19].

MTT cell viability assay

Rat pheochromocytoma PC12 cells (Leibniz Institute DSMZ, Braunschweig, Germany) were cultivated in DMEM medium supplemented with 10% fetal bovine serum and 5% horse serum. 10,000 cells per well were seeded on collagen-coated 96 well plates (Gibco, Life technology, Carlsberg, USA) and incubated in a 95% humidified atmosphere with 5% CO_2 at 37°C for 24 h. To yield oligomeric Aβ, monomerized Aβ(1–42) was preincubated for 4.5 h in sodium phosphate buffer at 21°C and 600 rpm agitation. DB peptide was then added at different concentrations and incubated for further 40 min at 21°C and 600 rpm agitation before addition to the PC12 cells. Final concentrations were 1 μM Aβ(1–42) and 0, 2, 1, or 5 μM DB3 or half of the molar peptide concentrations of DB3DB3. The PC12 cells were further incubated for 24 h in 95% humidified atmosphere with 5% CO_2 at 37°C after adding the Aβ-peptide mixture. Cell viability was then measured using the Cell proliferation Kit I (MTT) (Roche, Basel, Switzerland) according to the manufacturer's instruction. The absorbance of the formazan product was determined by measuring at 570 nm after subtracting the absorption at 660 nm. For absorption measurements, a Polarstar Optima plate reader (BMG, Offenburg, Germany) was used. All results were normalized to cells that were treated with buffer only.

Aβ Aggregation inhibition ELISA

Freshly dissolved monomeric Aβ(1–42) (400 nM in 500 mM Tris-buffer pH 7.4) was incubated with and without DB peptides in different concentrations (0.01, 0.05, 0.1, 0.5, 1, 5, 10, 50 and 100 μM for DB3 or half of the molar concentrations in case of DB3DB3) in a humidity chamber for 23 h at 37°C. The aggregation was analyzed by an enzyme-linked immunosorbent assay (ELISA). NP27 antibody in bicarbonate/carbonate buffer was used to coat the ELISA plate overnight. Then the plate was washed in PBS-Tween buffer (1x PBS + 0.05% Tween) and

blocked for 2 h at room temperature with 5% casein buffer. After washing, Aβ aggregate solutions were added to the plate and incubated for 1 h at room temperature. The plate was washed again and bound Aβ aggregates were detected by biotinylated 6E10/HRP-avidin mediated immunoreaction (BioLegend, San Diego, CA USA) using TMB as detection reagent. Each value was background corrected which were derived from ELISA of samples without capture antibody and normalized to the control without peptide (0% no inhibition, 100% full inhibition). Mean value and standard error were calculated from three independent experiments. EC_{50} was calculated by fitting the data to a logistic dose response function.

Aβ Aggregate disassembly ELISA

Freshly dissolved monomeric Aβ(1–42) (400 nM in 500 mM Tris-buffer pH 7.4) was incubated in a humidity chamber for 22 h at 37°C in order to preform Aβ(1–42) aggregates. These preformed aggregates were coincubated with D-peptide in different concentrations (0.01, 0.05, 0.1, 0.5, 1, 5, 10, 50, 100 μM for DB3 or with half of the molar concentrations in case of DB3DB3) for additional 22 h at 37°C. The content of Aβ aggregates was measured and evaluated in the same way as the aggregation inhibition ELISA.

Transmission electron microscopy (TEM)

10 μM of freshly dissolved monomeric Aβ(1–42) was incubated in 10 mM sodium phosphate buffer pH 7.4 with or without DB peptide in equal molar ratios for 24 h at 37°C. Afterwards, 20 μl of the samples were absorbed on formval/carbon coated copper grids (S162, Plano, Wetzlar, Germany) for 3 min, washed three times with water and negative stained with 1% v/v uranylacetate for 1 min. The images were acquired using a Libra 120 electron microscope (Zeiss, Oberkochen, Germany) at 120 kV.

Statistical analysis

Statistical analysis was performed using the Origin 8.5 (OriginLab Cooperation, Northampton, USA) software package.

Results

Screening for optimized D3 derivatives using peptide microarrays

We identified previously the Aβ oligomer eliminating D-enantiomeric peptide D3 via mirror image phage display [10, 16]. A possible explanation of the efficiency of D3 is that it binds to and stabilizes Aβ monomers within the various equilibria with Aβ oligomers and other Aβ assemblies. In order to identify more efficient derivatives, a systematic optimization of D3 regarding its binding affinity to monomeric Aβ(1–42) was performed using a two-step procedure. For the first step, every position of the original peptide D3 was replaced against each of the 19 other proteinogenic amino acids residues in their D-enantiomeric form. These 20x12 different peptides were spotted on a Pepspot membrane (JPT, Berlin, Germany) and the binding of monomeric Aβ(1–42) was measured according to the procedure described in the material and method part. To verify that the applied Aβ(1–42) was mainly monomeric even after the 1 h incubation period, a density gradient ultracentrifugation run was done with an aliquot of the applied Aβ(1–42) that was incubated 1 h, too. Even after 1 h incubation, only a very small fraction of Aβ(1–42) was found in fractions 4 and higher (Fig 1) indicating that by far the largest part of the Aβ is still monomeric and thus can be found in fractions 1 to 3 [14]. After washing, the amount of bound Aβ was determined by the Aβ-specific antibody 6E10, which is known to bind all Aβ species regardless of their assembly state, and a secondary detection

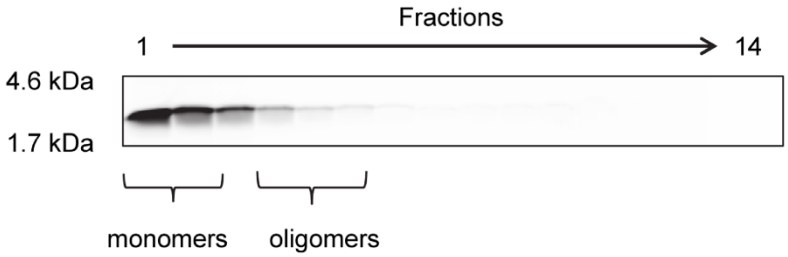

Fig 1. Aggregation state of monomeric Aβ(1–42) after 1 h incubation. For optimization of D3 with peptide microarrays, the peptide microarrays were incubated with 5 μM initially monomeric Aβ(1–42) for 1 h at room temperature. The aggregation state of this Aβ preparation was analyzed by density gradient centrifugation followed by 16% Tricine-SDS-PAGE. FITC-Aβ(1–42) was detected via FITC fluorescence and was only detectable in the first four lanes, which represent mainly monomeric and oligomeric FITC-Aβ [14].

doi:10.1371/journal.pone.0153035.g001

antibody (Fig 2A). The amino acid substitutions that yielded the highest Aβ binding activity, as measured by the dot staining density, were chosen for further combinations in the second round (Fig 2B and 2C). In particular, the substitutions R3I, R5T, H9D, R10Q, R10E, N11Q and N11D were found to bind more favorably to Aβ monomers. The residue H7 showed the highest potential for further improvement, because most substitutions at this position yielded higher affinity towards Aβ monomers. H7P, H7Q, H7R and H7S were selected as the most promising substitutions for H7. Substitution of R12 was excluded from the analysis because a minimum number of arginines has been recognized to be responsible for the superior pharmacokinetic properties of D3 [20]. Interestingly, nine of the eleven substitutions were located in the C-terminal half of D3 at positions 7, 9, 10 and 11.

For the second round of optimization, every possible combination of the eleven single residue replacements R3I, R5T, H7P, H7Q, H7R, H7S, H9D, R10Q, H10E, N11Q and N11D, were combined to yield 360 different peptides, which were spotted on a glass chip (Pepscan, Lelystad, Netherlands) (Fig 2C). To compare their binding activities to monomeric Aβ, the peptide microarrays were incubated with freshly dissolved monomeric FITC-Aβ(1–42) and fluorescence intensities of the Aβ-peptide interactions were measured. Five peptides that showed tight binding to Aβ monomers as deduced from high FITC fluorescence intensities were chosen for further *in vitro* characterization (Fig 2D and Table 1). The fluorescence intensities of these D3 derivatives, termed DB1 to DB5, were up to six times higher when compared with the fluorescence intensity obtained with D3 (Fig 2D). As shown in Table 1, the sequences of DB1 to DB5 had two to four amino acid substitutions to the original D3 template.

The influence of DB3 and DB3DB3 on Aβ fibril formation

To investigate the influence of DB1 to DB5 on Aβ fibril formation, a Thioflavin T (ThT) assay was performed. In an aqueous environment the benzothiazole dye has a low fluorescence. Upon interaction with regularly formed amyloid fibrils the fluorescence signal is significantly enhanced and excitation and emission maxima shift from 385 and 445 nm to 450 and 490 nm, respectively. The emission at 490 nm is directly proportional to the quantity of amyloid fibrils. Fibril formation of Aβ can be followed in real time by measuring the ThT fluorescence [21–23].

Therefore, the inhibitory effects of the D-peptides DB1 to DB5 and D3 were investigated by co-incubating these peptides with Aβ(1–42) and performing the ThT assay. Fluorescence emission data were compared after 5 h incubation, because after this period the Aβ(1–42) control (without added peptide) reached its fluorescence maximum. As shown in Fig 3, D3 inhibited

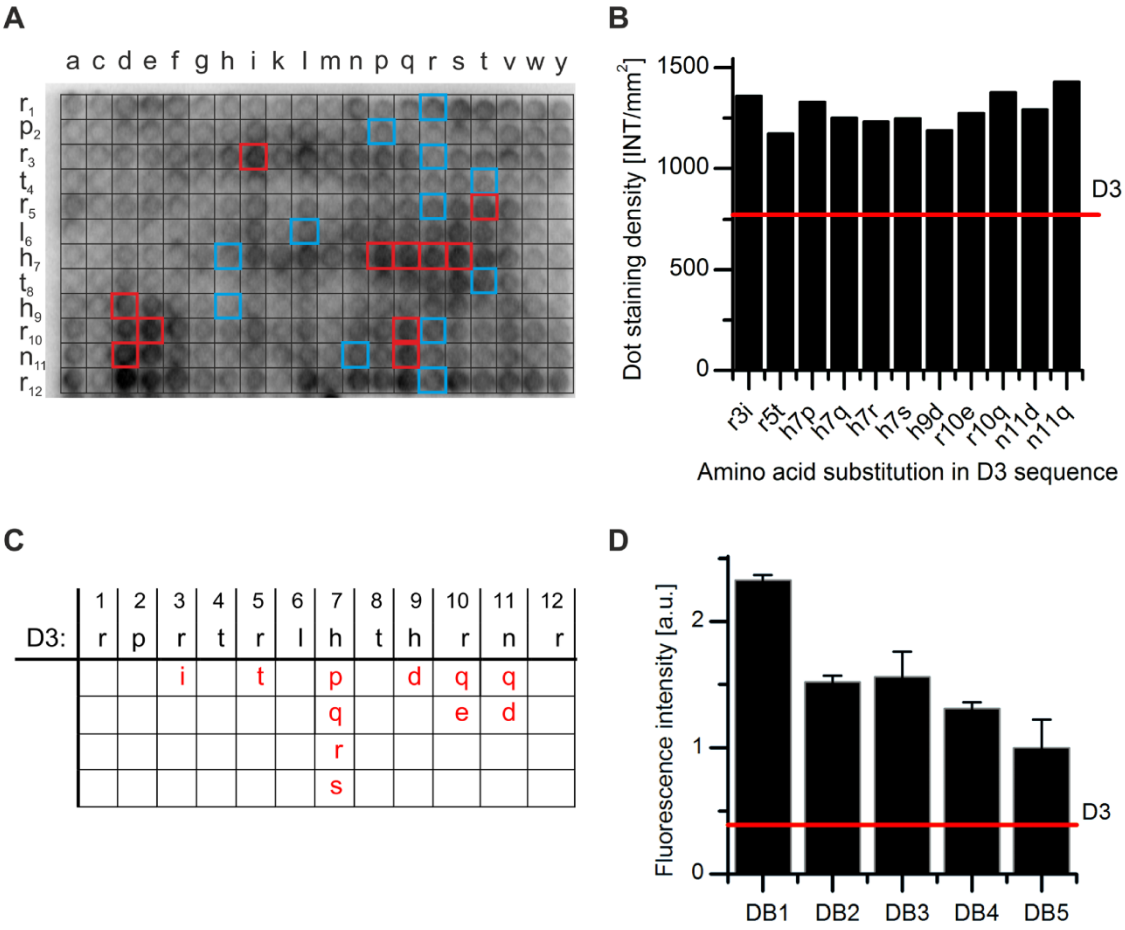

Fig 2. Selection of DB1 to DB5 based on two cycles of peptide microarray based screenings. A) Promising replacements in the sequence of D3 were selected via PepSpots peptide array. Binding of monomeric Aβ(1–42) to spotted D3 derivatives was detected using the Aβ antibody 6E10 and a HRP-labeled secondary antibody. Several of the dots with the highest staining density, representing the most promising single replacements, are marked in red. The original D3 controls are indicated in blue. B) The HRP-intensity was evaluated by the staining density of the peptide dots and plotted against the amino acid substitutions. Eleven promising substitutions that showed > 1.5 times increase in binding to monomeric Aβ(1–42) when compared with that of D3, were chosen for a second generation peptide microarray. The red line represents the mean dot staining intensity of D3. C) Schematic overview of the first generation microarray output. D) Binding of FITC-Aβ(1–42) to the peptides DB1 to DB5. The binding of FITC-Aβ(1–42) to the spotted peptides was analyzed by measuring the FITC-fluorescence intensity. All intensities were background corrected. The signal intensities of the top five peptides were plotted. The red line represents the mean fluorescence intensity of D3.

doi:10.1371/journal.pone.0153035.g002

Aβ(1–42) fibril formation by 30%, whereas DB3 inhibited the Aβ(1–42) fibril formation by 80%, DB5 by 76%, DB1 by 63% and DB2 by 49% when compared to the control (Fig 3). Surprisingly, DB4 had no effect on the fibril formation of Aβ.

The results of the ThT assay indicate that DB3 is the most promising peptide according to the inhibitory effect of fibril formation. Therefore, we selected DB3 for further in vitro studies. As a further potential optimization step of the DB peptides, we wanted to investigate the impact of avidity. Although the DB peptides were selected for monomer binding, elimination

Table 1. Amino acid sequences of D3 and DB1 to DB5.

name	sequence
D3	RPRTRLHTHRNR
DB1	RPITRLHT**D**RNR
DB2	RPI**TT**L**Q**TH**Q**NR
DB3	RPITRL**R**TH**Q**NR
DB4	RPRTRL**R**TH**Q**NR
DB5	RPITRL**Q**TH**EQ**R

All amino acids of the peptides are D-enantiomeric and their C-termini are amidated. The amino acid substitutions made to the D3 template are indicated in bold.

doi:10.1371/journal.pone.0153035.t001

of toxic oligomer species might require contacting monomer units within these oligomers. In order to make use of the multivalence of oligomers, multivalent DB3 could possibly have increased efficiency in oligomer elimination. As the simplest multivalent DB3 peptide, we designed a head-to-tail tandem peptide of DB3, named DB3DB3. In contrast to other divalent DB3 molecules, e.g. head-to-head or tail-to-tail orientations, the head-to-tail tandem of DB3 contains only peptide bonds between the amino acid residues and is thus easily accessible by standard peptide synthesis. As shown in Fig 3, 10 μM DB3DB3 inhibited the formation of ThT-positive aggregates as efficiently as 20 μM DB3.

Binding affinities of DB3 and DB3DB3 to Aβ(1–42) monomers

For further characterization of DB3 and DB3DB3, the equilibrium dissociation constants (K_D) of the D-peptides were determined for their interaction with Aβ(1–42) monomers using bio-layer interferometry (BLI) (Fig 4). For DB3, a K_D value of 75 μM was determined, whereas for the designed dimer peptide DB3DB3 a K_D value of 1 μM was obtained. Therefore, the binding affinity to Aβ(1–42) monomers was enhanced by 75-fold for the dimeric version of DB3.

Aβ aggregation inhibition by DB3 and DB3DB3

To confirm and further investigate the efficiency of DB3 and DB3DB3 activity on Aβ aggregation, an aggregation inhibition ELISA was performed. Initially monomeric Aβ(1–42) was incubated with different concentrations of DB3 or DB3DB3 and the Aβ(1–42) aggregates were specifically detected via ELISA. DB3 inhibits Aβ aggregate formation with an EC_{50} of 6 μM, whereas DB3DB3 inhibits Aβ aggregate formation with an EC_{50} of 8 nM (Fig 5A). Thus, DB3DB3 is 1000-fold more efficient in inhibiting Aβ aggregation when compared with that of DB3. Furthermore, the aggregation inhibition ELISA showed that the fibrillization of Aβ(1–42) was almost inhibited completely at a peptide concentration of 20 μM DB3 and 10 μM DB3DB3.

Aβ aggregates disassembly ability of DB3 and DB3DB3

The Aβ aggregate disassembly ELISA was used to analyze the effect of DB3 and DB3DB3 on preformed Aβ aggregates (Fig 5B). Preformed Aβ(1–42) aggregates were co-incubated with different concentrations of DB3 or DB3DB3 for 24 h. The Aβ aggregates specific ELISA was used to quantify Aβ aggregates. The raw data were normalized to Aβ aggregates without peptide. The results of measured Aβ aggregates normalized to the Aβ control were plotted against the peptide concentration. The EC_{50} was calculated by a logarithmic dose response function.

The EC_{50} value using D3 to dissemble the Aβ aggregates was 2.5 μM; however, the value for DB3DB3 could not be determined because the Aβ aggregates were already disassembled at very

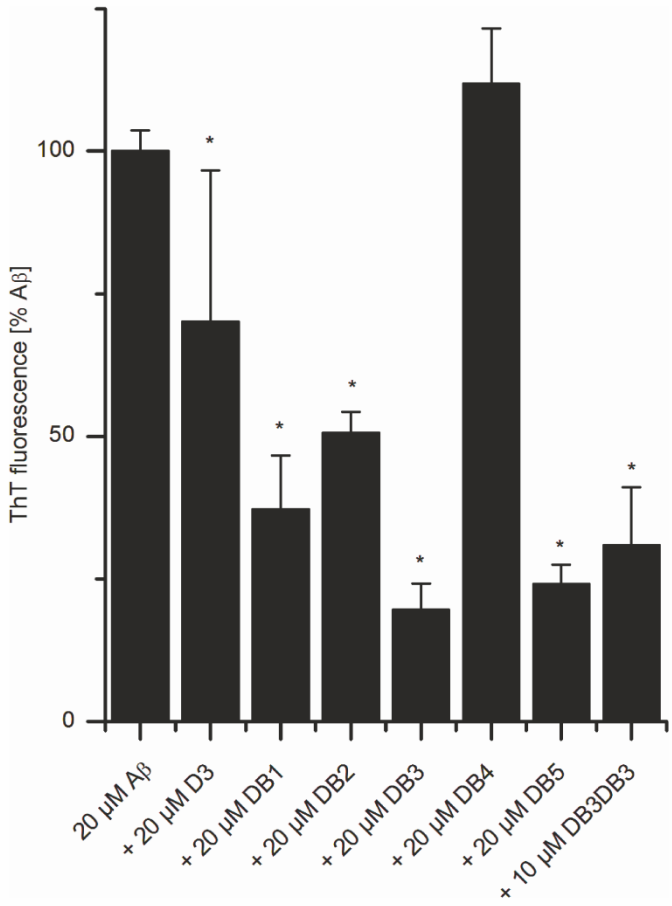

Fig 3. Thioflavin T fibril formation assay. 20 µM Aβ(1–42) was mixed with 20 µM DB1 to DB5 or 10 µM DB3DB3 and the ThT fluorescence was monitored. Aβ(1–42) without peptide addition was taken as the control. The ThT fluorescence of all samples were compared after 5 h, where the control, Aβ(1–42) only, reached its maximum in fluorescence emission. The Mann-Whitney-U-test was used for statistical analysis. * $p < 0.05$; ** $p < 0.01$; *** $p < 0.001$.

doi:10.1371/journal.pone.0153035.g003

low peptide concentrations, i.e., addition of 10 nM DB3DB3 to 400 nM Aβ gave 80% disassembly of the Aβ aggregates when compared to Aβ in the absence of peptide.

Elimination of Aβ oligomers

Aβ oligomers are the main toxic species and are discussed to be responsible for development and progression of AD [7]. A promising therapeutic approach is the elimination of Aβ oligomers. We have previously established an assay that determines quantitatively the Aβ oligomer elimination efficiency of a given substance (QIAD assay) [14]. By applying this assay the Aβ(1–42) oligomer elimination efficacy of DB3 and DB3DB3 (Fig 6) was determined. Incubation of 80 µM monomeric Aβ(1–42) for 4.5 h led to the formation of a mixture of Aβ monomers

(fractions 1–2), oligomers (fractions 4–6) and larger aggregates (other fractions) (Fig 6A). Addition of DB3 at different concentrations resulted in the elimination of Aβ oligomers in a concentration-dependent manner. Addition of 40 μM DB3 to Aβ oligomers yielded near complete elimination of the oligomers. In comparison, addition of 20 μM DB3DB3 to 80 μM Aβ eliminated the oligomer species completely. Moreover, the content of Aβ oligomers was also strongly reduced when applying 10 μM DB3DB3.

RP-HPLC was used to quantify the Aβ oligomer elimination efficiency (Fig 6B). 20 μM DB3 reduced the amount of Aβ oligomers by ~27% compared with that of the Aβ only control. 10 μM DB3DB3 reduced the content of Aβ oligomers by 82%, which is a significant improvement over the DB3 result. The content of large co-precipitates increased and represented the content of Aβ oligomers that were eliminated. The content of monomeric Aβ was not affected by DB3 and DB3DB3. Thus, DB3 and DB3DB3 eliminated Aβ oligomers without affecting the monomers and shifted the equilibrium from oligomeric Aβ to larger Aβ aggregates.

Reduction of Aβ toxicity

The MTT assay with rat PC12 cells was performed to analyze the influence of DB3 and DB3DB3 to Aβ-induced cytotoxicity (Fig 7). Monomeric Aβ(1–42) was pre-incubated for 4.5 h

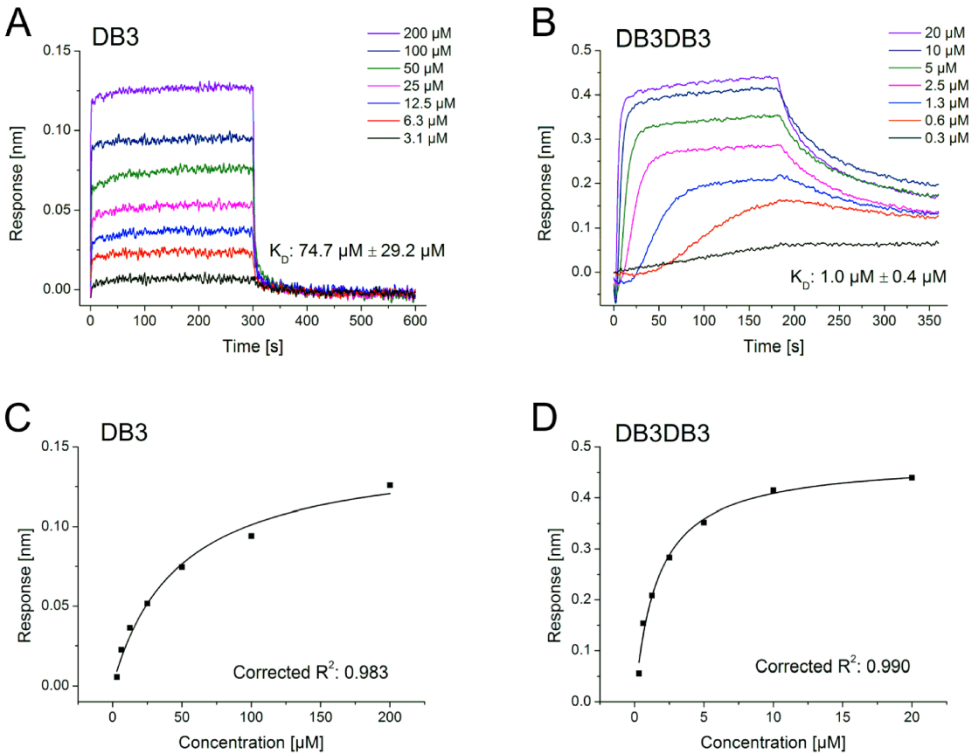

Fig 4. K_D determination of DB3 and DB3DB3 to monomeric Aβ using biolayer interferometry (BLI). N-terminally biotinylated Aβ(1–42) monomers were immobilized on streptavidin biosensors and the binding of DB3 and DB3DB3 was detected. Representative double referenced sensorgrams of a dilution series of DB3 (A) and DB3DB3 (B) are shown, including the equilibrium dissociation constants (K_D) as means ± SD of data recorded in triplicate. For steady state analysis Langmuir´s 1:1 binding model was applied. Representative fits of DB3 (C) and DB3DB3 (D) are depicted with the corresponding corrected R^2.

doi:10.1371/journal.pone.0153035.g004

to yield Aβ oligomers. After additional co-incubation with DB3 or DB3DB3 for 40 min, the mixture was added to PC12 cells and cell viability was analyzed after 24 h using the MTT assay.

In the absence of peptides a solution of 1 μM Aβ reduced the PC12 cell viability to 44% (Fig 7). In contrast, neither DB3 (5 μM) nor DB3DB3 (5 μM) exhibited any effect on PC12 cell viability, which indicates that both peptides are not toxic at the applied concentration. Addition of DB3 to 1 μM pre-incubated Aβ over the concentration range of 0.2 to 5 μM did not significantly increase cell viability. However, a significant concentration-dependent increase of cell viability was observed in the presence of 0.1 to 2.5 μM DB3DB3 in a concentration dependent manner up to 80% (Fig 7). Thus, DB3DB3 was able to inhibit Aβ-induced cytotoxicity.

Morphology of co-incubated Aβ

To analyze the morphology of Aβ co-complexes with DB3 and DB3DB3, initially monomeric Aβ(1–42) was incubated with DB3 and DB3DB3 for 24 h and TEM analysis performed. For

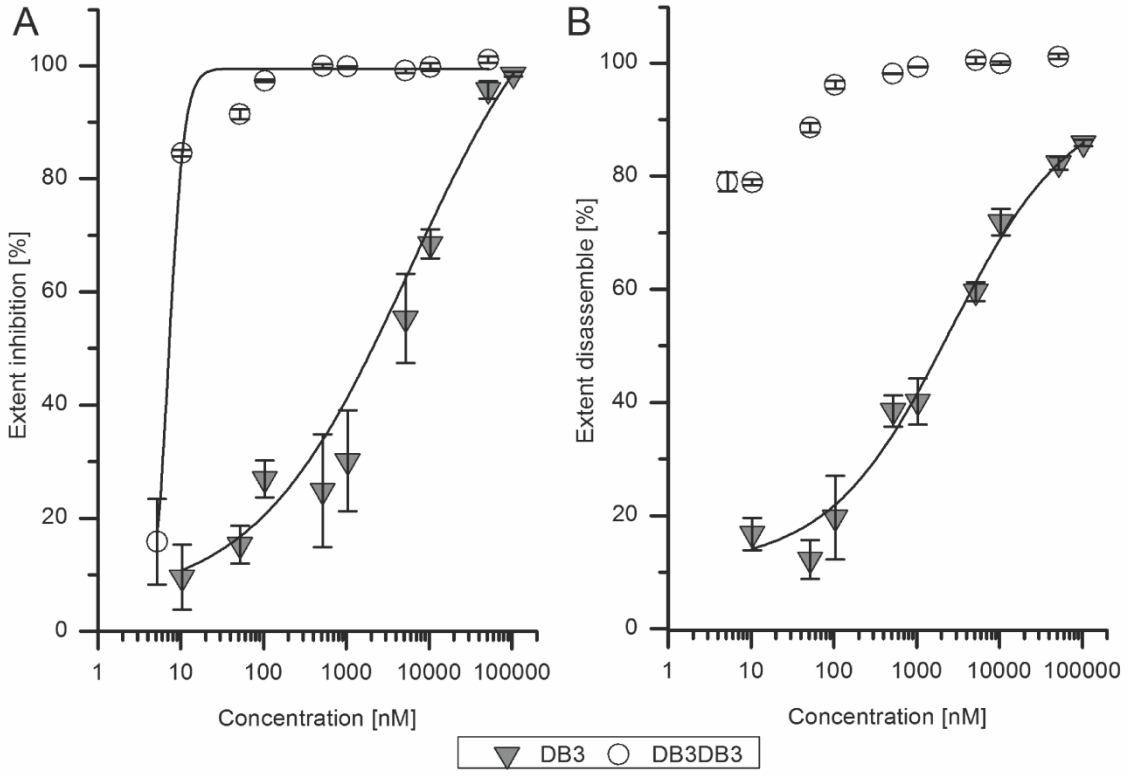

Fig 5. Inhibition of Aβ fibril formation and Aβ aggregation disassemble by DB3 and DB3DB3. A) Monomeric Aβ(1–42) (400 nM) was mixed with different concentrations of DB3 (0.01, 0.05, 0.1, 0.5, 1, 5, 10, 50, 100 μM) and the aggregation state of Aβ was analyzed using an Aβ aggregate specific ELISA. For DB3DB3 half of the molar concentrations compared to DB3 were used. Aβ without DB3 and DB3DB3 addition was taken as control. For DB3 an EC_{50} of 6 μM was calculated using a logistic fit model. DB3DB3 inhibited the formation of Aβ fibrils more efficiently with an EC_{50} of 7 nM. B) The disassembly properties of DB3 and DB3DB3 were measured using an Aβ aggregation specific ELISA. Monomeric Aβ(1–42) (400 nM) was preincubated in order to form fibrils and mixed with nine different concentrations of DB3 (0.01, 0.05, 0.1, 0.5, 1, 5, 10, 50, 100 μM). For DB3DB3, the molar concentrations were half those used for DB3. For DB3 an EC_{50} of 2.5 μM was determined. DB3DB3 disassembled Aβ aggregates at the lowest concentration (10 nM). Thus, the EC_{50} could not be determined, but is < 10 nM. All data were determined in triplicate. The Mann-Whitney-U-test was performed for statistical analysis. * $p < 0.05$; ** $p < 0.01$; *** $p < 0.001$

doi:10.1371/journal.pone.0153035.g005

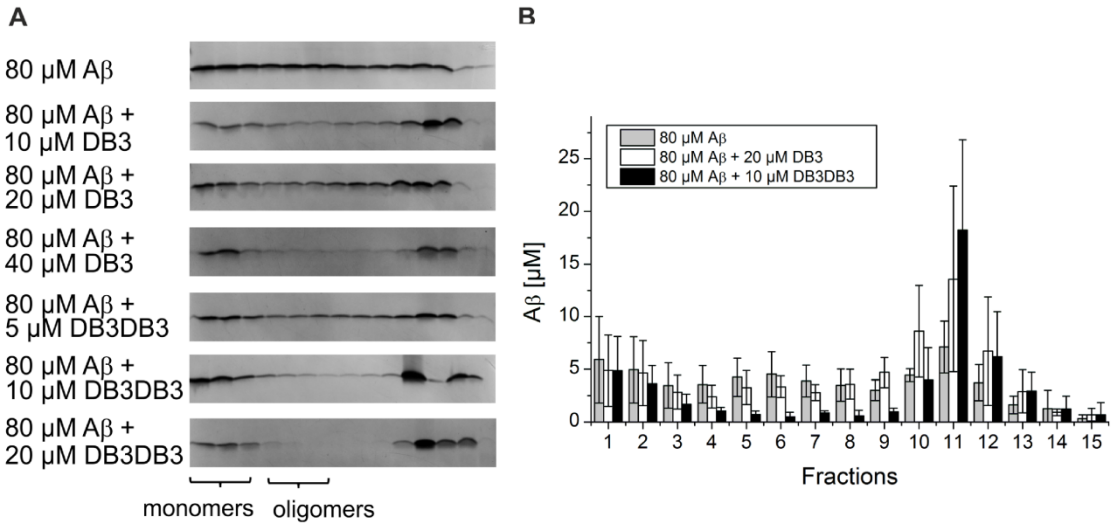

Fig 6. Effect of DB3 and DB3DB3 on different Aβ aggregation species. A) Analysis of Aβ(1–42) aggregation species with density gradient centrifugation and followed by analysis using silver-stained Tricine-SDS-PAGE to analyze the influence of DB3 and DB3DB3 on the distribution of Aβ assemblies. B) Quantification of Aβ(1–42) by RP-HPLC. All data were recorded in triplicate.

doi:10.1371/journal.pone.0153035.g006

TEM analysis, the samples were absorbed onto formval/copper grids and negatively stained using uranyl acetate.

Aβ formed large meshes of fibrils after 24 h incubation (Fig 8A). Co-incubation of Aβ with DB3 in an equal molar ratio resulted in the formation of substantially fewer and shorter fibrils (Fig 8B), which is in perfect accordance with the observation from the ThT assay that DB3 was able to reduce fibril formation by 80%. Co-incubation of Aβ with DB3DB3 yielded huge amorphous co-precipitates, which did not contain any fibrillar structures (Fig 8C). Obviously, at least under these artificially high concentrations, DB3DB3 did not yield mostly Aβ monomers, but high-molecular-weight non-fibrillar co-precipitates with Aβ (Fig 8C), as also observed in the QIAD assay (Fig 6).

Discussion

Currently, there is no causal therapy for Alzheimer's disease (AD). *In vitro* and *in vivo* studies showed that Aβ oligomers play an important role in the progression of AD [7]. Therefore, elimination of these toxic Aβ oligomers is a promising strategy to retard AD. Using peptide microarrays, we have optimized the amino acid sequence of the well-characterized D-enantiomeric Aβ oligomer-eliminating peptide D3. The most promising D3 derivatives, DB1–DB5, exhibit two to four different amino acids compared with D3. Besides DB4, the DB peptides have a lower net charge than D3, due to the substitution of R3, R5 and R10, and the introduction of negatively charged amino acids. The substitution of R10Q within DB4 was charge compensated through the substitution H7R. Additional substitutions that had no effect to the net charge were H7Q and N11Q. Combination of single amino acid residue replacements within D3 that each showed slightly enhanced binding capabilities to monomeric FITC-Aβ (Fig 2B) ultimately yielded D3 derivatives that are characterized by significantly enhanced binding capabilities to monomeric FITC-Aβ (Fig 2D). Increased binding capabilities to monomeric

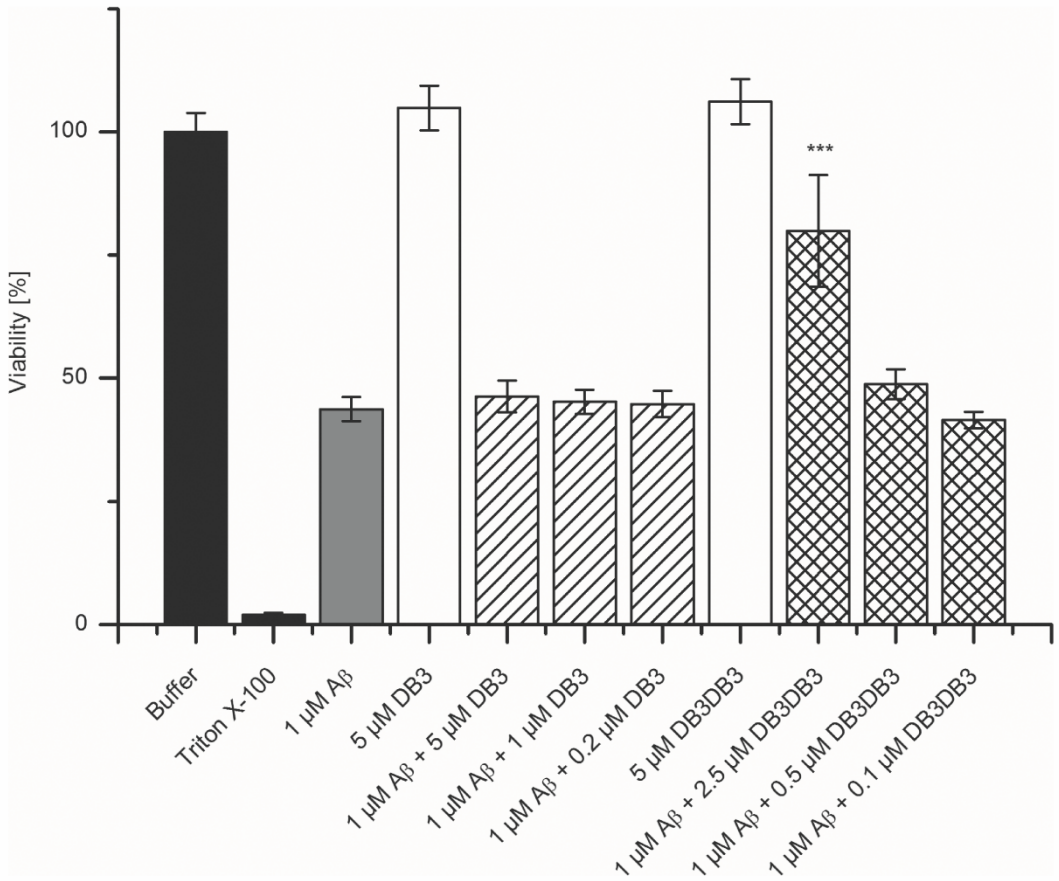

Fig 7. Influence of DB3 and DB3DB3 on Aβ-introduced cytotoxicity. The cell viability assay was performed using PC12 cells in a MTT test. Therefore, Aβ (1–42) was preincubated for 4.5 h and further coincubated with DB3 or DB3DB3 for 40 min. The cells were incubated for 24 h with the Aβ(1–42)-peptide mixture or Aβ(1–42) alone as a control. The absorption of buffer treated cells was set to 100% cell viability. The cell viability of cells treated with Aβ and DB3 or DB3DB3 were compared with cells treated with Aβ only. The Mann-Whitney-U-test was used for statistical analysis. * $p < 0.05$; ** $p < 0.01$; *** $p < 0.001$.

doi:10.1371/journal.pone.0153035.g007

FITC-Aβ were solely deduced from fluorescence intensities. Although we cannot prove that this assumption holds true for each peptide spot, it allowed us to pre-select the five most promising D3 derivatives that subsequently were compared to each other.

The inhibition efficacy of Aβ aggregation by DB1 to DB5 was investigated. DB3 was found to be the most promising D3 derivative that inhibited the Aβ aggregation by up to 80%. In contrast, D3 inhibited Aβ aggregation by only 30%. Considering the results of the ThT assay, DB3 was chosen for further *in vitro* characterization. BLI analysis revealed that DB3 interacts with Aβ monomers with a binding affinity of 75 μM, and an ELISA showed that DB3 inhibits the formation of Aβ aggregates with an EC_{50} of 6 μM.

The D-enantiomeric peptides D3 and DB1–DB5 were developed for elimination of Aβ oligomers. This was tested by the QIAD assay [14]. The addition of DB3 to Aβ reduced Aβ oligomers by 28%. Aβ monomers, which are assumed to have neuroprotective functions [24], were

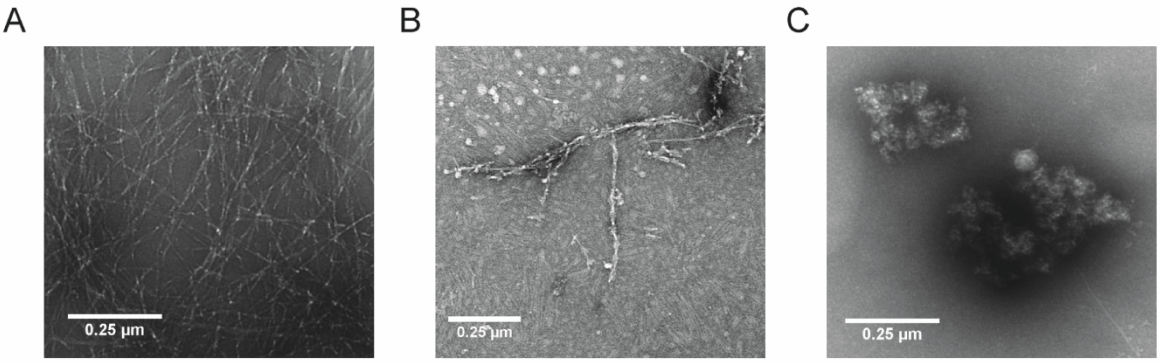

Fig 8. TEM of Aβ-DB3 and -DB3DB3 co-complexes. 10 µM initial monomeric Aβ(1–42) without (A) and with 10 µM DB3 (B) or 5 µM DB3DB3 (C) were coincubated for 24 h. Subsequently, the samples were absorbed onto formval/carbon coated copper grids and negative stained with 1% uranyl acetate. The images were obtained using a transmission electron microscope (TEM). Scale bar: 0.25 µm.

doi:10.1371/journal.pone.0153035.g008

not affected. The reduction of oligomeric Aβ resulted in an increase of large amorphous Aβ co-precipitates. TEM images showed that these aggregates possess a higher density. Typical Aβ fibrils, which are linear, unbranched and 5 to 10 nm wide [25], were not visible. Additionally, DB3 was able to disassemble preformed Aβ aggregates.

Since Aβ oligomers are a multivalent target, the divalent tandem peptide DB3DB3 was expected to be significantly more effective. DB3DB3 showed a 75-fold higher affinity for Aβ monomers. This increase in affinity resulted in an increase in the inhibition of Aβ fibrilation and an increased reduction in Aβ-induced cytotoxicity. Additionally, in the Aβ aggregation inhibition ELISA, DB3DB3 yielded an EC_{50} that was 1000-fold lower when compared with that of DB3. DB3DB3 was also able to efficiently eliminate Aβ oligomers as shown in the QIAD assay. Interestingly, DB3 and DB3DB3 did not significantly affect the Aβ monomer content. TEM images showed that these aggregates were not fibrillary structured.

In summary, our *in vitro* data show that the D3 derivative DB3 and its tandem version DB3DB3 were highly efficient at reducing Aβ oligomer content in samples. In particular, the tandem peptide DB3DB3 yielded a significant optimization step when compared with the original peptide DB3. *In vivo* studies will show whether the new compounds' *in vitro* properties can be translated into enhanced therapeutic activity in AD animal models.

Acknowledgments

D. W. was supported by grants from the "Portfolio Technology and Medicine", the "Portfolio Drug Research" and the Helmholtz-Validierungsfonds of the Impuls- und Vernetzungs-Fonds der Helmholtzgemeinschaft. D.W. was also supported by the TT-Fonds of the Technology Transfer Department of the Forschungszentrum Jülich.

Author Contributions

Conceived and designed the experiments: ANK TZ DB SAF OB LG JK DW. Performed the experiments: ANK TZ MT JB DB AB TW. Analyzed the data: ANK TZ MT DB AB TW. Contributed reagents/materials/analysis tools: JB DW EW. Wrote the paper: ANK TZ MT JB SAF JK AB EW DW.

References

1. Ferri CP, Prince M, Brayne C, Brodaty H, Fratiglioni L, Ganguli M, et al. Global prevalence of dementia: a Delphi consensus study. Lancet. 2005; 366(9503):2112–7. PMID: 16360788
2. Sperling RA, Jack CR, Aisen PS. Testing the Right Target and Right Drug at the Right Stage. Science Translational Medicine. 2011; 3(111):111cm33.
3. Hardy J, Selkoe DJ. The Amyloid Hypothesis of Alzheimer's Disease: Progress and Problems on the Road to Therapeutics. Science. 2002; 297(5580):353–6. PMID: 12130773
4. Selkoe DJ. Alzheimer's Disease: Genes, Proteins, and Therapy. 2001; 81(2):741–66.
5. Finder VH, Glockshuber R. Amyloid-β Aggregation. Neurodegenerative Diseases. 2007; 4(1):13–27. PMID: 17429215
6. McLean CA, Cherny RA, Fraser FW, Fuller SJ, Smith MJ, Konrad V, et al. Soluble pool of Aβ amyloid as a determinant of severity of neurodegeneration in Alzheimer's disease. Annals of Neurology. 1999; 46(6):860–6. PMID: 10589538
7. Shankar GM, Li S, Mehta TH, Garcia-Munoz A, Shepardson NE, Smith I, et al. Amyloid-β protein dimers isolated directly from Alzheimer's brains impair synaptic plasticity and memory. Nature medicine. 2008; 14(8):837–42. doi: 10.1038/nm1782 PMID: 18568035
8. Schumacher TN, Mayr LM, Minor DL Jr, Milhollen MA, Burgess MW, Kim PS. Identification of D-peptide ligands through mirror-image phage display. Science. 1996; 271(5257):1854–7. PMID: 8596952
9. Wiesehan K, Buder K, Linke RP, Patt S, Stoldt M, Unger E, et al. Selection of D-Amino-Acid Peptides That Bind to Alzheimer's Disease Amyloid Peptide Aβ1–42 by Mirror Image Phage Display. ChemBioChem. 2003; 4(8):748–53. PMID: 12898626
10. Funke SA, van Groen T, Kadish I, Bartnik D, Nagel-Steger L, Brener O, et al. Oral Treatment with the d-Enantiomeric Peptide D3 Improves the Pathology and Behavior of Alzheimer's Disease Transgenic Mice. ACS Chemical Neuroscience. 2010; 1(9):639–48. doi: 10.1021/cn100057j PMID: 22778851
11. Bartnik D, Funke SA, Andrei-Selmer L-C, Bacher M, Dodel R, Willbold D. Differently Selected d-Enantiomeric Peptides Act on Different Aβ Species. Rejuvenation Research. 2009; 13(2–3):202–5.
12. van Groen T, Kadish I, Wiesehan K, Funke SA, Willbold D. In vitro and in vivo Staining Characteristics of Small, Fluorescent, Aβ42-Binding D-Enantiomeric Peptides in Transgenic AD Mouse Models. ChemMedChem. 2009; 4(2):276–82. doi: 10.1002/cmdc.200800289 PMID: 19072935
13. Wiesehan K, Stöhr J, Nagel-Steger L, van Groen T, Riesner D, Willbold D. Inhibition of cytotoxicity and amyloid fibril formation by a d-amino acid peptide that specifically binds to Alzheimer's disease amyloid peptide. Protein Engineering Design and Selection. 2008; 21(4):241–6.
14. Brener O, Dunkelmann T, Gremer L, van Groen T, Mirecka EA, Kadish I, et al. QIAD assay for quantitating a compound's efficacy in elimination of toxic Aβ oligomers. Scientific Reports. 2015; 5:13222. doi: 10.1038/srep13222 PMID: 26394756
15. van Groen T, Kadish I, Funke SA, Bartnik D, Willbold D. Treatment with D3 Removes Amyloid Deposits, Reduces Inflammation, and Improves Cognition in Aged AβPP/PS1 Double Transgenic Mice. Journal of Alzheimer's Disease. 2013; 34(3):609–20. doi: 10.3233/JAD-121792 PMID: 23271316
16. van Groen T, Wiesehan K, Funke SA, Kadish I, Nagel-Steger L, Willbold D. Reduction of Alzheimer's Disease Amyloid Plaque Load in Transgenic Mice by D3, a D-Enantiomeric Peptide Identified by Mirror Image Phage Display. ChemMedChem. 2008; 3(12):1848–52. doi: 10.1002/cmdc.200800273 PMID: 19016284
17. Uttamchandani M, Yao SQ. Peptide Microarrays: Next Generation Biochips for Detection, Diagnostics and High-Throughput Screening. Current Pharmaceutical Design. 2008; 14(24):2428–38. PMID: 18781992
18. Foong YM, Fu J, Yao SQ, Uttamchandani M. Current advances in peptide and small molecule microarray technologies. Current Opinion in Chemical Biology. 2012; 16(1–2):234–42. doi: 10.1016/j.cbpa.2011.12.007 PMID: 22221853
19. Schagger H. Tricine-SDS-PAGE. Nat Protocols. 2006; 1(1):16–22. PMID: 17406207
20. Jiang N, Leithold LHE, Post J, Ziehm T, Mauler J, Gremer L, et al. Preclinical Pharmacokinetic Studies of the Tritium Labelled D-Enantiomeric Peptide D3 Developed for the Treatment of Alzheimer´s Disease. PloS one. 2015; 10(6):e0128553. doi: 10.1371/journal.pone.0128553 PMID: 26046986
21. LeVine H. Thioflavine T interaction with amyloid β-sheet structures. Amyloid. 1995; 2(1):1–6.
22. Levine H. Thioflavine T interaction with synthetic Alzheimer's disease β-amyloid peptides: Detection of amyloid aggregation in solution. Protein Science. 1993; 2(3):404–10. PMID: 8453378
23. Naiki H, Higuchi K, Hosokawa M, Takeda T. Fluorometric determination of amyloid fibrils in vitro using the fluorescent dye, thioflavine T. Analytical Biochemistry. 1989; 177(2):244–9. PMID: 2729542

24. Giuffrida ML, Caraci F, Pignataro B, Cataldo S, De Bona P, Bruno V, et al. β-Amyloid Monomers Are Neuroprotective. The Journal of Neuroscience. 2009; 29(34):10582–7. doi: 10.1523/JNEUROSCI.1736-09.2009 PMID: 19710311

25. Fändrich M, Schmidt M, Grigorieff N. Recent progress in understanding Alzheimer's β-amyloid structures. Trends in Biochemical Sciences. 2011; 36(6):338–45. doi: 10.1016/j.tibs.2011.02.002 PMID: 21411326

3.4 Optimization of D-peptides for Aβ monomer binding specificity enhances their potential to eliminate toxic Aβ oligomers

Antonia N Klein, Tamar Ziehm, Thomas van Groen, Inga Kadish, Anne Elfgen, Markus Tusche, Maren Thomaier, Kerstin Reiss, Oleksandr Brener, Lothar Gremer, Janine Kutzsche, Dieter Willbold

ACS Chem Neurosci. 2017 Sep 20;8(9):1889-1900

doi: 10.1021/acschemneuro.7b00045

http://pubs.acs.org/doi/abs/10.1021/acschemneuro.7b00045

ACS Chemical Neuroscience

Research Article

pubs.acs.org/chemneuro

Optimization of D-Peptides for Aβ Monomer Binding Specificity Enhances Their Potential to Eliminate Toxic Aβ Oligomers

Antonia Nicole Klein,[†] Tamar Ziehm,[†] Thomas van Groen,[‡] Inga Kadish,[‡] Anne Elfgen,[†] Markus Tusche,[†] Maren Thomaier,[†] Kerstin Reiss,[†] Oleksandr Brener,[†,§] Lothar Gremer,[†,§] Janine Kutzsche,[†] and Dieter Willbold*[,†,§]

[†]Institute of Complex Systems, Structural Biochemistry (ICS-6), Research Center Jülich, 52425 Jülich, Germany

[‡]Department of Cell, Developmental and Integrative Biology, University of Alabama at Birmingham, Birmingham, Alabama 35294, United States

[§]Institut für Physikalische Biologie, Heinrich-Heine-Universität Düsseldorf, 40225 Düsseldorf, Germany

Supporting Information

ABSTRACT: Amyloid-beta (Aβ) oligomers are thought to be causative for the development and progression of Alzheimer's disease (AD). Starting from the Aβ oligomer eliminating D-enantiomeric peptide D3, we developed and applied a two-step procedure based on peptide microarrays to identify D3 derivatives with increased binding affinity and specificity for monomeric Aβ(1−42) to further enhance the Aβ oligomer elimination efficacy. Out of more than 1000 D3 derivatives, we selected seven novel D-peptides, named ANK1 to ANK7, and characterized them in more detail in vitro. All ANK peptides bound to monomeric Aβ(1−42), eliminated Aβ(1−42) oligomers, inhibited Aβ(1−42) fibril formation, and reduced Aβ(1−42)-induced cytotoxicity more efficiently than D3. Additionally, ANK6 completely inhibited the prion-like propagation of preformed Aβ(1−42) seeds and showed a nonsignificant tendency for improving memory performance of tg-APPSwDI mice after i.p. application for 4 weeks. This supports the hypothesis that stabilization of Aβ monomers and thereby induced elimination of Aβ oligomers is a suitable therapeutic strategy.

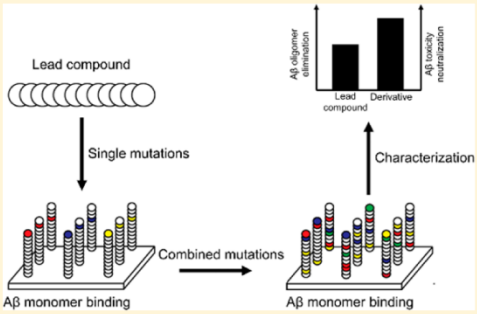

KEYWORDS: *Alzheimer's disease, amyloid-beta, drug development, D-peptides, peptide microarrays, optimization*

INTRODUCTION

Alzheimer's disease (AD) is the major type of dementia affecting more than 30 million people worldwide.[1] Memory deficits and cognitive decline are the key symptoms of AD.[2] According to the modified amyloid cascade hypothesis, the aggregation of amyloid-beta (Aβ) is thought to be responsible for the development and progression of this neurodegenerative disease.[3] Aβ is a product of the proteolytic cleavage of the amyloid precursor protein (APP) by β- and γ-secretases.[4] Aβ monomers aggregate into various oligomeric Aβ species and fibrils. Small, soluble Aβ oligomers are thought to be the most toxic species.[5] The level of cognitive defects in AD is reported to correlate with the level of Aβ oligomeric species in the brain.[6] Thus, the elimination of the oligomeric Aβ is, from the current point of view, the most promising objective for causal therapy of AD. One possible approach is to identify ligands that stabilize Aβ monomers within the various equilibria between them, Aβ oligomers and other Aβ assemblies.

Previously, we selected the D-enantiomeric peptide D3 by mirror image phage display against Aβ monomers.[7,8] The original idea of the D3 selection was to identify ligands, which bind to Aβ monomers, thereby stabilizing them and thus shifting the equilibrium away from oligomers toward monomers. D3 consists of 12 D-enantiomeric amino acid residues. It inhibits formation of Aβ(1−42) fibrils, eliminates Aβ(1−42) oligomers, and reduces Aβ(1−42)-induced cell toxicity. In vivo, D3 improves cognitive performance of transgenic AD mice and reduces plaque load and inflammation of transgenic AD mice after oral application.[9−15]

In order to support that D3's mechanism of action is based on its ability to bind and stabilize Aβ monomers, we aimed for the identification of D3 derivatives that show enhanced Aβ monomer binding affinity and specificity. If our hypothesis for the mechanism of action of D3−stabilization of Aβ monomers−is true, such derivatives are expected to be even more efficient than the original peptide D3.

RESULTS

Development of a Two-Step Procedure to Identify D3 Derivatives with Increased Binding Affinity and Specif-

Received: January 28, 2017
Accepted: June 5, 2017
Published: June 5, 2017

DOI: 10.1021/acschemneuro.7b00045
ACS Chem. Neurosci. 2017, 8, 1889−1900

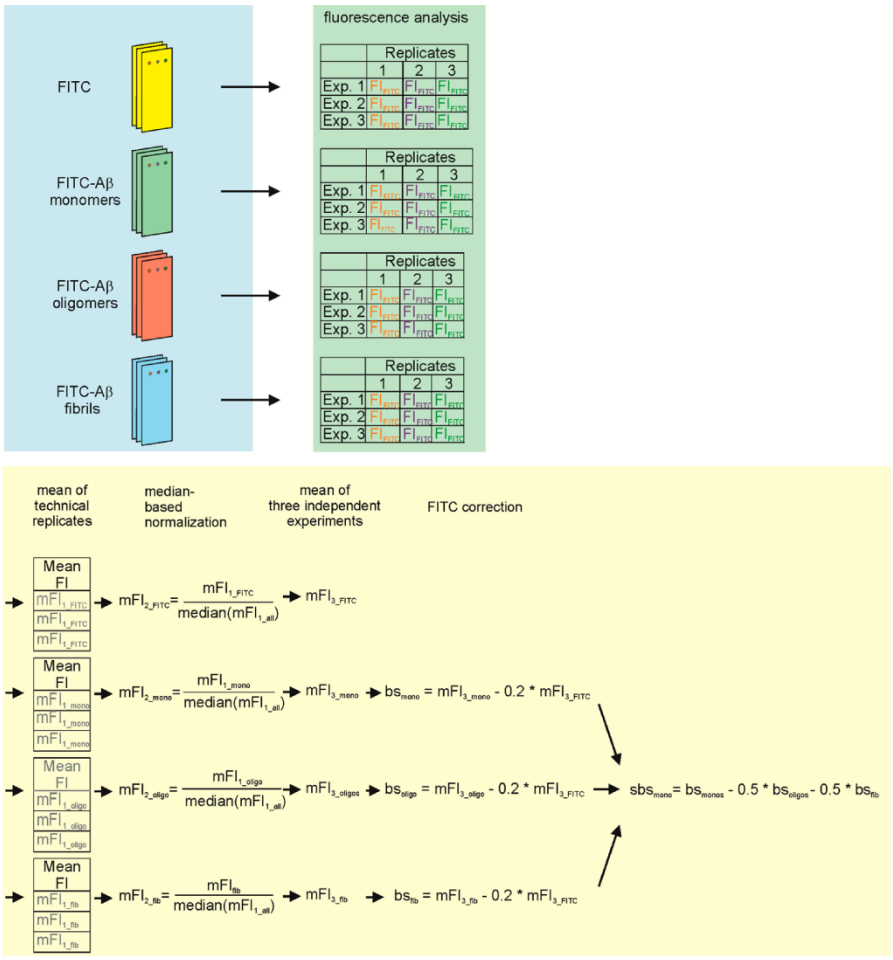

Figure 1. Schematic overview of the peptide microarray procedure. The experimental part, consisting of the incubation of peptide microarray slides with different FITC-Aβ species and FITC only as a control, is marked in blue and data acquisition in green. The data analysis to calculate the specific binding score (sbs) is marked in yellow. Three peptide microarray slides were incubated each separately with FITC-Aβ monomers, oligomers, fibrils or FITC. The interaction between the D-peptides, covalently coupled to the glass slide, and different FITC-Aβ species was measured via fluorescence, here termed FI (fluorescence intensity). Afterward, the specific binding score (sbs) of every D-peptide to Aβ monomers was calculated. Therefore, the mean fluorescence intensity (mFI_1) of the three technical replicates was calculated, a median-based normalization was performed (mFI_2) and therewith the mean value of the three biological replicates was calculated (mFI_3). After a FITC correction, the specific binding score (sbs) to monomeric Aβ was calculated by subtracting the binding score (bs) of oligomeric and fibrillar Aβ of the binding score of monomeric Aβ. Please note that the exact equations are shown and described in the Methods. The different Aβ conformation species are indicated as subscripts. mono, Aβ monomers; oligo, Aβ oligomers; fib, Aβ fibrils.

icity for Monomeric Aβ. In order to identify D3 derivatives with increased binding affinity and specificity for Aβ(1−42) monomers, we designed and performed a systematic amino acid replacement of D3 using peptide microarrays. Therefore, we designed two generations of peptide microarrays and developed an experimental and a data analysis procedure (Figures 1 and 2).

In the first step, a complete single amino acid replacement set of all 12 amino acid residues of D3 was performed (Figure 2A). Each amino acid residue of the D-enantiomeric D3 was substituted by all proteinogenic amino acids, except for cysteine. Cysteine had been excluded because of its unpredictable redox-based properties. These replacements already lead to 18 × 12 D3 derivatives and 12 times the original D-peptide D3. These copies of D3 resulted from the substitution of each of the 12 amino acid residues of D3 also with the original one. In addition to the 19 proteinogenic amino acid replacements for each D3 residue, we further added 13 nonproteinogenic amino acid residues to the replacement scheme (Figure S1) to allow much more conformational and functional freedom and potential properties. The nonproteinogenic amino acids were chosen based on increased or decreased structural flexibility, hydrophobicity, presence of aromatic ring systems, as well as the content of elements that may later be suitable for the use of the optimized derivatives as tracer ligands in PET imaging, like fluorine and iodine, and of course also on their availability by the manufacturer. All proteinogenic and nonproteinogenic amino acids that contained asymmetric

DOI: 10.1021/acschemneuro.7b00045
ACS Chem. Neurosci. 2017, 8, 1889−1900

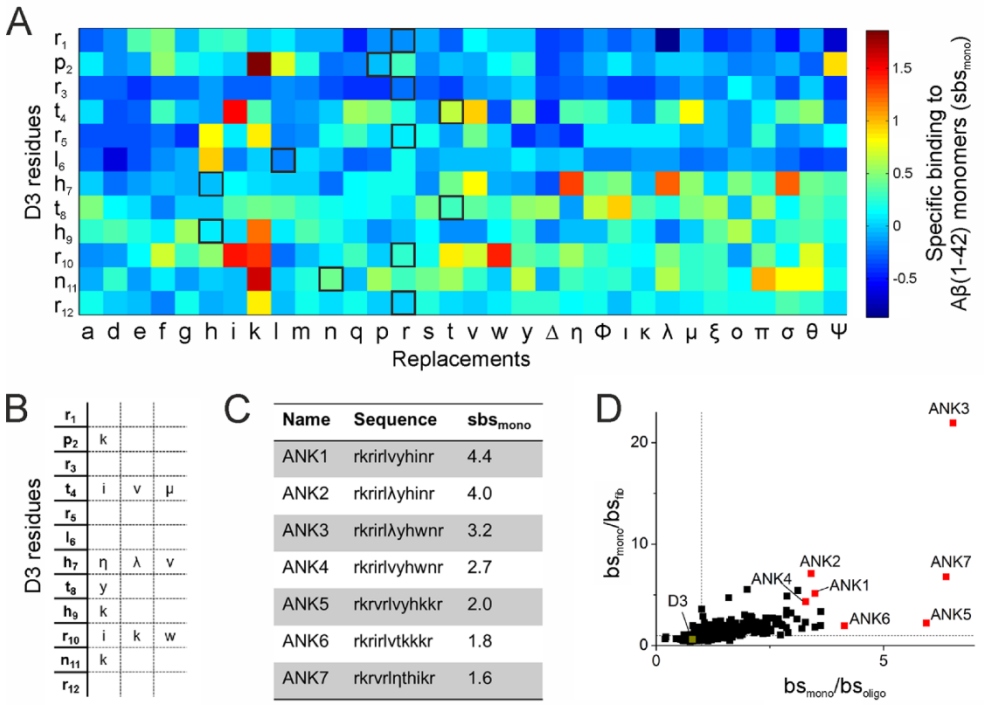

Figure 2. Selection of optimized D3 derivatives via peptide microarray analysis. (A) Heat map of Aβ monomer specific binding scores (sbs$_{mono}$) of all investigated D3 derivatives. The positions of original D3 controls are framed. (B) Layout of the second generation peptide microarray in which all promising amino acid replacements of the first generation peptide microarray were combined. Some promising replacements were not considered due to high SD of fluorescence intensities of the triplicate. (C) Sequences and sbs$_{mono}$ values of the novel D3 derivatives. All amino acid residues were in the D-enantiomeric conformation. (D) Aβ monomer binding specificities of the novel ANK peptides (red rectangles), all remaining D3 derivatives (black) and D3 (yellow). The ratio of sbs$_{mono}$ to sbs$_{fib}$ is plotted against the ratio of sbs$_{mono}$ to sbs$_{oligo}$. A specific binding to monomeric Aβ was achieved if the ratios were above 1 (dashed lines). Δ, *trans*-4-L-fluoro-proline; η, 4-fluoro-D-phenylalanine; θ, 4-benzyl-D-phenylalanine; ι, 1-naphthyl-D-alanine; κ, 3,5-diiodo-D-tyrosine; λ, D-phenylglycine; μ, D-homoarginine; ξ, D-homocitrulline; o, β-homoarginine; π, β-cyclohexyl-D-alanine; σ, cyclovaline; Φ, β-alanine; Ψ, γ-aminobutyric acid.

carbon centers were used in their D-enantiomeric form. Thus, our single residue replacement library of D3 contained 31 × 12 different D3 derivatives, which yielded 372 D3 derivatives. These D3 derivatives and 12 copies of D3 were spotted on a glass slide (Pepscan, Lelystad, Netherlands), each in triplicate, and represented the first peptide microarray used within our two-step optimization procedure.

To assess binding affinity and specificity of each D3 derivative for Aβ monomers, oligomers and fibrils, we carried out the following experimental procedure. The peptide microarrays were incubated with fluorescein isothiocyanate (FITC) labeled Aβ(1−42) monomers, oligomers and fibrils and with FITC itself as a control (see Methods and Supporting Information). To ensure the monomeric and oligomeric transition state during the microarray procedure, the distribution of these two solutions after 1 h of incubation was analyzed via density gradient centrifugation and subsequent SDS-PAGE. Aβ was visualized via FITC (Figure S2). The monomers were very stable under the assay conditions and only small amounts of the oligomers re-equilibrate into monomers and protofibrils. Therefore, the major fraction was still consisting of Aβ oligomers. Every peptide microarray slide was used only once and all incubations were done in triplicate. Thus, we used 12 identical peptide microarray slides for this step of the procedure.

After the final washing step, fluorescence intensities of bound FITC or FITC-Aβ species were quantified. It was assumed, that the FITC signal intensity at each spot correlates with the extent of FITC-Aβ bound to the spotted D3 derivative. Although this assumption may not be applicable to each D3 derivative at each spot, it allowed the prescreening of the peptide library by comparing the respective fluorescence intensities to each other.

To obtain a scoring system for binding affinity and specificity for Aβ monomers, we developed a procedure that highly weighed on Aβ monomer binding and subtracted binding to Aβ oligomers and fibrils. To compare different peptide microarrays, overall staining intensities for each peptide microarray replicate were taken into account. As a control, binding to the FITC control was subtracted to avoid selection of FITC binding derivatives. The exact data processing procedure is described in the Methods section and summarized within Figure 1.

The calculated specific binding score of each of the D3 derivatives for monomeric Aβ (sbs$_{mono}$) represented the capability of the respective D3 derivative to bind specifically to Aβ monomers and the raw data can be obtained from Table S1. These sbs$_{mono}$ scores are illustrated as a heat map at Figure 2A for the single amino acid replacement D3 derivatives. The

DOI: 10.1021/acschemneuro.7b00045
ACS Chem. Neurosci. 2017, 8, 1889−1900

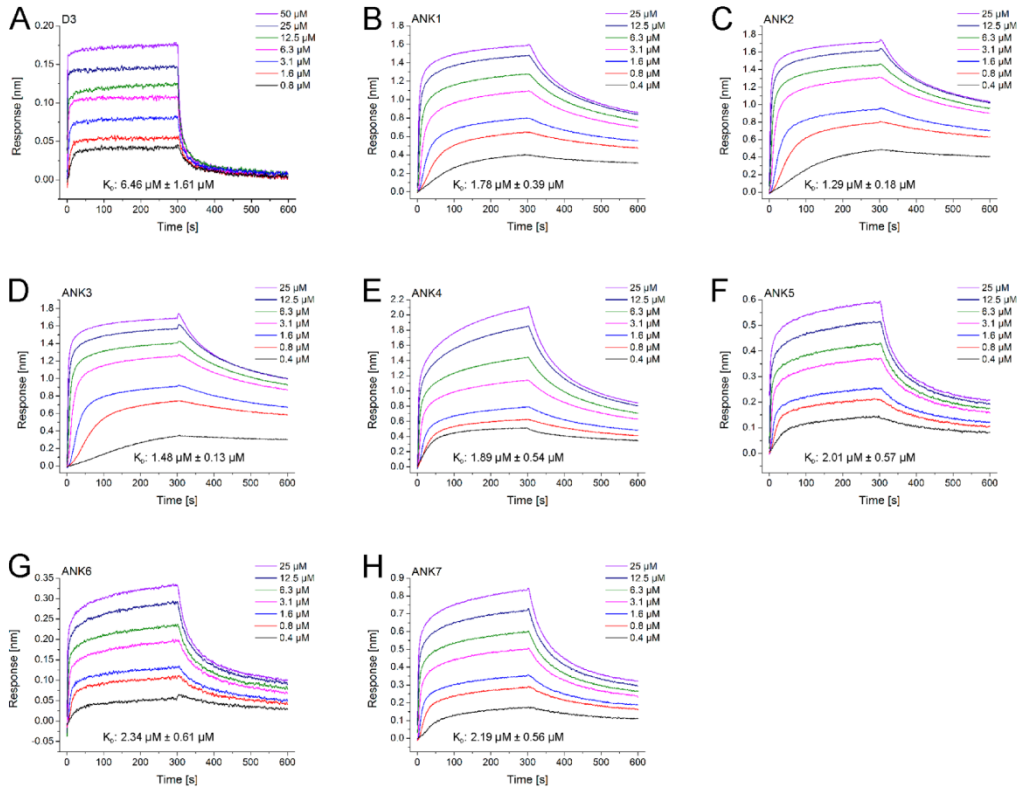

Figure 3. Sensorgrams and apparent equilibration dissociation constants (K_D) of D-peptide−Aβ(1−42) interactions. K_D values of D3 and ANK interactions with monomeric Aβ(1−42) were determined using biolayer interferometry (BLI). Biotinylated Aβ(1−42) was coupled to streptavidin biosensors and the D-peptides were used as analytes. By plotting the equilibrium response signals against the applied D-peptide concentrations, overall K_D values were determined. Data were fitted according to Langmuir's 1:1 binding model. The sensorgrams show one representative experiment and K_D values represent means ± SD of three independent experiments for (A) D3; (B) ANK1; (C) ANK2; (D) ANK3; (E) ANK4; (F) ANK5; (G) ANK6; (H) ANK7.

scale of the specific binding to Aβ monomers (sbs_{mono}) ranged from −0.5 (blue) to 1.9 (red). The higher the sbs_{mono} value, the higher was the affinity and specificity of the respective D-peptide to monomeric Aβ after subtracting the values from binding to Aβ oligomers and fibrils.

As shown in Figure 2A, the original D3 peptide was characterized by an sbs_{mono} value of 0.2 with a slight variation between the technical replicates, indicating that some derivatives achieved clearly enhanced affinity and specificity for Aβ monomers. Replacement of D3 residues 1 to 3 did not enhance the sbs_{mono} scores of the D-peptides, except for the replacement p2k. Replacement of the original C-terminal half of D3 (amino acid residues 7−11) frequently resulted in enhanced Aβ monomer affinity and specificity. Any replacement of residues 1, 3, and 6 did not alter the sbs_{mono} scores of D3 derivatives compared to D3. Whereas replacement of residues 7, 8, 10, and 11 showed the highest potential for enhancement of affinity and specificity to Aβ monomers as compared to D3, represented by high sbs_{mono} scores displayed in Figure 2A in yellow or red colors.

Selection of New D3 Derivatives with Increased Specific Binding Capability to Monomeric Aβ. To further increase Aβ monomer binding affinity and specificity, the 13 most promising single amino acid replacements within D3, based on the sbs_{mono} scores, were combined and the resulting 1024 D-peptides were spotted on a second generation peptide microarray, which was assayed analog to the first generation array (Figure 2B). After data analysis, the most promising D3 derivatives with more than two replaced amino acid residues were selected for further analysis (Figure 2C). Selection criteria were high sbs_{mono} scores representing increased affinity and specificity for Aβ monomers. The sbs_{mono} of D3 in the second generation of peptide microarray analysis was −0.6 and the most interesting D3 derivatives had sbs_{mono} scores between 4.4 and 1.6, already indicating that some derivatives bound to Aβ monomers with higher affinity and selectivity than D3. The seven most interesting D3 derivatives were selected for further in vitro characterization and named ANK1 to ANK7 (Figure 2C).

Additionally, the ratio of Aβ monomer binding to oligomer binding and fibril binding was calculated (see Methods and Figure 2D). For all ANK peptides, this ratio was above one. For example, the respective ratios of ANK3 were 6.5 and 22, indicating a 6.5 or 22 fold increased specific binding for Aβ monomers compared to Aβ oligomers or fibrils, respectively (Figure 2D). In comparison, the ratios for D3 were below one (0.8 and 0.6), indicating that D3 binds with a slightly higher affinity to Aβ oligomers and fibrils than to Aβ monomers.

DOI: 10.1021/acschemneuro.7b00045
ACS Chem. Neurosci. 2017, 8, 1889−1900

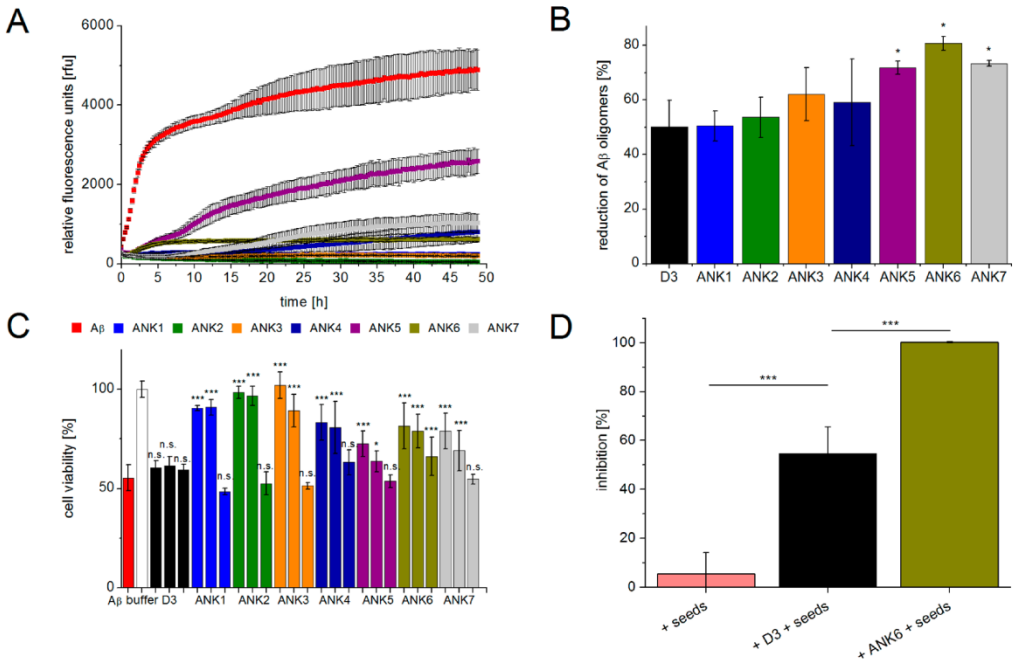

Figure 4. In vitro characterization of the ANK peptides. (A) Aβ fibril formation in the presence of the D-peptides was monitored by Thioflavin T (ThT). The data represent mean ± SD with $n = 3$ of one representative out of three independent experiments. (B) Elimination of Aβ oligomers was analyzed via QIAD assay. The mean values ± SD of four independent experiments are presented. (C) MTT-based Aβ cytotoxicity assay in the presence of D3 or the ANK peptides. Different Aβ:peptide ratios are presented (high (1:5), equimolar (1:1) and low (1:0.2) from left to right in one color). The data present mean ± SD of three independent experiments with $n = 5$ for each compound. Significant differences are with respect to the Aβ control (red) and were tested by using one-way ANOVA with Bonferroni posthoc test. (D) Analysis of the seeding potential of Aβ fibrils on monomeric Aβ in the presence of D3 or ANK6. The Aβ fibril formation was monitored using ThT and the inhibition (mean value ± SD) was calculated out of three independent experiments with $n = 3$ for each compound as described in the Methods. $^*p \leq 0.05$; $^{**}p \leq 0.01$; $^{***}p \leq 0.001$; n.s. not significant.

ANK1 to ANK7 Bound to Aβ Monomers with Increased Affinity. After selection of the D3 derivatives ANK1 to ANK7, their in vitro performance was investigated and compared to D3. First, the real time interaction between the D-peptides and monomeric Aβ(1−42) was examined using biolayer interferometry (BLI) (Figure 3). The sensorgrams of D3 binding to monomeric Aβ displayed a homogeneous 1:1 interaction (Figure 3A). ANK1 to ANK7 exhibited a heterogeneous binding behavior consisting of two kinetics with a slow final off-rate (Figure 3B−H). In order to describe these two kinetics quantitatively, a heterogeneous fit was applied (Figure S3). However, the equilibrium dissociation constants (K_D) of the second binding site could not reliably be determined, since the results were outside the instrument specifications ($<10^{-12}$ M) (Table S2). Therefore, we also carried out a steady state analysis of the data. This analysis is more conservative but based on a simple equation (eq 4) which makes it also very robust. The fitting curves of one representative experiment are shown in Figure S4. Since we were aware that this steady state fit based on a homogeneous binding model is not the most precise description of our data, we called the obtained K_D values "apparent overall K_D values". For steady state fit analysis, R^2 values ≥ 0.95 (Figure S4) were achieved which we considered as a reliable fit and K_D values were precisely determined with relative errors < 30% for triplicates (Figure 3). Therefore, we have taken the apparent overall K_D values from steady state analysis into account to directly compare ANK peptides among each other and relatively to D3.

D3 bound to Aβ monomers with a K_D value of 6.5 μM under the given assay conditions (Figure 3A). The K_D values of optimized D3 derivatives ANK1 to ANK7 ranged from 1.3 μM to 2.3 μM (Figure 3B−H). Thus, the ANK peptides had 3- to 5-fold increased binding affinities to monomeric Aβ compared to the original peptide D3.

ANK1 to ANK7 Inhibited Aβ Fibril Formation Highly Efficiently. To study the influence of the ANK peptides on the Aβ(1−42) fibril formation, a Thioflavin T (ThT) assay was performed. ThT is a benzothiazole, which interacts with β-sheet rich structures including Aβ oligomers, protofibrils and fibrils. Upon binding the fluorescence emission is increased at 490 nm.[16]

As demonstrated in Figure 4A, all ANK peptides inhibited the formation of ThT positive Aβ fibrils within 48 h. Co-incubation of 20 μM Aβ with equimolar concentrations of ANK1, ANK2, or ANK3 showed only 5%, 1%, and 4% of the fluorescence signal of Aβ alone after 48 h, indicating that Aβ oligomer and fibril formation was almost completely suppressed by the respective ANK peptides. ANK4, ANK6, and ANK7 significantly inhibited the Aβ fibril formation, which is shown by the decreased ThT fluorescence signal after 48 h to 16%, 13%, and 21% compared to the Aβ control. ANK5 co-incubated with Aβ resulted in a ThT fluorescence signal of 53%

DOI: 10.1021/acschemneuro.7b00045
ACS Chem. Neurosci. 2017, 8, 1889−1900

normalized to the control, indicating that ANK5 inhibited fibril formation by 47%.

ANK1 to ANK7 Eliminated Aβ Oligomers. A suitable method to assess a compound's efficacy to eliminate toxic Aβ oligomers is the QIAD assay, an assay for the quantitative determination of interference with Aβ aggregate size distribution.[14] As introduced by Brener et al., this assay is a powerful tool to measure oligomer elimination instead of oligomer binding. The QIAD assay consists of three steps: first, the generation of different Aβ species followed by a co-incubation of this mixture with therapeutics of interest; second, a separation of the different Aβ species by density gradient centrifugation followed by a fractionation; third, a quantification of Aβ within the different fractions via RP-HPLC. Previous work showed that especially Aβ(1−42) oligomers located in fractions 4 to 6 are sensitive to D3 and thus, these oligomers were characterized in detail by Brener et al.[14] The results showed that those oligomers consist of approximately 23 monomer units, have an average molecular weight of about 100 kDa and are extremely cytotoxic. Under the given conditions, the oligomer population is weighted to 35% relatively to the total Aβ distribution (Figure S5). ANK1 to ANK7 were compared to each other and to D3 according to their ability to eliminate these Aβ(1−42) oligomers. The quantification of Aβ within these fractions showed, that ANK5, ANK6, and ANK7 eliminated the Aβ oligomers significantly more efficient than D3 (Figure 4B). D3 eliminated 50% of the Aβ oligomers, while ANK6, ANK7 and ANK5 eliminated 81%, 73% and 72% of the Aβ oligomers, respectively. The concentration of Aβ monomers, present in fractions 1 and 2, was not significantly affected by the ANK-peptides (Figure S5). The elimination of Aβ oligomers by D3 or ANK peptides was balanced by an increase of Aβ in fractions 10 to 13. Thus, Aβ oligomers were coprecipitated into high-molecular-weight aggregates with the respective peptide, which were already described to be nontoxic.[17]

ANK1 to ANK7 Reduced the Aβ-Induced Cytotoxicity in a Concentration Dependent Manner. Aβ has a toxic effect on neuronal cells.[18] To study the influence of ANK peptides on the Aβ-induced cytotoxicity, a cell viability assay was performed. Therefore, 50 μM Aβ was preincubated to generate toxic Aβ species and co-incubated with or without D-peptides in three different Aβ/peptide ratios (a high ratio (1:5), an equimolar ratio (1:1) and a low ratio (1:0.2)). These Aβ-peptide mixtures were subsequently applied to SH-SY5Y human neuroblastoma cells for 24 h.

Aβ species formed in absence of ANK peptides significantly reduced SH-SY5Y cell viability by 45% (Figure 4C). Co-incubation of Aβ with D3 did not show any significant effects on the Aβ-induced cytotoxicity within all tested ratios (Figure 4C). Co-incubation of Aβ with ANK peptides reduced the cytotoxicity of Aβ especially at high and equimolar ratios. ANK1, ANK2, and ANK3 almost completely neutralize Aβ cytotoxicity under these conditions. The addition of ANK6 showed the highest rescue effect on Aβ-induced cytotoxicity already in the low ANK/Aβ ratio. As a control, the ANK peptides alone did not have any influence on the viability of SH-SY5Y cells (Supporting Information, Figure S6).

These results correlate overall with the results obtained from the QIAD assay for Aβ oligomer elimination. In both assays, ANK6 was the most efficient D3 derivative (Figure 4B). ANK6 eliminated more than 80% of the Aβ oligomers and significantly reduced the Aβ-induced toxicity on SH-SY5Y cells in all applied concentrations. Additionally, ANK6 bound to Aβ with a K_D value of 2.3 μM (Figure 3G) and inhibited the Aβ fibril formation almost completely (Figure 4A). Therefore, ANK6 was picked for further detailed in vitro and in vivo characterizations.

ANK6 Inhibited the Prion-like Propagation of Preformed Aβ Seeds. Aβ amyloidogenesis was described in vitro as a nucleated polymerization mechanism.[19−21] To investigate the ability of D3 and ANK6 to inhibit the prion-like propagation of preformed Aβ seeds by monomer sequestration, a seeding assay monitoring the aggregation of Aβ with ThT in real-time was performed (Figure S7). We examined the seeding potential of preformed Aβ fibrils on monomeric Aβ in the presence of D3 or ANK6 (Figure 4D). Since ANK6 was able to completely inhibit Aβ aggregation, we were only able to calculate the inhibition of fibril formation and not the half-time of the growth phase ($t_{1/2}$). However, the accelerated aggregation kinetics of Aβ monomers in the presence of seeds was observed in the time-resolved curves (Figure S7). D3 significantly inhibited seeded Aβ fibril formation by 55%. In comparison to D3, the efficacy of ANK6 to interfere with the seeded aggregation reaction was significantly improved, resulting in 100% inhibition of fibril formation.

ANK6 Converted Aβ Oligomers into Amorphous Aggregates. Previous studies showed that D3 converts Aβ into amorphous aggregates under unphysiologically high in vitro concentrations.[12] Since ANK6 is a derivative of D3, we hypothesized that ANK6 has a similar effect on Aβ(1−42). To investigate this, Aβ was preincubated for 4.5 h to enrich oligomers and co-incubated with ANK6 afterward. Transmission electron microscope (TEM) images confirmed our hypothesis. After 4.5 h of incubation, small oligomers were observed (Figure 5A). Aβ incubated for 28.5 h contained fibrillary structures, as shown in Figure 5B. Aβ co-incubated with ANK6 in the same molar ratio resulted in the formation of amorphous Aβ coprecipitates (Figure 5C). These results correlated with the observation, that ANK6 inhibited the formation of ThT positive Aβ fibrils.

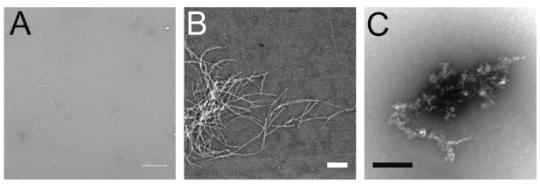

Figure 5. TEM images of initially 4.5 h preincubated Aβ(1−42) (A) without (B) and with (C) co-incubation with ANK6 (molar ratio 1:1) for further 24 h. Scale bars: 0.25 μm.

In vivo Study of ANK6 in Transgenic AD Mice. The therapeutic effect of ANK6 was investigated in the transgenic mouse model tg-APPSwDI.[22] Two groups of tg-APPSwDI mice (see Table S3) were treated either with saline or ANK6 (0.13 mg per mouse per day, i.p., for 4 weeks using Alzet minipumps). Their behavior was assessed using open field, zero maze, Morris water maze, and object recognition tests.

The open field and the zero maze tests provide data for the assessment of novel environment exploration and for the effects of drugs on anxiety-related behavior of mice. Changes in the behavior are hints for hypo- or hyperactivity.[23−25] Treatment

DOI: 10.1021/acschemneuro.7b00045
ACS Chem. Neurosci. 2017, 8, 1889−1900

with ANK6 had no influence on the general behavior of tg-APPSwDI (Figure S8).

Tendency of Reversal of Cognitive Deficits in tg-APPSwDI Mice Treated with ANK6. After 3 weeks of ANK6 treatment, a Morris water maze experiment was performed to investigate spatial learning and memory capabilities of the mice (Figure S9).[26] No significant differences in the swimming speed were observed (15.0 ± 0.6 m/s for saline and 16.4 ± 0.9 m/s for ANK6 treated mice) and both groups showed significant learning during 5 days of training. Thus, due to significant learning of the control group, any treatment effect of ANK6 was neither expected nor observed in the Morris water maze.

Furthermore, we studied the performance of both groups in the novel object recognition test. The assay investigates the spontaneous behavior of rodents to interact more intensively with a novel object compared to a familiar one.[27,28] Equal or similar interaction of the rodent with a familiar object and with a novel object points toward a lack of recall or loss of memory. Within our study, saline treated mice displayed deficits in episodic memory as demonstrated by the lack of preference for the new object (Figure 6, p = 0.75). ANK6 treated mice, however, showed increased preference for the new object (p = 0.075) indicating a tendency that ANK6 improved the cognition of tg-APPSwDI mice.

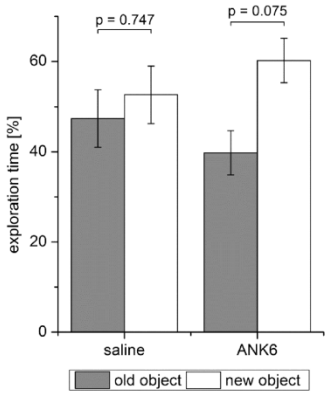

Figure 6. Object recognition test. Tg-APPSwDI mice were treated i.p. over 4 weeks with ANK6 or saline as a control. To investigate the cognitive abilities of the treated mice, an object recognition test was performed. The amount of time which the mice explored either the familiar or the new object is presented as mean values ± SEM. A two-sample t test was performed to compare the exploration times for both objects within one group.

No Significant Changes in Aβ Plaque Load in ANK6 Treated tg-APPSwDI Mice. Tg-APPSwDI mice are developing typical Aβ plaques, starting at the age of three months.[22] Although based on the suggested mechanism of action, we did not expect ANK6 treatment to change the plaque load, there was a slight chance to observe treatment impact on plaques. Therefore, mice were sacrificed after the behavioral experiments and we determined the plaque load of the mouse brains (Figure S10). No significant changes in the Aβ plaque load were observed between ANK6 and placebo treated groups.

■ DISCUSSION AND CONCLUSION

Previously, we selected via mirror image phage display the D-enantiomeric peptide D3 to identify specific ligands for monomeric Aβ as target.[12] The rationale behind this approach was that any ligand that specifically binds monomeric Aβ might stabilize monomeric Aβ and thus shifting the equilibrium away from aggregated Aβ species, for example Aβ oligomers. In the original selection procedure, we were not able to counter-select for binding to nonmonomeric Aβ species. Nevertheless, we identified D3 as a compound that eliminates toxic Aβ oligomers and converts them into nontoxic, amorphous coprecipitates in vitro.[8,13] In vivo, D3 improves spatial learning and decreases Aβ plaque load even after oral administration.[8] In order to investigate more on the hypothesis that stabilization of monomeric Aβ is beneficial for improved elimination of Aβ oligomers and enhancement of cognition, we set out amino acid residue replacements to identify D3 derivatives that are characterized by higher affinity and specificity to monomeric Aβ.

It is noteworthy that although D3 was selected from a phage displayed peptide library that contained about 10^9 different 12mer peptides, a fully randomized 12mer library would contain 20^{12} different peptides. Thus, the phage displayed peptide library of the original D3 selection did by far not contain all possible 12mer sequences leaving room for further optimization of D3.

In the past, we started several intents to carry out such optimization and to confirm the proof of principle. First, we identified Aβ monomer specific ligands by repeating the original mirror image phage display selection procedure,[8] but introducing additional counter-selection pressure for binding to Aβ oligomers and fibrils.[29] Second, we set out to exchange every amino acid residue of D3 with all proteinogenic, except cysteine, in D-enantiomeric confirmation.[30] In a second round, these replacements were combined for further selection. These approaches, however, were based on "seedless" Aβ instead of truly monomeric Aβ as a target. Additionally, a counter selection against Aβ oligomers and fibrils was not performed within the second approach.

Thus, for the first time, we hereby present the results of a more sophisticated approach to identify truly Aβ monomer specific ligands by D3 derivatization. We developed and applied a two-step peptide microarray selection procedure to identify D3 derivatives with increased binding affinity and specificity for monomeric Aβ(1−42) and at the same time for decreased binding affinity and specificity for oligomeric and fibrillar Aβ. Therefore, we used Aβ monomers obtained from SEC as drug target and Aβ oligomers and Aβ fibrils as counter target for scoring all investigated D3 derivatives.

Within the here performed screening, additional 13 non-proteinogenic amino acid residues were used in order to introduce more variety. The first peptide microarray consisted of 384 different D3 derivatives with a variation of each single amino acid residue with all proteinogenic amino acid residues, except cysteine, but in their D-enantiomeric conformation and 13 nonproteinogenic amino acid residues. These 384 different D3 derivatives were assayed for increased binding affinity and specificity to Aβ(1−42) monomers. In a second step, the most promising single replacements were combined with each other and the resulting 1024 compounds were again screened for increased Aβ(1−42) monomer binding affinity and specificity. Seven novel compounds, named ANK1 to ANK7, with five or six replacements compared to D3 were picked and further characterized in vitro. The positions 2, 4, 7, and 10 of D3 showed the highest potential for optimization. In all ANKs, the original p2 of D3 was replaced against k, the original t4 against i

DOI: 10.1021/acschemneuro.7b00045
ACS Chem. Neurosci. 2017, 8, 1889−1900

or v, the original h7 against v, phenylglycine or trans-4-fluorophenylalanine, and the original r10 against i, w or k. ANK5, ANK6 and ANK7 contain k at the C-terminus. Therefore, the positive net charge of these peptides was increased compared to D3 and the remaining ANK peptides. With this procedure, we could successfully identify D3 derivatives, named ANK peptides, with increased binding specificity for Aβ monomers.

Binding affinities of ANK1 to ANK7 to monomeric Aβ were 3−5-fold increased as compared to D3. Additionally, the binding mode deviated from a homogeneous interaction, which was deduced from the shape of the BLI sensorgrams and suggested the appearance of an additional slower off-rate for the ANK peptides as compared to D3. However, it needs to be further investigated whether the heterogeneous binding is just based on unspecific binding, e.g. due to the increased hydrophobicity compared to D3, or rather a second binding site.

Furthermore, the Aβ oligomer elimination efficacy, as analyzed by the QIAD assay, was enhanced for the ANKs as compared to D3. Aβ-induced cytotoxicity was reduced in the presence of ANK1 to ANK7, as expected. ANK6 showed the highest effect on elimination of Aβ oligomers and reduction of Aβ-induced cytotoxicity, and thus was selected for further analysis.

Aβ fibrils exhibit the ability to enhance self-aggregation and act as seeds for fibril formation of Aβ monomers.[19−21] The reduced seeding reaction of Aβ fibrils in the presence of D3 or ANK6 indicated that ANK6 was significantly more efficient than D3 to inhibit this process. Since ANK6 was able to completely inhibit this process, a highly efficient stabilization of monomers can be assumed which resulted in a sequestration of Aβ monomers from this acceleration reaction.

In vivo therapeutic effects of ANK6 were investigated in the transgenic mouse model tg-APPSwDI. Application of ANK6 over 4 weeks did not result in any side effects, like hypo- or hyperactivity. Although we have not carried out a full pharmacokinetic study with ANK6, it is well documented that the lead compound D3 and several other D3 derivatives penetrate the brain very efficiently and show brain to plasma ratios up to 1.0.[31−33] Therefore, we assume that also ANK6 was able to cross the blood-brain barrier and reached the brain. ANK6 showed a tendency for improving the cognition of tg-APPSwDI mice within the novel object recognition test (p = 0.075). One possible explanation why the typical significance level ($p < 0.05$) was not reached might be the relatively short treatment period compared to other studies.[34,35] Furthermore, no significant changes in Aβ plaque load were found, which is exactly what was expected based on our working hypothesis. Because ANK6 was not designed to interfere with Aβ production or clearance, and because we indeed did not find any differences in plaque loads between ANK6 treated and placebo treated mice, we did not further investigate Aβ levels in the animals. Nevertheless, this result indicates, that reduction of Aβ plaque pathology is not necessary to improve cognitive deficits, which is in accordance with the well described lack of correlation between Aβ plaques load and cognitive impairment and was also reported from our further studies.[36−38]

This ANK6 mice study is not directly comparable with previously published D3 studies. With ten months of age the here used tg-APPSwDI mice were relatively old compared to other D3 studies.[9,14] Additionally, earlier studies differed in mouse models, treatment durations, dosage and application forms.[9,11,14]

Taken together, this study shows that the strategy to identify derivatives of D3 with increased binding affinity and specificity for Aβ monomers resulted in even more potent D-peptides than the original lead compound D3. The ANK peptides showed highly efficient stabilization of monomers resulting in a sequestration of monomers from the aggregation reaction. Therefore, Aβ oligomer elimination efficacy was enhanced for ANK peptides as well as superior effects in other in vitro and in vivo experiments. The ANK peptides may become promising drug candidates for the treatment of AD and will be further investigated in vivo.

METHODS

Peptides. Synthetic Aβ(1−42), N-terminally biotinylated Aβ(1−42) and FITC-Aβ(1−42) were purchased from Bachem (Heidelberg, Germany). Recombinant Aβ(1−42) was purchased from Isoloid (Duesseldorf, Germany). The D-enantiomeric peptides D3 and ANK1 to ANK7 were purchased with a purity of 95% from peptides&elephants (Potsdam, Germany). The C-terminus of the D-peptides was amidated.

Preparation of Seedless Aβ(1−42) Stock Solutions. In general, synthetic Aβ(1−42) was used if not other stated and all Aβ preparations were carried out in Protein LoBind tubes (Eppendorf AG, Hamburg, Germany). Lyophilized Aβ(1−42), N-terminally biotinylated Aβ(1−42) and FITC-Aβ(1−42) were dissolved in 1,1,1,3,3,3-Hexafluor-2-propanol (HFIP) to a final concentration of 1 mg/mL overnight at room temperature and stored at −20 °C until further use. For experiments, required amounts were aliquoted and HFIP was evaporated using a vacuum concentrator (Concentrator 5301, Eppendorf, Germany) for 20 min.

Preparation of Different Aβ(1−42) Species in Solution. For incubation of the peptide microarrays with different Aβ(1−42) species, the preparation of monomeric and oligomeric FITC-Aβ(1−42) was carried out using size exclusion chromatography (SEC) as described before.[39] In brief, HFIP pretreated FITC-Aβ(1−42) was freshly dissolved in 10 mM sodium phosphate buffer pH 7.4 containing 150 mM NaCl to a concentration of 0.1 mM FITC-Aβ(1−42), centrifuged and supplied on a Superdex 75 10/300 GL column (GE Healthcare, Uppsala, Sweden) connected to an Äkta purifier system (GE Healthcare, Uppsala, Sweden). The separation of monomeric and oligomeric FITC-Aβ(1−42) was performed with a flow rate of 0.6 mL/min and recorded by measuring the absorption at 490 and 280 nm. 500 μL fractions were collected and fractions, containing monomeric or oligomeric FITC-Aβ(1−42), were pooled.

For preparation of Aβ fibrils, FITC-Aβ(1−42) was dissolved in 10 mM sodium phosphate buffer pH 7.4 as described above and incubated for 3 days at 37 °C. Generated fibrils were centrifuged at 14,000g and washed three times with buffer to remove soluble monomeric and oligomeric Aβ species.

Peptide Microarrays. The peptide microarrays were purchased from Pepscan (Lelystad, Netherlands). Different D-peptides were covalently coupled on glass microscope slides in triplicate (spots with a diameter of 100 μm). In a first generation peptide microarray, every position of the 12 amino acid residues of D3 was replaced against 19 naturally occurring amino acids (all amino acids except of cysteine) and 13 nonproteinogenic amino acids in their D-enantiomeric conformation. In a second generation peptide microarray, promising single replacements, which increased the specific binding of D3 derivatives to monomeric Aβ, were combined.

The peptide microarray procedure involved three parts: an experimental part, a data acquisition and a data analysis (Figure 1).

1. Experimental Part. As a pretreatment, the peptide microarray slides were shortly washed with ddH_2O and 20% ethanol. Peptide microarray slides were incubated with 5 μM fluorescein isothiocyanate (FITC), 1−5 μM monomeric, oligomeric or fibrillar FITC-Aβ(1−42), respectively, achieved as described above, in 10 mM sodium phosphate buffer pH 7.4 for 1 h at room temperature with gentle agitation. After incubation, the slides were washed three times with TBS-T (TBS with

DOI: 10.1021/acschemneuro.7b00045
ACS Chem. Neurosci. 2017, 8, 1889−1900

0.1% v/v Tween-20) for 10 min and three times with water for 10 min, following by drying with nitrogen. This experimental part was performed in triplicate.

2. Data Acquisition. The fluorescence intensities (FI) on the prepared slides were evaluated using a FLA800 fluorescence image system (Fujifilm Medical Systems USA Inc., Stamford, CT) with slide carrier employing a 473 nm laser for excitation and a 530 nm emission filter. Digital images with 5 μm resolution were generated. The fluorescence intensities were quantified using the software AIDA array Metrix (Raytest, Staubenhardt, Germany). The integral of the fluorescence intensities (diameter 80 μm) was calculated. Background subtraction was carried out by local dot rings. Therefore, background signals were measured from the ring area of 150−180 μm from the center of each D-peptide spot.

3. Data Analysis. Each peptide sequence has three replicates on each slide. The fluorescence intensities (FI) of these technical replicates were combined by calculating the mean value, named mean fluorescence intensity (mFI_1). To compare the fluorescence intensities of the different experiments, a median-based normalization was performed:

$$mFI_2 = \frac{mFI_1}{\text{median}(mFI_{1\_all})} \quad (1)$$

with mFI_2 being the normalized fluorescence intensity of one peptide on the microarray, mFI_1 being the mean fluorescence intensity of the technical replicates, and mFI_{1_all} being the mean fluorescence intensity of all sequences within one experiment. The mean value of mFI_2 for each peptide sequence of three independent experiments was calculated and named mFI_3. Afterward, the fluorescence intensities were corrected for unspecific binding of FITC by subtracting mFI_3 from peptide microarrays incubated with FITC only.

$$bs_{conf} = mFI_{3\_conf} - 0.2mFI_{3\_FITC} \quad (2)$$

with bs_{conf} being the FITC corrected binding score of one peptide incubated with one of the three Aβ conformation species, and mFI_{3_conf} and mFI_{3_FITC} being the mean fluorescence intensity of one peptide sequence over all three experiments incubated with an Aβ conformation species or FITC, respectively. To avoid overestimation of FITC binding, the mFI_3 values were multiplied by a factor of 0.2.

The specific monomeric Aβ binding score (sbs_{mono}) was calculated using the following equation:

$$sbs_{mono} = bs_{mono} - 0.5bs_{oligo} - 0.5bs_{fib} \quad (3)$$

with bs_{mono} being the binding score for Aβ monomers, bs_{oligo} being the binding score for Aβ oligomers, and bs_{fib} being the binding score for Aβ fibrils. To avoid overestimation of the sum of the binding scores for oligomers and fibrils, the bs_{oligo} and bs_{fib} values were multiplied by a factor of 0.5. The resulting sbs_{mono}, one score for each peptide sequence, was visualized in a heat map generated with MatLab (The MathWorks, Natick, MA) (Figure 2A).

Additionally, a specific binding ratio was calculated by forming the quotient of bs_{mono} and bs_{oligo} and bs_{mono} and bs_{fib} (Figure 2D).

Biolayer Interferometry (BLI). The equilibration dissociation constants (K_D) determination of D3 and ANK1 to ANK7 to monomeric Aβ(1−42) was examined using biolayer interferometry (BLI) where biotinylated Aβ(1−42) was immobilized to the sensor surface via biotin−streptavidin coupling and the peptides were used as analytes in solution.

The purification and immobilization of Aβ(1−42) monomers was performed as described before with minor changes.[40] Briefly, HFIP pretreated N-terminally biotinylated Aβ(1−42) was dissolved in 20 mM sodium phosphate buffer pH 7.2 to a final concentration of 80 μg/mL. Monomers were purified on a Superdex 75 10/300 GL column (GE Healthcare, Uppsala, Sweden) connected to an ÄKTA purifier system (GE Healthcare, Uppsala, Sweden). Purified monomers were directly immobilized on the sensor surface of Super Streptavidin biosensors (SSA) (fortéBIO, PALL Life Science, Menlo Park, CA) using an Octet RED96 instrument (fortéBIO, PALL Life Science, Menlo Park, CA) to a final level of 2 nm. Ligand and reference biosensors were quenched with 20 μg/mL biotin for 7 min.

The K_D determinations of D3 and ANK peptides to monomeric Aβ(1−42) were performed in multi cycle kinetics at 26 °C. Association of 0.8, 1.6, 3.1, 6.3, 12.5, 25 , and 50 μM D3 and 0.4, 0.8, 1.6, 3.1, 6.3, 12.5, and 25 μM ANK peptides diluted in 20 mM sodium phosphate, 50 mM sodium chloride, pH 7.4 was recorded for 300 s on ligand and reference biosensors, followed by a dissociation phase of 300 s. After each cycle, a regeneration step using 2 M guanidine hydrochloride for 30 s was implemented. After measurement, the sensorgrams were double referenced using the reference biosensors and a buffer cycle. Steady-state evaluation was performed by plotting the respective response levels against the applied peptide concentrations. The curves were fitted according to the following Langmuir's 1:1 binding model (Hill equation with $n = 1$) using OriginPro 8.5G (OriginLab, Northampton, MA):

$$y = \frac{R_{max}\, x}{K_D + x} \quad (4)$$

with y being the binding signal, R_{max} being the saturation binding signal, x being the applied peptide concentration, and K_D being the equilibrium dissociation constant.

Thioflavin T Assay. The Thioflavin T (ThT) assay was performed as described before.[39] In brief, HFIP pretreated Aβ(1−42) was dissolved to 20 μM in 10 mM sodium phosphate buffer, pH 7.4 and mixed with 20 μM ThT and 20 μM D-peptide. The ThT fluorescence was monitored over 48 h every 15 min at λ_{ex} = 440 nm and λ_{em} = 490 nm in a plate reader (Polarstar Optima, BMG, Ortenberg, Germany) at 37 °C. Each value was background corrected (all components without Aβ).

Quantitative Determination of Interference with Aβ(1−42) Aggregate Size Distribution (QIAD). The QIAD assay was performed according to Brener et al.[14] After a preincubation of 4.5 h in 10 mM sodium phosphate buffer, pH 7.4 at 21 °C and shaking at 600 rpm, 80 μM Aβ(1−42) was co-incubated with 10 μM D-peptide for 40 min under the same conditions. For separation of the different Aβ(1−42) species, a density gradient centrifugation with a discontinuous gradient ranging from 5 to 50% iodixanol (OptiPrep, Axis-Shield, Oslo, Norway) was performed by using an ultracentrifuge (Optima MAX-XP) with an TLS-55 rotor (both Beckman Coulter, Brea, CA). A volume of 100 μL of the sample was loaded on the top of the gradient. After centrifugation at 259, 00g for 3 h at 4 °C, 14 × 140 μL fractions were collected from the top to the bottom. To dissolve the pellet, representing the 15th fraction, 60 μL of 6 M guanidine hydrochloride was boiled for 5 min within the centrifuge tube. The samples were stored at −20 °C until further use.

For quantification of the Aβ content in each fraction, reverse phase high performance liquid chromatography (RP-HPLC) was used. A volume of 20 μL was supplied on a Zorbax SB-300 C8 column (Agilent, Böblingen, Germany) connected to an Agilent 1260 Infinity system. Thirty % v/v acetonitrile with 0.1% (v/v) trifluoroacetic acid (TFA) was used as mobile phase. The column was tempered at 80 °C and the UV absorption at 214 nm was detected. For quantification of the Aβ(1−42) amount, the area under the peak representing Aβ(1−42) was calculated and the molar concentration was determined using a calibration equation.

The recovery rate R was determined by using the following equation:

$$R = \frac{c_p V_p + \sum_{n=1}^{14} c_n V_F}{c_0 V_0} \quad (5)$$

with c_p being the Aβ(1−42) concentration in the last fraction (15th fraction), c_n being the Aβ(1−42) concentration in fractions 1−14, c_0 being the initial Aβ(1−42) concentration, V_F being the volume of the fractions 1−14, V_p being the volume of the last fraction, and V_0 being the volume of the initial sample. The total Aβ recovery rate was 94% for Aβ(1−42) without peptide and 92% for Aβ(1−42) co-incubated with D-peptides

DOI: 10.1021/acschemneuro.7b00045
ACS Chem. Neurosci. 2017, 8, 1889−1900

The elimination (E) of Aβ(1−42) oligomers by the D-peptides D3 and ANK1 to ANK7 were determined as followed:

$$E = 100\left(1 - \frac{\sum_{n=4}^{6} c_n}{\sum_{n=4}^{6} c_{A\beta}}\right) \quad (6)$$

with c_n being the Aβ(1−42) concentration in fractions 4−6 in the presence of D-peptide and $c_{A\beta}$ being the Aβ(1−42) concentration of the control without D-peptide.

The results were statistically analyzed using the Mann−Whitney U-test. Aβ(1−42) without ligand was measured 11 times, and Aβ(1−42) with D-peptide four times.

MTT Cell Viability Assay. The human neuroblastoma SH-SY5Y cells (Leibniz Institute DSMZ, Braunschweig, Germany) were cultivated in DMEM medium supplemented with 20% fetal calf serum. Here, 10 000 cells per well were seeded on collagen-coated 96 well plates (Gibco, Carlsbad, CA) and incubated in a humidified atmosphere with 95% air and 5% CO_2 at 37 °C for 24 h. 51 μM Aβ(1−42) was preincubated for 4.5 h in 10 mM sodium phosphate buffer pH 7.4 at 21 °C and 600 rpm and co-incubated with the ANK peptides or D3 for further 40 min under the same conditions. The cells were treated with 1 μM Aβ(1−42) and 0, 0.2, 1, or 5 μM final peptide concentrations. For quantification of the cell viability, the Cell Proliferation Kit I (MTT) (Roche, Mannheim, Germany) was used according to manufacturer's instructions. The absorbance of the formazan product was determined by measuring the absorption at 570 nm subtracted by the absorption at 660 nm in a plate reader (Polarstar Optima, BMG). The positive control, consisting of cells only, was set to 100% cell viability. One-way ANOVA with Bonferroni posthoc test was used for statistical analysis.

Seeding Assay. Recombinant Aβ(1−42), 50 μM, was incubated in 10 mM sodium phosphate buffer pH 7.4 over 3 days at 37 °C for seed preparation. After this time, we assumed that nearly 100% of monomers aggregated into fibrils. The sample was vortexed and sonicated for 2 min. Freshly prepared Aβ(1−42) monomers (10 μM) were mixed with 2% seeds (200 nM) regarding the monomer concentration in the seed solution and 10 μM D3 or ANK6. The buffer conditions were 10 mM sodium phosphate pH 7.4 containing 5 μM ThT. Aβ(1−42) monomers without seeds served as a control. The ThT fluorescence was measured at λ_{ex} = 440 nm and λ_{em} = 490 nm every 10 min for 21 h at 37 °C. After this time, the curves reached saturation and the amplitudes were determined by subtracting the fluorescence signals from the lag-phase from final signals at the end of the aggregation curves. The fibril masses were normalized to the Aβ(1−42) monomer curves and inhibition in % was calculated. The presented data are mean values and SD from three independent experiments with three technical replicates each. The results were statistically analyzed using the Mann−Whitney U-test.

Transmission Electron Microscopy (TEM). Oligomer-enriched Aβ(1−42) solution of the QIAD assay and samples used for the MTT assay with Aβ(1−42) and ANK6 in equimolar ratio were incubated 24 h and absorbed on Formvar/carbon coated copper grids (S162, Plano, Wetzlar, Germany) for 5 min. After three times washing with water, the samples were negatively stained with 1% (w/v) uranyl acetate for 1 min. Images were recorded using a Libra 120 transmission electron microscope (Zeiss, Oberkochen, Germany) operating at 120 kV.

Animals. In the present study, 10 month (±1 week) old female APPSwDI (human APP with Swedish K670N/M671L, Dutch E693Q, and Iowa D694N mutations on a C57BL/6 background) mice were used. The animals were housed five per cage in a controlled environment (temperature 22 °C, humidity 50−60% and light from 07:00 am to 07:00 pm), food and water were available ad libitum. The experiments were conducted in accordance with the local Institutional Animal Care and Use Committee (IACUC) guidelines. Group sizes were decided on the basis of previous data.[9]

ANK6 Treatment. Tg-APPSwDI mice (11 animals per group) were treated over 4 weeks with a total peptide amount of 3.7 mg via intraperitoneally implantedAlzet minipumps (model #1004; delivery rate: 0.11 μL/h).

Behavior. During the last week of treatment, animals were tested in three different behavioral tests to assess cognition and to monitor side effects like changes in general activity and anxiety. Experiments were performed double-blinded.

First, the open field test was conducted. The arena consisted of an arena of 42 × 42 cm^2 with clear Plexiglas walls (20 cm high). The animal was put into the arena and observed for 4 min with a camera driven tracker system (Ethovision 8.5, Noldus, Wageningen, The Netherlands). The arena was subdivided into two areas, the center and the area at the walls. The system recorded the position of the animal in the arena at 5 frames/second and the data were analyzed regarding time spent in each area (center vs wall). For disinfection and to avoid olfactory cues, the apparatus was cleaned with chlorhexidine and 70% ethanol and allowed to air-dry.

Next, the zero maze test was conducted. The maze consisted of a circular arena with a diameter of 70 cm and four areas of equal size, two with walls with the height of 0.5 cm and two walls with the height of 15 cm walls of nontransparent material. The animal was put in the arena and observed for 4 min with a camera driven tracking system (Ethovision 8.5, Noldus, Wageningen, The Netherlands). The time spent in each area (open vs closed) was recorded. After every trail, the box was cleaned with chlorhexidine and 70% ethanol and allowed to air-dry to avoid olfactory cues.

The water maze procedure has been described in detail before.[41] Briefly, a pool, 120 cm in diameter, and a see-through round platform, 10 cm in diameter, located 0.5 cm below the water surface, were used. During day 1 through day 5 of the testing period, the mice were trained to find a hidden platform that is kept in a constant position throughout these 5 days. Three trials a day were performed; each trial started at another starting position in random order. The mice had 60 s to find the platform and 10 s to stay on the platform. The intertrial interval was 2 min.

The object recognition test (ORT) was carried out in a maze consisting of a rectangular polycarbonate box, with partitions separating the box into three chambers. The partitions had openings that allowed the animal to move freely from one chamber to another. The animal was monitored by the Noldus tracking system Ethovision 8.5. The test consisted of two sessions: a training session and a testing session. In the training session, two identical objects were placed on each side in the box. The mouse was placed in the box and allowed to move freely throughout the apparatus for a 10 min training session. After 30 min, a new object replaced one of the old objects and the mouse was put in the box and allowed to move freely throughout the box over a 4 min test session. The time spent with each object was recorded. All objects used in this study were different in size and shape. They were fixed in the box to avoid movement and cleaned with chlorhexidine and 70% ethanol and allowed to air-dry to avoid olfactory cues. The apparatus was additionally cleaned with chlorhexidine followed by ethanol and water and dried with paper towels for each mouse tested.

Histochemistry. After the treatment period, mice were sacrificed for histochemical analysis. Therefore, the mice were anesthetized and transcardially perfused. The brain was removed, and the right hemisphere was fixed in 4% paraformaldehyde overnight. Afterward, it was cryoprotected in 30% sucrose for 24 h and antifreezed in 15% sucrose and 30% ethylene glycol in 0.05 M phosphate buffer, pH 7.4. The brain was cut into six sections (1−6) of coronal sections (30 μm). The first series of sections was mounted unstained; the second and third series were immunohistochemically stained, using the W0-2 antibody for human Aβ, according to van Groen et al.[42] The other series were stored in antifreeze at −20 °C. Plaque loads were determined as described before.[42,43]

■ ASSOCIATED CONTENT

Supporting Information

The Supporting Information is available free of charge on the ACS Publications website at DOI: 10.1021/acschemneuro.7b00045.

DOI: 10.1021/acschemneuro.7b00045
ACS Chem. Neurosci. 2017, 8, 1889−1900

Raw data of first generation peptide microarray, structure of nonproteinogenic amino acids, size distribution of Aβ monomers and oligomers used within the peptide microarrays, heterogeneous fit curves and results of BLI measurements, steady state fit curves of BLI measurements, effect of D3 or ANK peptides on the Aβ size distribution, MTT assay controls, seeding assay curves, effect on saline and ANK6 treated tg-APPSwDI mice in open field test, zero maze and Morris water maze, plaque load, summary of important quantities of the in vivo study and SI Methods (PDF)

AUTHOR INFORMATION

Corresponding Author

*E-mail: d.willbold@fz-juelich.de.

ORCID

Dieter Willbold: 0000-0002-0065-7366

Author Contributions

A.N.K, J.K., and D.W. designed the peptide combinations for the microarrays. A.N.K. carried out all experiments with the peptide microarrays, as well as the QIAD, TEM, and ThT assays. O.B. and L.G. designed the QIAD. T.Z. designed and M.Th. and T.Z. performed the binding studies. J.K. designed and M.T. performed the cell toxicity assays. T.Z. and A.E. designed and performed the seeding assay, T.v.G. and I.K. designed and performed the in vivo studies, and D.W. designed the overall study. A.N.K, T.Z., J.K., and D.W. wrote the manuscript. All other authors contributed to writing.

Funding

D.W. was supported by grants from the "Portfolio Technology and Medicine", the "Portfolio Drug Research", and the Helmholtz-Validierungsfonds of the "Impuls und Vernetzungs-Fonds der Helmholtzgemeinschaft". The study was supported by the TT-Fonds of the Technology Transfer Department of the Forschungszentrum Jülich.

Notes

The authors declare no competing financial interest.

ABBREVIATIONS

BLI, biolayer interferometry; FITC, fluorescein isothiocyanate; TEM, transmission electron microscopy; Tg-APPSwDI, transgene mice expressing human APP with Swedish K670N/M671L, Dutch E693Q and Iowa D694N mutations on a C57BL/6 background; ThT, Thioflavin T

REFERENCES

(1) Prince, M., Bryce, R., Albanese, E., Wimo, A., Ribeiro, W., and Ferri, C. P. (2013) The global prevalence of dementia: A systematic review and metaanalysis. *Alzheimer's Dementia 9*, 63−75.e2.

(2) Querfurth, H. W., and LaFerla, F. M. (2010) Alzheimer's Disease. *N. Engl. J. Med. 362*, 329−344.

(3) Hardy, J., and Selkoe, D. J. (2002) The Amyloid Hypothesis of Alzheimer's Disease: Progress and Problems on the Road to Therapeutics. *Science 297*, 353−356.

(4) Selkoe, D. J. (2001) Alzheimer's Disease: Genes, Proteins, and Therapy. *Physiol. Rev. 81*, 741−766.

(5) Finder, V. H., and Glockshuber, R. (2007) Amyloid-β Aggregation. *Neurodegener. Dis. 4*, 13−27.

(6) Lue, L.-F., Kuo, Y.-M., Roher, A. E., Brachova, L., Shen, Y., Sue, L., Beach, T., Kurth, J. H., Rydel, R. E., and Rogers, J. (1999) Soluble Amyloid β Peptide Concentration as a Predictor of Synaptic Change in Alzheimer's Disease. *Am. J. Pathol. 155*, 853−862.

(7) Schumacher, T. N., Mayr, L. M., Minor, D. L., Jr., Milhollen, M. A., Burgess, M. W., and Kim, P. S. (1996) Identification of D-peptide ligands through mirror-image phage display. *Science 271*, 1854−1857.

(8) Wiesehan, K., Buder, K., Linke, R. P., Patt, S., Stoldt, M., Unger, E., Schmitt, B., Bucci, E., and Willbold, D. (2003) Selection of D-Amino-Acid Peptides That Bind to Alzheimer's Disease Amyloid Peptide Aβ1−42 by Mirror Image Phage Display. *ChemBioChem 4*, 748−753.

(9) Funke, S. A., van Groen, T., Kadish, I., Bartnik, D., Nagel-Steger, L., Brener, O., Sehl, T., Batra-Safferling, R., Moriscot, C., Schoehn, G., Horn, A. H. C., Müller-Schiffmann, A., Korth, C., Sticht, H., and Willbold, D. (2010) Oral Treatment with the d-Enantiomeric Peptide D3 Improves the Pathology and Behavior of Alzheimer's Disease Transgenic Mice. *ACS Chem. Neurosci. 1*, 639−648.

(10) Bartnik, D., Funke, S. A., Andrei-Selmer, L.-C., Bacher, M., Dodel, R., and Willbold, D. (2010) Differently Selected d-Enantiomeric Peptides Act on Different Aβ Species. *Rejuvenation Res. 13*, 202−205.

(11) van Groen, T., Kadish, I., Funke, S. A., Bartnik, D., and Willbold, D. (2013) Treatment with D3 Removes Amyloid Deposits, Reduces Inflammation, and Improves Cognition in Aged AβPP/PS1 Double Transgenic Mice. *J. Alzheimer's Dis. 34*, 609−620.

(12) van Groen, T., Wiesehan, K., Funke, S. A., Kadish, I., Nagel-Steger, L., and Willbold, D. (2008) Reduction of Alzheimer's Disease Amyloid Plaque Load in Transgenic Mice by D3, a D-Enantiomeric Peptide Identified by Mirror Image Phage Display. *ChemMedChem 3*, 1848−1852.

(13) Wiesehan, K., Stöhr, J., Nagel-Steger, L., van Groen, T., Riesner, D., and Willbold, D. (2008) Inhibition of cytotoxicity and amyloid fibril formation by a d-amino acid peptide that specifically binds to Alzheimer's disease amyloid peptide. *Protein Eng., Des. Sel. 21*, 241−246.

(14) Brener, O., Dunkelmann, T., Gremer, L., van Groen, T., Mirecka, E. A., Kadish, I., Willuweit, A., Kutzsche, J., Jürgens, D., Rudolph, S., Tusche, M., Bongen, P., Pietruszka, J., Oesterhelt, F., Langen, K.-J., Demuth, H.-U., Janssen, A., Hoyer, W., Funke, S. A., Nagel-Steger, L., and Willbold, D. (2015) QIAD assay for quantitating a compound's efficacy in elimination of toxic Aβ oligomers. *Sci. Rep. 5*, 13222.

(15) van Groen, T., Kadish, I., Wiesehan, K., Funke, S. A., and Willbold, D. (2009) In vitro and in vivo Staining Characteristics of Small, Fluorescent, Aβ42-Binding D-Enantiomeric Peptides in Transgenic AD Mouse Models. *ChemMedChem 4*, 276−282.

(16) LeVine, H. (1995) Thioflavine T interaction with amyloid β-sheet structures. *Amyloid 2*, 1−6.

(17) Aileen Funke, S., van Groen, T., Kadish, I., Bartnik, D., Nagel-Steger, L., Brener, O., Sehl, T., Batra-Safferling, R., Moriscot, C., Schoehn, G., Horn, A. H., Muller-Schiffmann, A., Korth, C., Sticht, H., and Willbold, D. (2010) Oral treatment with the d-enantiomeric peptide D3 improves the pathology and behavior of Alzheimer's Disease transgenic mice. *ACS Chem. Neurosci. 1*, 639−648.

(18) Iversen, L. L., Mortishire-Smith, R. J., Pollack, S. J., and Shearman, M. S. (1995) The toxicity in vitro of beta-amyloid protein. *Biochem. J. 311*, 1−16.

(19) Cohen, S. I. A., Linse, S., Luheshi, L. M., Hellstrand, E., White, D. A., Rajah, L., Otzen, D. E., Vendruscolo, M., Dobson, C. M., and Knowles, T. P. J. (2013) Proliferation of amyloid-β42 aggregates occurs through a secondary nucleation mechanism. *Proc. Natl. Acad. Sci. U. S. A. 110*, 9758−9763.

(20) Jarrett, J. T., Berger, E. P., and Lansbury, P. T. (1993) The carboxy terminus of the.beta. amyloid protein is critical for the seeding of amyloid formation: Implications for the pathogenesis of Alzheimer's disease. *Biochemistry 32*, 4693−4697.

(21) Petkova, A. T., Leapman, R. D., Guo, Z., Yau, W.-M., Mattson, M. P., and Tycko, R. (2005) Self-Propagating, Molecular-Level Polymorphism in Alzheimer's ß-Amyloid Fibrils. *Science 307*, 262−265.

(22) Davis, J., Xu, F., Deane, R., Romanov, G., Previti, M. L., Zeigler, K., Zlokovic, B. V., and Van Nostrand, W. E. (2004) Early-onset and Robust Cerebral Microvascular Accumulation of Amyloid β-Protein in

DOI: 10.1021/acschemneuro.7b00045
ACS Chem. Neurosci. 2017, 8, 1889−1900

Transgenic Mice Expressing Low Levels of a Vasculotropic Dutch/Iowa Mutant Form of Amyloid β-Protein Precursor. *J. Biol. Chem. 279*, 20296−20306.
(23) Lalonde, R., Fukuchi, K., and Strazielle, C. (2012) Neurologic and motor dysfunctions in APP transgenic mice. *Rev. Neurosci. 23*, 363−379.
(24) Xu, F., Grande, A. M., Robinson, J. K., Previti, M. L., Vasek, M., Davis, J., and Van Nostrand, W. E. (2007) Early-onset subicular microvascular amyloid and neuroinflammation correlate with behavioral deficits in vasculotropic mutant amyloid beta-protein precursor transgenic mice. *Neuroscience 146*, 98−107.
(25) Prut, L., and Belzung, C. (2003) The open field as a paradigm to measure the effects of drugs on anxiety-like behaviors: a review. *Eur. J. Pharmacol. 463*, 3−33.
(26) D'Hooge, R., and De Deyn, P. P. (2001) Applications of the Morris water maze in the study of learning and memory. *Brain Res. Rev. 36*, 60−90.
(27) Zhang, R., Xue, G., Wang, S., Zhang, L., Shi, C., and Xie, X. (2012) Novel Object Recognition as a Facile Behavior Test for Evaluating Drug Effects in AβPP/PS1 Alzheimer's Disease Mouse Model. *J. Alzheimer's Dis. 31*, 801−812.
(28) Ennaceur, A., and Delacour, J. (1988) A new one-trial test for neurobiological studies of memory in rats. 1: Behavioral data. *Behav. Brain Res. 31*, 47−59.
(29) Rudolph, S., Klein, A. N., Tusche, M., Schlosser, C., Elfgen, A., Brener, O., Teunissen, C., Gremer, L., Funke, S. A., Kutzsche, J., and Willbold, D. (2016) Competitive Mirror Image Phage Display Derived Peptide Modulates Amyloid Beta Aggregation and Toxicity. *PLoS One 11*, e0147470.
(30) Klein, A. N., Ziehm, T., Tusche, M., Buitenhuis, J., Bartnik, D., Boeddrich, A., Wiglenda, T., Wanker, E., Funke, S. A., Brener, O., Gremer, L., Kutzsche, J., and Willbold, D. (2016) Optimization of the All-D Peptide D3 for A? Oligomer Elimination. *PLoS One 11*, e0153035.
(31) Jiang, N., Leithold, L. H., Post, J., Ziehm, T., Mauler, J., Gremer, L., Cremer, M., Schartmann, E., Shah, N. J., Kutzsche, J., Langen, K. J., Breitkreutz, J., Willbold, D., and Willuweit, A. (2015) Preclinical Pharmacokinetic Studies of the Tritium Labelled D-Enantiomeric Peptide D3 Developed for the Treatment of Alzheimer s Disease. *PLoS One 10*, e0128553.
(32) Leithold, L. H., Jiang, N., Post, J., Niemietz, N., Schartmann, E., Ziehm, T., Kutzsche, J., Shah, N. J., Breitkreutz, J., Langen, K. J., Willuweit, A., and Willbold, D. (2016) Pharmacokinetic properties of tandem d-peptides designed for treatment of Alzheimer's disease. *Eur. J. Pharm. Sci. 89*, 31−38.
(33) Leithold, L. H., Jiang, N., Post, J., Ziehm, T., Schartmann, E., Kutzsche, J., Shah, N. J., Breitkreutz, J., Langen, K. J., Willuweit, A., and Willbold, D. (2016) Pharmacokinetic Properties of a Novel D-Peptide Developed to be Therapeutically Active Against Toxic beta-Amyloid Oligomers. *Pharm. Res. 33*, 328−336.
(34) Fukumoto, H., Takahashi, H., Tarui, N., Matsui, J., Tomita, T., Hirode, M., Sagayama, M., Maeda, R., Kawamoto, M., Hirai, K., Terauchi, J., Sakura, Y., Kakihana, M., Kato, K., Iwatsubo, T., and Miyamoto, M. (2010) A Noncompetitive BACE1 Inhibitor TAK-070 Ameliorates Aβ Pathology and Behavioral Deficits in a Mouse Model of Alzheimer's Disease. *J. Neurosci. 30*, 11157−11166.
(35) Scholtzova, H., Wadghiri, Y. Z., Douadi, M., Sigurdsson, E. M., Li, Y.-S., Quartermain, D., Banerjee, P., and Wisniewski, T. (2008) Memantine Leads to Behavioral Improvement and Amyloid Reduction in Alzheimer's-Disease-Model Transgenic Mice Shown as by Micromagnetic Resonance Imaging. *J. Neurosci. Res. 86*, 2784−2791.
(36) Dodart, J.-C., Bales, K. R., Gannon, K. S., Greene, S. J., DeMattos, R. B., Mathis, C., DeLong, C. A., Wu, S., Wu, X., Holtzman, D. M., and Paul, S. M. (2002) Immunization reverses memory deficits without reducing brain A[beta] burden in Alzheimer's disease model. *Nat. Neurosci. 5*, 452−457.
(37) Cuadrado-Tejedor, M., Hervías, I., Ricobaraza, A., Puerta, E., Pérez-Roldán, J. M., García-Barroso, C., Franco, R., Aguirre, N., and García-Osta, A. (2011) Sildenafil restores cognitive function without affecting β-amyloid burden in a mouse model of Alzheimer's disease. *Br. J. Pharmacol. 164*, 2029−2041.
(38) Ziehm, T., Brener, O., van Groen, T., Kadish, I., Frenzel, D., Tusche, M., Kutzsche, J., Reiß, K., Gremer, L., Nagel-Steger, L., and Willbold, D. (2016) Increase of Positive Net Charge and Conformational Rigidity Enhances the Efficacy of d-Enantiomeric Peptides Designed to Eliminate Cytotoxic Aβ Species. *ACS Chem. Neurosci. 7*, 1088−1096.
(39) Widera, M., Klein, A., Cinar, Y., Funke, S., Willbold, D., and Schaal, H. (2014) The D-amino acid peptide D3 reduces amyloid fibril boosted HIV-1 infectivity. *AIDS Res. Ther. 11*, 1.
(40) Frenzel, D., Glück, J. M., Brener, O., Oesterhelt, F., Nagel-Steger, L., and Willbold, D. (2014) Immobilization of Homogeneous Monomeric, Oligomeric and Fibrillar Aβ Species for Reliable SPR Measurements. *PLoS One 9*, e89490.
(41) Liu, L., Ikonen, S., Heikkinen, T., Heikkila, M., Puolivali, J., van Groen, T., and Tanila, H. (2002) Effects of fimbria-fornix lesion and amyloid pathology on spatial learning and memory in transgenic APP+PS1 mice. *Behav. Brain Res. 134*, 433−445.
(42) van Groen, T., Kiliaan, A. J., and Kadish, I. (2006) Deposition of mouse amyloid β in human APP/PS1 double and single AD model transgenic mice. *Neurobiol. Dis. 23*, 653−662.
(43) Kadish, I., Pradier, L., and van Groen, T. (2002) Transgenic mice expressing the human presenilin 1 gene demonstrate enhanced hippocampal reorganization following entorhinal cortex lesions. *Brain Res. Bull. 57*, 587−594.

DOI: 10.1021/acschemneuro.7b00045
ACS Chem. Neurosci. 2017, 8, 1889−1900

Supporting Information

Optimization of D-peptides for Aβ monomer binding specificity enhances their potential to eliminate toxic Aβ oligomers

Antonia Nicole Klein[1], Tamar Ziehm[1], Thomas van Groen[2], Inga Kadish[2], Anne Elfgen[1], Markus Tusche[1], Maren Thomaier[1], Kerstin Reiss[1], Oleksandr Brener[3], Lothar Gremer[1,3], Janine Kutzsche[1], Dieter Willbold[1,3,*]

[1] Institute of Complex Systems, Structural Biochemistry (ICS-6), Research Center Jülich, 52425 Jülich, Germany

[2] Department of Cell, Developmental and Integrative Biology, University of Alabama at Birmingham, Birmingham, AL, USA

[3] Institut für Physikalische Biologie, Heinrich-Heine-Universität Düsseldorf, 40225 Düsseldorf, Germany

*Correspondence: d.willbold@fz-juelich.de

Table S1| Raw data of sbs_{mono} values obtained from the first generation peptide microarray.

	r	p	r	t	r	l	h	t	h	r	n	r
a	-0.28	0.08	-0.28	0.06	-0.35	-0.30	0.00	0.47	0.26	-0.18	-0.06	0.17
d	-0.18	-0.15	-0.29	-0.32	-0.35	-0.62	-0.26	0.12	0.34	-0.10	0.26	0.00
e	0.36	-0.08	-0.41	-0.29	-0.35	-0.34	-0.13	0.04	0.24	0.15	-0.11	-0.02
f	0.49	0.51	-0.30	0.30	-0.23	-0.17	-0.03	-0.22	0.09	0.67	0.09	-0.22
g	-0.03	0.22	-0.31	-0.02	-0.44	-0.08	-0.08	0.00	0.57	0.31	-0.12	0.17
h	0.27	0.09	-0.10	-0.11	0.81	0.94	-0.02	0.00	0.11	0.50	0.02	-0.07
i	0.32	0.00	-0.30	1.48	0.08	-0.21	0.15	0.36	0.04	1.47	-0.03	-0.02
k	0.00	1.86	-0.29	0.36	0.87	0.00	0.04	0.42	1.20	1.39	1.61	0.85
l	0.08	0.75	-0.18	-0.18	-0.22	-0.21	0.00	0.41	0.10	-0.26	0.02	-0.05
m	-0.08	0.22	-0.21	-0.13	-0.16	0.06	0.00	0.28	0.36	-0.04	0.23	0.19
n	-0.07	-0.27	-0.34	-0.01	0.20	-0.03	-0.25	0.18	0.23	0.11	0.44	0.06
p	-0.45	-0.19	-0.40	0.57	0.32	-0.27	0.13	0.15	0.07	0.29	-0.03	0.19
q	-0.17	-0.04	-0.41	0.49	0.06	-0.24	0.17	0.18	-0.16	0.01	0.55	0.00
r	-0.17	0.32	-0.24	0.24	0.10	0.19	0.20	0.03	-0.06	0.25	0.30	0.00
s	-0.06	-0.18	-0.30	-0.11	0.18	-0.11	-0.18	0.44	0.14	0.19	0.44	0.23
t	-0.28	-0.03	-0.37	0.64	-0.12	-0.02	0.43	0.32	-0.17	0.84	0.57	0.07
v	0.15	-0.09	-0.14	0.96	0.43	-0.03	0.81	0.41	-0.15	0.67	0.26	0.00
w	0.00	0.14	-0.06	-0.32	0.01	-0.04	-0.10	0.25	0.16	1.42	0.00	0.10
y	0.00	0.28	0.00	0.51	-0.43	0.08	-0.11	0.53	0.30	0.41	0.63	0.25
Δ	-0.37	-0.39	-0.34	-0.46	-0.27	-0.02	-0.34	0.54	-0.20	0.29	-0.06	0.26
η	-0.33	-0.27	-0.28	0.34	-0.40	0.01	1.34	-0.11	-0.05	0.56	0.32	0.15
θ	-0.16	-0.08	-0.23	0.31	0.10	-0.20	0.39	0.65	-0.04	0.29	0.23	0.17
ι	-0.31	0.11	-0.36	0.06	0.11	-0.20	0.47	0.95	0.32	0.19	0.25	-0.02
κ	-0.15	-0.11	-0.39	-0.23	0.10	-0.12	-0.03	0.35	0.10	0.12	0.06	0.17
λ	-0.87	0.00	-0.24	0.28	0.10	-0.10	1.26	0.23	-0.26	0.47	0.59	0.04
μ	-0.13	-0.01	-0.13	0.83	-0.06	-0.24	0.51	0.48	0.03	0.26	0.25	0.08
ξ	-0.44	-0.09	-0.21	-0.05	-0.05	-0.19	0.06	0.55	0.38	0.29	0.30	0.22
o	-0.32	-0.23	0.15	-0.17	-0.15	-0.09	0.48	-0.02	0.62	-0.12	0.12	0.19
π	-0.21	-0.17	-0.10	0.09	0.28	-0.13	0.26	0.57	0.06	0.44	1.02	0.16
σ	-0.50	-0.06	-0.34	0.39	-0.16	-0.25	1.25	0.13	0.32	0.12	0.83	0.35
Φ	-0.14	-0.31	0.00	0.52	-0.07	-0.36	0.44	0.41	0.37	0.73	0.83	0.28
Ψ	-0.66	0.91	-0.42	-0.27	0.15	-0.33	0.37	0.27	0.17	0.11	0.18	0.04

Δ	trans-4-fluoro-L-proline	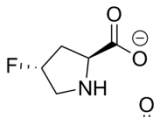
η	4-fluoro-D-phenylalanine	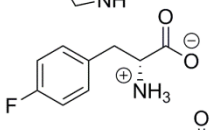
θ	4-benzyl-D-phenylalanine	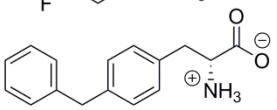
ι	1-naphthyl-D-alanine	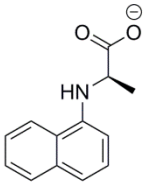
κ	3,5-diiodo-D-tyrosin	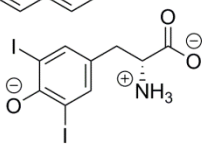
λ	D-phenylglycine	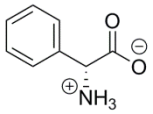
μ	D-homoarginine	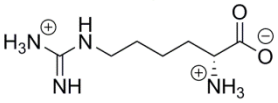
ξ	D-homocitrulline	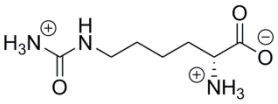
ο	β-homoarginine	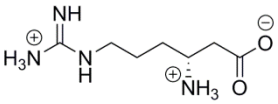
π	β-cyclohexyl-D-alanine	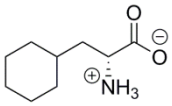
σ	cyclovalin	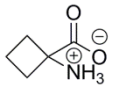
Φ	β-alanine	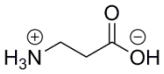
Ψ	γ-aminobutyric acid	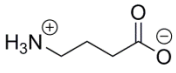

Figure S1| Non-proteinogenic amino acids used within the two-step peptide microarray procedure. To increase the variability of D3 derivatives, 13 non-proteinogenic amino acids were introduced. The amino acids were in D-enantiomeric conformation, if possible, except of trans-4-fluoro-L-proline.

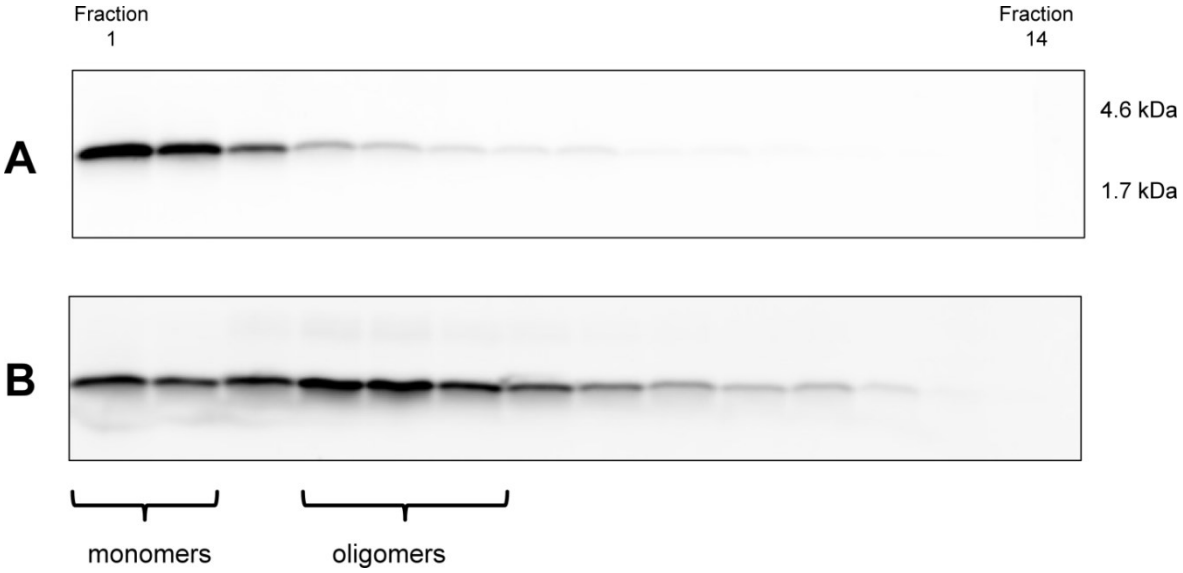

Figure S2| Size distribution of FITC-Aβ(1-42) monomers (A) and oligomers (B) after size exclusion chromatography and additional 1 h incubation at room temperature. Aβ species were verified by density gradient centrifugation, fractionated within 14 fractions, visualized by SDS-PAGE and detecting the FITC tag by fluorescence.

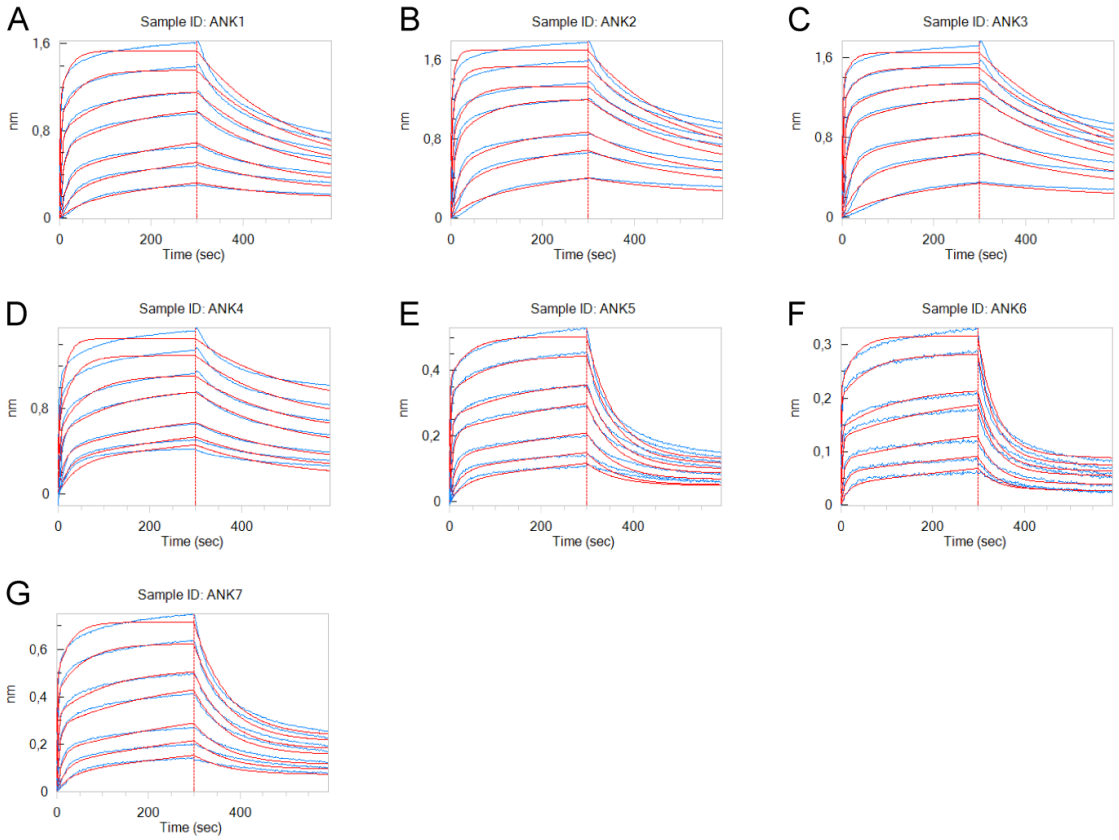

Figure S3| Heterogeneous fit curves of one representative interaction study using biolayer interferometry (BLI). Since heterogeneous binding curves were observed for ANK peptides, the data were fitted using a heterogeneous ligand fit model (ForteBio Data Analysis 8.0). A) ANK1; B) ANK2; C) ANK3; D) ANK4; E) ANK5; F) ANK6; G) ANK7.

Table S2| Mean values of fit results of three independent interaction studies obtained from the heterogeneous ligand binding model. With few exceptions, obtained K_{D2} values were outside the instrument specification (10^{-12} M). In these cases, mean values and SD could not be determined.

	K_{D1} [M]	SD [M]	K_{D2} [M]	SD [M]
ANK1	8.70E-07	1.03E-06	<1.0E-12	
ANK2	1.58E-07	6.69E-08	<1.0E-12	
ANK3	2.10E-07	1.28E-07	<1.0E-12	
ANK4	1.35E-06	1.76E-06	<1.0E-12	
ANK5	1.27E-06	1.29E-06	<1.0E-12	
ANK6	2.33E-06	2.87E-06	3.99E-07	1.37E-07
ANK7	1.95E-06	2.36E-06	<1.0E-12	

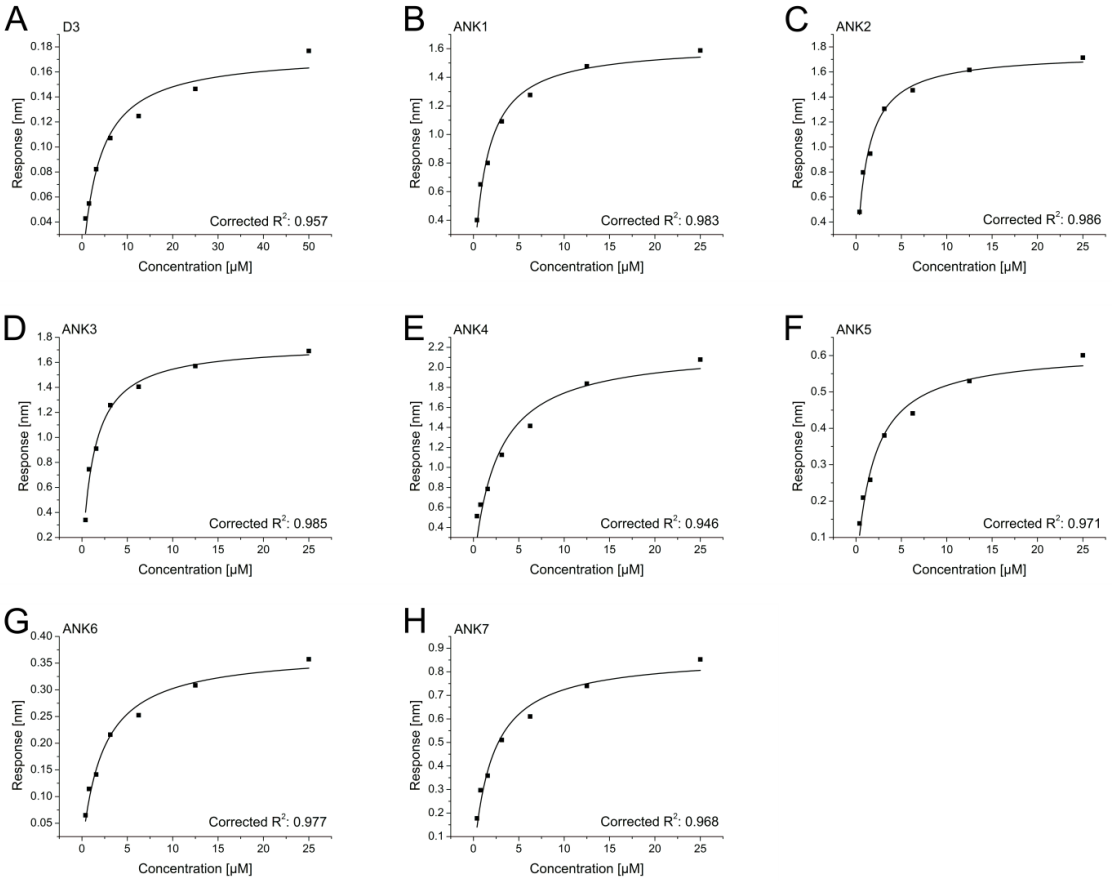

Figure S4| Steady state fit curves of one representative interaction study using biolayer interferometry (BLI). Apparent equilibration dissociation constants of peptide-Aβ(1-42) interactions were determined applying Langmuir´s 1:1 binding model. A) D3; B) ANK1; C) ANK2; D) ANK3; E) ANK4; F) ANK5; G) ANK6; H) ANK7. Corrected R^2 values represent the goodness of the fit.

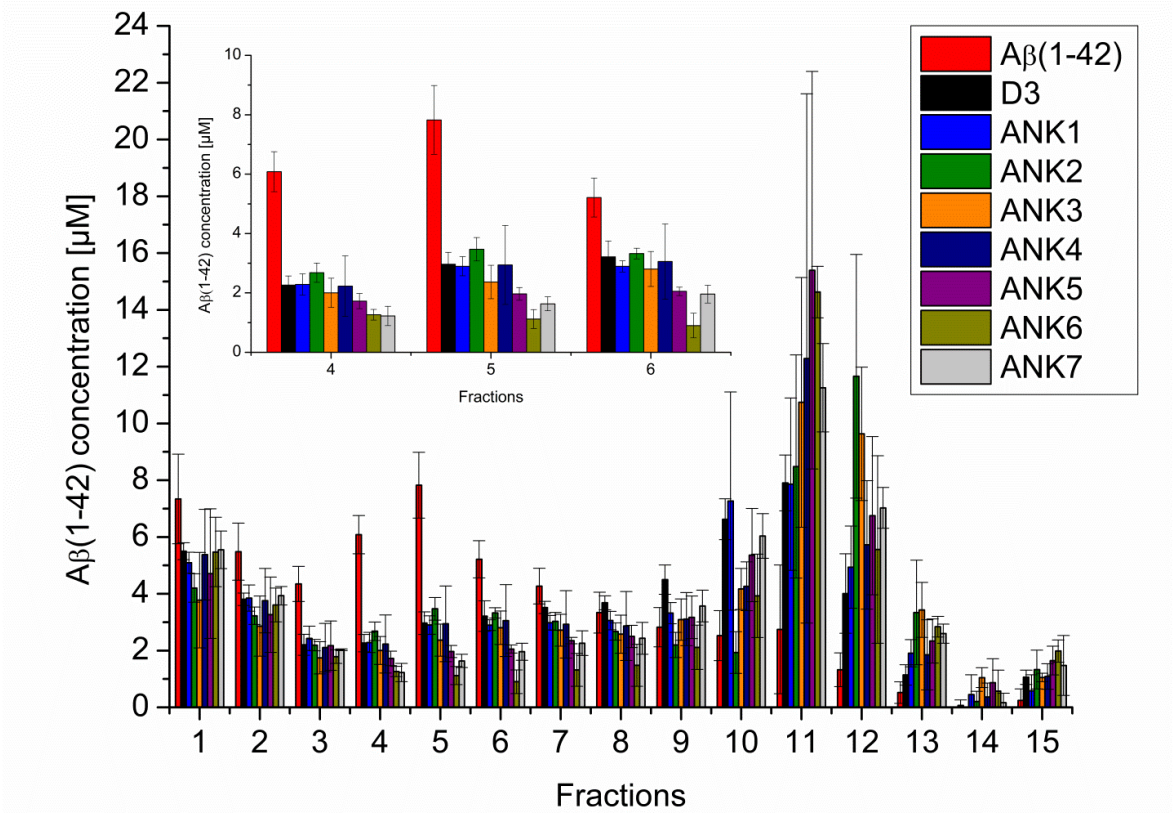

Figure S5| Effects of ANK1 to ANK7 on Aβ(1-42) assemblies. 80 µM pre-incubated Aβ (4.5 h at 21 °C, 600 rpm) was co-incubated with 10 µM D3 or ANK1 to ANK7 (40 min, 21 °C, 600 rpm). Afterwards, the different Aβ aggregates were separated via density gradient centrifugation, fractionated into 15 fractions and quantified via RP-HPLC according to their Aβ content. Fractions 1 and 2 represented monomeric Aβ and fractions 4 to 6 oligomeric Aβ. Aβ oligomer concentrations present in fractions 4 to 6 are shown in the inlet. Mean value and SD of four independent experiments are shown.

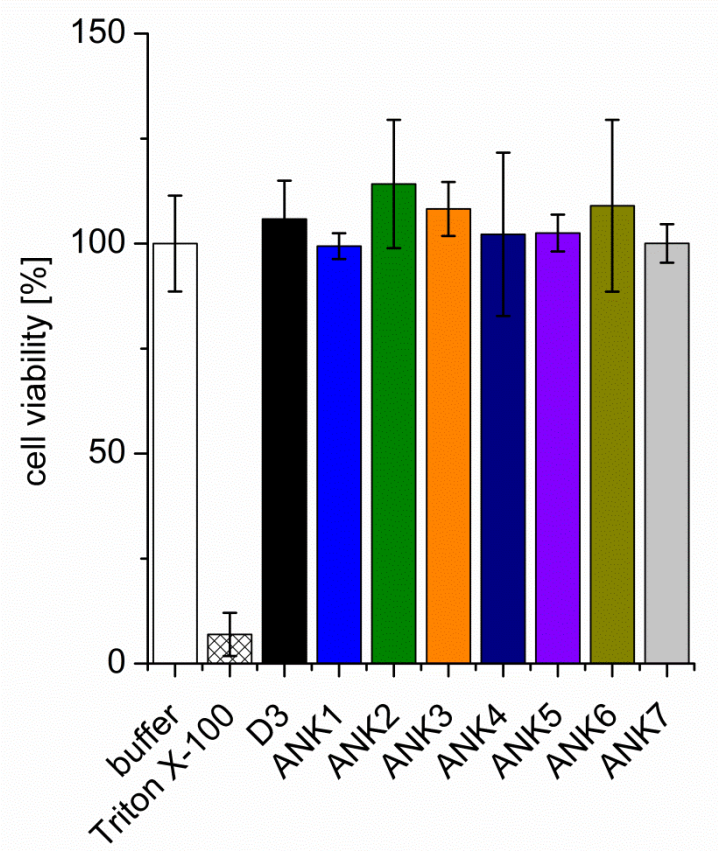

Figure S6| Controls for cell viability assay. The influence of 5 µM D3 and 5 µM ANK1 to ANK7 without Aβ on the cell viability was determined. Cell viabilities were measured by measuring the absorption of MTT at 570 nm subtracted by the absorption at 660 nm and normalized to non-treated cells. As a negative control, the influence of 0.125 % Triton X-100 on the cell viability was measured. Mean values and SD are shown.

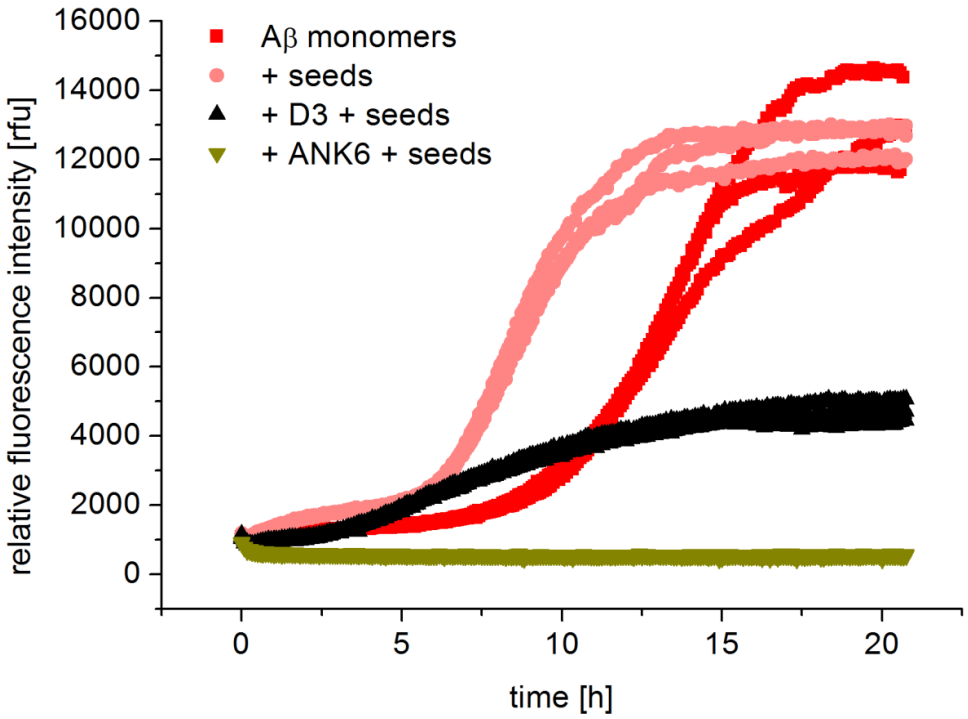

Figure S7| Effect of D3 or ANK6 on the Aβ seeding potential. 10 µM Aβ(1-42) monomers were seeded with 2 % fibrils in the presence or absence of 10 µM D3 or ANK6. The aggregation was monitored for 21 h at 37 °C by ThT fluorescence. Three technical replicates are presented and the data are exemplary for three independent experiments.

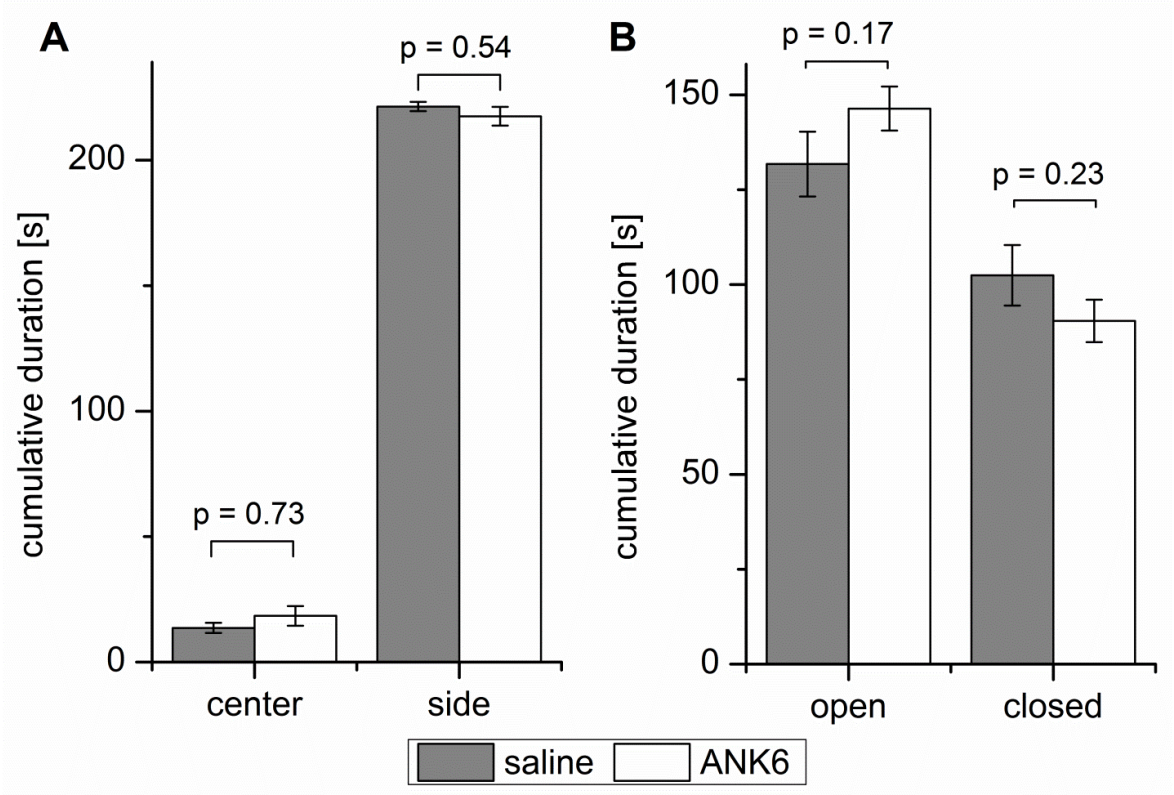

Figure S8| Effects of treatment on general activity or anxiety studied via A) open field test and B) zero maze test. A) A squared arena was divided into the center and the side near the walls. B) A circular maze was divided into four parts with equal size. Two parts have nonvisible walls (closed) and two parts have open arms (open). For both tests, the time the mice spent in both parts was compared between both groups. For statistical analysis, Mann-Whitney U-test was performed.

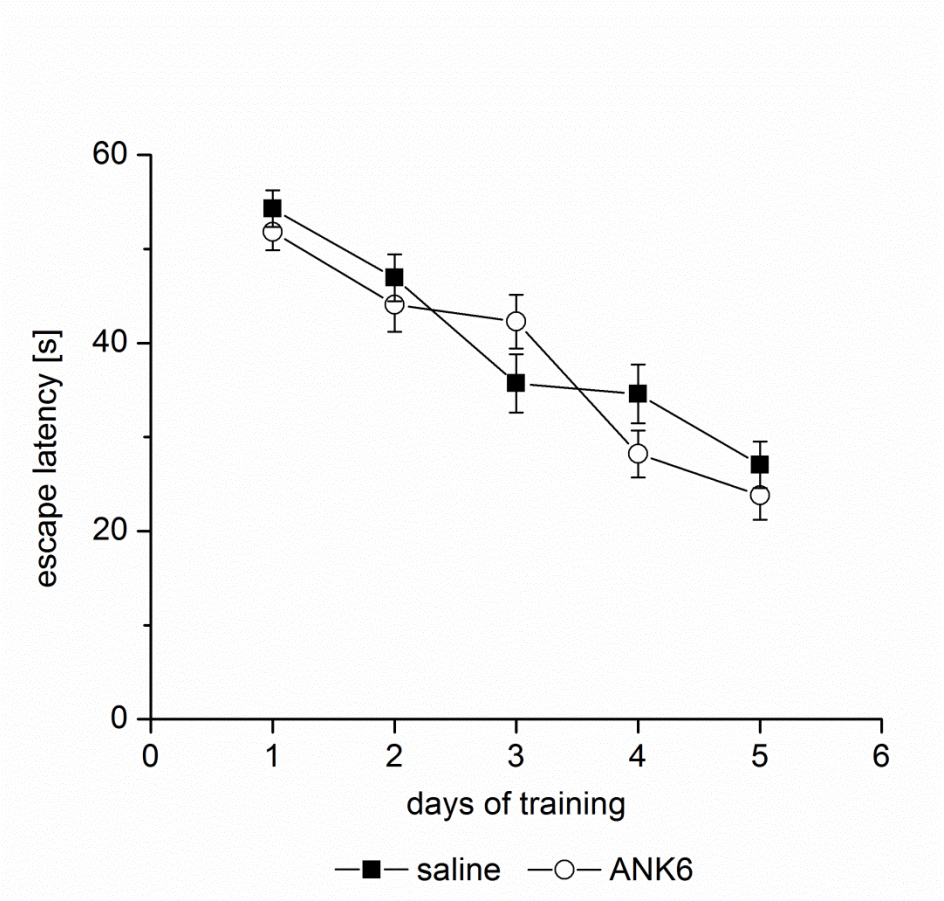

Figure S9| Morris water maze performance of saline and ANK6 treated tg-APPSwDI mice. The time spend in the water until they found the hidden platform was investigated daily over a period of five days. The mean values ± SEM are shown. For statistical analysis, a Friedman-ANOVA was performed. Both groups significantly learned within this training interval; $p = 1.04 \times 10^{-6}$ for saline and $p = 1.33 \times 10^{-5}$ for ANK6.

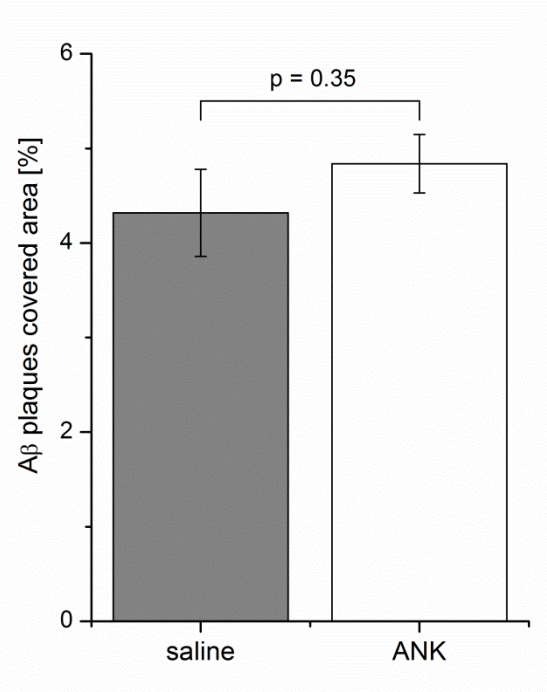

Figure S10| Aβ plaque loads of saline- and ANK-treated tg-APPSwDI mice at the hippocampus and dorsal cortex. After behavioral studies, the mice were sacrificed and brain slices were analyzed according to the Aβ plaque load. For statistical analysis, a t-test was performed.

Table S3| Summary of important quantities of the *in vivo* study.

Group	control	ANK6
Infusion	saline	ANK6 peptide
Number	n = 11	n = 11
Body weight [g]		
Before treatment	35.4 ± 5.2	33.2 ± 4.6
After treatment	31.8 ± 2.9	25.8 ± 3.7

[a] Intraperitoneal (i.p.) Alzet pumps, treatment with 3.696 mg / 4 weeks

[b] Number of animal per group

SI Methods

Tricine-SDS-PAGE. Tricine-SDS-PAGE was performed according to Schagger[1]. In brief, all samples were mixed with 4x Tris-Tricine loading buffer (4 % SDS (w/v), 12 % glycerol (v/v), 50 mM Tris, 2 % β-mercaptoethanol (v/v), 0.01 % SERVA BlueG (w/v), pH 6.8), boiled for 5 min, and the proteins were separated on a 16 % Tricine-SDS-Gel at 100 V constantly. The ultra-low range Color Protein marker (C6210, Sigma-Aldrich, St. Louis, USA) was used as a size standard. For visualization, the Chemidoc MP system (Biorad, Hercules, USA) was used.

Heterogeneous fitting of BLI data. Performance of biolayer interferometry (BLI) measurements and data processing were described in the Methods section of the main manuscript. For kinetic evaluation of the BLI data according to a heterogeneous binding model, the data were fitted using the heterogeneous ligand fit model implemented in the ForteBio Data Analysis Software, 8.0. In brief, this fit model assumes the presence of two independent 1:1 binding sites or binding modes of the analyte on the ligand surface. Therefore, two different rate constants are given, one for each site:

$$A + B_1 \underset{k_{off1}}{\overset{k_{on1}}{\leftrightarrow}} AB_1 \qquad \text{(S1)}$$

$$A + B_2 \underset{k_{off2}}{\overset{k_{on2}}{\leftrightarrow}} AB_2 \qquad \text{(S2)}$$

with A as analyte concentraton, B the immobilized ligand, k_{on} the association rate constant, k_{off} the dissociation rate constant and AB the complex. B_1 and B_2 are either two different epitopes on the same ligand or two different ligands on the surface. The corresponding equilibrium dissociation constants (K_{D1} and K_{D2}) are calculated separately for each binding site by the following equations:

$$K_{D1} = \frac{k_{off1}}{k_{on1}} \qquad \text{(S3)}$$

$$K_{D2} = \frac{k_{off2}}{k_{on2}} \qquad \text{(S4)}$$

SI References

1. Schagger, H., Tricine-SDS-PAGE. Nat. Protocols 2006, 1 (1), 16-22.

3.5 The role of hydrophobicity and charge of amyloid-beta oligomer eliminating D-peptides in the interaction with amyloid-beta monomers

Tamar Ziehm[1], Alexander K. Buell[2], Dieter Willbold[1,2,*]

[1]Institute of Complex Systems, Structural Biochemistry (ICS-6), Forschungszentrum Jülich, 52425 Jülich, Germany

[2]Institut für Physikalische Biologie, Heinrich-Heine-Universität Düsseldorf, 40225 Düsseldorf, Germany

[*]Correspondence: d.willbold@fz-juelich.de

Keywords: Alzheimer´s disease, drug discovery, amyloid-beta, D-peptides, thermodynamics

Abstract

Inhibition of the self-assembly process of amyloid-beta and even more the destruction of already existing toxic amyloid-beta assemblies represents a promising therapeutic strategy to prevent Alzheimer´s disease. To approach this aim, we selected a D-enantiomeric peptide by phage-display based on the interaction with amyloid-beta monomers. This lead compound was successfully optimized by peptide microarrays with respect to its affinity and specificity to the target resulting in D-peptides with both increased hydrophobicity and net charge. Here, we present a detailed biophysical characterization of the interaction between these optimized D-peptides and amyloid-beta monomers in comparison to the original lead compound in order to obtain a more thorough understanding of the physico-chemical determinants of the interactions. Kinetics and stoichiometry of complex formation were studied using surface plasmon resonance. Potential modes of binding to amyloid-beta were identified and the influence of ionic strength on complex stability was investigated. The results elucidate a very different mode of interaction of the optimized D-peptides based on a combination of electrostatic and hydrophobic interactions as compared to the fully electrostatically driven interaction of the lead compound. These conclusions were supported by the thermodynamic profiles of the interaction between optimized D-peptides and Aβ monomers, which indicate an increase in binding entropy.

Introduction

Alzheimer´s disease (AD) is a neurodegenerative disorder with progressive loss of memory and cognitive decline as major symptoms. Although the precise etiology remains unclear, aggregation of amyloid-beta (Aβ) is a hallmark of AD. This aggregation process is characterized by oligomeric precursors, which are considered to be the most neurotoxic species, and highly ordered, insoluble amyloid fibrils, which make up the basis of amyloid plaques (1-4). Therefore, inhibiting the Aβ oligomer formation or even more the destruction of already existing Aβ oligomers is a promising and widely pursued strategy for a causative therapy. However, the unstable and transient nature of Aβ oligomers renders them very challenging to study and hence to target. Aβ monomers, on the other hand, are easier to study and targeting monomers could be a promising early intervention strategy, preventing the formation of toxic oligomers and pursuing the destabilization of preformed oligomers (5,6). We hypothesize that specific interactions with monomeric Aβ can shift the equilibrium away from oligomeric states and simultaneously inhibit further aggregation. To test this hypothesis, the D-enantiomeric peptide D3 (D-peptide, amino acid sequence rprtrlhthrnr) was selected as the first representative of a novel class of therapeutics. D3 was found to bind to Aβ monomers and inhibit Aβ amyloid fibril formation in vitro (7-9). Additionally, preformed oligomers were eliminated by D3 resulting in a rescue effect of oligomer induced cytotoxicity. The molecular mechanism of the inhibitory effect was shown to be the D3-induced formation of off-pathway non-toxic, amorphous co-precipitates (10). This is in contrast to most known inhibitors such as chaperones or antibodies that mostly slow down the formation of amyloid fibrils and do not open additional aggregation channels (11-13), and therefore represents a novel mode of inhibition of amyloid fibril formation. In vivo, D3 improved cognition of transgenic AD mice and reduced Aβ plaque load as well as cerebral inflammation (7,10,14). In order to increase drug efficacy, this lead compound was systematically optimized regarding the affinity and specificity to Aβ monomers by peptide microarrays. The seven D-peptides with strongest binding signatures to monomeric Aβ are represented by the ANK D-peptides (15). In vitro, it was shown that these D-peptides indeed show improved efficacy as compared to D3, i.e., increased binding affinity as well as efficacy in eliminating Aβ oligomers and in neutralization of toxicity, indicating a successful lead optimization process. Regarding the binding mode, it was observed that the interaction with Aβ monomers changed from a homogeneous interaction to a heterogeneous one without quantitatively describing the kinetics. One component of the interactions between Aβ and the ANK D-peptides might be based on electrostatics which was previously found to be

the major driving force of D3 interaction with Aβ (9,16) and we hypothesize, that ANK binding might additionally be driven by hydrophobic interactions, consistent with the increased sequence hydrophobicity. Here, we address this question by studying the influence of charge and hydrophobicity of the D-peptides on the interaction with Aβ monomers in detail. The binding kinetics and stoichiometry were determined, as well as affinities to Aβ fragments in order to identify potential epitopes. The influence of the ionic strength of the solution, and hence the role of electrostatic interactions on the interaction was investigated by stepwise increasing the salt concentration in the buffer. The conclusions from these experiments were confirmed by performing aggregation assays of Aβ under the same ionic strength conditions. Furthermore, thermodynamic profiles including enthalpic and entropic contributions were analyzed which provide further insights into the driving forces for the binding of the D-peptides to Aβ, information that is relevant for decision making in the lead optimization process (17-19). Since Aβ species, especially Aβ oligomers, are converted into non-amyloid, non-toxic amorphous co-precipitates in the presence of ANK D-peptides, solution-based techniques are not easily applicable for accurate interaction analysis between Aβ monomers and D-peptides. Thus, the surface-based sensing technique surface plasmon resonance (SPR) has been used with Aβ monomers attached to the surface matrix in order to prevent D-peptide-induced aggregation. This method enables the reliable analysis of binding affinity, kinetics and stoichiometry to surface-bound Aβ monomers (20). Additionally, the thermodynamic signature of the interaction can be examined by performing a van´t Hoff analysis where the change in affinity over a temperature range is investigated.

Since the ANK D-peptides are highly similar in sequence and also in efficacy in vitro, only a representative selection was included in this study. Two D-peptides out of seven were chosen: ANK3 and ANK6. The physico-chemical characteristics including sequence, charge and hydrophobicity in comparison to D3 are depicted in Table 1. ANK3 is one of the D-peptides with highly increased hydrophobicity due to an exchange of four polar to hydrophobic amino acid residues whereas the net charge of the D-peptide is the same as for D3. ANK6 exhibits the highest number of positive charges. However, hydrophobicity is only slightly enhanced as a result of two polar to aliphatic substitutions which were mainly compensated by introducing hydrophilic lysine residues. Therefore, a direct comparison between D3 and ANK3 provides further insights into the role of hydrophobicity on the interaction with Aβ whereas ANK6 is characterized by both increased net charge and slightly enhanced hydrophobicity.

Results

Kinetics and stoichiometry of complex formation between surface-bound Aβ and D-peptides

The interactions of different D3, ANK3 and ANK6 concentrations with immobilized Aβ molecules were measured by SPR (Figure 1). Deduced from the sensorgram shape it was assumed, that D3 bound homogeneously to Aβ with single rate constants whereas ANK D-peptides exhibited a second association and dissociation phase, indicating a heterogeneous interaction consisting of two kinetic rate constants. Hence, the sensorgrams were globally fitted using three different models; a homogeneous interaction model which considers a single type of interaction on the surface, a two-state reaction model considering a conformational change which stabilizes the complex upon binding, and a heterogeneous interaction model where D-peptides are allowed to interact heterogeneously with surface-bound Aβ via two independent binding modes (Figure 1). The goodness of the respective fit was expressed as χ^2 values. The homogeneous fit model was sufficient to describe the binding curves of D3 since χ^2 values were only slightly decreased by applying a more complex model (Figure 1A, D, G). In contrast, this simple fit model and the more complex two-state reaction model were not able to describe ANK3 (Figure 1B and E) and ANK6 sensorgrams Figure 1C and F). However, the heterogeneous fit model described the entire data sets of ANK D-peptides with minimal χ^2 values (Figure 1H and I), yielding two ligand binding modes with two pairs of rate constants. The quantitative description of the kinetics was very reproducible with low deviation between replicates (Figure 2A). For D3, a very fast association rate constant (k_{on}) of $5 \cdot 10^4$ $M^{-1}s^{-1}$ and also a very fast dissociation rate constant (k_{off}) of $7 \cdot 10^{-1}$ s^{-1} were determined, indicating that the complex is rapidly formed but not very stable. Both kinetics of ANK3 and ANK6 were very similar to each other. For binding mode 1, k_{on} values of $2 \cdot 10^4$ $M^{-1}s^{-1}$ and $3 \cdot 10^4$ $M^{-1}s^{-1}$ and a k_{off} of $1 \cdot 10^{-1}$ s^{-1} were determined and binding mode 2 was characterized by a k_{on} of $2 \cdot 10^5$ $M^{-1}s^{-1}$ and k_{off} values of $2 \cdot 10^{-3}$ s^{-1} and $4 \cdot 10^{-3}$ s^{-1}. The resulting equilibrium dissociation constants (K_d) were 14 µM for D3, 7 µM (binding mode 1) and 13 nM (binding mode 2) for ANK3 and 3 µM (binding mode 1) and 28 nM (binding mode 2) for ANK6. In general, binding mode 1 was characterized by affinity in the low micromolar range for all D-peptides and binding mode 2 represented a high affinity site for ANK3 and ANK6 with a K_d in the low nanomolar range. Thus, binding kinetics of ANK3 and ANK6 were comparable. However, by evaluation of the fitted saturation levels (R_{max}) of the two binding modes it was observed that the extent of the high affinity binding mode differed between these two D-peptides. For ANK6, this site represented 13% of the total

binding while for ANK3 the high affinity binding mode was more pronounced and amounted to 26% (Figure 2B). Regarding the stoichiometry, a substoichiometric binding of all three D-peptides to the quantity of Aβ attached to the sensor surface was observed (Figure 2B). For D3, an overall binding of 0.19 molecules per Aβ molecule was determined meaning that one molecule of D3 bound per 5.3 attached Aβ molecules. The low affinity binding mode of ANK3 showed the same stoichiometry as compared to D3 but including the high affinity site increased the total stoichiometry to 0.28 ANK3 molecules per Aβ molecule, leading to a final ratio of one molecule ANK3 per 3.6 Aβ molecules. For ANK6, a lower stoichiometric ratio was determined for both binding modes; 0.12 molecules bound to one Aβ molecule on the low affinity binding mode and 0.02 molecules per Aβ molecule on the high affinity binding mode. This resulted in a total stoichiometry of 0.14 molecules ANK6 per Aβ molecule, meaning that one ANK6 molecule bound to 7.0 Aβ molecules.

Identification of epitopes

In order to analyze whether a distinct epitope on the Aβ sequence is responsible for the heterogeneous binding, especially of ANK3, an epitope mapping approach was conducted. Seven Aβ fragments were designed with 15 amino acids in length with an overlap of ten amino acids and a frame shift of five amino acids (Figure 3A). Only fragments 6 and 7 had a frame shift of two amino acids to investigate the affinities to the two isoforms Aβ(1-40) and Aβ(1-42) separately. Interestingly, the binding of the ANK D-peptides to all Aβ fragments could be fitted with the homogeneous model, which allowed the determination of a single K_d value for each fragment (Figure 3B), facilitating convenient comparison. D3 and ANK6 bound to the fragments 1 to 5 with a K_d ranging from 14 to 85 µM and 3 to 16 µM, respectively. Both D-peptides showed no binding to fragments 6 and 7 in the applied concentrations. ANK3 bound to all seven fragments with a K_d ranging from 1 to 41 µM. Thus, the D-peptides did not exhibit a well-defined epitope and the effective K_d values determined for the full length Aβ sequence are likely to stem from a combination of multiple indistinct binding modes on the Aβ sequence and resulting avidity effects. D3 and ANK6 bound to all fragments, which contained negatively charged residues located on the N-terminal part of the sequence. ANK3 also bound to these fragments but interestingly, it additionally bound to the hydrophobic C-terminal region which does not include any negative charges, except the C-terminal carboxyl group. None of the D-peptides distinguished between Aβ(1-40) and Aβ(1-42), since they all bound similarly to fragments 6 and 7, i.e., either not detectably (D3 and ANK6) or with the same affinity (ANK3).

Influence of ionic strength on the interaction

As the epitope mapping approach suggested that the interaction of ANK3 with Aβ might be driven not only by electrostatic interactions, the binding to Aβ was analyzed at increased ionic strength in order to screen electrostatic interactions and strengthen hydrophobic interactions simultaneously (21). A constant D-peptide concentration was brought into contact with Aβ at four different sodium chloride concentrations, i.e., 150 mM, 300 mM, 600 mM and 1200 mM. 50 µM D3 showed a clear binding signal at 150 mM NaCl, which was already reduced by 80% at 300 mM (Figure 4A). At higher ionic strength (600 mM and 1200 mM), no binding could be detected, indicating high NaCl sensitivity of D3 binding. Binding of 25 µM ANK6 was also strongly affected by the increased ionic strength (Figure 4C). At 300 mM, the signal was reduced by 60% as compared to 150 mM and at 600 mM and 1200 mM, only 10% remained. This result revealed that the main contribution of the interaction of ANK6 with Aβ was sensitive to NaCl as well but that 10% of the interaction was independent of salt concentration, possibly representing the hydrophobic contribution. Contrary to D3 and ANK6, 60% of the binding signal from 25 µM ANK3 at 150 mM NaCl was still detected at 1200 mM NaCl, indicating that ANK3 interaction is highly stable at increasing NaCl concentrations (Figure 4B). All measurements at different NaCl concentrations were performed on the same sensor chip and the immobilized Aβ was stable under these conditions (Figure S1).

In addition to probing the interactions with Aβ by SPR, the D-peptides were also tested with respect to their function as inhibitors of Aβ amyloid fibril formation at different ionic strength. Aβ fibril formation kinetics were monitored by Thioflavin-T (ThT) fluorescence in the presence or absence of the respective D-peptide at 150 mM, 300 mM, 600 mM and 1200 mM NaCl (Figure 5A-D). It was observed that the absolute ThT fluorescence levels of 10 µM fibrillar Aβ decreased with increasing salt concentrations, most probably due to interference of NaCl with ThT binding to mature fibrils (22). This is plausible due to the fact that the electrostatic interactions between Aβ (negatively charged) and ThT (positively charged) are favorable. At 1200 mM, the kinetic data was of poor quality but still allowed qualitative statements regarding the inhibitory function of the D-peptides. At 150 mM NaCl, D3 inhibited Aβ fibril formation by 30% as judged from the final ThT intensity but at 300 mM NaCl, the inhibition efficacy was already reduced to 15%. At 600 mM and upwards no inhibitory effect by D3 was observed. ANK6 nearly completely inhibited Aβ fibril formation at 150 mM NaCl indicating a higher efficacy as D3 but at 300 mM, the efficacy was reduced to 60%. At 600 mM and 1200 mM, ANK6 was also not able to inhibit Aβ fibril formation. In contrast, ANK3 showed a complete inhibition of Aβ fibril formation at

all tested salt concentrations, even at 1200 mM. Thus, Aβ fibril formation assays were in very good agreement with SPR-derived data at different NaCl concentrations and indicated that ANK3 is an efficient inhibitor of Aβ amyloid fibril formation independently of the ionic strength.

Thermodynamics of the interactions

To further investigate the physico-chemical mechanism and its driving forces, the thermodynamic signatures of the interaction of the D-peptides with Aβ were studied. First, the solution-based technique isothermal titration calorimetry (ITC) was applied which is the method of choice for thermodynamic analysis of interactions due to the fact that it can simultaneously yield the free energy, enthalpy and entropy of interaction (23, 24). However, the measured heat signal from the titration of D3 into Aβ solution was not distinguishable from background heat (Figure S2). If no heat signal is recorded in an ITC experiment, either the binding event is entirely entropy-driven or no binding occurs. The second appeared unlikely as direct interaction was demonstrated by SPR. Thus, SPR-based van´t Hoff analyses were performed, which have been reported in the past to correlate well with ITC experiments (25, 26).

K_d values of the homogeneous D3 and heterogeneous ANK interactions with Aβ monomers were determined at different temperatures ranging from 11 to 39°C. Based on a linear relationship between the logarithm of the dissociation constants and the inverse absolute temperature (R^2 > 0.9) (Figure S3), the analysis of enthalpic (ΔH) and entropic ($-T\Delta S$) contributions at 25°C of Gibbs free energy of binding (ΔG) was performed according to van´t Hoff as described in the experimental procedures. The low affinity binding mode 1 with a K_d in the micromolar range corresponded to a free energy of binding of around -20 kJ mol^{-1} for all D-peptides (Figure 6A). However, the enthalpic and entropic contributions differed between D3 and ANK D-peptides. D3 binding was characterized by a slightly negative but very low enthalpy (-4 kJ mol^{-1}), which resulted in a nearly completely entropy-driven binding. Interestingly, the binding enthalpy of the low affinity binding mode 1 of ANK D-peptides changed from negative to positive resulting in an increase in entropy as compared to D3. The profiles of the high affinity binding mode 2 of ANK3 and ANK6 were very similar for both D-peptides Figure 6B). The K_d values in the nanomolar range corresponded to a free energy of binding of around -40 kJ mol^{-1} with an enthalpic contribution of around +40 kJ mol^{-1} and entropic contribution of -80 kJ mol^{-1}, respectively.

Discussion

The process of drug discovery often starts with a rather hydrophilic lead compound where hydrogen bonding and electrostatic interactions are likely to contribute significantly to affinity, often resulting in micromolar binding affinity to the target protein. The process of lead optimization typically includes a high-throughput screening and yields lead derivatives with increased hydrophobicity, leading to increased affinity of hit compounds and entropy-driven binding (27-30). This strategy was successfully applied to our target Aβ. The hydrophilic polycationic D-peptide D3 as lead compound was systematically modified by peptide microarrays, resulting in optimized D-peptides (15). In order to gain a more detailed understanding of the physico-chemical determinants of interaction with Aβ, D3 and two of the optimized D-peptides were included in the current study: ANK3 and ANK6. We showed that D3 rapidly interacts with Aβ involving all negatively charged amino acid residues and the interaction was strongly dependent on the ionic strength of the solution. As a consequence, the inhibitory effect on Aβ amyloid fibril formation by D3 decreased with increasing ionic strength. At concentrations > 300 mM NaCl, neither binding nor inhibitory action was observed. It was demonstrated that the interaction between D3 and Aβ was principally driven by electrostatic interactions and that the binding event of D3 was indeed responsible for the inhibitory action. Quantitative analysis of the SPR-derived kinetics of the interactions with Aβ revealed a low affinity binding mode in the micromolar range for ANK3 and ANK6 as well. The rate constants and resulting K_d values of this low affinity binding mode were all of comparable magnitude as those determined for D3. Thus, increased hydrophobicity of ANK3 and increased net charge of ANK6 had a very little influence on this mode of interaction. However, ANK3 and ANK6 binding curves showed heterogeneous binding behavior to Aβ and global fitting revealed an additional high affinity binding mode with affinity in the nanomolar range, which differed in the stoichiometry from the low affinity binding mode. For ANK6, this high affinity binding mode amounted to 13% of the total binding and this corresponded to the proportion of ANK6 binding which was resistant to increased ionic strength. Therefore, we concluded that the high affinity binding mode was driven by hydrophobic rather than electrostatic interactions. Nevertheless, the proportion of 13% was not sufficient to inhibit Aβ fibril formation at NaCl concentrations higher than 300 mM and we concluded that electrostatic interactions were relevant for the inhibitory function of ANK6. In the case of ANK3, it was shown that increased hydrophobicity resulted in an increased proportion of the high affinity binding mode (26%) and, in contrast to D3 and ANK6, ANK3 additionally showed interactions with the hydrophobic C-terminus of Aβ beginning at S26. This region

of Aβ is known to be part of the fibril core and thus, plays an important role in the self-assembly process (31-33). Despite the fact that the hydrophobic contribution of ANK3 binding to Aβ amounted to 26%, 60% of the binding signal remained stable at NaCl concentrations > 1 M and this interaction was sufficient to completely inhibit Aβ amyloid fibril formation. Thus, targeting the hydrophobic C-terminus of Aβ might be a relevant feature for increased efficacy of drug candidates for AD.

All D-peptides were characterized by a substoichiometric binding to Aβ monomers, possibly suggesting cross-linking or bridging of multiple Aβ monomers by one polyvalent D-peptide molecule which might be attributed to the high number of positively charged residues and hydrophobic interaction sites for ANK3. For a standard Biacore CM5 sensor chip it was described that 100 RU of immobilized ligand corresponds to a bulk concentration of 1 mg ml^{-1} in the surface matrix (34,35). Based on this value, an immobilization level of 1800 RU is equivalent to a local Aβ concentration of 4 mM which corresponds to an average distance between Aβ molecules of less than 8 nm, rendering at least partial cross-linking of surface-bound Aβ by the D-peptides plausible. The fact, that Aβ is rapidly converted into amorphous co-precipitates in the presence of D3 and ANK D-peptides in solution supports this proposed mechanism (15). A further possible explanation for the substoichiometry is that a certain fraction of the Aβ molecules is not accessible to the D-peptides. This could be either due to the fact that the Aβ is partly attached to the surface in oligomeric form, or that the attachment to the dextran matrix of the SPR sensor renders some Aβ molecules inaccessible, potentially due to reduced mobility of the positively charged D-peptides within the negatively charged dextran matrix. Furthermore, the referencing procedure, whereby the signal from D-peptides that bind non-specifically to the dextran matrix is subtracted from the signal in the presence of surface-attached Aβ, could be incomplete in this case. Despite these potential complications stemming from the use of a surface-based biosensing technique, SPR has the advantage that the surface-bound Aβ is stably attached and hence a reliable binding constant can be established, because the same number and conformation of Aβ molecules are exposed to the various D-peptide concentrations.

In order to further validate these results, we analyzed the thermodynamic profiles of the individual binding modes which revealed that all binding modes are entropy-driven. The thermodynamic profile of D3 interaction with Aβ showed a slightly negative enthalpic contribution to the Gibbs free energy of binding which resulted in a nearly completely entropy-driven interaction. This type of thermodynamic signature has already been described for purely electrostatic interactions, for example in the case of the interaction

between DNA and polyvalent cations, i.e., lysine, Mg^{2+} and polycationic proteins (36,37). The enthalpic contributions of these interactions are explained by the counterion condensation theory which describes the partial release of counterions to the bulk solution, resulting in cratic entropy gain, as proposed by Manning (38,39) as well as by Privalov et al. (40). In contrast to this, the mechanism of binding mode 1 changed from a weakly exothermic to a weakly endothermic process for ANK D-peptides suggesting that the net effect of ANK binding to Aβ involved breakage of energetically favorable noncovalent interactions, e.g., van der Waals contacts and hydrogen bonds. This enthalpy gain was compensated by a corresponding entropy gain. Furthermore, the high affinity binding mode 2 of ANK D-peptides was also entropy-driven and it is well-established that hydrophobic interactions are mainly entropic in nature, at least in the case of small hydrophobes (41). Thus, the thermodynamic analysis of the binding modes supported the idea that the second binding mode of ANK might be based on hydrophobic interactions.

Conclusion

The present study provided new insights into the physico-chemical determinants of the interactions between the lead compound D3 and optimized D-peptides ANK3 and ANK6 with their target, the Aβ peptide. We conclude that D3 interacts with Aβ via electrostatic interactions, leading to micromolar affinity. In addition to this mode of interaction, ANK3 and ANK6 exhibited a second binding mode with nanomolar affinity. This second binding mode was more pronounced in the case of the hydrophobic D-peptide ANK3 than for ANK6 which is more positively charged and involved hydrophobic interactions with the C-terminus of Aβ, the latter being known to play an important role in the self-assembly process. Therefore, both electrostatic and hydrophobic interactions significantly contributed to the driving force for binding of ANK3, leading to a more robust complex formation with Aβ. A decomposition of the free energy of binding into enthalpic and entropic contributions supported these findings. In vivo, increased hydrophobicity is linked to improved pharmacokinetic and pre-clinical ADMET (absorption, distribution, metabolism, excretion and toxicity) properties resulting in increased chances of success in drug development (17,42,43). Thus, ANK3 is highly relevant for further fit-for-purpose studies in vivo investigating if increased hydrophobicity indeed leads to an optimized drug for the treatment of AD.

Experimental procedures

D-peptides

D3, ANK3 and ANK6 consisted of D-enantiomeric amino acids and were purchased from peptides&elephants (Germany) with C-terminal amidation and > 95% purity.

Hydrophobicity calculation

The grand average of hydropathy (GRAVY) of the D-peptides was calculated according to Kyte and Doolittle (44) using the online tool ProtParam. The higher the GRAVY score, the more hydrophobic the D-peptide. Amidation of the C-terminus was not taken into account for the calculation and the unnatural amino acid phenylglycine (λ) was substituted by phenylalanine for the calculation of the GRAVY score of ANK3. Since all D-peptides consist of twelve amino acid residues, the GRAVY scores represent not only hydropathy but also hydrophobicity of the D-peptides.

Aβ samples and their preparation

To ensure the monomeric state of full-length Aβ, recombinant Aβ(1-42) (Isoloid, Germany) and N-terminally biotinylated Aβ(1-42) (Bachem, Switzerland) were dissolved in hexafluoroisopropanol (HFIP), aliquoted and lyophilized. As required, Aβ was dissolved in 2 mM NaOH to a concentration of 1 mg ml^{-1}, diluted in HBS (20 mM HEPES, 150 mM NaCl, pH 7.4) and directly used.
N-terminally biotinylated Aβ fragments (peptides&elephants, Germany) were dissolved in dimethylformamide (DMF) and diluted in HBS for the SPR coupling procedure. Fragments 5 and 7 were heated up to 50°C for better solubility.

Kinetic interaction analysis

Kinetic analysis of the interaction between Aβ(1-42) and D-peptides was performed by SPR using a Biacore T200 instrument (GE Healthcare, Sweden) at 25°C. N-terminally biotinylated Aβ(1-42) (Bachem, Switzerland) was coupled on Series S SA Sensor chips (GE Healthcare, Sweden) at a concentration of 10 µg ml^{-1} to final levels of 1500-1800 RU. The Aβ flow cell and a reference flow cell without ligand were quenched with biotin. Titration series of D-peptides ranging from 3.2 µM to 50 µM for D3 and from 1.6 µM to 25 µM for ANK D-peptides were prepared in HBS including 150 mM NaCl, unless otherwise stated, and injected over the sensor surface. For experiments at higher NaCl concentrations, the D-peptide concentrations were adapted to the K_d values for D3

(6.3 µM - 200 µM) and ANK6 (3.1 µM - 100 µM). After each cycle, a conditional regeneration step using 2 M GdnHCl was implemented. For evaluation, the curves were double referenced using a buffer cycle and the reference flow cell and fitted according to the homogeneous 1:1 fit model, the two-state reaction model and the heterogeneous ligand model with *RI* = 0, respectively (Biacore T200 Evaluation Software 2.0, GE Healthcare).

Stoichiometry

The fitted saturation levels were taken from kinetic interaction analysis to estimate the stoichiometry of the complexes by the following equation:

$$N_L = \frac{R_{max} M_L}{R M_A}$$

where N_L is the valency of the ligand, R_{max} is the fitted saturation level of the analyte, R is the immobilization level of Aβ, M_L is the molecular weight of Aβ, M_A is the molecular weight of the D-peptide. 100% ligand activity and accessibility were assumed.

Aβ fibril formation kinetics

The Aβ fibril formation kinetics were measured in 20 mM HEPES buffer, pH 7.4, including 150 mM (HBS), 300 mM, 600 mM or 1200 mM NaCl. All buffers were supplemented with 5 µM Thioflavin-T dye and 10 µM of the respective D-peptide (D3, ANK3 or ANK6). Recombinant Aβ(1-42) was dissolved in the presence or absence of D-peptides to a final concentration of 10 µM. The fluorescence intensity (λ_{Ex} = 440 nm, λ_{Em} = 490 nm) was recorded in black non-binding 96-well plates (Greiner, Austria) every 450 s at 37°C over 27 h under quiescent conditions. The curves were corrected for buffer and D-peptide background.

Affinity determination for Aβ fragments

To evaluate the affinities for Aβ fragment binding, SPR experiments were conducted as described in the `Kinetic analysis` section but using N-terminally biotinylated Aβ fragments as ligands. For the coupling reactions, the concentrations were increased to 70 - 100 µg ml^{-1}. The analyte concentrations ranged from 3.1 µM to 100 µM for D3 and ANK6 and from 1.6 µM to 50 µM for ANK3. Obtained signals below 10 RU from the highest concentration were considered as non-binding. Since the sensorgrams of ANK3 and ANK6 showed less signatures of heterogeneous binding to the fragments as

compared to the full-length Aβ, K_d values for a 1:1 interaction were calculated, which provided fits of satisfactory quality. For evaluation, the final responses at the end of the association phase were plotted against the applied concentrations and fitted with the 1:1 steady state affinity model (*RI* = 0) (Biacore T200 Evaluation Software 2.0, GE Healthcare).

Thermodynamics

The thermodynamic profiles of the interaction between the D-peptides and Aβ monomers were determined by van´t Hoff analysis. For equilibrium thermodynamics, the van't Hoff equation states:

$$\Delta G = -RT\ln\left(\frac{1}{K_d}\right) = RT\ln(K_d)$$

where Δ*G* is the Gibbs free energy of binding, *R* is the gas constant, *T* is the absolute temperature, K_d is the equilibrium dissociation constant.
Substituting in the expression

$$\Delta G = \Delta H - T\Delta S$$

and rearranging yields:

$$\ln(K_d) = \frac{\Delta H}{RT} - \frac{\Delta S}{R}$$

where Δ*H* is the standard enthalpy, Δ*S* is the standard entropy.

K_d values were analyzed in HBS by SPR-based affinity determination as described above at different temperatures ranging from 11°C to 39°C. For D3, the homogeneous 1:1 fit model was applied (*RI* = 0) and for ANK D-peptides, the heterogeneous ligand model (*RI* = 0) (Biacore T200 Evaluation Software 2.0, GE Healthcare). By plotting $\ln(K_d)$ against the reciprocal temperature, Δ*H* and Δ*S* were extracted from the slope (Δ*H*/*R*) and intercept on the y-axis (-Δ*S*/*R*) of the linear regression.

Tables and figures

Table 1 Physico-chemical characteristics of the D-peptides involved in the study. All D-peptides were purchased in D-enantiomeric configuration with an amidated C-terminus which was considered for the calculation of net charge at neutral pH. ANK3 contains the unnatural amino acid phenylglycine (λ). Hydrophobicity was determined according to Kyte and Doolittle (46) as described in the experimental procedures and expressed as GRAVY score.

Compound	Sequence	Net charge	GRAVY score
D3	rprtrlhthrnr	+6	-2.6
ANK3	rkrirlλyhwnr	+6	-1.6
ANK6	rkrirlvtkkkr	+9	-1.8

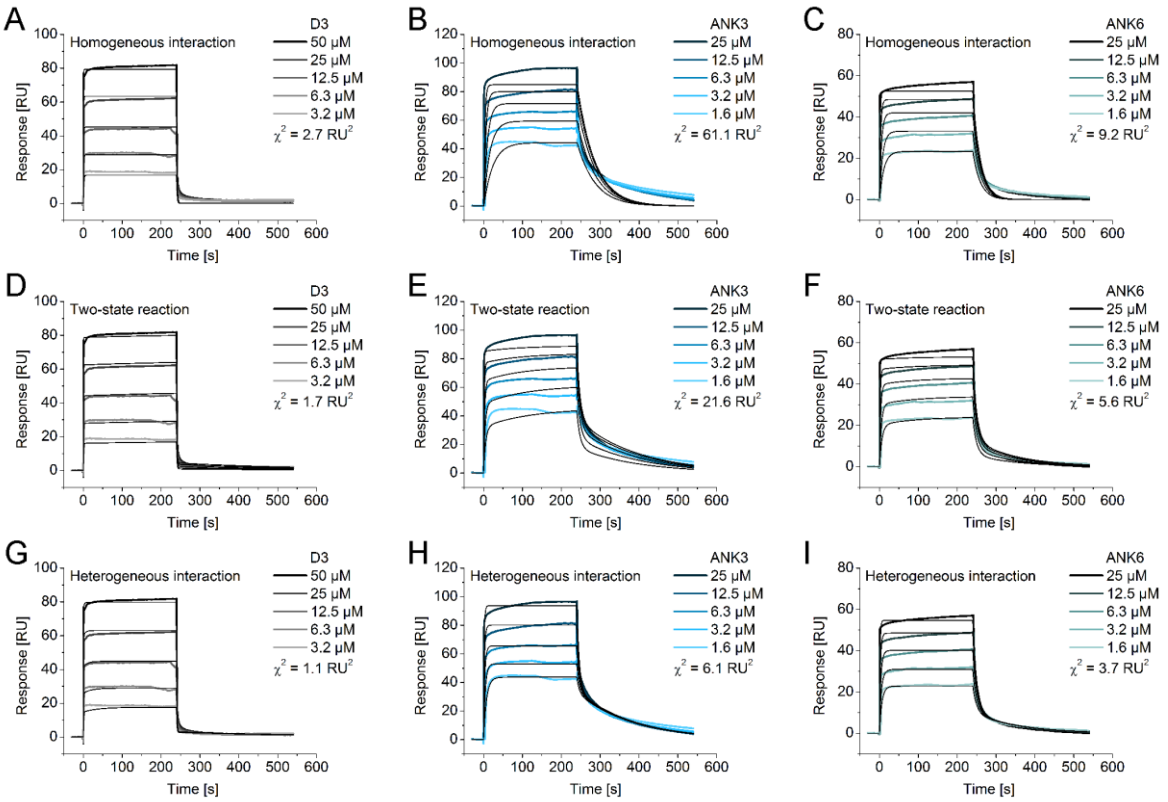

Figure 1 Real-time interaction between the D-peptides and Aβ monomers and corresponding fits. SPR sensorgrams of a titration series of D3 (A, D, G), ANK3 (B, E, H) and ANK6 (C, F, I) binding to immobilized Aβ monomers. Data were globally fitted according to a homogeneous (A-C), a two-state reaction (D-F) and a heterogeneous binding model (G-I). Sensorgrams are representative for seven independent kinetic measurements. χ^2 values present the goodness of the respective fit.

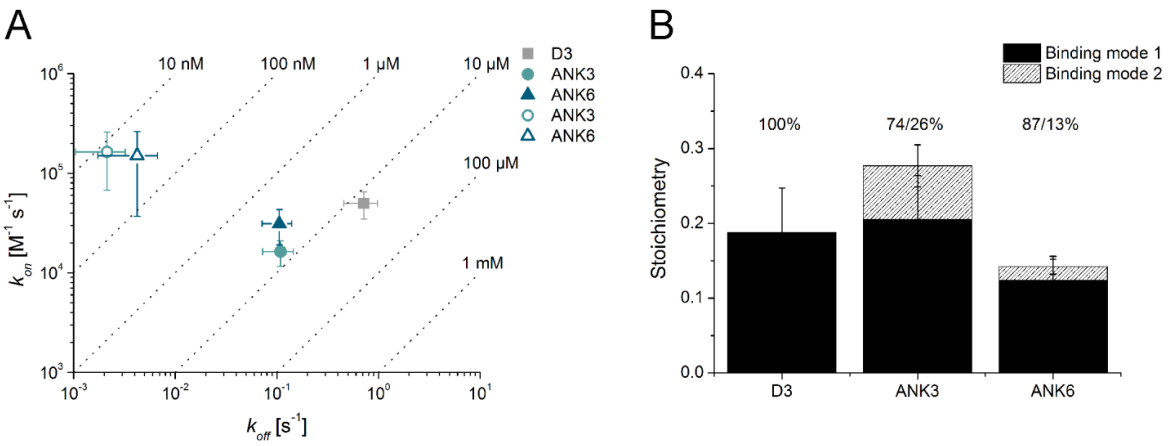

Figure 2 Kinetic rate constants and stoichiometry of the interaction of the D-peptides with Aβ. Kinetic rate constants of D3, ANK3 and ANK6 interactions with Aβ monomers were analyzed by SPR (A). Association rate constants (k_{on}) and dissociation rate constants (k_{off}) of D3 derived from global homogeneous fits while ANK3 and ANK6 were fitted heterogeneously, leading to two pairs of rate constants. Closed symbols represent binding mode 1 and open symbols binding mode 2. Equilibrium dissociation constants (K_d) resulting from k_{off} divided by k_{on} are depicted as dotted lines. The stoichiometry of saturated complexes was analyzed separately for each binding mode based on SPR data and shown as D-peptide to Aβ ratios (B). The numbers indicate the proportion of each binding mode. Presented data are mean values ± SD from seven independent measurements on various sensor surface preparations.

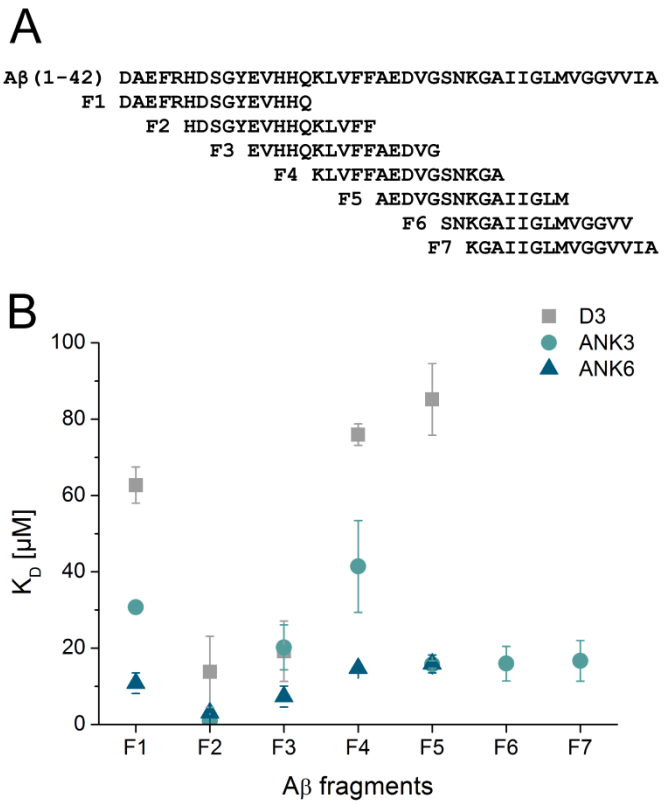

Figure 3 Epitope mapping of D3, ANK3 and ANK6. Aβ(1-42) sequence was divided into seven peptides with a length of 15 amino acids and an overlap of ten amino acids (A). The affinity of D3, ANK3 and ANK6 to the fragments 1 to 7 (F1 – F7) was determined by SPR (B). D3 and ANK6 showed no binding to fragments 6 and 7 in the applied concentrations. Presented data are mean values ± SD of three independent experiments.

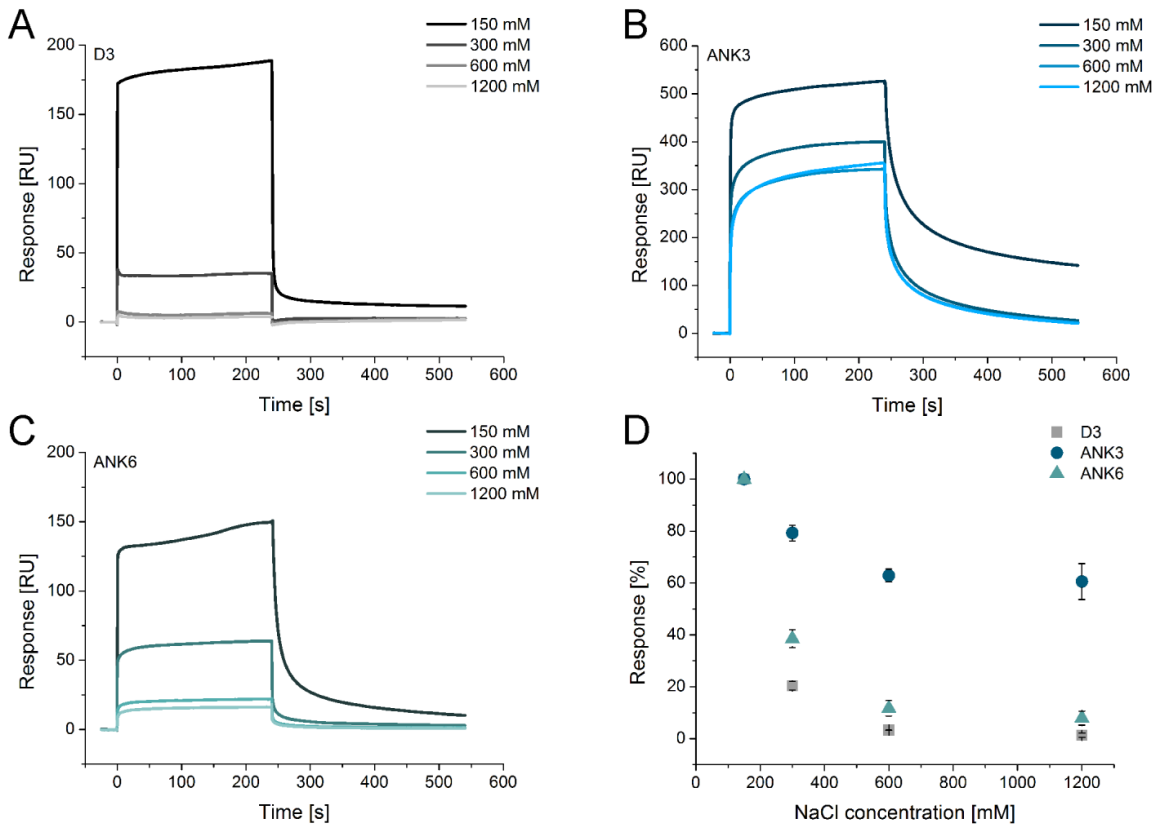

Figure 4 Interaction of the D-peptides with Aβ at different NaCl concentrations. The influence of ionic strength on the interaction of 50 µM D3 (A), 25 µM ANK3 (B) and 25 µM ANK6 (C) with Aβ monomers was analyzed by SPR at four different NaCl concentrations: 150 mM, 300 mM, 600 mM and 1200 mM. Sensorgrams are representative for two independent measurements. For quantitative analysis of the two data sets, the responses were normalized to the response at 150 mM and plotted as mean values ± SD over the NaCl concentration (D).

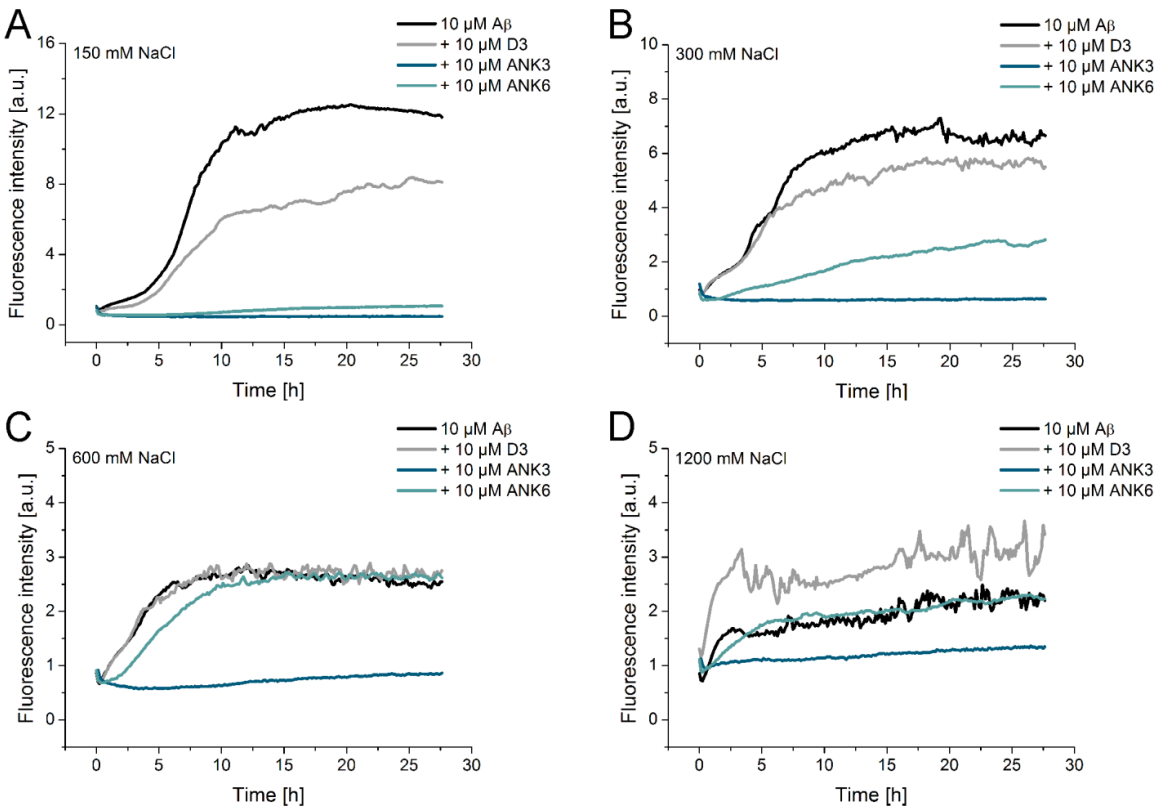

Figure 5 Inhibition of Aβ fibril formation by D3, ANK3 and ANK6 at different NaCl concentrations. The efficacy of D3, ANK3 and ANK6 to inhibit Aβ fibril formation was investigated at increasing ionic strength, adjusted by NaCl, 150 mM (A), 300 mM (B), 600 mM (C) and 1200 mM (D). All experiments were performed using 10 µM Aβ in the presence or absence of 10 µM D-peptide. The aggregation kinetics were monitored using Thioflavin-T fluorescence. Presented curves are mean values of three experiments.

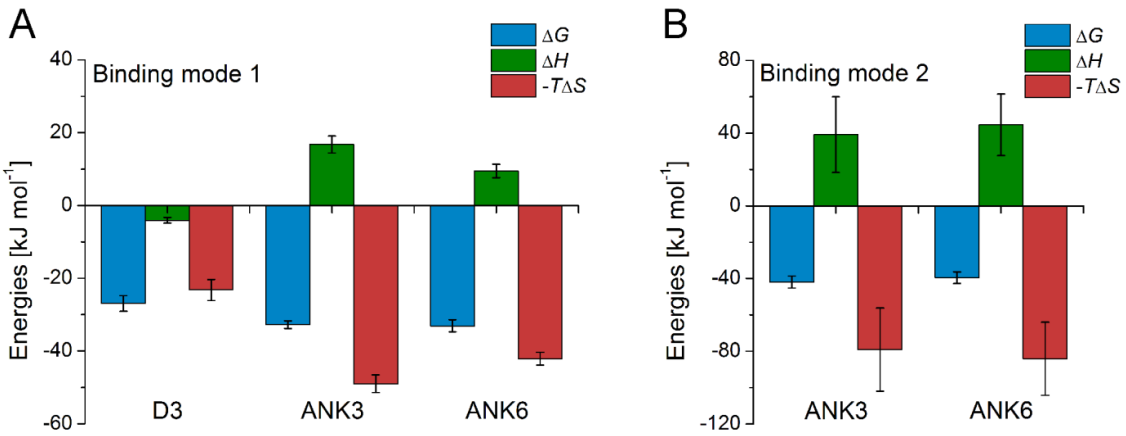

Figure 6 Thermodynamic analysis of the interaction with Aβ. The binding energies including Gibbs free energy of binding (ΔG), enthalpy (ΔH) and entropy ($-T\Delta S$) at 25°C were determined by van´t Hoff analysis. Due to heterogeneous binding of ANK D-peptides, thermodynamic profiles were separately analyzed for binding mode 1 (A) and binding mode 2 (B). Presented data are mean values ± SD of four independent analyses.

Supplemental data

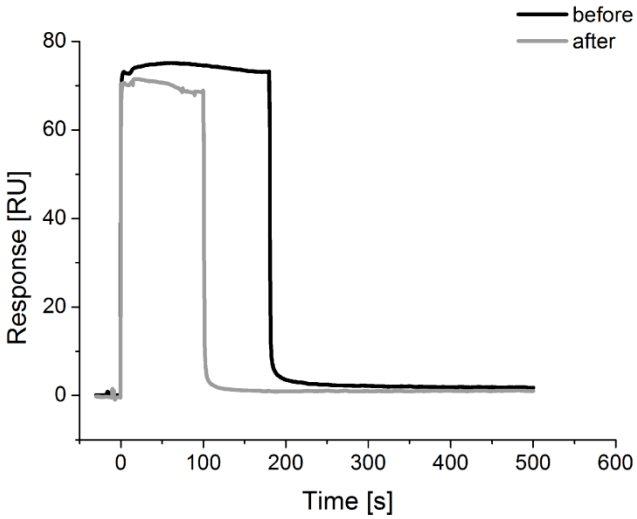

Figure S1 Control of immobilized Aβ after high salt conditions by SPR. Binding of 100 µM D3 was analyzed on a sensor chip directly after the immobilization procedure of Aβ monomers (before) and after more than 30 cycles with salt concentrations higher than 1 M NaCl (after). Since the response levels were the same, it was assumed that Aβ monomers are stable on the surface under these assay conditions.

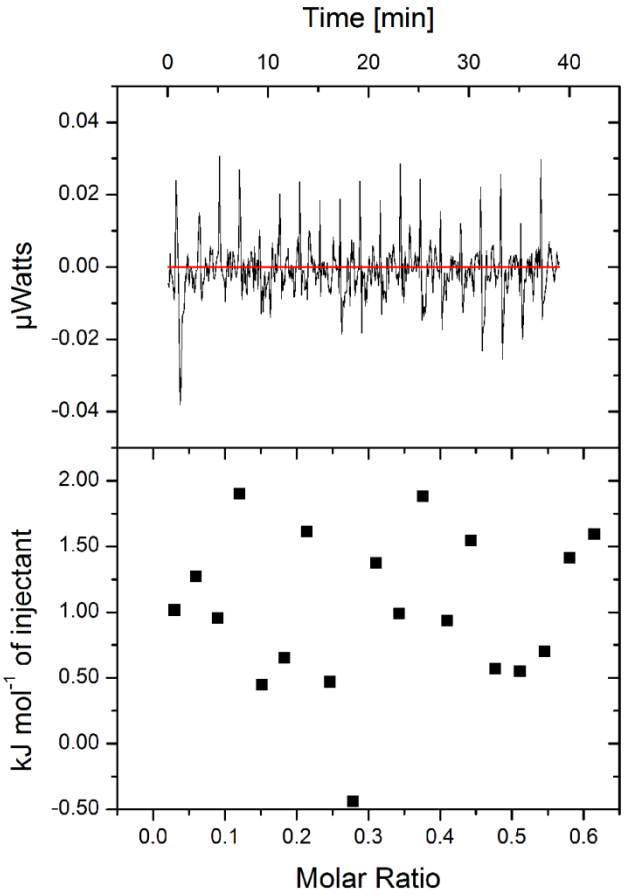

Figure S2 Titration curve of D3 into Aβ solution by ITC. Representatively, one isothermal titration calorimetry (ITC) experiment is shown for the titration of 300 µM D3 in 100 µM Aβ(1-40) solution at 25°C. The titrations of D3 in buffer (HBS) and buffer in Aβ solution were performed as control experiments and subtracted from the titration curve. Based on van´t Hoff analysis, very low entropy of -4 kJ mol^{-1} was expected which was not detected with this system.

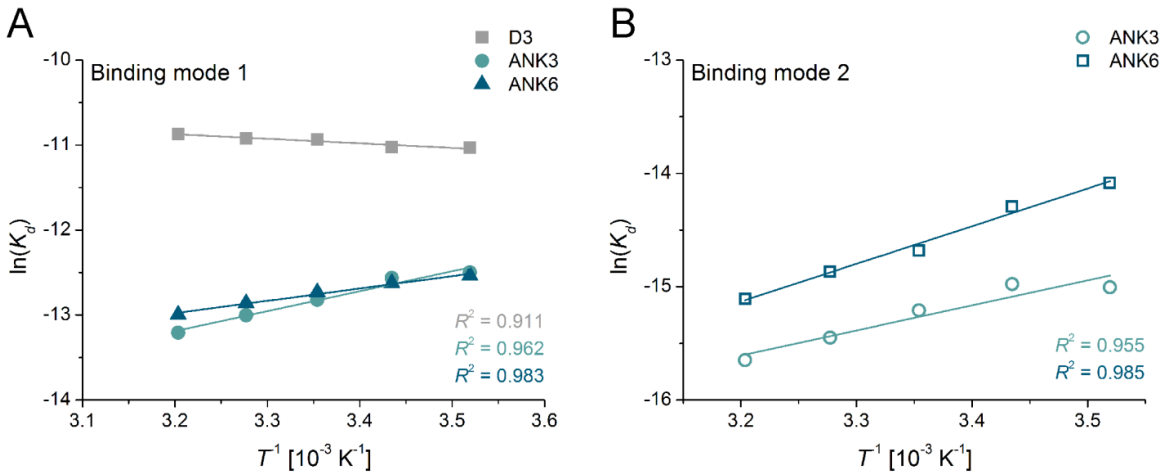

Figure S3 Temperature dependence of K_d values (van´t Hoff plot). K_d values of D3, ANK3 and ANK6 were determined at different temperatures using SPR. At each temperature, binding curves of D3 were homogeneously fitted whereas ANK D-peptides were analyzed heterogeneously, which resulted in two binding modes with two K_d values. Logarithm of dissociation constants were plotted against reciprocal temperature and fitted with a linear regression model. Closed symbols represent binding mode 1 (A) and open symbols binding mode 2 (B). Presented data are representative for four independent experiments.

References

1. Knowles, T. P., Vendruscolo, M., and Dobson, C. M. (2014) The amyloid state and its association with protein misfolding diseases. Nat Rev Mol Cell Biol 15, 384-396

2. Haass, C., and Selkoe, D. J. (2007) Soluble protein oligomers in neurodegeneration: lessons from the Alzheimer's amyloid beta-peptide. Nat Rev Mol Cell Biol 8, 101-112

3. Walsh, D. M., Klyubin, I., Fadeeva, J. V., Rowan, M. J., and Selkoe, D. J. (2002) Amyloid-beta oligomers: their production, toxicity and therapeutic inhibition. Biochem Soc T 30, 552-557

4. Finder, V. H., and Glockshuber, R. (2007) Amyloid-beta aggregation. Neurodegenerative Diseases 4, 13-27

5. Kumar, J., and Sim, V. (2014) D-amino acid-based peptide inhibitors as early or preventative therapy in Alzheimer disease. Prion 8, 119-124

6. Habchi, J., Chia, S., Limbocker, R., Mannini, B., Ahn, M., Perni, M., Hansson, O., Arosio, P., Kumita, J. R., Challa, P. K., Cohen, S. I., Linse, S., Dobson, C. M., Knowles, T. P., and Vendruscolo, M. (2017) Systematic development of small molecules to inhibit specific microscopic steps of Abeta42 aggregation in Alzheimer's disease. Proc Natl Acad Sci U S A 114, E200-E208

7. van Groen, T., Wiesehan, K., Funke, S. A., Kadish, I., Nagel-Steger, L., and Willbold, D. (2008) Reduction of Alzheimer's disease amyloid plaque load in transgenic mice by D3, A D-enantiomeric peptide identified by mirror image phage display. ChemMedChem 3, 1848-1852

8. Brener, O., Dunkelmann, T., Gremer, L., van Groen, T., Mirecka, E. A., Kadish, I., Willuweit, A., Kutzsche, J., Jurgens, D., Rudolph, S., Tusche, M., Bongen, P., Pietruszka, J., Oesterhelt, F., Langen, K. J., Demuth, H. U., Janssen, A., Hoyer, W., Funke, S. A., Nagel-Steger, L., and Willbold, D. (2015) QIAD assay for quantitating a compound's efficacy in elimination of toxic A beta oligomers. Sci Rep-Uk 5

9. Ziehm, T., Brener, O., van Groen, T., Kadish, I., Frenzel, D., Tusche, M., Kutzsche, J., Reiss, K., Gremer, L., Nagel-Steger, L., and Willbold, D. (2016) Increase of Positive Net Charge and Conformational Rigidity Enhances the Efficacy of d-Enantiomeric Peptides Designed to Eliminate Cytotoxic Abeta Species. ACS chemical neuroscience 7, 1088-1096

10. Funke, S. A., van Groen, T., Kadish, I., Bartnik, D., Nagel-Steger, L., Brener, O., Sehl, T., Batra-Safferling, R., Moriscot, C., Schoehn, G., Horn, A. H. C., Muller-Schiffmann, A., Korth, C., Sticht, H., and Willbold, D. (2010) Oral Treatment with the D-Enantiomeric Peptide D3 Improves the Pathology and Behavior of Alzheimer's Disease Transgenic Mice. ACS chemical neuroscience 1, 639-648

11. Aprile, F. A., Sormanni, P., Perni, M., Arosio, P., Linse, S., Knowles, T. P. J., Dobson, C. M., and Vendruscolo, M. (2017) Selective targeting of primary and secondary nucleation pathways in Abeta42 aggregation using a rational antibody scanning method. Sci Adv 3, e1700488

12. Arosio, P., Michaels, T. C., Linse, S., Mansson, C., Emanuelsson, C., Presto, J., Johansson, J., Vendruscolo, M., Dobson, C. M., and Knowles, T. P. (2016) Kinetic analysis reveals the diversity of microscopic mechanisms through which molecular chaperones suppress amyloid formation. Nat Commun 7, 10948

13. Cohen, S. I., Arosio, P., Presto, J., Kurudenkandy, F. R., Biverstal, H., Dolfe, L., Dunning, C., Yang, X., Frohm, B., Vendruscolo, M., Johansson, J., Dobson, C. M., Fisahn, A., Knowles, T. P., and Linse, S. (2015) A molecular chaperone breaks the catalytic cycle that generates toxic Abeta oligomers. Nat Struct Mol Biol 22, 207-213

14. van Groen, T., Kadish, I., Funke, A., Bartnik, D., and Willbold, D. (2012) Treatment with Abeta42 binding D-amino acid peptides reduce amyloid deposition and inflammation in APP/PS1 double transgenic mice. Advances in protein chemistry and structural biology 88, 133-152

15. Klein, A. N., Ziehm, T., van Groen, T., Kadish, I., Elfgen, A., Tusche, M., Thomaier, M., Reiss, K., Brener, O., Gremer, L., Kutzsche, J., and Willbold, D. (2017) Optimization of d-Peptides for Abeta Monomer Binding Specificity Enhances Their Potential to Eliminate Toxic Abeta Oligomers. ACS chemical neuroscience 8, 1889-1900

16. Olubiyi, O. O., Frenzel, D., Bartnik, D., Gluck, J. M., Brener, O., Nagel-Steger, L., Funke, S. A., Willbold, D., and Strodel, B. (2014) Amyloid aggregation inhibitory mechanism of arginine-rich D-peptides. Current medicinal chemistry 21, 1448-1457

17. Klebe, G. (2015) Applying thermodynamic profiling in lead finding and optimization. Nat Rev Drug Discov 14, 95-110

18. Geschwindner, S., Ulander, J., and Johansson, P. (2015) Ligand Binding Thermodynamics in Drug Discovery: Still a Hot Tip? Journal of medicinal chemistry 58, 6321-6335

19. Schon, A., and Freire, E. (2016) Enthalpy screen of drug candidates. Anal Biochem 513, 1-6

20. Frenzel, D., Gluck, J. M., Brener, O., Oesterhelt, F., Nagel-Steger, L., and Willbold, D. (2014) Immobilization of homogeneous monomeric, oligomeric and fibrillar Abeta species for reliable SPR measurements. PloS one 9, e89490

21. Melander, W., and Horvath, C. (1977) Salt Effects on Hydrophobic Interactions in Precipitation and Chromatography of Proteins - Interpretation of Lyotropic Series. Arch Biochem Biophys 183, 200-215

22. Buell, A. K., Hung, P., Salvatella, X., Welland, M. E., Dobson, C. M., and Knowles, T. P. (2013) Electrostatic effects in filamentous protein aggregation. Biophys J 104, 1116-1126

23. Krainer, G., and Keller, S. (2015) Single-experiment displacement assay for quantifying high-affinity binding by isothermal titration calorimetry. Methods 76, 116-123

24. Holdgate, G. A. (2001) Making cool drugs hot: isothermal titration calorimetry as a tool to study binding energetics. Biotechniques 31, 164-166, 168, 170 passim

25. Day, Y. S., Baird, C. L., Rich, R. L., and Myszka, D. G. (2002) Direct comparison of binding equilibrium, thermodynamic, and rate constants determined by surface- and solution-based biophysical methods. Protein Sci 11, 1017-1025

26. Navratilova, I., Papalia, G. A., Rich, R. L., Bedinger, D., Brophy, S., Condon, B., Deng, T., Emerick, A. W., Guan, H. W., Hayden, T., Heutmekers, T., Hoorelbeke, B., McCroskey, M. C., Murphy, M. M., Nakagawa, T., Parmeggiani, F., Qin, X., Rebe, S., Tomasevic, N., Tsang, T., Waddell, M. B., Zhang, F. F., Leavitt, S., and Myszka, D. G. (2007) Thermodynamic benchmark study using Biacore technology. Anal Biochem 364, 67-77

27. Oprea, T. I., Davis, A. M., Teague, S. J., and Leeson, P. D. (2001) Is there a difference between leads and drugs? A historical perspective. J Chem Inf Comp Sci 41, 1308-1315

28. Blundell, T. L., Jhoti, H., and Abell, C. (2002) High-throughput crystallography for lead discovery in drug design. Nature Reviews Drug Discovery 1, 45-54

29. de Kloe, G. E., Bailey, D., Leurs, R., and de Esch, I. J. P. (2009) Transforming fragments into candidates: small becomes big in medicinal chemistry. Drug discovery today 14, 630-646

30. Zhao, H. (2007) Scaffold selection and scaffold hopping in lead generation: a medicinal chemistry perspective. Drug discovery today 12, 149-155

31. Colvin, M. T., Silvers, R., Ni, Q. Z., Can, T. V., Sergeyev, I., Rosay, M., Donovan, K. J., Michael, B., Wall, J., Linse, S., and Griffin, R. G. (2016) Atomic Resolution Structure of Monomorphic Abeta42 Amyloid Fibrils. Journal of the American Chemical Society 138, 9663-9674

32. Walti, M. A., Ravotti, F., Arai, H., Glabe, C. G., Wall, J. S., Bockmann, A., Guntert, P., Meier, B. H., and Riek, R. (2016) Atomic-resolution structure of a disease-relevant Abeta(1-42) amyloid fibril. Proc Natl Acad Sci U S A 113, E4976-4984

33. Gremer, L., Scholzel, D., Schenk, C., Reinartz, E., Labahn, J., Ravelli, R. B. G., Tusche, M., Lopez-Iglesias, C., Hoyer, W., Heise, H., Willbold, D., and Schroder, G. F. (2017) Fibril structure of amyloid-beta(1-42) by cryo-electron microscopy. Science 358, 116-119

34. Muller, K. M., Arndt, K. M., and Pluckthun, A. (1998) Model and simulation of multivalent binding to fixed ligands. Anal Biochem 261, 149-158

35. Stenberg, E., Persson, B., Roos, H., and Urbaniczky, C. (1991) Quantitative-Determination of Surface Concentration of Protein with Surface-Plasmon Resonance Using Radiolabeled Proteins. J Colloid Interf Sci 143, 513-526

36. Ross, P. D., and Shapiro, J. T. (1974) Heat of Interaction of DNA with Polylysine, Spermine, and Mg++. Biopolymers 13, 415-416

37. Record, M. T., Lohman, T. M., and Dehaseth, P. (1976) Ion Effects on Ligand-Nucleic Acid Interactions. Journal of molecular biology 107, 145-158

38. Manning, G. S. (1969) Limiting Laws and Counterion Condensation in Polyelectrolyte Solutions .I. Colligative Properties. Journal of Chemical Physics 51, 924-&

39. Manning, G. S. (1978) The molecular theory of polyelectrolyte solutions with applications to the electrostatic properties of polynucleotides. Q Rev Biophys 11, 179-246

40. Privalov, P. L., Dragan, A. I., and Crane-Robinson, C. (2011) Interpreting protein/DNA interactions: distinguishing specific from non-specific and electrostatic from non-electrostatic components. Nucleic Acids Res 39, 2483-2491

41. Chandler, D. (2005) Interfaces and the driving force of hydrophobic assembly. Nature 437, 640-647

42. Testa, B., Crivori, P., Reist, M., and Carrupt, P. A. (2000) The influence of lipophilicity on the pharmacokinetic behavior of drugs: Concepts and examples. Perspect Drug Discov 19, 179-211

43. Arnott, J. A., and Planey, S. L. (2012) The influence of lipophilicity in drug discovery and design. Expert Opin Drug Dis 7, 863-875

44. Kyte, J., and Doolittle, R. F. (1982) A Simple Method for Displaying the Hydropathic Character of a Protein. Journal of molecular biology 157, 105-132

3.6 Aβ oligomer eliminating compounds interfere successfully with pEAβ(3-42) induced motor neurodegenerative phenotype in transgenic mice

Tina Dunkelmann, Kerstin Teichmann, Tamar Ziehm, Sarah Schemmert, Daniel Frenzel, Markus Tusche, Christina Dammers, Dagmar Jürgens, Karl-Josef Langen, Hans-Ulrich Demuth, Nadim Jon Shah, Janine Kutzsche, Antje Willuweit, Dieter Willbold

Neuropeptides. 2018 Feb;67:27-35

doi: 10.1016/j.npep.2017.11.011

https://www.sciencedirect.com/science/article/pii/S0143417917301531

Neuropeptides 67 (2018) 27–35

Contents lists available at ScienceDirect

Neuropeptides

journal homepage: www.elsevier.com/locate/npep

Aβ oligomer eliminating compounds interfere successfully with pEAβ(3–42) induced motor neurodegenerative phenotype in transgenic mice

Tina Dunkelmann[a,1], Kerstin Teichmann[a,2], Tamar Ziehm[a], Sarah Schemmert[a], Daniel Frenzel[a,3], Markus Tusche[a], Christina Dammers[a,4], Dagmar Jürgens[a], Karl-Josef Langen[b,c], Hans-Ulrich Demuth[d], Nadim Jon Shah[b,e,f], Janine Kutzsche[a], Antje Willuweit[b,**], Dieter Willbold[a,g,*]

[a] Institute of Complex Systems, Structural Biochemistry (ICS-6), Forschungszentrum Jülich GmbH, Wilhelm-Johnen Straße, 52425 Jülich, Germany
[b] Institute of Neuroscience and Medicine (INM-4), Medical Imaging Physics, Forschungszentrum Jülich GmbH, Wilhelm-Johnen Straße, 52425 Jülich, Germany
[c] Department of Nuclear Medicine, Faculty of Medicine, RWTH Aachen University, Pauwelsstraße 30, 52074 Aachen, Germany
[d] Fraunhofer-Institute of Cell Therapy and Immunology (IZI), Leipzig, Department of Drug Design and Target Validation (MWT), Biozentrum, Weinbergweg 22, 06120 Halle, Germany
[e] Department of Neurology, Faculty of Medicine, JARA, RWTH Aachen University, Pauwelsstraße 30, 52074 Aachen, Germany
[f] Department of Electrical and Computer Systems Engineering and Monash Biomedical Imaging, School of Psychological Sciences, Monash University, Melbourne, Victoria, Australia
[g] Institut für Physikalische Biologie, Heinrich Heine Universität Düsseldorf, Universitätsstraße 1, 40225 Düsseldorf, Germany

ARTICLE INFO

Keywords:
pEAβ(3–42)
D3
D3D3
Neurodegeneration
Alzheimer's disease
Animal model
Treatment
All-D-enantiomeric peptides
TBA2.1

ABSTRACT

Currently, there are no causative or disease modifying treatments available for Alzheimer's disease (AD). Previously, it has been shown that D3, a small, fully D-enantiomeric peptide is able to eliminate low molecular weight Aβ oligomers in vitro, enhance cognition and reduce plaque load in AD transgenic mice. To further characterise the therapeutic potential of D3 towards N-terminally truncated and pyroglutamated Aβ (pEAβ(3–42)) we tested D3 and its head-to-tail tandem derivative D3D3 both in vitro and in vivo in the new mouse model TBA2.1. These mice produce human pEAβ(3–42) leading to a strong, early onset motor neurodegenerative phenotype. In the present study, we were able to demonstrate 1) strong binding affinity of both D3 and D3D3 to pEAβ(3–42) in comparison to Aβ(1–42) and 2) increased affinity of the tandem derivative D3D3 in comparison to D3. Subsequently we tested the therapeutic potentials of both peptides in the TBA2.1 animal model. Truly therapeutic, non-preventive treatment with D3 and D3D3 clearly slowed the progression of the neurodegenerative TBA2.1 phenotype, indicating the strong therapeutic potential of both peptides against pEAβ(3–42) induced neurodegeneration.

1. Introduction

The number of patients suffering from Alzheimer's disease (AD) is expected to increase dramatically if no causal therapy becomes available (Brookmeyer et al., 2007). Major hallmarks of AD are progressive neurodegeneration, and the deposition of tau protein containing neurofibrillary tangles and amyloid β peptide (Aβ) containing extracellular plaques (Parihar and Hemnani, 2004). Aβ is produced by the cleavage of the amyloid precursor protein (APP) through β- and γ-secretases. Under pathological conditions, correlating with age, ultimately, Aβ monomers will assemble into different Aβ aggregates, e.g. the Aβ oligomers, which are thought to play an important role in the development and progression of the disease (Finder and Glockshuber, 2007). Currently, there is no causal treatment available to halt or even slow down AD progression (Bateman, 2015). Previously, the potential Aβ-binding D-enantiomeric peptide D3 has been identified by mirror image

* Correspondence to: D. Willbold, Institute of Complex Systems, Structural Biochemistry (ICS-6), Forschungszentrum Jülich GmbH, Wilhelm-Johnen Straße, 52425 Jülich, Germany.
** Corresponding author.
E-mail addresses: a.willuweit@fz-juelich.de (A. Willuweit), d.willbold@fz-juelich.de (D. Willbold).
[1] Present address: Clinical Development, Prima BioMed, Nürnberger Str. 49, 10789 Berlin, Germany.
[2] Present address: Evotec AG, Manfred Eigen Campus, Essener Bogen 7, 22419 Hamburg, Germany.
[3] Present address: European Molecular Biology Laboratory, Meyerhofstraße 1, 69117 Heidelberg, Germany.
[4] Present address: Analytical Development Biologicals, Boehringer Ingelheim Pharma GmbH & Co.KG, Birkendorfer Strasse 65, 88397 Biberach an der Riss, Germany.

https://doi.org/10.1016/j.npep.2017.11.011
Received 26 April 2017; Received in revised form 24 November 2017; Accepted 26 November 2017
Available online 27 November 2017

phage display (Schumacher et al., 1996) for binding to Aβ (Wiesehan and Willbold, 2003; Funke and Willbold, 2009). It has been shown that the two advantages of peptides consisting solely of D-enantiomeric amino acid residues are the lower immunogenic potential and the higher resistance to proteases as compared to L-peptides (Dintzis et al., 1993; Soto et al., 1996; Funke and Willbold, 2012; Jiang et al., 2015; Leithold et al., 2016). It was shown that D3 reduces Aβ(1–42) mediated cell toxicity, prevents further aggregation of Aβ(1–42) (van Groen et al., 2008) and converts toxic oligomers into large, non-toxic amorphous aggregates in vitro (Funke et al., 2010). Oral administration of D3 improves the spatial learning behaviour in the Morris water maze, reduces Aβ load and the inflammatory situation in transgenic APP/PS1 mice (van Groen et al., 2008; Funke et al., 2010; van Groen et al., 2013).

Animal models of AD have been successfully used to gain deeper insight into the pathogenesis of this condition and are currently without viable alternative. However, despite this utility, most of the models currently used lack the neurodegenerative pathology required to develop a curative treatment option. The transgenic TBA2.1 mouse model expresses human N-terminally truncated Aβ which is post-translationally modified to form pyroglutamate modified Aβ (pEAβ(3–42)) (Alexandru et al., 2011). pEAβ(3–42) is one of the principal components of senile plaques in human brains (Harigaya et al., 2000). Owing to its very fast aggregation and formation of toxic oligomers, pEAβ(3–42) is thought to be involved in the initiation of the amyloid cascade (Jawhar et al., 2011). Homozygous TBA2.1 mice develop a progressive motor neurodegenerative phenotype. Here, we investigated the treatment potential of D3 and its head-to-tail tandem version D3D3 in homozygous TBA2.1 mice to elucidate their potential in ameliorating pEAβ(3–42) aggregation induced pathology and neurodegeneration. This study demonstrates that a truly therapeutic, non-preventive treatment with D3 and D3D3 decelerated the progression of the pEAβ(3–42) induced neurodegenerative TBA2.1 phenotype underlining the strong therapeutic potentials of both compounds for Alzheimer's disease.

2. Material and methods

2.1. Experimental design

We determined the binding affinities of D3 and D3D3 to Aβ(1–42) and pEAβ(3–42) via SPR and tested their influence on the cytotoxicity of pEAβ(3–42) using MTT cytotoxicity analysis in cell culture. For these experiments, recombinant Aβ(1–42) was purchased from Isoloid (Germany) and recombinant pEAβ(3–42) was purified as described recently (Dammers et al., 2015). Both Aβ variants were dissolved in HFIP overnight prior to usage to destroy any existing aggregates and lyophilised to remove HFIP.

After the positive evaluation of both compounds in vitro, it was planned to determine their therapeutic properties in the TBA2.1 mouse model. Due to animal welfare we decided to use male TBA2.1 mice for phenotype characterisation and female mice for the treatment study. The phenotype assessment and the motor balance were determined longitudinally by testing ten wild type and eleven homozygous mice every four weeks starting at two months of age. For the treatment studies, four-months-old female mice were stratified into groups according to their SHIRPA score, resulting in 7 animals receiving placebo, 8 animals D3 and 8 animals D3D3. The mice were treated intraperitoneally by implanting Alzet osmotic minipumps, in order to achieve high and fast drug exposure in the brain during a short therapeutic treatment period. Additionally, the mice were tested before and after treatment in the accelerating Rotarod. All experimenters were blind to genotype or treatment and all tests were carried out at the same time of day. After the last behavioural test animals were sacrificed and brains were dissected. One hemisphere was collected for biochemical analysis and one for immunostainings. Several hemispheres were lost during processing for immunohistochemistry resulting in 4 placebo, 4 D3 and 5 D3D3 specimens. ELISA measurements were performed with samples from each animal included in the study (7 to 8 per group).

2.2. SPR spectroscopy

SPR measurements were performed using a Biacore T200 instrument (GE Healthcare, Sweden) at 25 °C with 20 mM sodium phosphate, 50 mM sodium chloride, pH 7.4 as running buffer. For preparation of the flow cells, a CM5 sensor chip (GE Healthcare, Sweden) was activated with EDC/NHS (0.2 M/0.05 M) and Aβ(1–42) (300 µg/ml) and pEAβ(3–42) (100 µg/ml), diluted in 10 mM sodium acetate pH 4.0, were immobilized to final levels of 8000 RU (pEAβ(3–42)) and 1000 RU (Aβ(1–42)). Ligand and reference flow cells were deactivated with 1 M ethanolamine-HCl. D3 and D3D3 affinity determinations were performed in multi cycle kinetics at 30 µl/min flow rate. The analytes were diluted in running buffer to the final concentrations of 100, 33.33, 11.11, 3.70, 1.23 and 0.41 µM for D3 and 10, 3.33, 1.11, 0.37, 0.12 and 0.04 µM for D3D3. Association of the peptides was recorded for 120 s, followed by a dissociation of 240 s. After each cycle, a conditional regeneration step with 2 M guanidine hydrochloride was implemented. After measurement, the sensorgrams were double referenced using the reference flow cell and a buffer cycle. Evaluation was performed by plotting the respective response levels against the applied peptide concentrations. The curves were fitted using Langmuir's 1:1 binding model (Hill function with $n = 1$, OriginPro 8.5G, OriginLab, Northampton, USA).

2.3. MTT-assay

Lyophilized pEAβ(3–42) was dissolved in 10 mM sodium phosphate buffer, pH 7.4 to a total concentration of 51 µM and the D-peptides D3 and D3D3 (molar ratio of 1:0, 1:0.1, 1:1, 1:10 for pEAβ(3–42):D3 and 1:0, 1:0.2, 1:1, 1:5 for pEAβ(3–42):D3D3) were added, respectively, and incubated at 37 °C for 5 days without shaking resulting in pEAβ(3–42) fibrils. The highest concentration of D-peptides, i.e. 510 µM (0,81 mg/ml) for D3 and 255 µM (0,81 mg/ml) for D3D3, were treated the same without co-incubation of pEAβ(3–42).

PC-12 cells (Leibniz-Institut DSMZ-Deutsche Sammlung von Mikroorganismen und Zellkulturen GmbH, Braunschweig, Germany) were cultured in Dulbecco's modified Eagle's medium (DMEM) (Sigma-Aldrich Chemie GmbH, Taufkirchen, Germany) supplemented with 10% fetal bovine serum (FCS) (Sigma-Aldrich Chemie GmbH, Taufkirchen, Germany) and 5% horse serum (HS) (Sigma-Aldrich Chemie GmbH, Taufkirchen, Germany) at 37 °C and 5% CO_2. Cells were harvested and seeded onto 96-well plates (Gibco, Life Technologies, Carlsbad, California) at 1×10^3 cells/well and incubated at 37 °C and 5% CO_2 for 24 h. The cells were treated with 1 µM incubated pEAβ(3–42) and 1 µM pEAβ(3–42) co-incubated with D3 (in molar ratios of 1:0.1, 1:1 and 1:1) or D3D3 (in molar ratios of 1:0.2, 1:1 and 1:5), respectively, as well as 10 µM D3, 10 µM D3D3 and the buffer alone (10 mM sodium phosphate, pH 7.4). The buffer containing 0.125% Triton X-100 (AppliChem, Darmstadt, Germany) was used as negative control. All samples were added five-fold in a three-fold-determination. The treated cells were incubated at 37 °C and 5% CO_2 for 24 h. MTT-assay was performed using the "Cell Proliferation Kit 1" (Roche, Mannheim, Germany) according to the manufacturer's instructions. The 96-well plate was analysed using a MicroPlate Reader (PolarStar Optima, BMG Labtech, Offenburg, Deutschland) by measuring the absorbance at 570 nm and 660 nm and background corrected.

2.4. Animals

Experiments were conducted using homozygous TBA2.1 mice and wild type littermates as control mice. Transgenic TBA2.1 mice exhibited

neuronal expression of Aβ(Q3–42) on a C57BL/6 × DBA1 background. Aβ(Q3–42) was modified by glutaminyl cyclase to pEAβ(3–42) within the secretory pathway in TBA2.1 mice (Alexandru et al., 2011). All animal procedures were performed in accordance with the German law for the protection of animals and approved by LANUV North-Rhine-Westphalia (Germany, AZ84-02.04.2011.A359). The animals were kept in a controlled environment on a 12/12-hours light/dark cycle (lights on from 7 a.m.–7 p.m.), with 54% humidity and a temperature of 22 °C. Up to four mice per cage were housed with food and water available ad libitum. Only heterozygous TBA2.1 mice were used for breeding and homozygous mice were sacrificed at five months of age to prevent suffering due to the severity of the phenotype.

2.5. Peptides

The D-enantiomeric peptides D3 (rprtrlhthrnr, all amino acids are D-enantiomers) and D3D3 (rprtrlhthrnrrprtrlhthrnr, all amino acids are D-enantiomers) with ≥ 95% purity were purchased C-terminally amidated from JPT Peptide Technologies GmbH, Germany.

2.6. Phenotype assessment

For phenotype assessment the primary screen of the SHIRPA test battery was used (Rogers et al., 1997). This includes the following subtests: abnormal body carriage, alertness, abnormal gait, startle response, loss of righting reflex, touch response, pinna reflex, cornea reflex, forelimb placing reflex, hanging behaviour and pain response. Additionally, the body weight was measured. For individual observation and analysis an arena of 42.5 cm × 18 cm × 26.5 cm (L × H × W) was used. The observations were scored from 0 (similar to wild type) to 3 (extremely abnormal from wild type). The sum of all subtests per animal was used for analysis.

2.7. Accelerating Rotarod

To analyse motor coordination and motor balance TBA2.1 mice were placed on a Rotarod apparatus (Ugo Basile Srl, Italy). Testing was performed according to the previously published protocol (Alexandru et al., 2011). In the morning of the first day mice were trained to stay on the rod for at least 60 s at a constant 10 rpm. The test sessions were performed in the afternoon as well as the following morning and afternoon. Before starting the test session the mice were habituated for 30 min in single cages. In one test session the mice had to run in three trials on the beam accelerating from 4 to 40 rpm. The escape latency of running was measured. Maximum time was 10 min. For analysis the mean value of all nine trials was used.

2.8. Treatment with D3 and D3D3

Wild type and homozygous four months old TBA2.1 mice were treated intraperitoneally for four weeks with a daily dosage of 5 mg per kg peptide in PBS (pH 7.4) or vehicle (PBS, pH 7.4) using Alzet mini-osmotic pumps (model 1004, DURECT Corporation, USA). The body weight and conditions of the mice were controlled twice a week. A loss of 15% body weight and severe conspicuities were defined as exclusion criteria. No animal was affected by these exclusion criteria.

2.9. Tissue preparation

The mice were sacrificed and the brain was harvested. The right hemisphere was used for immunohistochemical analysis and the left was used for enzyme-linked immunosorbent assay (ELISA) measurements. Both hemispheres were stored at − 80 °C until further processing.

2.10. Immunofluorescence

Immunofluorescence analysis was assessed to determine the Aβ load, DAPI positive nuclei and astrocyte staining. The right hemisphere was cryosectioned sagittally into 10 µm thin sections. Six sections per animal were fixed with 4% paraformaldehyde and treated with 70% formic acid for antigen retrieval. After washing and blocking with Mouse Ig Blocking Reagent (Vector Laboratories, Inc., USA) slides were treated with either primary antibody against Aβ (6E10, Covance Inc., USA) or against activated astrocytes (GFAP, Dako Deutschland GmbH, Germany) overnight. After washing the secondary antibody (mouse anti goat 488, Life Technologies GmbH, Germany) was incubated for two hours. After washing slides were covered with 4′, 6-Diamidin-2-phenylindol (DAPI, Merck KGaA, Germany) for 10 min. Images were taken with a LMD6000 microscope (Leica Camera, Germany) with a DFC310 FX camera (Leica Camera, Germany). The number of stained Aβ aggregates (Aβ particle count) of either the whole hemisphere, or hippocampus, striatum and midbrain as well as DAPI counts and GFAP (astrocyte staining, % positive area) of the CA1 region were quantified on five to six sections per animal using ImageJ (National Institute of Health, USA).

2.11. ELISA

In brief, an Aβ ELISA (N3pE-42, IBL International GmbH, Germany) was used to quantify the pEAβ(3–42) levels. Therefore, left hemispheres were homogenised with Tris buffer (20 mM Tris pH 8.3, 250 mM NaCl, Roche EDTA free Complete Protease Inhibitor) using the PreCellys24 homogeniser (2 × 20 sec at 6500 rpm, Bertin Technologies, France). After vortexing, a 15 min sonification and additional vortexing the homogenate was then centrifuged (175,000g, 4 °C, 30 min). The resulting pellet was incubated and resuspended with diethanolamine (DEA) on ice and again centrifuged. The supernatant represents the DEA soluble fraction which was used for analysis. The pellet was incubated and resuspended with 70% formic acid on ice. After the final centrifugation step the interphase was taken and neutralised with 1 M Tris pH 11.3 representing the insoluble Aβ fraction. DEA soluble and insoluble Aβ fractions were subjected to the ELISA to determine the pEAβ(3–42) concentrations according to the manufacturer's protocol. The samples were normalised to their protein concentration. For the DEA-soluble fraction, the Micro BCA Protein Assay Kit (Pierce Biotechnology, USA) was used and for the insoluble fraction, the Bio-Rad Protein Assay (Bio-Rad, Germany).

2.12. Statistical analysis

To assess Gaussian distribution, all data were tested using the Shapiro-Wilk-Test or in a normality probability plot. In the case of normally distributed data the Repeated-Measures Parametric Analyses, Two- or One-Way-ANOVA with Bonferroni post hoc analysis or (paired) *t*-test were used, respectively. For the non-parametric analysis, the Friedman test or Kruskal-Wallis test were used. Multiple Comparison Tests by Dunn was used for appropriate non-parametric post hoc analysis. All data were expressed as mean with SEM. Results are considered as significantly different to $p \leq 0.05$. All statistical analyses were performed using GraphPad PRISM 5 (GraphPad Software, Inc., USA) and InVivoStat 2.5 (InVivoStat by Simon Bate and Robin Clark, United Kingdom (Clark et al., 2012).

3. Results

3.1. In vitro binding activity of D3 and D3D3 for Aβ(1–42) and pEAβ(3–42)

In order to increase the potency of D3, we chose a head-to-tail tandem version of it, D3D3, which was expected to bind with higher

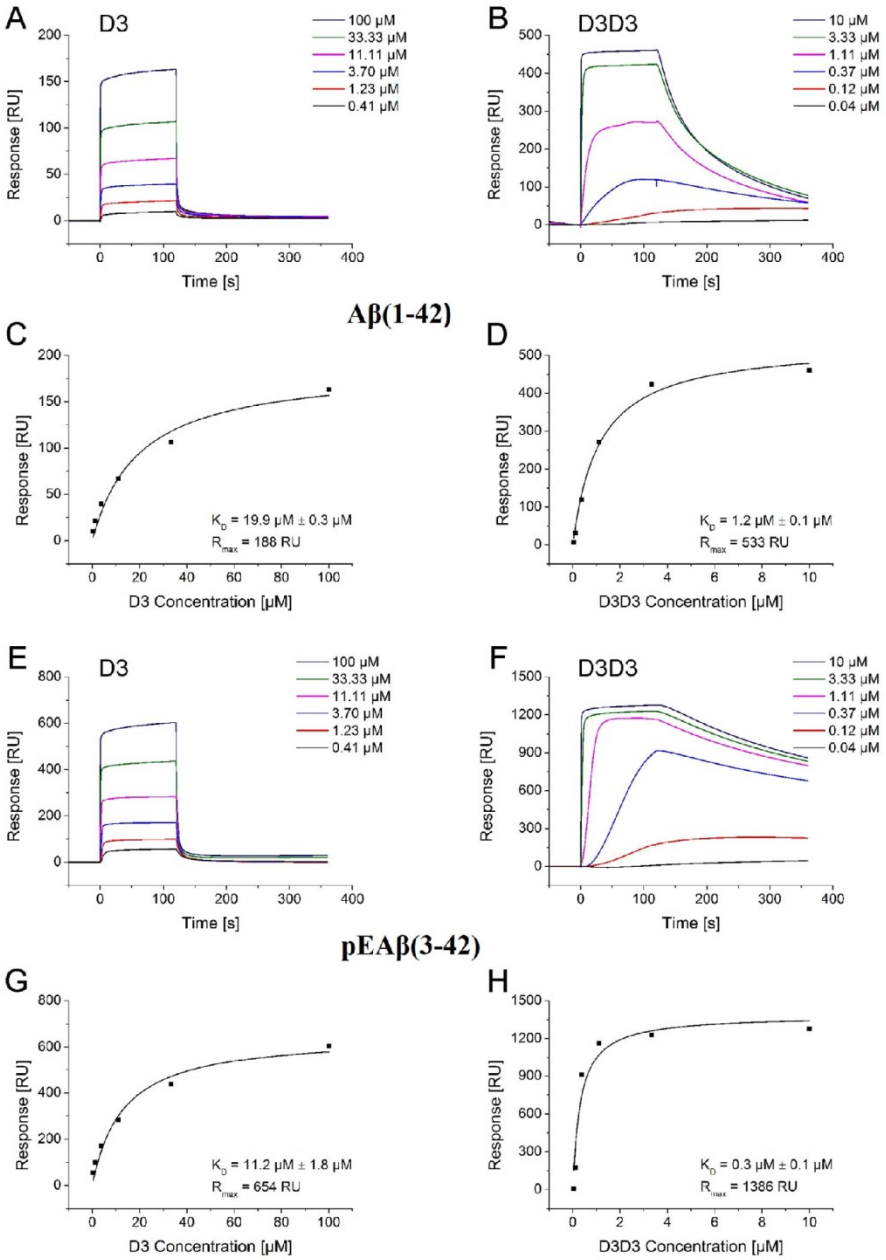

Fig. 1. Affinity determination of D3 and D3D3 to Aβ(1–42) and pEAβ(3–42) by SPR spectroscopy. (A) Sensorgrams of D3 and (B) D3D3 interaction with Aβ(1–42). (C,D) The data were fitted by plotting the response levels (RU) against applied peptide concentrations using a steady-state 1:1 binding model. Sensorgrams of (E) D3 and (F) D3D3 interaction with pEAβ(3–42) and corresponding fit results (G,H). K_D values are represented as mean with SD of two independent measurements. Representative sensorgrams and fits are shown for both measurements.

affinity to the target Aβ due to increased avidity. To validate this in vitro, equilibrium dissociation constants (K_D) of both peptides for Aβ(1–42) and pEAβ(3–42) were determined under the same assay conditions and compared with each other. As expected, D3D3 showed a higher binding affinity than D3 as indicated by lower K_D values (Fig. 1) which might be associated to increased avidity. For D3, the affinities for both Aβ species, Aβ(3–42) and pEAβ(3–42), were similar to each other with slightly higher binding affinities of D3 and D3D3 for pEAβ(3–42) as compared to Aβ(1–42) (Fig. 1).

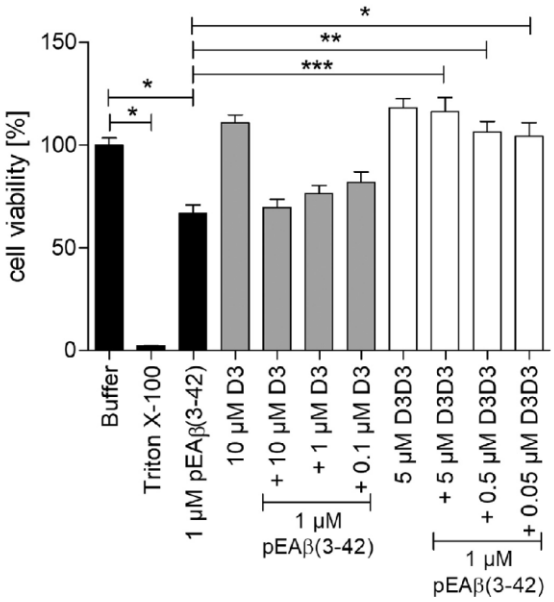

Fig. 2. MTT analysis of the interactions between D3 and D3D3 with pEAβ(3–42). MTT analysis revealed a reduced cell viability upon addition of 1 µM pEAβ(3–42). This was reversed by treatment with D3D3. Data is presented as mean with SEM; $^{*}p \leq 0.05$, $^{**}p \leq 0.01$ and $^{***}p \leq 0.001$.

3.2. Inhibition of pEAβ(3–42) mediated toxicity by D3 and D3D3

Encouraged by the binding experiments to pEAβ(3–42), we then compared the abilities of D3 and D3D3 to neutralize the cytotoxicity of recombinant pEAβ(3–42) in PC-12 cells (Fig. 2). Already a concentration of 1 µM recombinant pEAβ(3–42) reduced the cell viability by > 30% (15 measurements per treatment in 3 tests; Kruskal-Wallis test, $p \leq 0.0001$, post hoc Buffer vs. 1 µM pEAβ(3–42)). Treatment with D3 had no significant influence on this effect (post hoc 1 µM pEAβ(3–42) vs. D3 at any concentration, not significant (ns)), although this does not mean that D3 when applied at higher concentrations would not have rescued the pEAβ(3–42) mediated reduction of cell viability. However, the addition of D3D3 at concentrations of 0.05 µM or higher resulted in a significant rescue of cell viability (post hoc 1 µM pEAβ(3–42) vs. addition of 5 µM D3D3 $p \leq 0.001$, 1 µM pEAβ(3–42) vs. addition of 0.5 µM D3D3 $p \leq 0.01$, 1 µM pEAβ(3–42) vs. addition of 0.05 µM D3D3 $p \leq 0.05$).

Thus, as expected, the increased avidity of D3D3 over D3 led to superior efficacy of D3D3 in vitro (Brener et al., 2015).

3.3. Characterisation of the motor phenotype of TBA2.1 mice

Based on the results of the SPR and cytotoxicity experiments, it was our aim to prove our hypothesis in vivo by treatment of homozygous TBA2.1 mice with D3 and D3D3 against placebo. Accordingly, we determined the motor performance and overall phenotype of transgenic TBA2.1 mice. Subsequently, we treated homozygous mice with either D3 or D3D3 for four weeks.

We characterised the motor neurodegenerative phenotype of this mouse model longitudinally using wild type (WT) and homozygous (HOM) TBA2.1 mice up to five months of age. Phenotype assessment revealed HOM TBA2.1 mice to have a significant phenotype by the age of two months (Fig. 3). Scored observations revealed HOM TBA 2.1 mice to have severely impaired sensorimotor function, which in conjunction with other deficits, rapidly resulted in a hunched body posture, wobbly and rigid gait. By two months of age HOM TBA2.1 mice had four times the score of wild type littermates, a disparity that continued to increase with time, becoming ten times greater at five months (number of animals: 10 WT and 11 HOM; Repeated-Measures-Parametric Analyses, genotype ($F_{(2,25)} = 59.01$, $p \leq 0.001$), interaction genotype with age ($F_{(6,75)} = 20.30$, $p \leq 0.001$), pairwise tests WT vs. HOM $p \leq 0.001$ at all ages, Fig. 3A). In addition, the weight gain from two to five months of age differed significantly between the groups (number of animals: 10 WT and 11 HOM; Repeated-Measures-Parametric Analyses, weight ($F_{(3,75)} = 136.19$, $p \leq 0.001$), interaction genotype with age ($F_{(6,75)} = 4.88$, $p \leq 0.001$)). More precisely, the body weight of WT TBA2.1 mice increased successively up to five months of age (pairwise tests $p \leq 0.01$), whereas in HOM TBA2.1 significant weight gain was only observed up to the fourth month of age (pairwise tests of two to four months old HOM $p \leq 0.05$ and pairwise test four to five months HOM ns) (Fig. 3C).

Analysis of the motor coordination of HOM TBA2.1 mice showed a significant deficit beginning at the age of three months which remained for all subsequent time points tested (number of animals: 10 WT and 11 HOM; Repeated-Measures-Parametric Analyses, genotype ($F_{(2,25)} = 3.59$ and $p = 0.043$), pairwise WT vs. HOM at two months ns and at three to five months $p \leq 0.05$) (Fig. 3B). Overall, these results indicated the rapid progression of the phenotype in HOM TBA2.1 mice from two to five months of age.

3.4. Treatment with D3 and D3D3

Since the motor neurodegenerative phenotype of male HOM TBA2.1 mice was highly prominent at five months of age we decided to start the treatment at four months of age over four weeks to test the truly therapeutic rather than preventive power of D3 and D3D3. Before treating female HOM and WT TBA2.1 mice, all mice were stratified into groups according to their SHIRPA score in the phenotype assessment test. Comparing the scores of WT (1.4 ± 0.22) and HOM (12.2 ± 0.71) mice clearly demonstrated that female HOM mice also developed a severe phenotype with the same baseline as the males. When comparing the outcome of the motor performance before and after treatment of female HOM TBA2.1 mice, the motor balance of placebo treated mice decreased (number of treated animals: placebo 7, D3 8, D3D3 8; Repeated-Measures-Parametric Analyses, before vs. after ($F_{(1,20)} = 2.76$, $p = 0.1122$, pairwise tests before vs. after treatment $p \leq 0.05$), indicating a progression of the phenotype over the four weeks treatment period. In contrast, treatment with D3 or D3D3 inhibited the worsening of the Rotarod performance of HOM TBA2.1 mice (Fig. 4A, pairwise tests before vs. after treatment ns). Of note, the rate of progression is the decisive factor in this model, since the phenotype can only be delayed or ideally stopped but not be reversed. Analysis of the pEAβ(3–42) concentration in the brain of HOM TBA2.1 mice showed an increase in DEA-soluble pEAβ(3–42) after the administration of D3D3 in contrast to the placebo and D3 treated groups (Fig. 4C, number of analysed samples: placebo 7, D3 8; D3D3 8; One-Way-ANOVA $p = 0.0055$, post hoc analysis placebo vs. D3 ns, placebo vs. D3D3 $p \leq 0.05$), while no significant differences were detectable between the insoluble fractions of the three groups (Fig. 4D; number of analysed samples: placebo 7, D3 8; D3D3 8; Kruskal-Wallis test $p = 0.9253$; post hoc analysis ns). The latter was confirmed by quantification of Aβ immunostaining in different brain areas in which Aβ aggregates were found (Fig. 5; 6 slices per animal, number of analysed animals: placebo 4, D3 4, D3D3 5; total brain, One-Way-ANOVA $p = 0.18$; striatum, Kruskal-Wallis test $p = 0.67$; CA1, Kruskal-Wallis test $p = 0.34$; midbrain, One-Way-ANOVA $p = 0.21$; post hoc placebo vs. D3 or D3D3 ns). To evaluate the incidence of hippocampal neurodegeneration (neuron loss and gliosis), cell nuclei and activated astrocytes in the CA1 region of D3, D3D3 and placebo-treated HOM TBA2.1 mice were stained. Quantification of stainings revealed an increasing

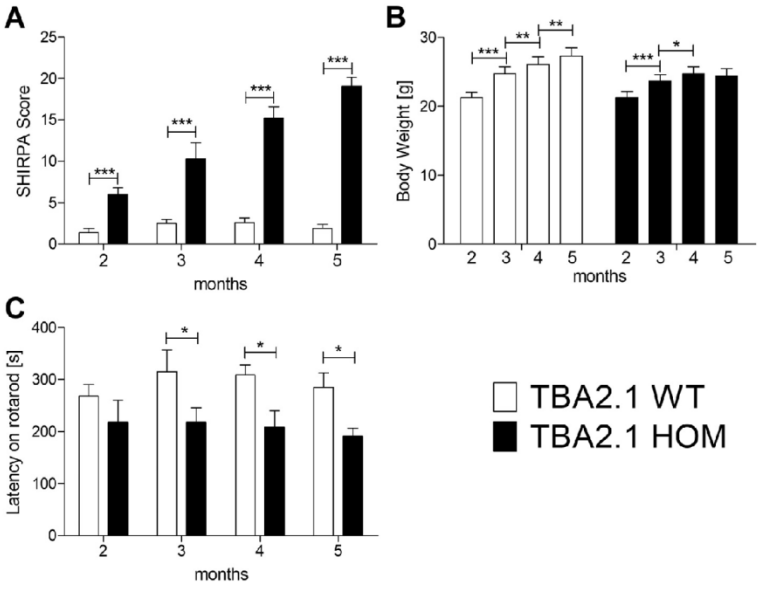

Fig. 3. Longitudinal determination of the sensorimotor phenotype of wild type (WT) and homozygous (HOM) TBA2.1 mice at 2, 3, 4 and 5 months of age. (A) Assessment using the SHIRPA test battery revealed the continuously increasing phenotype of HOM TBA2.1 mice. (B) Body weight of WT mice increased from two to five months of age, but weight gain of HOM was stable from four to five months of age. (C) Between three and five months of age the Rotarod motor performance of HOM mice was reduced when compared to control. Data are presented as mean with SEM; *p < 0.05, **p < 0.01 and ***p < 0.001.

trend in the DAPI count and a decreasing trend in GFAP positive astrocytes of D3 or D3D3 treated animals in comparison to placebo animals, although quantification revealed no significant differences (Fig. 6; 5 to 6 slices per animal, number of analysed animals: placebo 4, D3 3, D3D3 5; GFAP: Kruskal-Wallis test, $p = 0.3953$, post hoc placebo vs.D3 or D3D3 ns and DAPI: Kruskal-Wallis test, $p = 0.0867$, post hoc placebo vs. D3 or D3D3 ns).

Additionally, WT TBA2.1 mice were treated with D3 or D3D3 to exclude unrelated effects of the compounds. No differences between these groups could be observed in the Rotarod test, indicating the effects of D3 and D3D3 were restricted to HOM TBA2.1 mice (Fig. 4B, number of treated animals: placebo 6, D3 7, D3D3 7; Friedman test $p = 0.1667$, post hoc analysis ns).

Overall, both D3 and D3D3 were able to inhibit the deterioration of the motor neuronal degenerative phenotype in HOM TBA2.1, and D3D3 was able to induce a concentration shift towards the DEA-soluble pEAβ(3–42) pool.

4. Discussion

The D-enantiomeric peptide D3 has been shown to be a promising lead compound for the treatment of AD. D3 was originally developed as an Aβ(1–42) monomer stabilizing ligand in order to destabilize and eliminate Aβ oligomers, which are thought to be the most toxic Aβ species and decisive for development and progression of AD. In vitro tests with D3 showed its potential to eliminate toxic Aβ(1–42) oligomers (Funke et al., 2010). The potential of D3 was further proven by inhibition of Aβ(1–42) toxicity in cell culture, the improvement of

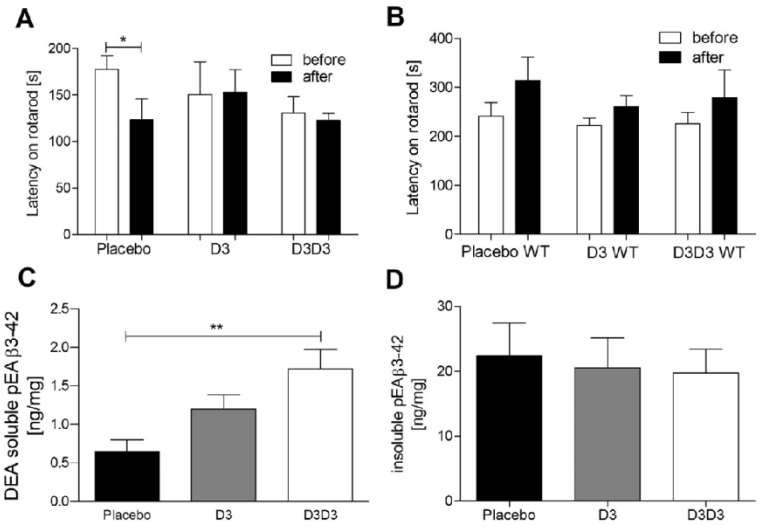

Fig. 4. Treatment of homozygous TBA2.1 mice with the D-enantiomeric peptides D3 and D3D3. Homozygous TBA2.1 (HOM) and wild-type (WT) mice were treated intraperitoneally over four weeks with vehicle (placebo) or with 5 mg per kg body weight D3 or D3D3 per day. Rotarod analysis of HOM demonstrates a worsening of the motor phenotype in placebo-treated mice whereas D3 and D3D3 administration inhibited this process. (A) Data before and after treatment per HOM mouse are shown. (B) The Rotarod performance of WT mice before and after treatment is illustrated. (C) Biochemical quantification of DEA-soluble pEAβ(3–42) in the brain of HOM revealed a significantly higher concentration in D3D3 compared to placebo treated mice. (D) Quantification of insoluble pEAβ(3–42) from the brains of HOM animals is unchanged between treatment groups. Data are presented as mean with SEM (B, C, D); *p ≤ 0.05, **p ≤ 0.01 and ***p ≤ 0.001.

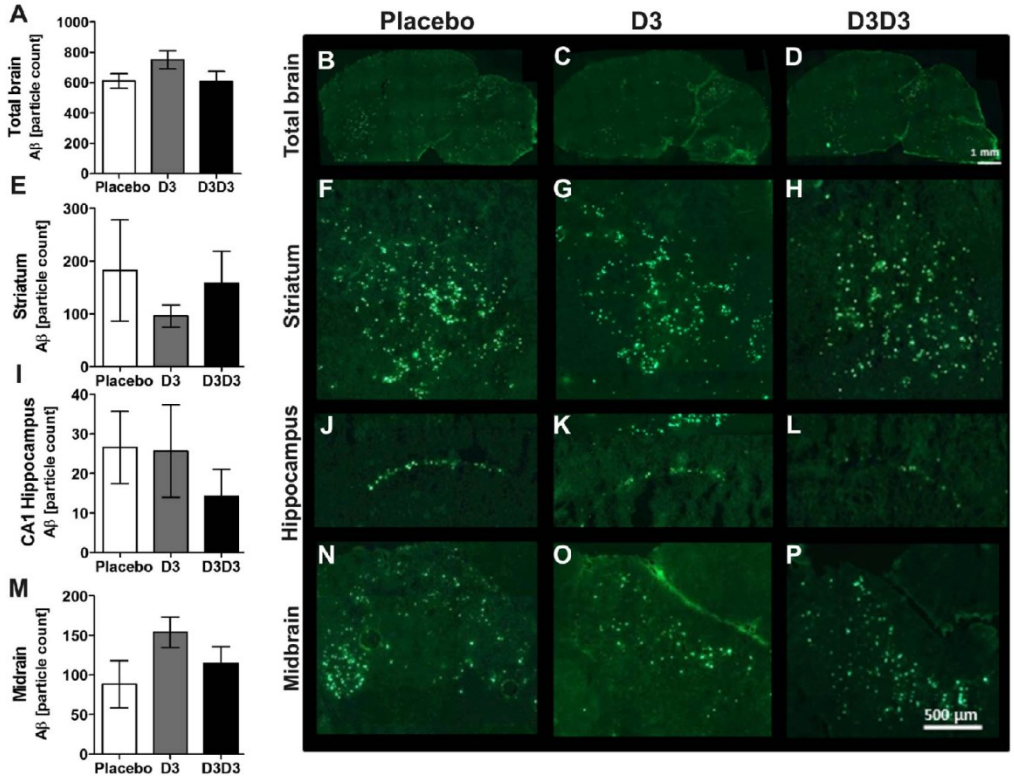

Fig. 5. Aβ immunofluorescence staining and quantification of homozygous mice treated with D3 or D3D3. After treatment, hemispheres of D3, D3D3 or placebo-treated homozygous TBA2.1 mice were harvested. Brain slices of each group were stained against Aβ (antibody 6E10). Immunofluorescence figures show the whole brain hemispheres (B–D), the striatum (F–H), the hippocampus (J–L) or midbrain (N–P) of placebo, D3 and D3D3 treated mice. Quantification of the Aβ particle count in the whole hemisphere (A), striatum (E), CA1 region of the hippocampus (I) or midbrain (M) revealed no significant differences between these groups. Data are presented as mean with SEM. Bars indicating length in (D) and (P) are representative for pictures (B–D) and (F–P), respectively.

spatial learning behaviour and the reduction of the Aβ plaque load in APP/PS1 double transgenic mice (van Groen et al., 2008; Funke et al., 2010). D3D3 was rationally designed to yield a di-valent version of D3 with increased avidity and hence increased affinity to its Aβ target species. In the present study, we have for the first time validated the higher binding affinity of the derivative D3D3 to Aβ(1–42) in comparison to D3. Furthermore, we were able to show that both peptides, and especially D3D3, show increased binding affinity to pEAβ(3–42) as compared to Aβ(1–42). We evaluated the inhibition potentials of both compounds against pEAβ(3–42) mediated toxicity in PC12 cells. Low concentrations of pEAβ(3–42) reduced cell viability, an effect blocked by minute amounts of D3D3. In contrast, D3 was unable to significantly improve cell viability at any of the concentrations tested. To validate the potentials of D3 and D3D3 in vivo, we analysed the therapeutic efficacies in the new mouse model, TBA2.1, which exhibits a motor neurodegenerative phenotype induced by the expression of human pEAβ(3–42).

From two months of age the progression of the phenotype influencing posture, gait and motor function of TBA2.1 mice was severe. Additionally, from the age of three months these mice displayed impaired motor coordination. In contrast, WT TBA2.1 mice failed to display any abnormalities over the entire period of observation. These results are in agreement with previously published observations (Alexandru et al., 2011) and confirm the strong motor neurodegenerative phenotype of HOM TBA2.1 mice.

Treatment studies with D3 or D3D3 in diseased HOM TBA2.1 over a period of four weeks with a daily dosage of 5 mg per kg of body weight showed that both compounds have strong therapeutic potential. Both compounds were able to stabilise the motor coordination of the HOM TBA 2.1 mice and to reduce phenotype progression to non-significant levels during the treatment period. In contrast, placebo-treated mice showed significant progression of their phenotype during that time. In addition, WT mice demonstrated no adverse effects caused by the treatment, which confirmed the effects of D3 and D3D3 were specific to HOM TBA2.1 mice. These findings suggest these D-enantiomeric proteins have a specific therapeutic effect against the pEAβ(3–42) induced neurodegenerative phenotype as they halted disease progression, maintaining performance to that observed at the beginning of treatment. This conclusion is also supported by Brener et al., 2015 showing D3D3 was able to delay the overall behaviour and sensorimotor progression in homozygous TBA mice. In contrast to the present report, in which both D3 and D3D3 stopped progression of the motor deficit as measured by the Rotarod test, Brener et al., 2015 demonstrated that the SIIIRPA assay was able to distinguish the efficiencies of D3D3 and D3 in slowing down the progression of the motor neurodegenerative phenotype. Although this observation is in line with results of the present study demonstrating higher in vitro efficiency of D3D3 over D3, one has to keep in mind that in vitro results do not necessarily directly translate to respective in vivo efficiencies due to potentially different pharmacokinetic properties of the respective compounds. Also, the repeated Rotarod measurements for assessment of motor performance might be less sensitive than the SIIIRPA derived judgements due to training

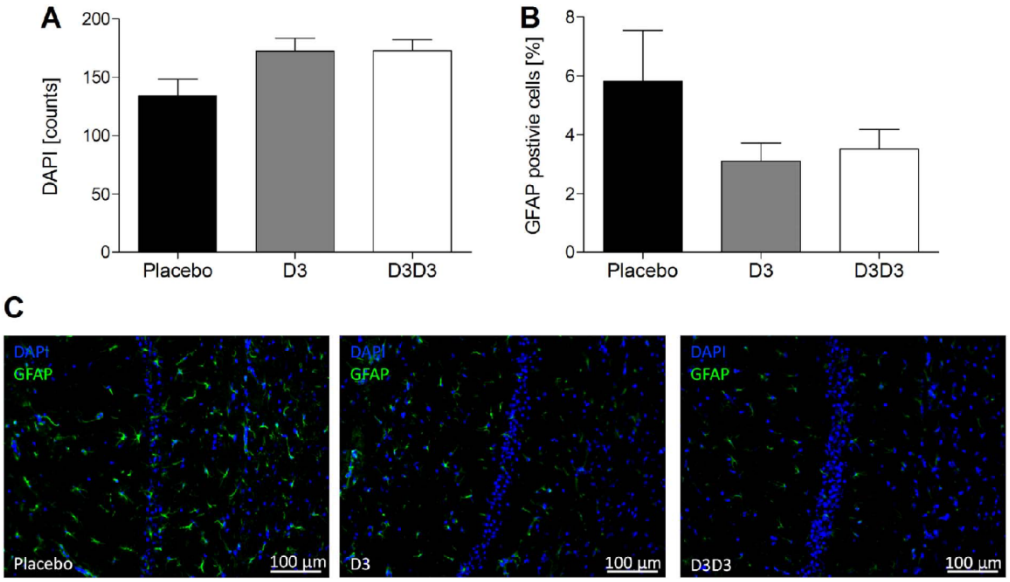

Fig. 6. DAPI and GFAP immunofluorescence stainings of homozygous mice treated with D3 and D3D3. Brain sections of D3, D3D3 or placebo-treated homozygous mice were stained for activated astrocytes with antibodies raised against GFAP and nuclei were counter stained by DAPI. DAPI positive nuclei (A) and activated astrocytes (B) were quantified in the CA1 region of the hippocampus. (C) CA1 region of merged DAPI and GFAP stainings after treatment with D3, D3D3 or placebo-treated homozygous mice. (A, B) Data are presented as mean with SEM.

effects inherently connected to the Rotarod assay. Also, by trend neuron loss was improved and correspondingly gliosis reduced in D3 and D3D3 treated HOM mice. Although statistical analyses revealed no significance of the quantification, this was most probably due to the low number of samples, which were left for this analysis. Nevertheless, it supports the hypothesis that D3 and D3D3 seem to interfere with hippocampal neurodegeneration. Besides neuronal toxicity, it is well known that oligomeric species of Aβ also interfere with neuronal function. Disturbances of synaptic transmission, either pre- or postsynaptically, synaptic loss and inhibition of synaptic plasticity via modulation of neurotransmitter receptors are discussed, which are all independent of neuronal toxicity and neuronal death (Carrillo-Mora et al., 2014). These synaptotoxic effects may also act via, or in conjunction with Tau. Recently, it was reported that oligomeric Tau exerts selective synaptotoxicity without affecting cell viability (Kaniyappan et al., 2017), and combination of oligomeric Aβ and Tau species have been shown to impair long-term-potentiation and memory (Fa et al., 2016). Thus, by reducing oligomeric Aβ D3 and D3D3 could mediate a therapeutic effect and halt in phenotype progression of TBA2.1 mice even without interfering with neurodegeneration.

The development of a disease-modifying or even curative treatment for AD is one the biggest challenges of 21st century medicine, but unfortunately most of the potential compounds that are chosen for clinical research fail. One potential reason for this is that most of the animal models used for preclinical research do not show neurodegeneration. Here we use the TBA2.1 mouse – a model exhibiting a dramatically increasing motor neurodegenerative phenotype. The principle aim of the present study was to investigate the truly therapeutic potentials of the fully D-enantiomeric peptides D3 and its derivative D3D3 in this neurodegenerative animal model. In this respect, reversal of cerebral damage and increase of motor performance cannot be expected by this kind of treatment as the animals used suffer already from distinct neurodegeneration in the brain by this age (Alexandru et al., 2011). Instead, any halt of phenotype progression has to be regarded as a treatment success. In particular, we show that the pEAβ(3–42) induced neurodegenerative phenotype of TBA2.1 mice can not only be inhibited by a preventive treatment, but arrested by a truly therapeutic treatment with D3 and D3D3, most probably by direct action against pEAβ(3–42) assemblies, e.g. pEAβ(3–42) oligomers.

Earlier in vitro studies demonstrated that these D-enantiomeric peptides are capable of binding Aβ species and convert them into non-toxic, non-fibrillar forms (Funke et al., 2010; Brener et al., 2015). In vivo, using mouse models that produce mainly Aβ(1–40) and Aβ(1–42), and develop a plaque pathology comparable to AD patients, a reduction of the Aβ load was observed after several weeks of treatment with D3 (van Groen et al., 2008; Funke et al., 2010). The exact mechanism of action in vivo has not been unraveled yet. However, all experimental data collected so far suggests the following hypothesis: By binding of D3 to Aβ monomers and oligomers the chemical equilibrium is shifted away from fibrillary species which is obviously able to result in a reduction of existing, or in prevention of newly formed plaques. In the present study, the used mouse model TBA2.1 produces aggregates consistent of Aβ and pEAβ(3–42) (Alexandru et al., 2011). Not much information is available about the chemical equilibrium of aggregates containing pEAβ(3–42), but it has been shown that those aggregates are more stable (Dammers et al., 2017). In consequence, D3 and D3D3 can probably not be expected to dissolve already formed pEAβ(3–42) aggregates or significantly prevent their formation within the short treatment window used here. Instead, we hypothesize a mechanism by which toxic oligomeric species are reduced by binding to D3 or D3D3, as has been shown for Aβ(1–42) in vitro (Brener et al., 2015). In line with our in vitro data on cell viability presented here, this may prevent neuronal cell death also in vivo resulting in the observed halt in phenotype progression in TBA2.1 mice.

We have observed a significant increase of pEAβ(3–42) in the DEA-soluble fraction upon treatment with D3D3 and a trend upon D3 treatment in the HOM TBA2.1 mice. It is not absolutely clear which Aβ species are located in the DEA fraction. Since DEA solubilizes protein complexes, one could speculate that complexes between pEAβ(3–42) and D3D3 or D3 are enriched in this fraction, which would also support our working hypothesis of shifted equilibriums, as outlined above. However, so far it is not clear whether the observed increase in the DEA

fraction is therapeutically relevant and actually does correlate with the delay in phenotype progression observed in the mice. In any case it could be a hint of target engagement by D3D3 in vivo.

TBA2.1 mice expressing pEAβ(3–42) is a very potent model delivering a highly interesting drug target. But to date, only a few compounds have been identified as targeting pEAβ(3–42). The main effects of these compounds were reducing the plaques and/or Aβ species using either active (e.g. pGlu-3 mimotope, (Schneeberger et al., 2009)) or passive immunisation (e.g. 9D5 (Wirths et al., 2010), or NT4X (Antonios et al., 2015)) in different mouse models of amyloidosis. To our knowledge these data are mostly lacking behavioural analyses or functional benefits or show preventive rather than therapeutic effects (Frost et al., 2015). Moreover, there are several challenges to overcome with these immunogenic strategies. For example, passive immunisation is deficient in bridging the blood brain barrier, which is essential to have substantial effects. The risk of active immunisation is that the immune system of AD patients might not be capable enough for the patients´ benefit. Additionally, the probability of upcoming adverse events has to be discussed (Cynis et al., 2016). Comparing these challenges to the present study, D-enantiomeric peptides are less immunogenic than L-enantiomers which seems to be an advantage (Funke and Willbold, 2012). Moreover, it is already known that D-enantiomeric peptides like D3 are passing the blood brain barrier (Jiang et al., 2015; Jiang et al., 2016). Additionally, pharmacokinetic studies showed high biological stability, long plasma half-lives and constant levels of D3 and D3D3 in the target organ brain (Jiang et al., 2015; Leithold et al., 2016).

In conclusion, D3 and D3D3 represent a potentially interesting new class of compounds with promising properties to cope with the challenge of treating Alzheimer's disease.

Funding sources

Financial support of D.W. was provided by "Portfolio Technology and Medicine", the Helmholtz-Validierungsfonds of the Impuls and Vernetzungs-Fonds der Helmholtzgemeinschaft. D.W. and K.-J.L. were supported by the "Portfolio Drug Research" of the Impuls and Vernetzungs-Fonds der Helmholtzgemeinschaft. TD was associated fellow of the graduate school "Molecules of Infection".

Conflict of interests

None.

Acknowledgements

The first breeding pairs of TBA2.1 mice were a generous gift by Probiodrug AG. We thank Elke Butzküven and Verena Graf for excellent technical assistance.

References

Alexandru, A., Jagla, W., Graubner, S., Becker, A., Bäuscher, C., Kohlmann, S., Sedlmeier, R., Raber, K., Cynis, H., Rönicke, R., Reymann, K., Petrasch-Parwez, E., Hartlage-Rübsamen, M., Waniek, A., Rossner, S., Schilling, S., Osmand, A., Demuth, H.-U., von Hörsten, S., 2011. Selective hippocampal neurodegeneration in transgenic mice expressing small amounts of truncated Aβ is induced by pyroglutamate-Aβ formation. J. Neurosci. 31 (36), 12790–12801.

Antonios, G., Borgers, H., Richard, B.C., Brauss, A., Meissner, J., Weggen, S., Pena, V., Pillot, T., Davies, S.L., Bakrania, P., Matthews, D., Brownlees, J., Bouter, Y., Bayer, T.A., 2015. Alzheimer therapy with an antibody against N-terminal Abeta 4-X and pyroglutamate Abeta 3-X. Sci. Rep. 5, 17338.

Bateman, R., 2015. Alzheimer's disease and other dementias: advances in 2014. Lancet Neurol. 14 (1), 4–6.

Brener, O., Dunkelmann, T., Gremer, L., van Groen, T., Mirecka, E.A., Kadish, I., Willuweit, A., Kutzsche, J., Jürgens, D., Rudolph, S., Tusche, M., Bongen, P., Pietruszka, J., Oesterhelt, F., Langen, K.-J., Demuth, H.-U., Janssen, A., Hoyer, W., Funke, S.A., Nagel-Steger, L., Willbold, D., 2015. QIAD assay for quantitating a compound's efficacy in elimination of toxic Abeta oligomers. Sci. Rep. 5, 13222–13234.

Brookmeyer, R., Johnson, E., Ziegler-Graham, K., Arrighi, H.M., 2007. Forecasting the global burden of Alzheimer's disease. Alzheimers Dement. 3 (3), 186–191.

Carrillo-Mora, P., Luna, R., Colín-Barenque, L., 2014. Amyloid beta: multiple mechanisms of toxicity and only some protective effects? Oxidative Med. Cell. Longev. 2014, 795375.

Clark, R.A., Shoaib, M., Hewitt, K.N., Stanford, S.C., Bate, S.T., 2012. A comparison of InVivoStat with other statistical software packages for analysis of data generated from animal experiments. J. Psychopharmacol. 26 (8), 1136–1142.

Cynis, H., Frost, J.L., Crehan, H., Lemere, C.A., 2016. Immunotherapy targeting pyroglutamate-3 Abeta: prospects and challenges. Mol. Neurodegener. 11 (1), 48.

Dammers, C., Gremer, L., Neudecker, P., Demuth, H.U., Schwarten, M., Willbold, D., 2015. Purification and characterization of recombinant N-terminally pyroglutamate-modified amyloid-beta variants and structural analysis by solution NMR spectroscopy. PLoS One 10 (10), e0139710.

Dammers, C., Reiss, K., Gremer, L., Lecher, J., Ziehm, T., Stoldt, M., Schwarten, M., Willbold, D., 2017. Pyroglutamate-modified amyloid-beta(3-42) shows alpha-helical intermediates before amyloid formation. Biophys. J. 112 (8), 1621–1633.

Dintzis, H.M., Symer, D.E., Dintzis, R.Z., Zawadzke, L.E., Berg, J.M., 1993. A comparison of the immunogenicity of a pair of enantiomeric proteins. Proteins 16 (3), 306–308.

Fa, M., Puzzo, D., Piacentini, R., Staniszewski, A., Zhang, H., Baltrons, M.A., Li Puma, D.D., Chatterjee, I., Li, J., Saeed, F., Berman, H.L., Ripoli, C., Gulisano, W., Gonzalez, J., Tian, H., Costa, J.A., Lopez, P., Davidowitz, E., Yu, W.H., Haroutunian, V., Brown, L.M., Palmeri, A., Sigurdsson, E.M., Duff, K.E., Teich, A.F., Honig, L.S., Sierks, M., Mce, J.G., D'Adamio, L., Grassi, C., Kanaan, N.M., Fraser, P.E., Arancio, O., 2016. Extracellular tau oligomers produce an immediate impairment of LTP and memory. Sci. Rep. 6, 19393.

Finder, V.H., Glockshuber, R., 2007. Amyloid-beta aggregation. Neurodegener. Dis. 4 (1), 13–27.

Frost, J.L., Liu, B., Rahfeld, J.U., Kleinschmidt, M., O'Nuallain, B., Le, K.X., Lues, I., Caldarone, B.J., Schilling, S., Demuth, H.U., Lemere, C.A., 2015. An anti-pyroglutamate-3 Abeta vaccine reduces plaques and improves cognition in APPswe/PS1DeltaE9 mice. Neurobiol. Aging 36 (12), 3187–3199.

Funke, S.A., Willbold, D., 2009. Mirror image phage display—a method to generate D-peptide ligands for use in diagnostic or therapeutical applications. Mol. BioSyst. 5 (8), 783–786.

Funke, S.A., Willbold, D., 2012. Peptides for therapy and diagnosis of Alzheimer's disease. Curr. Pharm. Des. 18 (6), 755–767.

Funke, S., van Groen, T., Kadish, I., Bartnik, D., Nagel-Steger, L., Brener, O., Sehl, T., Batra-Safferling, R., Moriscot, C., Schoehn, G., Horn, A.H., Muller-Schiffmann, A., Korth, C., Sticht, H., Willbold, D., 2010. Oral treatment with the D-enantiomeric peptide D3 improves the pathology and behavior of Alzheimer's disease transgenic mice. ACS Chem. Neurosci. 1 (9), 639–648.

van Groen, T., Wiesehan, K., Funke, S.A., Kadish, I., Nagel-Steger, L., Willbold, D., 2008. Reduction of Alzheimer's disease amyloid plaque load in transgenic mice by D3, A D-enantiomeric peptide identified by mirror image phage display. ChemMedChem 3 (12), 1848–1852.

van Groen, T., Kadish, I., Funke, S.A., Bartnik, D., Willbold, D., 2013. Treatment with D3 removes amyloid deposits, reduces inflammation, and improves cognition in aged AbetaPP/PS1 double transgenic mice. J. Alzheimers Dis. 34 (3), 609–620.

Harigaya, Y., Saido, T.C., Eckman, C.B., Prada, C.M., Shoji, M., Younkin, S.G., 2000. Amyloid beta protein starting pyroglutamate at position 3 is a major component of the amyloid deposits in the Alzheimer's disease brain. Biochem. Biophys. Res. Commun. 276 (2), 422–427.

Jawhar, S., Wirths, O., Bayer, T.A., 2011. Pyroglutamate amyloid-beta (Abeta): a hatchet man in Alzheimer disease. J. Biol. Chem. 286 (45), 38825–38832.

Jiang, N., Leithold, L.H., Post, J., Ziehm, T., Mauler, J., Gremer, L., Cremer, M., Schartmann, E., Shah, N.J., Kutzsche, J., Langen, K.J., Breitkreutz, J., Willbold, D., Willuweit, A., 2015. Preclinical pharmacokinetic studies of the tritium labelled D-enantiomeric peptide D3 developed for the treatment of Alzheimer s disease. PLoS One 10 (6), e0128553.

Jiang, N., Frenzel, D., Schartmann, E., van Groen, T., Kadish, I., Shah, N.J., Langen, K.J., Willbold, D., Willuweit, A., 2016. Blood-brain barrier penetration of an Abeta-targeted, arginine-rich, D-enantiomeric peptide. Biochim. Biophys. Acta 1858 (11), 2717–2724.

Kaniyappan, S., Chandupatla, R.R., Mandelkow, E.M., Mandelkow, E., 2017. Extracellular low-n oligomers of tau cause selective synaptotoxicity without affecting cell viability. Alzheimers Dement. 13 (11), 1270–1291.

Leithold, L.H., Jiang, N., Post, J., Niemietz, N., Schartmann, E., Ziehm, T., Kutzsche, J., Shah, N.J., Breitkreutz, J., Langen, K.J., Willuweit, A., Willbold, D., 2016. Pharmacokinetic properties of tandem d-peptides designed for treatment of Alzheimer's disease. Eur. J. Pharm. Sci. 89, 31–38.

Parihar, M.S., Hemnani, T., 2004. Alzheimer's disease pathogenesis and therapeutic interventions. J. Clin. Neurosci. 11 (5), 456–467.

Rogers, D.C., Fisher, E.M., Brown, S.D., Peters, J., Hunter, A.J., Martin, J.E., 1997. Behavioral and functional analysis of mouse phenotype: SHIRPA, a proposed protocol for comprehensive phenotype assessment. Mamm. Genome 8 (10), 711–713.

Schneeberger, A., Mandler, M., Otawa, O., Zauner, W., Mattner, F., Schmidt, W., 2009. Development of AFFITOPE vaccines for Alzheimer's disease (AD)—from concept to clinical testing. J. Nutr. Health Aging 13 (3), 264–267.

Schumacher, T.N., Mayr, L.M., Minor Jr., D.L., Milhollen, M.A., Burgess, M.W., Kim, P.S., 1996. Identification of D-peptide ligands through mirror-image phage display. Science 271 (5257), 1854–1857.

Soto, C., Kindy, M.S., Baumann, M., Frangione, B., 1996. Inhibition of Alzheimer's amyloidosis by peptides that prevent beta-sheet conformation. Biochem. Biophys. Res. Commun. 226 (3), 672–680.

Wiesehan, K., Willbold, D., 2003. Mirror-image phage display: aiming at the mirror. Chembiochem 4 (9), 811–815.

Wirths, O., Erck, C., Martens, H., Harmeier, A., Geumann, C., Jawhar, S., Kumar, S., Multhaup, G., Walter, J., Ingelsson, M., Degerman-Gunnarsson, M., Kalimo, H., Huitinga, I., Lannfelt, L., Bayer, T.A., 2010. Identification of low molecular weight pyroglutamate A{beta} oligomers in Alzheimer disease: a novel tool for therapy and diagnosis. J. Biol. Chem. 285 (53), 41517–41524.

4 Summary and conclusion

AD is a neurodegenerative disorder with progressive loss of memory and cognitive decline as major symptoms. Although the precise etiology remains unclear, aggregation of Aβ has become the fundamental framework of AD (LaFerla et al. 2007). This aggregation process is characterized by monomers, oligomeric precursors which are considered to be the most neurotoxic species and highly ordered, insoluble amyloid fibrils (Cohen et al. 2013). To develop a curative therapy for AD, we hypothesize that stabilization of monomers and sequester them from the aggregation cascade will shift the thermodynamic equilibration away from oligomer generation and simultaneously eliminate pre-formed cytotoxic Aβ oligomers. To validate this strategy, the lead compound D3, a D-peptide, was selected by mirror image phage display and intensively characterized in vitro and in vivo regarding its efficacy and potency as a potential therapeutic for AD (see 1.2.4). These results evidenced that D3 is ready for further fit-for-purpose studies including pre-clinical parameters

In the present study, the pharmacokinetic profile of tritium-labeled D3 was analyzed for different administration routes to study its distribution in vivo and the metabolic stability in ex vivo material. Additionally, plasma protein binding was analyzed in vitro in order to estimate the unbound fraction of compound in plasma.

After validating suitable pre-clinical properties for D3, this lead compound was further optimized regarding its efficacy and potency for AD therapy. Two different strategies, rational and systematic approaches, were applied resulting in various D3 derivatives. Those were characterized in vitro regarding their efficacy to bind Aβ monomers, eliminate oligomers and Aβ-induced cytotoxicity. Additionally, two compounds resulting from peptide microarrays, ANK3 and ANK6, were analyzed in detail regarding their interaction with Aβ in order to gain a better understanding of the molecular mechanism. Kinetics, stoichiometry, epitopes and thermodynamics of complex formation were studied using surface plasmon resonance (SPR). Thereby, the main driving forces of D3 and optimized compounds binding to Aβ were identified.

Due to high prevalence of pEAβ(3-42) in senile plaques of AD patients, this posttranslationally modified Aβ isoform is thought to play an important role in triggering neurodegeneration (Wirths et al. 2009). pEAβ(3-42) is characterizes by increased aggregation propensity as compared to Aβ(1-42) and the resulting assemblies have a stronger cross-seeding potential for other Aβ isoforms (Schilling et al. 2006, D'Arrigo et al.

2009). Therefore, the cross-reactivity of D3 and derivatives for pEAβ(3-42) was further investigated and the suitability of those compounds for pEAβ-directed therapy evaluated.

Certain D3 derivatives derived from rational or systematic optimization strategies were further tested in transgenic AD mice with respect to improvement of neurodegeneration. An overview of investigated compounds involved in this thesis can be found in Table 1.

Table 1 Overview of D3 and its derivatives involved in this thesis. D3 yielded from phage display (PD) and derivatives from either rational design (RD) or systematic peptide microarray (MA) approaches. All compounds were in D-enantiomeric configuration with an amidated C-terminus, if not other stated. Net charge was calculated at neutral pH. Certain ANK compounds contain unnatural amino acid residues. λ, phenylglycine; μ, 4-fluorophenylalanine.

Compound	Source	Sequence	Charge	Comment
D3	PD	rprtrlhthrnr	+6	
$D3_{COOH}$	RD	rprtrlhthrnr	+5	D3 with free C-terminus
cD3	RD	rprtrlhthrnr	+5	head-to-tail cyclization of D3
cD3r	RD	rprtrlhthrnrr	+6	cD3 with additional arginine residue
D3D3	RD	rprtrlhthrnrrprtrlhthrnr	+11	tandem head-to-tail version of D3
DB3	MA	rpitrlrthqnr	+5	
DB3DB3	RD	rpitrlrthqnrrpitrlrthqnr	+9	tandem head-to-tail version of DB3
ANK1	MA	rkrirlvyhinr	+6	
ANK2	MA	rkrirlλyhinr	+6	
ANK3	MA	rkrirlλyhwnr	+6	
ANK4	MA	rkrirlvyhwnr	+6	
ANK5	MA	rkrvrlvyhkkr	+8	
ANK6	MA	rkrirlvtkkkr	+9	
ANK7	MA	rkrvrlμthikr	+7	

4.1 Pre-clinical parameters of D3

The pharmacokinetic profile of tritium-labeled compound revealed high oral bioavailability and long plasma half-lives for D3 which might be based on very high metabolic stability as shown for the D-peptide in comparison to the L-enantiomer. Therefore, D3 exhibits all favorable characteristics of D-peptides which were mentioned in 1.2.1. Furthermore, constant levels of D3 in the target organ brain were detected indicating that D3 can cross the blood brain barrier in vivo.

Binding of D3 to human serum albumin (HSA) and α1-acid glycoprotein (AGP) was analyzed in vitro in order to calculate the unbound fraction in plasma. HSA comprises 40 % of the total plasma proteins and AGP accounts for 1-3 % (Mandic 2012). Therefore, the majority of human plasma proteins are covered by investigating those two proteins. For AGP, a K_D value of 1.8 µM was determined and for HSA, the K_D was over the detection limit of the assay which was 1.4 mM. Therefore, plasma protein binding was mainly affected by AGP binding which was expected since it is known that acidic and lipophilic drugs mainly bind to albumin whereas basic drugs have higher affinity to AGP (Hage et al. 2011). Accounting AGP and HSA binding, the estimated free fraction of D3 in plasma was calculated to be approx. 8% which is typically not considered as high protein binding for drugs (Liu et al. 2014).

4.2 Rational optimization of D3

Due to a high content of positively charged amino acid residues, charge of D3 obviously plays a central role in the mechanism of action. Therefore, the effect of net charge was investigated as an optimization strategy for D3. Furthermore, the well-known tool for peptides optimization, cyclization, was applied to D3 (1.2.2). Indeed, in vitro investigations, i.e. affinity determination to Aβ(1−42), elimination efficacy of cytotoxic oligomers and subsequent neutralization of oligomer-induced cytotoxicity, elucidated that the efficacy of D3 can be already optimized by charge increase. Most probably, the electrostatic driven interaction of D3 with negatively charged residues of Aβ is enhanced by this. Additionally, cyclization implied another optimization step with a similar degree of optimization. By applying both modifications, D3 was successfully upgraded into the superior compound cD3r. Furthermore, the design of multivalent compounds, e.g. bivalent peptides, was emphasized to yield a high grade of optimization. In the study investigating pEAβ-targeting therapy, the K_D values of D3 and D3D3 to non-modified Aβ(1-42) were analyzed. Here, a 16-fold increase in affinity was observed by developing the head-to-tail tandem version. For DB3, this effect was even more pronounced. The K_D values of DB3 and DB3DB3 indicated a 75-fold improvement. Increased affinity of tandem compounds were further linked to increased characteristics such as oligomer elimination efficacy and subsequent rescue of cytotoxicity. Most probably, the high number of positive charged residues results in avidity effects.

4.3 Systematic optimization of D3

Peptide microarrays were proven to be a powerful tool for systematic peptide optimization. Attributed to relatively high throughput, several parameters can be investigated in parallel (1.2.2). We have applied peptide microarrays for systematic optimization of D3 regarding its affinity and specificity to Aβ(1-42) monomers using oligomers and fibrils as counter targets. The most promising derivatives derived from this approach were the seven ANK compounds. As compared to D3, all compounds exhibit higher hydrophobicity and were characterized by enhanced binding affinity, oligomer elimination efficacy and neutralization ability of Aβ-induced cytotoxicity. However, the net charge of the ANK compounds ranges from +6 (as for D3) to +9. Therefore, the influence of charge and hydrophobicity on the interaction with Aβ was investigated in a detailed biophysical study involving ANK3 and ANK6. In comparison to D3, the binding mode changed from a homogeneous interaction with a K_D in the micromolar range to a heterogeneous one with an additional binding mode in the nanomolar range for both compounds. The proportion of this high affinity binding mode correlates with the hydrophobicity. Additionally, an epitope mapping approach showed that this binding mode involves the hydrophobic C-terminus of Aβ which is known to play an important role in the self-assembly process (Colvin et al. 2016, Walti et al. 2016). The Aβ interaction of the more hydrophobic compound ANK3 was characterized by a high resistance to ionic strength (> 1 M) resulting in highly efficient inhibitory function of Aβ aggregation under these conditions. The thermodynamic profiles supported these findings by an increase in entropic contributions. Thus, we concluded that D3 interacted with Aβ via electrostatic interactions only and the hydrophobic contributions of ANK6 interaction were too low to benefit from this. In contrast to this, electrostatic and hydrophobic interactions were both substantially involved in the binding process of ANK3.

4.4 pEAβ-directed therapy with D3 and a derivative

Quantitative K_D determinations revealed a comparable binding affinity of D3 to Aβ(1-42) and pEAβ(3-42) indicating that D3 is characterized by high cross-reactivity. However, the effect of bivalent D3 differed for both isoforms. For Aβ(1-42), affinity increased by factor 16 and this effect was double for pEAβ(3-42). High affinity of D3D3 to pEAβ(3-42) was confirmed by cell viability assays where it was able to completely rescue pEAβ-derived cytotoxicity in a concentration range where D3 showed no significant effects. Thus, D3 but especially D3D3 show a high therapeutic potential for pEAβ-driven neurodegeneration.

4.5 Correlation between in vitro and in vivo outcome

After all, high potential in vitro requires to be validated in vivo. Indeed, certain D3 derivatives were already significantly proven to be therapeutically active in transgenic AD mice. Although various other mechanisms of action might underlay the observed potency, the elimination of Aβ oligomers is one potential mechanism.

Treatment with cD3r yielded spatial cognition and memory improvement in Tg-SwDI mice without changing Aβ plaque load or inflammation markers. Previously, also D3 was shown to improve cognition, reduce Aβ plaque load and inflammation in APP/PS1 mice (1.2.4). The potency of D3 and D3D3 for pEAβ-induced neurodegenerative phenotype was confirmed using the transgenic mouse model TBA2.1. Both compounds D3 and D3D3 were able to stabilize the motor coordination and reduce phenotype progression down to non-significant levels. Thus, D3 and D3D3 were proven to be therapeutically active by stopping pEAβ-driven phenotype progression after treatment. In contrast, ANK6 which is a highly promising candidate regarding its in vitro performance only showed a non-significant tendency for cognitive improvement so far. However, performed in vivo studies cannot be compared with each other regarding their outcome due to various variable parameters. The mentioned studies differed in mouse model, age and gender of mice, dosage, duration and application route of treatment. Thus, each compound can only be assessed qualitatively within one study by comparing compound-treated with placebo-treated animals.

4.6 General conclusion and perspectives

Pre-clinical results validated that D-peptides in general are characterized by favorable characteristics and especially that D3 is a promising candidate for further evaluation. Furthermore, detailed biophysical characterization of the interaction between optimized compounds and their target Aβ(1-42) elucidated that not only charge but also hydrophobicity is a crucial characteristic in the lead optimization process of D3. Additionally, we gained a deeper understanding of the molecular mechanism of interaction in comparison to the original compound D3 regarding kinetics, stoichiometry, epitopes and thermodynamics. This information was crucial and partially associated with potency characteristics such as Aβ oligomer elimination and toxicity neutralization efficacy.

After systematic optimization of D3 leading to highly potent ANK compounds, rational optimization tools such as increase of charge, cyclization and multivalence can be applied Those are readily implemented and might provide high potential to further increase the therapeutic effect since they were already proven to be efficient for D3. For example, a cyclic version of ANK3 might be more potent as compared to the linear one or a heterodimer of ANK3 and ANK6 might combine the positive effects of both compounds. Furthermore, in vivo efficacy and pre-clinical parameters of ANK compounds would be interesting, especially for ANK3 since hydrophobicity is supposed to positively influence ADMET properties resulting in increased chances of success in drug development (Testa et al. 2000, Klebe 2015).

References

Alzheimer's Association (2017). "2017 Alzheimer's disease facts and figures". *Alzheimers Dement* 13: 325-373

Alzheimer A (1907). "Über eine eigenartige Erkrankung der Hirnrinde". *Allgemeine Zeitschrift fur Psychiatrie und Psychisch-gerichtliche Medizin* 64: 146-148

Arai T, Araya T, Sasaki D, Taniguchi A, Sato T, Sohma Y and Kanai M (2014). "Rational design and identification of a non-peptidic aggregation inhibitor of amyloid-beta based on a pharmacophore motif obtained from cyclo[-Lys-Leu-Val-Phe-Phe-]". *Angew Chem Int Ed Engl* 53(31): 8236-8239

Ballard C, Gauthier S, Corbett A, Brayne C, Aarsland D and Jones E (2011). "Alzheimer's disease". *Lancet* 377(9770): 1019-1031

Beach TG, Monsell SE, Phillips LE and Kukull W (2012). "Accuracy of the Clinical Diagnosis of Alzheimer Disease at National Institute on Aging Alzheimer Disease Centers, 2005-2010". *Journal of Neuropathology and Experimental Neurology* 71(4): 266-273

Bekris LM, Yu CE, Bird TD and Tsuang DW (2010). "Genetics of Alzheimer disease". *J Geriatr Psychiatry Neurol* 23(4): 213-227

Beyreuther K and Masters CL (1991). "Amyloid precursor protein (APP) and beta A4 amyloid in the etiology of Alzheimer's disease: precursor-product relationships in the derangement of neuronal function". *Brain Pathol* 1(4): 241-251

Bird TD (1993). "Alzheimer Disease Overview". *GeneReviews*. R. A. Pagon, M. P. Adam, H. H. Ardinger et al. Seattle (WA), last revision: September 2015.

Blennow K, de Leon MJ and Zetterberg H (2006). "Alzheimer's disease". *Lancet* 368(9533): 387-403

Blennow K, Hampel H, Weiner M and Zetterberg H (2010). "Cerebrospinal fluid and plasma biomarkers in Alzheimer disease". *Nature Reviews Neurology* 6(3): 131-144

Blessed G, Tomlinson BE and Roth M (1968). "The association between quantitative measures of dementia and of senile change in the cerebral grey matter of elderly subjects". *Br J Psychiatry* 114(512): 797-811

Brener O, Dunkelmann T, Gremer L, van Groen T, Mirecka EA, Kadish I, Willuweit A, Kutzsche J, Jurgens D, Rudolph S, Tusche M, Bongen P, Pietruszka J, Oesterhelt F, Langen KJ, Demuth HU, Janssen A, Hoyer W, Funke SA, Nagel-Steger L and Willbold D (2015). "QIAD assay for quantitating a compound's efficacy in elimination of toxic Abeta oligomers". *Sci Rep* 5: 13222

Chalifour RJ, McLaughlin RW, Lavoie L, Morissette C, Tremblay N, Boule M, Sarazin P, Stea D, Lacombe D, Tremblay P and Gervais F (2003). "Stereoselective interactions of peptide inhibitors with the beta-amyloid peptide". *Journal of Biological Chemistry* 278(37): 34874-34881

Cohen SI, Arosio P, Presto J, Kurudenkandy FR, Biverstal H, Dolfe L, Dunning C, Yang X, Frohm B, Vendruscolo M, Johansson J, Dobson CM, Fisahn A, Knowles TP and Linse S

(2015). "A molecular chaperone breaks the catalytic cycle that generates toxic Abeta oligomers". *Nat Struct Mol Biol* 22(3): 207-213

Cohen SI, Linse S, Luheshi LM, Hellstrand E, White DA, Rajah L, Otzen DE, Vendruscolo M, Dobson CM and Knowles TP (2013). "Proliferation of amyloid-beta42 aggregates occurs through a secondary nucleation mechanism". *Proc Natl Acad Sci U S A* 110(24): 9758-9763

Colvin MT, Silvers R, Ni QZ, Can TV, Sergeyev I, Rosay M, Donovan KJ, Michael B, Wall J, Linse S and Griffin RG (2016). "Atomic Resolution Structure of Monomorphic Abeta42 Amyloid Fibrils". *J Am Chem Soc* 138(30): 9663-9674

D'Arrigo C, Tabaton M and Perico A (2009). "N-Terminal Truncated Pyroglutamyl beta Amyloid Peptide A beta py3-42 Shows a Faster Aggregation Kinetics than the Full-Length A beta 1-42". *Biopolymers* 91(10): 861-873

Dintzis HM, Symer DE, Dintzis RZ, Zawadzke LE and Berg JM (1993). "A comparison of the immunogenicity of a pair of enantiomeric proteins". *Proteins* 16(3): 306-308

Dubois B, Feldman HH, Jacova C, Dekosky ST, Barberger-Gateau P, Cummings J, Delacourte A, Galasko D, Gauthier S, Jicha G, Meguro K, O'Brien J, Pasquier F, Robert P, Rossor M, Salloway S, Stern Y, Visser PJ and Scheltens P (2007). "Research criteria for the diagnosis of Alzheimer's disease: revising the NINCDS-ADRDA criteria". *Lancet Neurol* 6(8): 734-746

Dubois B, Feldman HH, Jacova C, Hampel H, Molinuevo JL, Blennow K, Dekosky ST, Gauthier S, Selkoe D, Bateman R, Cappa S, Crutch S, Engelborghs S, Frisoni GB, Fox NC, Galasko D, Habert MO, Jicha GA, Nordberg A, Pasquier F, Rabinovici G, Robert P, Rowe C, Salloway S, Sarazin M, Epelbaum S, de Souza LC, Vellas B, Visser PJ, Schneider L, Stern Y, Scheltens P and Cummings JL (2014). "Advancing research diagnostic criteria for Alzheimer's disease: the IWG-2 criteria". *Lancet Neurology* 13(6): 614-629

Duggineni S, Mitra S, Lamberto I, Han X, Xu Y, An J, Pasquale EB and Huang Z (2013). "Design and Synthesis of Potent Bivalent Peptide Agonists Targeting the EphA2 Receptor". *ACS Med Chem Lett* 4(3)

Dunkelmann T, Teichmann K, Ziehm T, Schemmert S, Frenzel D, Tusche M, Dammers C, Jurgens D, Langen KJ, Demuth HU, Shah NJ, Kutzsche J, Willuweit A and Willbold D (2018). "Abeta oligomer eliminating compounds interfere successfully with pEAbeta(3-42) induced motor neurodegenerative phenotype in transgenic mice". *Neuropeptides* 67: 27-35

Edman P (1959). "Chemistry of Amino Acids and Peptides". *Annual Review of Biochemistry* 28: 69-96

Esteras-Chopo A, Pastor MT, Serrano L and de la Paz ML (2008). "New strategy for the generation of specific D-peptide amyloid inhibitors". *Journal of Molecular Biology* 377(5): 1372-1381

Farrer LA, Cupples LA, Haines JL, Hyman B, Kukull WA, Mayeux R, Myers RH, Pericak-Vance MA, Risch N and van Duijn CM (1997). "Effects of age, sex, and ethnicity on the association between apolipoprotein E genotype and Alzheimer disease. A meta-analysis. APOE and Alzheimer Disease Meta Analysis Consortium". *JAMA* 278(16): 1349-1356

Findeis MA, Musso GM, Arico-Muendel CC, Benjamin HW, Hundal AM, Lee JJ, Chin J, Kelley M, Wakefield J, Hayward NJ and Molineaux SM (1999). "Modified-peptide inhibitors of amyloid beta-peptide polymerization". *Biochemistry* 38(21): 6791-6800

Folstein MF, Folstein SE and McHugh PR (1975). ""Mini-mental state". A practical method for grading the cognitive state of patients for the clinician". *J Psychiatr Res* 12(3): 189-198

Francis PT (2005). "The interplay of neurotransmitters in Alzheimer's disease". *CNS Spectr* 10(11 Suppl 18): 6-9

Funke SA, van Groen T, Kadish I, Bartnik D, Nagel-Steger L, Brener O, Sehl T, Batra-Safferling R, Moriscot C, Schoehn G, Horn AH, Muller-Schiffmann A, Korth C, Sticht H and Willbold D (2010). "Oral treatment with the d-enantiomeric peptide D3 improves the pathology and behavior of Alzheimer's Disease transgenic mice". *ACS Chem Neurosci* 1(9): 639-648

Glenner GG and Wong CW (1984). "Alzheimer's disease: initial report of the purification and characterization of a novel cerebrovascular amyloid protein". *Biochem Biophys Res Commun* 120(3): 885-890

Goate A, Chartier-Harlin MC, Mullan M, Brown J, Crawford F, Fidani L, Giuffra L, Haynes A, Irving N, James L and et al. (1991). "Segregation of a missense mutation in the amyloid precursor protein gene with familial Alzheimer's disease". *Nature* 349(6311): 704-706

Golde TE, Schneider LS and Koo EH (2011). "Anti-abeta therapeutics in Alzheimer's disease: the need for a paradigm shift". *Neuron* 69(2): 203-213

Gunn AP, Masters CL and Cherny RA (2010). "Pyroglutamate-A beta: Role in the natural history of Alzheimer's disease". *International Journal of Biochemistry & Cell Biology* 42(12): 1915-1918

Hage DS, Anguizola J, Barnaby O, Jackson A, Yoo MJ, Papastavros E, Pfaunmiller E, Sobansky M and Tong ZH (2011). "Characterization of Drug Interactions with Serum Proteins by Using High-Performance Affinity Chromatography". *Current Drug Metabolism* 12(4): 313-328

Hamamoto K, Kida Y, Zhang Y, Shimizu T and Kuwano K (2002). "Antimicrobial activity and stability to proteolysis of small linear cationic peptides with D-amino acid substitutions". *Microbiology and Immunology* 46(11): 741-749

Hamman JH, Enslin GM and Kotze AF (2005). "Oral delivery of peptide drugs - Barriers and developments". *Biodrugs* 19(3): 165-177

Hardy J and Allsop D (1991). "Amyloid Deposition as the Central Event in the Etiology of Alzheimers-Disease". *Trends in Pharmacological Sciences* 12(10): 383-388

Hardy J and Selkoe DJ (2002). "The amyloid hypothesis of Alzheimer's disease: progress and problems on the road to therapeutics". *Science* 297(5580): 353-356

Horton DA, Bourne GT and Smythe ML (2000). "Exploring privileged structures: The combinatorial synthesis of cyclic peptides". *Molecular Diversity* 5(4): 289-304

Hummel G, Reineke U and Reimer U (2006). "Translating peptides into small molecules". *Mol Biosyst* 2(10): 499-508

Jack CR, Jr., Albert MS, Knopman DS, McKhann GM, Sperling RA, Carrillo MC, Thies B and Phelps CH (2011). "Introduction to the recommendations from the National Institute on Aging-Alzheimer's Association workgroups on diagnostic guidelines for Alzheimer's disease". *Alzheimers Dement* 7(3): 257-262

Joo SH (2012). "Cyclic Peptides as Therapeutic Agents and Biochemical Tools". *Biomolecules & Therapeutics* 20(1): 19-26

Karran E and De Strooper B (2016). "The amyloid cascade hypothesis: are we poised for success or failure?". *Journal of Neurochemistry* 139: 237-252

Khazanov NA and Carlson HA (2013). "Exploring the composition of protein-ligand binding sites on a large scale". *PLoS Comput Biol* 9(11): e1003321

Klebe G (2015). "Applying thermodynamic profiling in lead finding and optimization". *Nat Rev Drug Discov* 14(2): 95-110

Klein AN, Ziehm T, van Groen T, Kadish I, Elfgen A, Tusche M, Thomaier M, Reiss K, Brener O, Gremer L, Kutzsche J and Willbold D (2017). "Optimization of d-Peptides for Abeta Monomer Binding Specificity Enhances Their Potential to Eliminate Toxic Abeta Oligomers". *ACS Chem Neurosci* 8(9): 1889-1900

Klunk WE, Engler H, Nordberg A, Wang YM, Blomqvist G, Holt DP, Bergstrom M, Savitcheva I, Huang GF, Estrada S, Ausen B, Debnath ML, Barletta J, Price JC, Sandell J, Lopresti BJ, Wall A, Koivisto P, Antoni G, Mathis CA and Langstrom B (2004). "Imaging brain amyloid in Alzheimer's disease with Pittsburgh Compound-B". *Annals of Neurology* 55(3): 306-319

Knight MJ, McCann B, Kauppinen RA and Coulthard EJ (2016). "Magnetic Resonance Imaging to Detect Early Molecular and Cellular Changes in Alzheimer's Disease". *Front Aging Neurosci* 8: 139

Kumar J and Sim V (2014). "D-amino acid-based peptide inhibitors as early or preventative therapy in Alzheimer disease". *Prion* 8(1): 119-124

LaFerla FM, Green KN and Oddo S (2007). "Intracellular amyloid-beta in Alzheimer's disease". *Nature Reviews Neuroscience* 8(7): 499-509

Levy-Lahad E, Wasco W, Poorkaj P, Romano DM, Oshima J, Pettingell WH, Yu CE, Jondro PD, Schmidt SD, Wang K and et al. (1995). "Candidate gene for the chromosome 1 familial Alzheimer's disease locus". *Science* 269(5226): 973-977

Lin J, Bardina L, Shreffler WG, Andreae DA, Ge YC, Wang JL, Bruni FM, Fu ZY, Han YS and Sampson HA (2009). "Development of a novel peptide microarray for large-scale epitope mapping of food allergens". *Journal of Allergy and Clinical Immunology* 124(2): 315-322

Liu H, Funke SA and Willbold D (2010). "Transport of Alzheimer disease amyloid-beta-binding D-amino acid peptides across an in vitro blood-brain barrier model". *Rejuvenation Res* 13(2-3): 210-213

Liu XR, Wright M and Hop CECA (2014). "Rational Use of Plasma Protein and Tissue Binding Data in Drug Design". *Journal of Medicinal Chemistry* 57(20): 8238-8248

Liu Y, Lu Z, Mei L, Yu Q, Tai X, Wang Y, Shi K, Zhang Z and He Q (2017). "Tandem Peptide Based on Structural Modification of Poly-Arginine for Enhancing Tumor Targeting Efficiency and Therapeutic Effect". *ACS Appl Mater Interfaces* 9(3): 2083-2092

Lowe TL, Strzelec A, Kiessling LL and Murphy RM (2001). "Structure-function relationships for inhibitors of beta-amyloid toxicity containing the recognition sequence KLVFF". *Biochemistry* 40(26): 7882-7889

Mandic Z (2012). "Physico Chemical Methods in Drug Discovery and Development". *IAPC Publishing*

Marx V (2005). "Watching peptide drugs grow up". *Chemical & Engineering News* 83(11): 17-24

Masters CL, Simms G, Weinman NA, Multhaup G, McDonald BL and Beyreuther K (1985). "Amyloid plaque core protein in Alzheimer disease and Down syndrome". *Proc Natl Acad Sci U S A* 82(12): 4245-4249

Mayeux R (2003). "Epidemiology of neurodegeneration". *Annu Rev Neurosci* 26: 81-104

McKhann GM, Albert MS and Sperling RA (2012). "Changing Diagnostic Concepts of Alzheimer's Disease". *Alzheimer's Disease - Modernizing Concept, Biological Diagnosis and Therapy* 28: 115-121

Mosconi L, Berti V, Glodzik L, Pupi A, De Santi S and de Leon MJ (2010). "Pre-Clinical Detection of Alzheimer's Disease Using FDG-PET, with or without Amyloid Imaging". *Journal of Alzheimers Disease* 20(3): 843-854

Murphy MP and LeVine H (2010). "Alzheimer's Disease and the Amyloid-beta Peptide". *Journal of Alzheimers Disease* 19(1): 311-323

Neuberger A (1948). "Stereochemistry of amino acids". *Adv Protein Chem* 4: 297-383

Newberg A, Alavi A and Reivich M (2002). "Determination of regional cerebral function with FDG-PET imaging in neuropsychiatric disorders". *Semin Nucl Med* 32(1): 13-34

Noetzli M and Eap CB (2013). "Pharmacodynamic, pharmacokinetic and pharmacogenetic aspects of drugs used in the treatment of Alzheimer's disease". *Clin Pharmacokinet* 52(4): 225-241

Olubiyi OO, Frenzel D, Bartnik D, Gluck JM, Brener O, Nagel-Steger L, Funke SA, Willbold D and Strodel B (2014). "Amyloid aggregation inhibitory mechanism of arginine-rich D-peptides". *Curr Med Chem* 21(12): 1448-1457

Olubiyi OO and Strodel B (2012). "Structures of the Amyloid beta-Peptides A beta(1-40) and A beta(1-42) as Influenced by pH and a D-Peptide". *Journal of Physical Chemistry B* 116(10): 3280-3291

Otvos L, Jr. and Wade JD (2014). "Current challenges in peptide-based drug discovery". *Front Chem* 2: 62

Perl DP (2010). "Neuropathology of Alzheimer's Disease". *Mount Sinai Journal of Medicine* 77(1): 32-42

Prince M, Comas-Herrera A, Knapp M, Guerchet M and Karagiannidou M (2016). World Alzheimer Report - Improving healthcare for people living with dementia.

Radkov AD and Moe LA (2014). "Bacterial synthesis of D-amino acids". *Appl Microbiol Biotechnol* 98(12): 5363-5374

Schilling S, Lauber T, Schaupp M, Manhart S, Scheel E, Bohm G and Demuth HU (2006). "On the seeding and oligomerization of pGlu-amyloid peptides (in vitro)". *Biochemistry* 45(41): 12393-12399

Schumacher TNM, Mayr LM, Minor DL, Milhollen MA, Burgess MW and Kim PS (1996). "Identification of D-peptide ligands through mirror-image phage display". *Science* 271(5257): 1854-1857

Selkoe DJ (1991). "The molecular pathology of Alzheimer's disease". *Neuron* 6(4): 487-498

Selkoe DJ (2001). "Alzheimer's disease: Genes, proteins, and therapy". *Physiological Reviews* 81(2): 741-766

Selkoe DJ and Hardy J (2016). "The amyloid hypothesis of Alzheimer's disease at 25 years". *EMBO Mol Med* 8(6): 595-608

Sherrington R, Rogaev EI, Liang Y, Rogaeva EA, Levesque G, Ikeda M, Chi H, Lin C, Li G, Holman K, Tsuda T, Mar L, Foncin JF, Bruni AC, Montesi MP, Sorbi S, Rainero I, Pinessi L, Nee L, Chumakov I, Pollen D, Brookes A, Sanseau P, Polinsky RJ, Wasco W, Da Silva HA, Haines JL, Perkicak-Vance MA, Tanzi RE, Roses AD, Fraser PE, Rommens JM and St George-Hyslop PH (1995). "Cloning of a gene bearing missense mutations in early-onset familial Alzheimer's disease". *Nature* 375(6534): 754-760

Soto C, Kindy MS, Baumann M and Frangione B (1996). "Inhibition of Alzheimer's amyloidosis by peptides that prevent beta-sheet conformation". *Biochemical and Biophysical Research Communications* 226(3): 672-680

Stevens CM, Halpern PE and Gigger RP (1951). "Occurrence of D-amino acids in some natural materials". *J Biol Chem* 190(2): 705-710

Sun N, Funke SA and Willbold D (2012). "A Survey of Peptides with Effective Therapeutic Potential in Alzheimer's Disease Rodent Models or in Human Clinical Studies". *Mini-Reviews in Medicinal Chemistry* 12(5): 388-398

Testa B, Crivori P, Reist M and Carrupt PA (2000). "The influence of lipophilicity on the pharmacokinetic behavior of drugs: Concepts and examples". *Perspectives in Drug Discovery and Design* 19(1): 179-211

Tjernberg LO, Lilliehook C, Callaway DJE, Naslund J, Hahne S, Thyberg J, Terenius L and Nordstedt C (1997). "Controlling amyloid beta-peptide fibril formation with protease-stable ligands". *Journal of Biological Chemistry* 272(19): 12601-12605

van Groen T, Kadish I, Funke SA, Bartnik D and Willbold D (2012). "Treatment with Abeta42 binding D-amino acid peptides reduce amyloid deposition and inflammation in APP/PS1 double transgenic mice". *Adv Protein Chem Struct Biol* 88: 133-152

van Groen T, Kadish I, Funke SA, Bartnik D and Willbold D (2013). "Treatment with D3 removes amyloid deposits, reduces inflammation, and improves cognition in aged AbetaPP/PS1 double transgenic mice". *J Alzheimers Dis* 34(3): 609-620

van Groen T, Wiesehan K, Funke SA, Kadish I, Nagel-Steger L and Willbold D (2008). "Reduction of Alzheimer's Disease Amyloid Plaque Load in Transgenic Mice by D3, a D-Enantiomeric Peptide Identified by Mirror Image Phage Display". *Chemmedchem* 3(12): 1848-1852

van Regenmortel MHV and Muller S (1998). "D-peptides as immunogens and diagnostic reagents". *Current Opinion in Biotechnology* 9(4): 377-382

Vlassenko AG, Benzinger TLS and Morris JC (2012). "PET amyloid-beta imaging in preclinical Alzheimer's disease". *Biochimica Et Biophysica Acta-Molecular Basis of Disease* 1822(3): 370-379

Vlieghe P, Lisowski V, Martinez J and Khrestchatisky M (2010). "Synthetic therapeutic peptides: science and market". *Drug Discovery Today* 15(1-2): 40-56

Walsh DM and Selkoe DJ (2007). "A beta oligomers - a decade of discovery". *J Neurochem* 101(5): 1172-1184

Walti MA, Ravotti F, Arai H, Glabe CG, Wall JS, Bockmann A, Guntert P, Meier BH and Riek R (2016). "Atomic-resolution structure of a disease-relevant Abeta(1-42) amyloid fibril". *Proc Natl Acad Sci U S A* 113(34): E4976-4984

Werle M and Bernkop-Schnurch A (2006). "Strategies to improve plasma half life time of peptide and protein drugs". *Amino Acids* 30(4): 351-367

Wirths O, Breyhan H, Cynis H, Schilling S, Demuth HU and Bayer TA (2009). "Intraneuronal pyroglutamate-Abeta 3-42 triggers neurodegeneration and lethal neurological deficits in a transgenic mouse model". *Acta Neuropathologica* 118(4): 487-496

Witt KA, Gillespie TJ, Huber JD, Egleton RD and Davis TP (2001). "Peptide drug modifications to enhance bioavailability and blood-brain barrier permeability". *Peptides* 22(12): 2329-2343

Wolosker H, Dumin E, Balan L and Foltyn VN (2008). "D-amino acids in the brain: D-serine in neurotransmission and neurodegeneration". *FEBS J* 275(14): 3514-3526

Ziehm T, Brener O, van Groen T, Kadish I, Frenzel D, Tusche M, Kutzsche J, Reiss K, Gremer L, Nagel-Steger L and Willbold D (2016). "Increase of Positive Net Charge and Conformational Rigidity Enhances the Efficacy of d-Enantiomeric Peptides Designed to Eliminate Cytotoxic Abeta Species". *ACS Chem Neurosci* 7(8): 1088-1096

Danksagung

Ein großer Dank geht an Prof. Dieter Willbold für die Bereitstellung eines Themas, wie ich es mir vorgestellt habe, in einer perfekt ausgestatteten Umgebung. Weiterhin danke ich Dir für Deine Unterstützung und die permanente Förderung. Außerdem schätze ich es sehr, dass Du mir die Teilnahme an verschiedensten nationalen und internationalen Konferenzen ermöglicht hast.

Weiterhin danke ich Jun.-Prof. Alexander Büll für die Übernahme des Korreferats mit allen dazugehörigen Aufgaben. Die Diskussionen mit Dir haben mir viel Spaß gemacht, mich stets motiviert weiterzumachen und mir viele neue Denkweisen bereitet. Danke für Deinen Einsatz, ich habe viel von Dir gelernt.

Der Graduiertenschule IHRS BioSoft, insbesondere Thorsten, danke ich für eine tolle Zeit. Ihr habt mir neue wissenschaftliche Perspektiven eröffnet.

Weiterhin danke ich der gesamten „Alzheimer-Therapie“-Gruppe für eine freundliche und hilfsbereite Zusammenarbeit über die gesamten drei Jahre und ein offenes Ohr für jede Fragestellung: Janine, Antonia, Anne, Markus, Sarah, Elena und Stephan. Auch Wolfgang, Melanie und Lothar danke ich für die vielen fachlichen Diskussionen und Gespräche.

Franzi, Yvonne und den ehemaligen Kolleginnen und Kollegen Justin, Kerstin, Christina, Kateryna, Maren und Katja danke ich für den wissenschaftlichen Austausch, viel Spaß und der Hilfe bei Problemen aller Art.

Ein großer Dank geht auch an alle übrigen Mitarbeiterinnen und Mitarbeiter des ICS-6. Ihr habt dazu beigetragen, dass ich mich immer wohl gefühlt habe.

Besonders danke ich meiner ganzen Familie, insbesondere meinen Eltern, für Eure große Unterstützung mein Leben lang und dass Ihr immer an mich geglaubt habt.

Martin, Dir danke ich von Herzen für alles, was Du in den vielen Jahren für mich getan hast. Du hast mich unterstützt, wo es ging, viel Verständnis gezeigt und motiviert weiterzumachen.

Eidesstattliche Erklärung

Ich versichere an Eides Statt, dass die Dissertation von mir selbständig und ohne unzulässige fremde Hilfe unter Beachtung der „Grundsätze zur Sicherung guter wissenschaftlicher Praxis an der Heinrich-Heine-Universität Düsseldorf“ erstellt worden ist und ich Zitate deutlich kenntlich gemacht habe.

Ferner erkläre ich, dass ich in keinem anderen Dissertationsverfahren mit oder ohne Erfolg versucht habe, diese Dissertation einzureichen.

Jülich,

List of publications

2018

Ziehm T, Buell AK, Willbold D. “The role of hydrophobicity and charge of amyloid-beta oligomer eliminating D-peptides in the interaction with amyloid-beta monomers”. *Chem Sci* (submitted)

Dunkelmann T, Teichmann K, Ziehm T, Schemmert S, Frenzel D, Tusche M, Dammers C, Jürgens D, Langen KJ, Demuth HU, Shah NJ, Kutzsche J, Willuweit A, Willbold D. “Aβ oligomer eliminating compounds interfere successfully with pEAβ(3-42) induced motor neurodegenerative phenotype in transgenic mice”. *Neuropeptides* 2018 Feb;67:27-35

Yerabham ASK, Müller-Schiffmann A, Ziehm T, Stadler A, Köber S, Indurkhya X, Marreiros R, Trossbach SV, Bradshaw NJ, Prikulis I, Willbold D, Weiergräber OH, Korth C. “Biophysical insights from a single chain camelid antibody directed against the Disrupted-in-Schizophrenia 1 protein”. *PLoS One* 2018 Jan 11;13(1):e0191162

2017

Schartmann E, Schemmert S, Ziehm T, Leithold LHE, Jiang N, Tusche M, Joni Shah N, Langen KJ, Kutzsche J, Willbold D, Willuweit A. “Comparison of blood-brain barrier penetration efficiencies between linear and cyclic all-D-enantiomeric peptides developed for the treatment of Alzheimer's disease”. *Eur J Pharm Sci* 2017 Dec 7;114:93-102

van Groen T, Schemmert S, Brener O, Gremer L, Ziehm T, Tusche M, Nagel-Steger L, Kadish I, Schartmann E, Elfgen A, Jürgens D, Willuweit A, Kutzsche J, Willbold D. “The Aβ oligomer eliminating D-enantiomeric peptide RD2 improves cognition without changing plaque pathology”. *Sci Rep* 2017 Nov 24;7(1):16275

Klein AN, Ziehm T, van Groen T, Kadish I, Elfgen A, Tusche M, Thomaier M, Reiss K, Brener O, Gremer L, Kutzsche J, Willbold D. “Optimization of D-peptides for Aβ monomer binding specificity enhances their potential to eliminate toxic Aβ oligomers”. *ACS Chem Neurosci* 2017 Sep 20;8(9):1889-1900

Dammers C, Reiss K, Gremer L, Lecher J, Ziehm T, Stoldt M, Schwarten M, Willbold D. “Pyroglutamate-modified amyloid-β(3-42) shows α-helical intermediates prior to amyloid formation”. *Biophys J* 2017 Apr 25;112(8):1621-1633

2016

Ziehm T, Brener O, van Groen T, Kadish I, Frenzel D, Tusche M, Kutzsche J, Reiß K, Gremer L, Nagel-Steger L, Willbold D. “Increase of Positive Net Charge and Conformational Rigidity Enhances the Efficacy of D-Enantiomeric Peptides Designed to Eliminate Cytotoxic Aβ Species”. *ACS Chem Neurosci* 2016 Aug 17;7(8):1088-96

Klein AN, Ziehm T, Tusche M, Buitenhuis J, Bartnik D, Boeddrich A, Wiglenda T, Wanker E, Funke SA, Brener O, Gremer L, Kutzsche J, Willbold D. “Optimization of the All-D Peptide D3 for Aβ Oligomer Elimination”. *PLoS One* 2016 Apr 22;11(4):e0153035

Leithold LH, Jiang N, Post J, Niemietz N, Schartmann E, Ziehm T, Kutzsche J, Shah NJ, Breitkreutz J, Langen KJ, Willuweit A, Willbold D. “Pharmacokinetic properties of tandem

D-peptides designed for treatment of Alzheimer's disease". *Eur J Pharm Sci* 2016 Jun 30;89:31-8

Leithold LH, Jiang N, Post J, Ziehm T, Schartmann E, Kutzsche J, Shah NJ, Breitkreutz J, Langen KJ, Willuweit A, Willbold D. "Pharmacokinetic Properties of a Novel D-Peptide Developed to be Therapeutically Active Against Toxic β-Amyloid Oligomers". *Pharm Res* 2016 Feb;33(2):328-36

2015

Jiang N, Leithold LH, Post J, Ziehm T, Mauler J, Gremer L, Cremer M, Schartmann E, Shah NJ, Kutzsche J, Langen KJ, Breitkreutz J, Willbold D, Willuweit A. "Preclinical Pharmacokinetic Studies of the Tritium Labelled D-Enantiomeric Peptide D3 Developed for the Treatment of Alzheimer´s Disease". *PLoS One* 2015 Jun 5;10(6):e0128553

List of conference contributions

2017

Ziehm T, Buell AK, Willbold D. “Detailed biophysical analysis of the interaction between amyloid-beta and aggregation inhibitors: Role of charge and hydrophobicity”. *Ulm Meeting Biophysics of Amyloid Formation* (Ulm, Germany). Poster presentation.

Ziehm T, Klein AN, Kutzsche J, Willbold D. “Biophysical studies of the interaction between optimized peptides and amyloid-beta elucidate a completely novel binding mode”. *Biophysical Society 61st Annual Meeting* (New Orleans, LA, USA). Oral presentation.

2016

Ziehm T, Willbold D. “A reproducible method for characterization of specific ligand interactions with different amyloid-beta assembly states”. *2nd Drug Discovery Forum* (Munich, Germany). Invited oral presentation.

Ziehm T, Brener O, van Groen T, Kadish I, Tusche M, Kutzsche J, Willbold D. “Increase of positive net charge and conformational rigidity enhances the efficacy of D-enantiomeric peptides designed to eliminate cytotoxic Aβ species”. *10th Annual Drug Discovery for Neurodegeneration Conference* (Miami, FL, USA). Poster presentation.

2015

Ziehm T, Brener O, van Groen T, Kadish I, Tusche M, Kutzsche J, Willbold D. “Cyclization and charge elevation: two minor modifications of an amyloid-beta targeting peptide with major impact on oligomer elimination efficacy”. *1st Düsseldorf-Jülich Symposium on Neurodegenerative Diseases* (Düsseldorf, Germany). Poster presentation.

Ziehm T, Frenzel D, Willbold D. “A facile approach to immobilize different amyloid beta assembly states”. *Biacore User Meeting* (Berlin, Germany). Invited oral presentation.

Ziehm T, Brener O, van Groen T, Kadish I, Tusche M, Kutzsche J, Willbold D. “Optimization of D-enantiomeric peptides by chemical modifications for the treatment of Alzheimer´s disease”. *Alzheimer’s and Parkinson’s Diseases Congress - AD/PD* (Nice, France). Poster presentation.

Print permissions

Increase of Positive Net Charge and Conformational Rigidity Enhances the Efficacy of D-Enantiomeric Peptides Designed to Eliminate Cytotoxic Aβ Species

Tamar Ziehm, Oleksandr Brener, Thomas van Groen, Inga Kadish, Daniel Frenzel, Markus Tusche, Janine Kutzsche, Kerstin Reiß, Lothar Gremer, Luitgard Nagel-Steger, Dieter Willbold

ACS Chem Neurosci. 2016 Aug 17;7(8):1088-96

doi: 10.1021/acschemneuro.6b00047

http://pubs.acs.org/doi/abs/10.1021/acschemneuro.6b00047

Optimization of D-peptides for Aβ monomer binding specificity enhances their potential to eliminate toxic Aβ oligomers

Antonia N Klein, Tamar Ziehm, Thomas van Groen, Inga Kadish, Anne Elfgen, Markus Tusche, Maren Thomaier, Kerstin Reiss, Oleksandr Brener, Lothar Gremer, Janine Kutzsche, Dieter Willbold

ACS Chem Neurosci. 2017 Sep 20;8(9):1889-1900

doi: 10.1021/acschemneuro.7b00045

http://pubs.acs.org/doi/abs/10.1021/acschemneuro.7b00045

Aβ oligomer eliminating compounds interfere successfully with pEAβ(3-42) induced motor neurodegenerative phenotype in transgenic mice

Tina Dunkelmann, Kerstin Teichmann, Tamar Ziehm, Sarah Schemmert, Daniel Frenzel, Markus Tusche, Christina Dammers, Dagmar Jürgens, Karl-Josef Langen, Hans-Ulrich Demuth, Nadim Jon Shah, Janine Kutzsche, Antje Willuweit, Dieter Willbold

Neuropeptides. 2018 Feb;67:27-35

doi: 10.1016/j.npep.2017.11.011

https://www.sciencedirect.com/science/article/pii/S0143417917301531